Université de Montréal

Monocouches peptidiques auto-assemblées et applications dans le domaine des biocapteurs de résonance de plasmon de surfaces

par :

Olivier R. Bolduc

Département de Chimie

Faculté des arts et des sciences

Thèse présentée à la Faculté des arts et des sciences

en vue de l'obtention du grade de Philosophiae Doctor (Ph.D.)

en Chimie

Août, 2011

Université de Montréal

Faculté des arts et des sciences

Cette thèse intitulée :

Monocouches peptidiques auto-assemblées et applications dans le domaine des biocapteurs de résonance de plasmon de surfaces

Présentée par :

Olivier R. Bolduc

a été évaluée par un jury composé des personnes suivantes :

Karen C. Waldron, président-rapporteur

Jean-François Masson, directeur de recherche

Pierre Chaurand, membre du jury

Denis Boudreau, examinateur externe

Karen C. Waldron, représentante du doyen de la FES

Résumé

Ces travaux visent à étendre les applications de la résonance de plasmons de surface (SPR) L'objectif est d'offrir des outils diagnostics plus rapides, efficaces et simple d'utilisation pour diagnostiquer ou effectuer le suivi de conditions cliniques. Pour se faire, un nouveau type d'instrumentation SPR basé sur l'utilisation d'un prisme d'inversion (dove) a permis d'atteindre une limite de détection (LOD) de 10^{-6} unité d'indice de réfraction (RIU), une valeur comparable aux instruments commerciaux complexes tout en demeurant peu dispendieux, robuste et simple d'utilisation. Les travaux présentés dans cet ouvrage visent, dans un second temps, à réduire les interactions nonspécifiques (NSB) entre la surface des biocapteurs SPR et les composants de la matrice biologique complexe telles que: l'urine, le lysat cellulaire, le sérum et le sang. Ces dernières induisent des réponses empêchant l'utilisation de biocapteurs SPR en milieux complexes. Les acides aminés (AA) offrent une grande variété de propriétés physico-chimiques permettant la mise au point de monocouches auto-assemblées (SAM) aux propriétés diverses. Initialement, 19 des 20 acides aminés naturels ont été attachés à l'acide 3-mercaptopropionique (3-MPA) formant des SAMs peptidomimétiques. La quantité d'interactions nonspécifiques engendrées par ces différentes surfaces a été mesurée en exposant ces surfaces au sérum sanguin bovin complet variant de 400 ng/cm² jusqu'à 800 ng/cm². La détection à l'aide de ces surfaces de la β-lactamase (une enzyme responsable de la résistance aux antibiotiques au niveau μM) a démontré la possibilité d'employer ces surfaces pour bâtir des biocapteurs SPR. Des peptides de longueur allant de 2 à 5 résidus attachés à 3-MPA ont été synthétisés sur support solide. Cette étude a démontré que l'augmentation de la longueur des peptides formés d'AA résistants aux NBS accroit leur résistance jusqu'à 5 résidus. Le composé le

plus performant de ce type (3-MPA-$(Ser)_5$-OH) a permis d'atteindre 180 ng/cm². Cette valeur est similaire à celle des meilleures surfaces disponibles commercialement, notamment les surfaces de polyethylène glycol (PEG) à 100 ng/cm². Des surfaces de 3-MPA-$(Ser)_5$-OH ont permis l'étalonnage de la β-lactamase et sa quantification directe dans un lysat cellulaire. La LOD pour ces biocapteurs est de 10 nM. Une troisième génération de surfaces peptidiques binaires a permis la réduction de la NSB jusqu'à un niveau de 23±10 ng/cm² une valeur comparable aux meilleures surfaces disponibles. Ces surfaces ont permis l'étalonnage d'un indicateur potentiel du cancer la metalloprotéinase-3 de matrice (MMP-3). Les surfaces formées de peptides binaires (3-MPA-H_3D_2-OH) ont permis la quantification directe de la MMP-3 dans le sérum sanguin complet. Une quatrième génération de surfaces peptidiques a permis de réduire davantage le niveau de NSB jusqu'à une valeur de 12 ± 11 ng/cm². Ces surfaces ont été modifiées en y attachant une terminaison de type acide nitriloacétique (NTA) afin d'y attacher des biomolécules marquées par six résidus histidines terminaux. Ces surfaces ont permis le développement d'une méthode rapide de balayage des ligands ciblant le « cluster of differenciation-36 » (CD36). L'étude d'électroformation des monocouches de peptide a permis de déterminer les conditions de formation optimales d'une couche de 3-MPA-HHHDD-OH permettant ainsi la formation de monocouches résistantes au NSB en moins de 6 minutes en appliquant un potentiel de formation de 200mV vs Ag/AgCl.

Mots-Clés

Interactions nonspécifiques, Résonance de plasmons de surface, Biocapteurs, Capteurs chimiques, Monocouches auto-assemblées, Peptides, Pharmaceutique, Électroformation, Outils diagnostiques, Couches chimiques, Adsorption.

Abstract

The work presented in this thesis aims to extend the use of surface plasmon resonance (SPR) biosensors to generate more rapid, cost efficient and simple to use diagnostic tools to diagnose or follow serious medical conditions. This task required the development of a new SPR instrument that relies on an inversion prism (dove) and is able to reach a limit of detection (LOD) in the 10^{-6} refractive index unit (RIU) range, a value comparable to more complex commercial instruments. The developed SPR instrumentation is inexpensive, robust and very simple to manipulate. The other work presented in this thesis is based on reducing nonspecific interactions between the surface of SPR sensors and components in biological matrices such as urine, cell lysate, serum and whole blood. These nonspecific interactions induce SPR responses that have typically prohibited the use of SPR in these complex matrices. Amino acidshavebeen investigated for reduction of nonspecific binding (NSB) because they offer a wide variety of physico-chemical properties capable of tuning the physical properties of surfaces in a self-assembled monolayer (SAM) format. Initially, the attachment of one of 19 physiological 20 amino acids to 3-mercaptopropionic acid (3-MPA) allowed the formation of amino acid SAMs. Exposure of these surfaces to bovine serum revealed nonspecific interactions ranging from 400 ng/cm² to 800 ng/cm². Detection assays for β-lactamase (an enzyme produced by drug resistant bacteria at a micromolar level) demonstrated that the amino acid SAM is suitable for SPR biosensing. By using a solid phase approach, peptides were of 2 to 5 residues were synthesized to investigate NSB properties. The result of this study showed that adding amino acids decreased nonspecific interactions up to a peptide length of 5 amino acids. The best performing peptide, 3-MPA-$(Serine)_5$-OH, resulted in low nonspecific adsorption of bovine

serum proteins to a level of 180 ng/cm². This value is similar to nonspecific adsorption obtained under identical conditions for one of the best reported surfaces: polyethylene glycol-based SAMs at 100 ng/cm². The 3-MPA-$(Serine)_5$-OH based SAM was used to calibrate β-lactamase, leading to its direct quantification in crude cell lysate. The detection limit for this analyte was 10 nM. A third generation of peptide, which is binary patterned, decreased significantly nonspecific adsorption to a level as low as 23 ± 10 ng/cm², a value comparable to the best surfaces known. This surface SAM allowed the calibration of matrix metalloproteinase-3 (MMP-3), a potential indicator of cancer. Direct quantification assays of MMP-3 in whole blood serum were achieved with the binary patterned peptides developed. The LOD for MMP-3 was 0.2nM over a 50 nM linear domain. A fourth generation of peptide based surfaces was developed, reducing the level of nonspecific adsorption of blood serum proteins to 12 ± 11 ng/cm^2. These new surfaces were modified to attach His-tagged biomolecules enabling rapid screening of small ligands targeting the Cluster of differentiation-36 (CD36). Finally, the electroformation of peptide monolayers was studied to determine the optimal conditions needed to form an ultralow biofouling surface. It was demonstrated that the difference in potential applied during the formation of a peptide based layer influences the kinetics of formation and the arrangement of this layer. An optimal layer of 3-MPA-HHHDD-OH could be obtained in less than 6 min by applying a potential of 200mV vs Ag/AgCl to the SPR sensor.

Keywords

Nonspecific interactions, Surface plasmon resonance, Biosensors, Chemical sensors, Self-assembled monolayers, Peptides, Pharmaceutical, Eectroformation, Diagnostic tools, Chemical layers, Adsorption.

Table des matières

Liste des tableaux

Liste des figures

Liste des sigles et abréviations

Δ	Variation
16-MHA	16-mercaptohexadecanoic acid ($HS-(CH2)_{15}-COOH$)
	(Acide 16-mercaptohexadécanoique)
3-MPA	3-mercaptopropionic acid ($HS-(CH2)_2-COOH$)
	(Acide 3-mercapto propionique)
AA	Acide aminé
ADN	Acide désoxyribonucléïque
Ag/AgCl	Électrode de référence : Argent/Chlorure d'argent
APTES	3-aminopropyl triethoxysilane
	(3-aminopropyle triéthoxysilane) – Agent couplant avec Si-O
APTMS	3-aminopropyl trimethoxysilane
	(3-aminopropyle triméthoxysilane) – Agent couplant avec Si-O
ARN	Acide ribonucléïque
ATR	Attenuated total reflectance
	(Réflexion totale atténuée)
BK7	Borosilicate crown glass
	(Verre de borosilicate)
BSA	Bovine serum albumine
	(Albumine bovine du sérum)
CCD	Charge-coupled device
	(Capteur photographique)
CD	circular dichroism
	(Dichroïsme circulaire)

CD36	Cluster of differenciation - 36
	(Complexe de différenciation-36)
CE	Capillary electrophoresis
	(Électrophorèse capillaire)
CM-dextran	Carboxymethyl-dextran
	(Carboxymethyl-dextran)
DCC	N,N'-dicyclohexylcarbodiimide
DCM	Dichlorométhane
DHF	Dihydroxyfolate
DIEA	N-ethyldiisopropylamine
DMAP	4-(dimethylamino)pyridine
DMF	N,N-dimethylformamide
DOPA	L-3,4-dihydroxyphenylamine
EC50	Half maximal effective concentration
	(Concentration efficace à mi-hauteur)
EDC	N-Ethyl-N'-(3-dimethylaminopropyl)carbodiimide
EDTA	Ethylene diaminetetraacetic acid
ESI	Electrospray ionization
	(Ionisation par éléctronébulisation)
FTIR	Fourier transform infrared spectroscopy
	(Spectroscopie infrarouge à Transformée de Fourier)
GATR	Germanium attenuated total reflection
	(Réflexion totale atténuée sur cristal de Germanium)
HBTU	2-(1H-Benzotriazole-1-yl)-1,1,3,3-tetramethyluronium

hDHFR	human Dihydroxyfolate reductase (Dihydroxyfolate réductase humaine)
His-tag ou H_6	-(Histidine)$_6$-OH
HPLC	High-performance liquid chromatography (Chromatographie liquide à haute performance)
IgG	Immunoglobuline-Gamma
K_d	Constante de dissociation
laser	Light Amplification by Stimulated Emission of Radiation (Amplification de la lumière par émission stimulée de rayonnement)
LC	Chromatographie liquide
l_d	Distance de pénétration
LED	Light-emitting diode (Diode lumineuse)
LOD	Limit of detection (Limite de détection)
m	Sensibilité
MALDI	Matrix assisted laser desorption ionization (Ionisation par désorption laser assistée par matrice)
MBP	Maltose binding protein (Protéine liant le maltose)
MES	2-(N-morpholino)ethanesulfonic acid (acide 2-(N-morpholino)éthane sulfonique)
MMP-3	matrix metalloproteinase-3 (Métalloprotéinase de matrice-3)

MS	Spectrométrie de masse
MTX	Methotrexate
NA	Numerical aperture
	(Ouverture numérique)
NADPH	Nicotinamide adenine dinucleotide phosphate
	(Nicotinamide adénine dinucléotide phosphate)
NHS	N-hydroxysuccinimide
NIR	Proche infrarouge
NSB	Nonspecific binding
	(Interactions nonspécifiques)
NTA	Nitrilotriacetic acid
	(Acide nitriloacétique)
OLLS	Ordinary linear least squares
	(Moindres carrés ordinaires)
PBS	Phosphate buffer saline (concentration 1x)
	(Tampon salin phosphate)
PE	Polyethylene
	(Polyethylène)
PEO	Polyethylene oxide
	(Oxyde de polyethylène)
ppb	Parties par milliards
ppm	Partie par millions
RI	Refractive index
	(Indice de réfraction)

RIU	Refractive index unit
	(Unité d'indice de réfraction)
SAM	self-assembled monolayer
	(Monocouche auto-assemblée)
SERS	Surface Enhanced Raman Sacttering
	(Diffusion Raman exaltée par les surfaces)
SP	Surface plasmon
	(Plasmon de surface)
SPE	Solid phase extraction
	(Extraction sur phase solide)
SPR	Surface Plasmon Resonance
	(Résonance des plasmons de surface)
STM	Scanning Tunneling Microscopy
SVD	Singular value decomposition
	(Décomposition en valeur singulière)
TES	Triethylsilane
TFA	Trifluoro acetic acid
	(Acide trifluoroacétique)
UV/Vis	Lumière ultraviolet/visible
VIS	Visible ou lumière visible
XPS	X-ray photoelectron spectroscopy
	(spectrométrie de photoélectrons induits par rayons-X)
θ_c	Angle de contact
λ	Longueur d'onde

ρ	Densité volumique
Γ	Couverture de surface

Dédicace

Cette thèse est dédié à tout ceux qui offrent leur vie afin que nous soyons des scientifiques en temps de paix parmi eux : mon ami Frédéric Bouchard décédé le 16 août 2011 et ma petite sœur Virginie.

Merci, - *Olivier*

Remerciements

Cette thèse n'aurait jamais vu le jour sans mon directeur de recherche le Professeur Jean-François Masson de l'Université de Montréal qui a fait de moi le premier membre étudiant de son groupe de recherche en hiver 2008. Je le remercie d'avoir su reconnaître et développer en moi mes qualités de chercheur. Je le remercie de m'avoir montré les rouages de la fondation d'un groupe de recherche ainsi que de sa gestion quotidienne ce qui constitue un outil de taille pour l'avenir. Je le remercie d'avoir fait de moi une meilleure personne sur le plan personnel.

Je remercie ma conjointe, Audrey Ste-Marie, d'être à mes côtés à chaque instant de ma vie. Elle m'a encouragé à entreprendre ces travaux et m'a soutenu tout au long de ces derniers.

Je remercie mes collègues étudiants et chercheurs postdoctoraux du groupe de recherche Masson pour leur collaboration, soutien et compréhension. J'aimerais plus particulièrement remercier les stagiaires ayant œuvré à mes côtés : Audrey Cunche, Alexandra Aubé, Michael Pruneau, Émilie Canuel et Mimosa Nguyen. J'aimerais remercier Julien Breault-Turcot, Ludovic S. Live, Sandy S. Zhao, Dr. Mathieu Branca et Mathieu Ratel de leur contribution à mes travaux de recherche.

Je remercie le corps professoral du département de chimie de l'Université de Montréal pour avoir fait de moi le scientifique que je suis devenu au travers des trois cycles d'études universitaires. J'aimerais remercier particulièrement les professeurs Joelle N. Pelletier, Andreea R. Schmitzer, Antonella Badia et Christian Pellerin ainsi que leur

groupe de recherche pour leurs conseils précis, ainsi que pour m'avoir ouvert la porte de leur laboratoire.

J'aimerais remercier l'équipe de soutien technique du département de chimie pour m'avoir fourni les outils nécessaires à la réalisation de ces travaux. Plus spécifiquement, M. Jean-François Myre et M. Martin Lambert pour avoir concrétisé les instrumentations développées au cours de ces travaux. Je remercie l'équipe des laboratoires d'enseignement pour leur soutien au niveau de l'instrumentation analytique et pour leur aide au cours de mes tâches d'auxiliaire d'enseignement.

CHAPITRE 1 : Introduction générale

1.1 Les biocapteurs

1.1.1 Descriptions et applications

Les capteurs chimiques et biologiques sont des instruments analytiques intégrant tous les composants nécessaires à détecter, amplifier, analyser, traiter le signal et afficher les résultats en un seul et même système. Les capteurs chimiques permettent la détection ou la quantification de molécules chimiques; alors que les capteurs biologiques nommés biocapteurs détectent ou quantifient des analytes de nature biologique. Les différentes composantes d'un biocapteur standard sont représentés en Figure 1-1.[1]

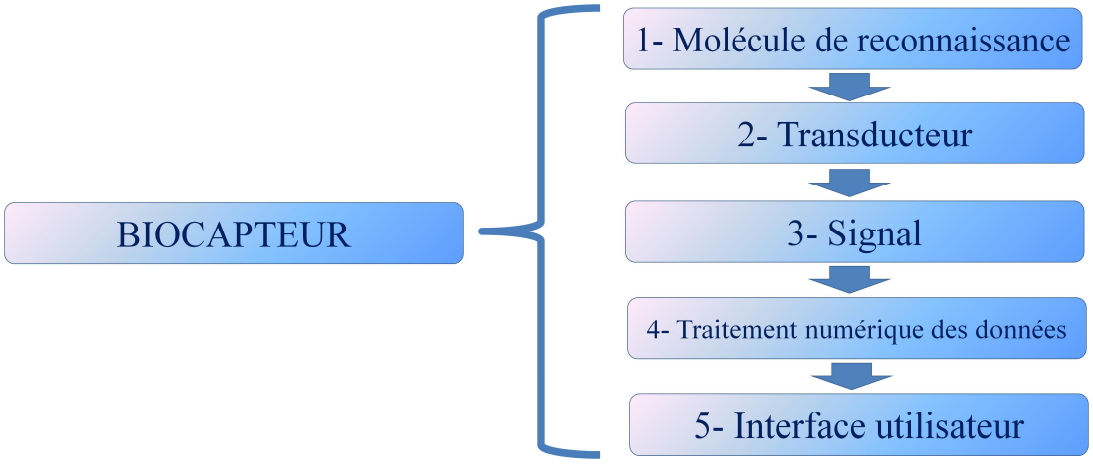

Figure 1-1. Représentation graphique des composantes d'un biocapteur standard

La molécule de reconnaissance assure la sélectivité de la surface du biocapteur pour l'analyte à détecter ou à quantifier. Le transducteur est la portion du biocapteur permettant de transformer un évènement physique propre au système biologique sous investigation, soit un changement de propriété chimique ou physique à une interface, en signal électrique concret par exemple un flux d'électrons. Le courant ainsi généré suite à une réaction chimique peut être modulé ou amplifié au besoin pour permettre le traitement de données

approprié afin de quantifier l'analyte présent en solution. L'interface utilisateur est la portion permettant d'afficher l'état de la détection ou la quantité détectée pour un utilisateur. Par exemple, l'interface utilisateur d'un biocapteur destiné à la détection d'agents neurotoxiques pourrait n'être composée que d'un voyant lumineux de couleur rouge indiquant au soldat la présence d'agents toxiques.

Le développement des biocapteurs suit donc des lignes de pensées menant à la production de systèmes hautement portables, robustes, simples d'utilisation et aussi le plus abordables que possible. La portabilité des biocapteurs est essentielle pour réduire au maximum le matériel à déplacer dans le cadre de mesures sur le terrain, par exemple lors d'études environnementales. Dans un cadre clinique, une bonne portabilité permet de réduire de manière optimale les impacts sur la vie de tous les jours d'un patient possédant un système de suivi en temps réel d'une condition médicale. Une bonne portabilité implique aussi le développement de biocapteurs non seulement de faibles tailles, mais aussi peu énergivores. La robustesse des biocapteurs est essentielle à la portabilité, mais aussi au maintien de leur potentiel de détection ayant une influence directe sur la fiabilité des résultats obtenus à l'aide de ces derniers. Certains types de biocapteurs pourraient être exposés à des températures extrêmes, des conditions d'humidité variables ou à l'exposition prolongée à la lumière. L'utilisation des biocapteurs pourrait s'effectuer autant en Antarctique qu'au Sahara et l'élaboration des composantes de ces derniers doit donc s'effectuer en conséquence. Les biocapteurs se voulant des outils accessibles au grand public, il est essentiel que leur manipulation et leur utilisation soient aussi simples que possible tant au niveau de la manipulation de l'échantillon, que de l'opération du biocapteur et de la compréhension des résultats obtenus suite à la mesure. Les biocapteurs étant

souvent composés de molécules de détection périssables et constituant un premier outil de détection menant au besoin à des analyses plus poussées, mais aussi souvent plus fastidieuses et coûteuses à l'aide de techniques analytiques conventionnelles plus efficaces, il est alors essentiel de diminuer le coût des biocapteurs autant que possible. Ces caractéristiques font des biocapteurs des outils ayant un très grand potentiel dans des domaines tels que : le domaine médical, le domaine environnemental, le domaine alimentaire et la sécurité/défense[2], mais dont le développement engendre de nombreux défis à relever.

1.1.2 Types de biocapteurs

Plusieurs types de capteurs chimiques et de biocapteurs basés sur différentes réactions et interactions chimiques ou biologiques ont été développés. Le plus grand succès commercial des biocapteurs étant le glucomètre, un biocapteur de type électrochimique. Le grand succès du glucomètre est dû à la forte croissance du diabète, à des concentrations de glucoses dans le sang de l'ordre du mM et à l'existence d'une enzyme (glucose oxydase) robuste permettant d'oxyder l'analyte, le glucose, produisant, par le biais de médiateurs chimiques, un courant mesurable par le transducteur, une électrode, simple à fabriquer à base de matériaux peu dispendieux. L'ajout de médiateurs et la découverte de nouvelles méthodes plus sélectives pour oxyder le glucose ont poussé la popularité du glucomètre au sommet des ventes de biocapteurs avec près de 85% du marché mondial.[3] Les biocapteurs électrochimiques ne sont pas limités qu'à la détection du glucose. Plusieurs recherches portent sur le développement de biocapteurs électrochimiques pour la détection d'ADN[4], de bactéries pathogènes dans l'alimentation[5], de composés pharmaceutiques[6], d'agents biologiques militaires[7], de pesticides[8] et autres. Un autre type de biocapteurs dépend de

transducteurs piézoélectriques. Ces biocapteurs mesurent des signaux dans le domaine des ondes acoustiques dans des médias, tel que le cristal de quartz, permettant ainsi la mesure des variations de masses à l'interface solide-liquide ou solide-gaz de ces cristaux et du milieu à analyser.[9] Toutefois, les méthodes optiques présentées plus bas offrent de meilleures performances dues à leur surface de détection plus importante et à leur sensibilité supérieure.[10]

Une autre famille importante de biocapteurs est basée sur l'utilisation de méthodes optiques de type éllipsométrique, spectroscopique (luminescence, fluorescence phosphorescence, Raman), interférométrique, à guide d'onde optique et à résonance de plasmon de surface (SPR). Les biocapteurs éllipsométriques permettent de mesurer des changements de polarisation de la lumière dus à des variations d'épaisseurs de molécules biologiques à une interface engendrant un changement d'indice de réfraction. Ce type de biocapteur a permis la mesure de l'immobilisation de protéines sanguines à la surface des biocapteurs éllipsométriques.[11] Les biocapteurs spectroscopiques dépendent directement des propriétés optiques de l'analyte ou d'une molécule de reconnaissance qui peuvent être marquées au besoin. Plusieurs versions de ce type de biocapteur ont été développées et plusieurs modes de détections ont été explorés.[12, 13] Les biocapteurs basés sur l'utilisation de guides d'ondes s'appuient sur des interactions multiples entre le champ évanescent, provenant d'une onde lumineuse, et l'analyte immobilisé sur une surface sélective.[14] Les biocapteurs SPR seront décrits de manière détaillée plus loin.

1.1.3 Limites des biocapteurs

Bien que les biocapteurs offrent de nombreux avantages pratiques et économiques, ils sont aussi limités par leur nature. Les biocapteurs sont généralement conçus pour

détecter un seul analyte ou un seul type d'analyte précis, ce qui n'est pas le cas des instrumentations basées sur les méthodes analytiques classiques telles que la spectroscopie d'absorption ou de fluorescence couplée à la chromatographie liquide ou encore de la spectrométrie de masse couplée à un détecteur à transformée de Fourier. Un biocapteur créé spécifiquement pour détecter un analyte ou un type d'analyte est donc un instrument moins versatile qu'un système analytique complet, mais il est possible de modifier leur conception pour en modifier les applications. Leur conception impliquant l'utilisation de composants miniaturisés et souvent de plus faible résolution que ceux d'un système analytique standard, leurs limites de détection sont souvent supérieures à celle des méthodes de mesure conventionnelles. Par exemple, les travaux de Rainina et al. ont mené au développement d'un biocapteur piézoélectrique quantifiant des neurotoxines organophosphorés jusqu'à une limite de détection de 1μM[15] là où la spectrométrie de masse engendre une LOD typique de l'ordre du pM ou moins sans préconcentration.[16] Malgré les limites mentionnées dans cette section, la portabilité, la rapidité de mesure et les bonnes limites de détection font des biocapteurs une alternative attrayante pour la détection sur le site d'analyse avec un minimum de moyen. Toutefois, il est à noté que les techniques analytiques conventionnelles, bénéficient elles aussi de la capacité de miniaturisation provenant des avancées significatives en nanofabrication et des avancées en matériaux. Par exemple, Tulej et al, ont conçu un spectromètre de masse ne pesant que 1,5 kg et ne mesurant que 120mm x 60 mm destiné à l'exploration spatiale.[17] Toutefois, cette instrumentation nécessite des sources d'énergie non négligeables, impliquant donc l'intégration d'accumulateurs de forte masse/taille ou d'une grande quantité d'unités de production

électrique. De plus, leur résolution (m/Δm), ne dépasse guère 600, ce qui est nettement inférieur à une instrumentation pleine taille tout en demeurant très dispendieuse.

1.2 Les biocapteurs SPR

1.2.1 Description des biocapteurs SPR et de leur fonctionnement

Un biocapteur SPR en configuration Kretschmann typique est montré en Figure 1-2. Un média optique, tel que du verre, est recouvert d'un film mince d'Au typiquement d'une épaisseur de 50 nm au-dessus duquel se trouve une solution à analyser. Un faisceau de lumière soit blanche collimaté, soit monochromatique provenant d'un laser (trait large rouge, Figure 1-2) atteint l'interface verre-Au en conditions de réflexion totale interne. Puisque la lumière est une onde électromagnétique, elle se compose donc d'une composante électrique et d'une composante magnétique perpendiculaire à cette première. Lorsque le faisceau lumineux est réfléchi, le caractère ondulatoire des ondes permet une pénétration du champ électrique de la lumière dans le métal sous la forme d'une onde evanescente (oscillation verte). Le champ électrique peut donc intéragir avec les charges à l'interface métal-liquide, soit avec les électrons abondants dans la bande de conduction de l'Au. Les plasmons de surfaces existent de manière intrinsèque à l'interface Au-solution. Dans des conditions bien particulières, des photons dans de domaine du spectre électro-magnétique UV-visible et proche infrarouge, peuvent exiter efficacement les électrons, afin d'entrer en résonance (oscillation rouge). Cette oscillation des électrons, ayant un caractère ondulatoire, est nommée résonance des plasmons de surface et a une portée de 200nm au-dessus de cette interface. (voir section suivante) La Figure 1-2 montre la surface d'Au où sont immobilisées des molécules de roconnaissance permettant la détection spécifique de l'analyte en solution.

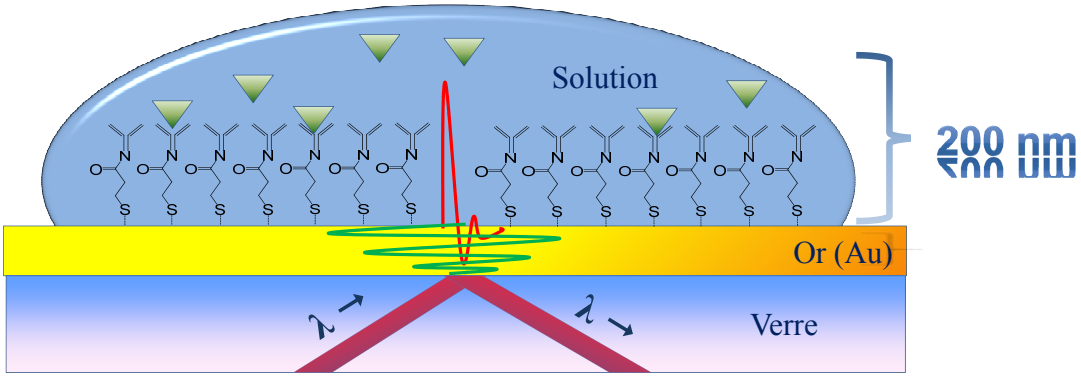

Figure 1-2. Biocapteur SPR en configuration Kretschmann. La lumière incidente frappe l'interface Verre-Au engendrant une onde évanescente (vert) ce qui peut entrainer la résonance des plasmons de surface (rouge) qui sonderont l'indice de réfraction des premiers 200 nm de la solution à l'interface d'une surface fonctionnalisée à l'aide de molécules thiolés. Des molécules de reconnaissance (noir) sélectives aux analytes sont immobilisées à la surface du capteur, afin de détecter et de quantifier l'analyte (triangles verts).

L'entrée en résonance des ces ondes se traduit par l'absorption de photon pour un couple (angle d'indidence (θ_i), longueur d'onde précis (λ)). Puisque ce phénomène nécessite la pénétration du champ électrique de l'Au, l'utilisation de lumière polarisée permet de moduler l'importance de la pénétration du champ électrique. Le cas où la composante électrique est perpendiculaire à l'interface verre-Au est dit p-polarisé et maximise la résonance des plasmons de surface. Le cas opposé où la composante électrique est dans le plan de l'interface verre-Au est dit s-polarisé et ne s'accompagne d'aucune résonance des plasmons de surface. Le phénomène de la résonance des plasmons de surface est alors dit : transverse magnétique.

L'entrée en résonance des plasmons de surface est fortement dépendante de l'indice de réfraction des molécules se trouvant dans les premiers 200 nm au-dessus de la surface de l'Au en solution. Une variation locale d'indice de réfraction dans cette zone entrainera

alors un chgangement du couple (θ_i,λ) pour lequel la résonance des plasmons de surfaces est observée. Il est alors possible de fixer l'un des deux paramètres en employant un laser à angle incident variable ou en utilisant de la lumière blanche collimitée à un angle fixe pour suivre des changements d'indice de réfraction locaux au-dessus l'interface Au-solution. L'ajout d'une monocouche organique à la surface de l'Au induira ainsi un changement observable en temps réel du signal observé, tout comme l'immobilisation d'une molécule de reconnaissance pour finalement détecter un analyte, puisque ces derniers ont généralement des indice de réfraction plus élevés que la matrice elle-même (Typiquement, protéine n = 1,45-1,57).

Pour une instrumentation fonctionnant en mode d'interogation des longueurs d'onde, soit en fixant l'angle d'incidence, θ_i, les spectres lumineux en lumière s-polarisée (Figure 1-3 A) sont tout d'abord acquis pour servir de référence (absence de résonance des plasmons de surface). Les intéractions moléculaires à l'interface Au-solution sont alors mesurée lumineux en lumière p-polarisée (Figure 1-3 B). Il est possible de recueillir des spectres lumineux de manière dynamique pour suivre les intéractions à l'interface. Le signal en lumière p-polarisé est alors divisé par le signal de référence pour obtenir un ratio dont la longueur d'onde affichant un minimum sera déterminé à chaque moment de l'analyse (λ_{SPR}) (Figure 1-3 C), puis reportée sur un graphique nommé « sensorgramme » (Figure 1-3 D) illustrant l'importance des interactions à la surface à chaque moment de l'analyse. Une augmentation de l'indice de réfraction s'illustre alors par une augmentation de λ_{SPR}.[18-20]

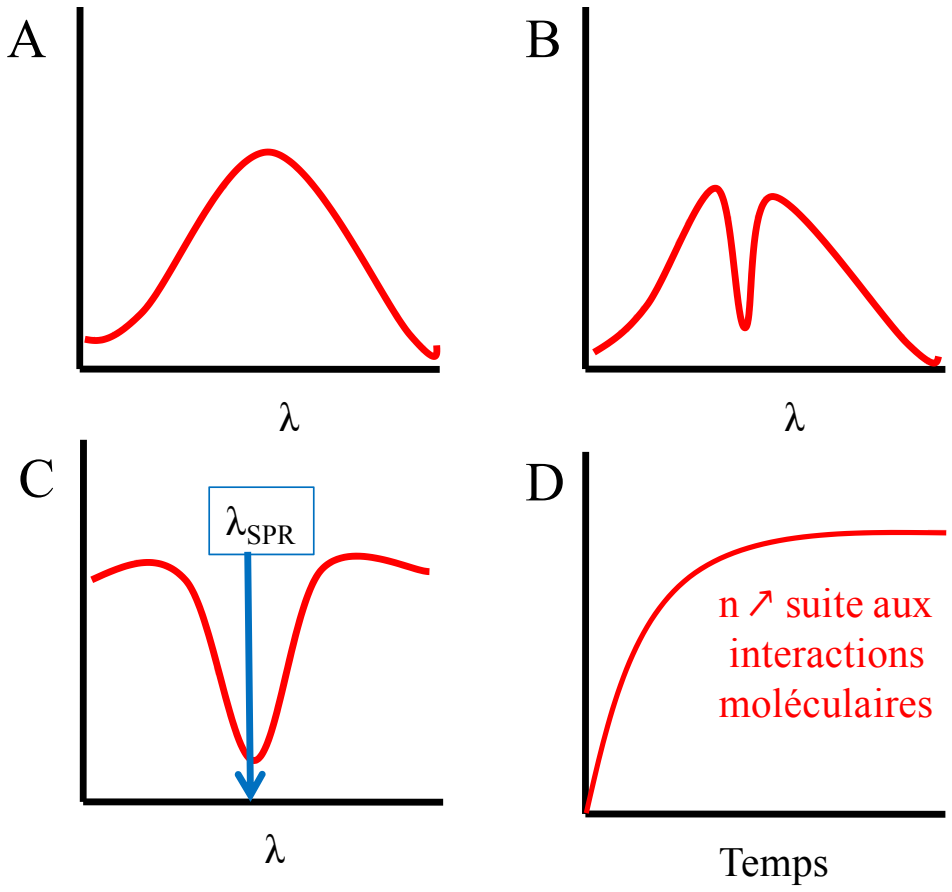

Figure 1-3. Détermination du signal SPR pour un instrument en mode d'intérogation par longueur d'onde. (A) Spectre de la lumière s-polarisée (spectre de la source en lumière polarisée). (B) Spectre de la lumière p-polarisée. (C) Ratio des spectres lumineux p-polarisée / s-polarisée pour détermination de la longueur d'onde SPR (λ_{SPR}). (D) Suivi de λ_{SPR} en temps réel.

La Figure 1-4 compare les composants généraux des biocapteurs SPR avec celles des glucomètres, le plus grand succès commercial des biocapteurs.

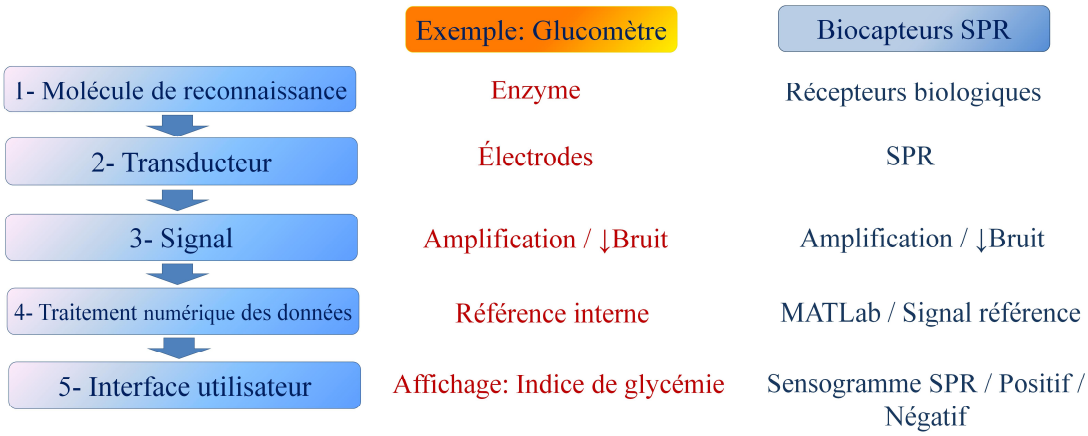

Figure 1-4. Composantes principales des biocapteurs SPR comparés au glucomètre.

Les travaux présentés dans cet ouvrage portent donc sur les composants qui assurent la reconnaissance des biocapteurs SPR, puisqu'un objectif de cette thèse est d'améliorer la sélectivité de ce type de biocapteur. Des travaux visant l'amélioration des transducteurs SPR ont aussi été conduits en parallèle par l'utilisation de couches métalliques microstructurées permettant l'amplification des signaux SPR. Ces deux composantes ont été intégrées pour permettre l'amélioration du signal SPR par un facteur de 2 lors de la détection de marqueurs biologiques par rapport à un film métallique continu. Ces travaux ont été publiés par Live et al.[21] Les composantes instrumentales sont décrites plus en détails dans la section 2.1.

La molécule de reconnaissance et le transducteur en SPR conventionnel se composent donc d'une surface métallique fonctionnalisée à l'aide d'une molécule de reconnaissance sélectif pour un analyte ciblé. Deux configurations sont alors envisageables, soit la configuration d'Otto ou soit la configuration de Kretschmann. Ces deux configurations sont montrées en Figure 1-5. Toutefois, la configuration de Kretschmann où le métal est directement disposé au-dessus du prisme (souvent en verre),

demeure la configuration employée pour les instruments de recherche et commerciaux.[19] La configuration d'Otto ne demeure qu'une configuration historique n'ayant aucune d'application pratique. Dans certains cas particuliers, comme lors de la mesure simultanée de techniques basées sur les ondes acoustiques, ces configurations peuvent être complémentaires.[22] D'autres configurations ont été développées, mais ces deux configurations demeurent le cœur des applications et des simulations actuellement en développement.[23]

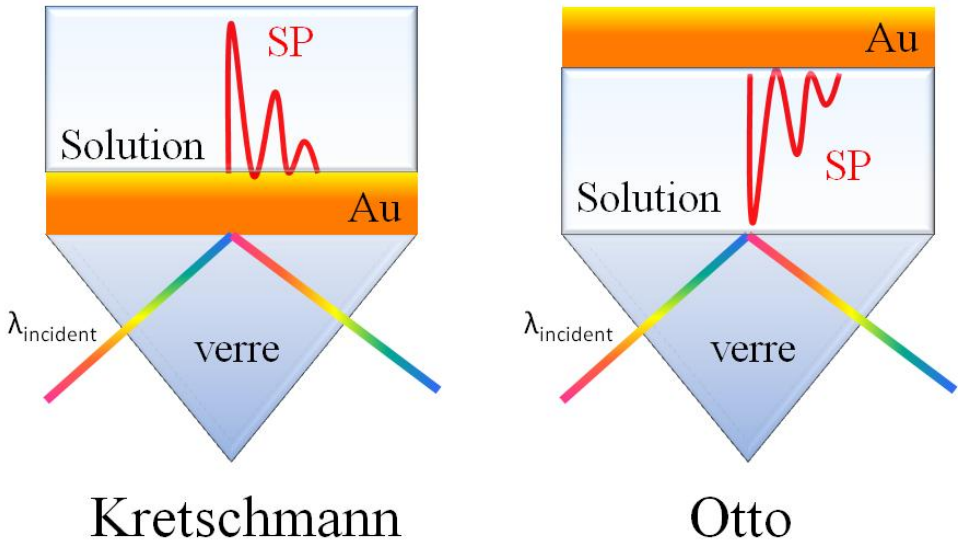

Figure 1-5. Configurations possibles en SPR

1.2.2 Le phénomène de la résonance des plasmons de surface (SPR)

Les ondes de plasmon de surface (SP) sont des ondes électromagnétiques se propageant le long d'une interface métal-diélectrique. Ce phénomène est de nature transverse magnétique ce qui signifie que la composante électrique est perpendiculaire au plan de l'interface métal-diélectrique. Dans certaines conditions bien précises, ces plasmons peuvent entrer en résonance ce qui est associé à l'oscillation des charges se

trouvant à l'interface métal-diélectrique. Pour que les conditions de résonance des plasmons de surface soit rencontrées, il faut que le vecteur d'onde des SP, k_{SP}, Éqn (1-1) et que le vecteur d'onde de la lumière incidente, k_{photon}, Éqn (1-2) concordent[18-20], soit les équations :

$$k_{SP} = \frac{2\pi}{\lambda}\sqrt{\frac{\varepsilon_m \varepsilon_s}{\varepsilon_m + \varepsilon_s}} \approx \frac{2\pi}{\lambda}\sqrt{\frac{\varepsilon_m n_s^2}{\varepsilon_m + n_s^2}}\ puisque\ \varepsilon = n^2 \qquad (1-1)$$

$$k_{photon} = \frac{2\pi}{\lambda} n_{verre} \sin\theta_{incidente} \qquad (1-2)$$

Ces équations établissent clairement le lien avec les indices de réfraction de la solution, n_s, au-dessus la surface métallique de constante diélectrique ε_m exposé à un faisceau de longueur d'onde λ arrivant à l'interface à un angle $\theta_{incident}$, tel que montre en Figure 1-6. Normalement, les deux vecteurs d'onde ne se recoupent pas ne permettant donc pas d'atteindre les conditions de résonance des plasmons de surface. Dans des conditions particulières, comme lorsque la lumière incidente arrive à l'interface avec le métal d'un milieu de fort indice de réfraction comme du verre et à un angle permettant le passage de l'onde lumineuse en onde évanescente, ces vecteurs peuvent se recouper.

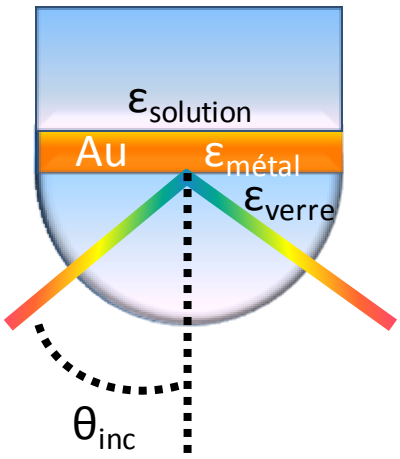

Figure 1-6. Représentation schématique simplifiée d'un montage SPR.

En condition de résonance des plasmons de surface, la lumière est absorbée ce qui se traduit par une baisse de l'intensité lumineuse détectée après la réflexion de la lumière. Les équations (1-1) et (1-2) montrent clairement le lien direct entre l'indice de réfraction, n_s du milieu et l'angle d'incidence, $\theta_{incidente}$ selon la longueur d'onde, λ en présence.[20] Il est alors possible d'envisager deux manières de mesurer l'indice de réfraction du milieu, (i) fixer la longueur d'onde (exemple : laser) et faire varier l'angle d'incidence pour en mesurer l'intensité et déterminer l'angle pour lequel ce phénomène est optimal, soit pour lequel la réflectance est la plus faible. (ii) Il est aussi possible de fixer l'angle et d'employer une source lumineuse à large spectre (exemple : diode lumineuse) en mesurant le spectre de réflectance pour en déterminer la longueur d'onde engendrant le minimum de réflectance, λ_{SPR}. Ces différentes variantes seront présentées en section 1.3 Instrumentation SPR.

Puisque le phénomène de résonance des plasmons de surface dépend de la constante diélectrique du métal à l'interface, seuls certains métaux engendrent le phénomène SPR. Typiquement, l'or (Au) et l'argent (Ag) sont les métaux les plus employés pour la qualité

des signaux obtenus pour ces métaux dans le domaine de la lumière visible, l'Au ayant l'avantage supplémentaire de la stabilité en milieu aqueux grâce à son haut potentiel standard d'oxydation. Le cuivre (Cu) permet aussi d'atteindre ces conditions de résonance avec la lumière visible, mais sa faible stabilité à l'oxydation rend son utilisation plus marginale.[24] D'autres métaux comme l'aluminium (Al) peuvent aussi permettre la résonance des plasmons de surface dans le domaine de la lumière UV, ce qui peut être employé pour exciter d'autres phénomènes optiques, tel que la fluorescence.[25]

L'utilisation commune de l'Au et l'Ag peut aussi être justifiée par la possibilité d'y immobiliser des molécules contenant une extrémité thiolée (-SH) permettant un attachement spontané du soufre via la formation spontanée (sans apport d'énergie ou catalyse) d'un lien covalent avec ces surfaces formant ainsi des couches dites auto-assemblées. Les molécules thiolés formeront alors une monocouche de densité importante, mais dépendante de leur nature chimique. Ces molécules formanant les monocouches peuvent alors contenir des groupements fonctionnels permettant l'attachement d'une molécule de reconnaissance. Un des objectifs des travaux présentés dans cette thèse est de développer des surfaces de type peptidique permettant l'amélioration des performances des biocapteurs SPR.[26] La formation d'une monocouche auto-assemblée se fera donc selon la réaction suivante[27] :

$$Au^0 + R - SH \leftrightarrows Au - S - R + \acute{e}^- + H^+ \qquad (1-3)$$

1.2.3 Types de biocapteurs SPR

Puisque les biocapteurs SPR permettent le suivi d'interactions ayant lieu à une interface par le biais d'un changement local d'indice de réfraction, il est possible de

concevoir trois types distincts de détection. Les essais SPR **directs** nécessitent tout d'abord l'attachement d'une molécule de reconnaissance moléculaire sélective à un analyte d'intérêt à l'interface métal-liquide via une chimie de surface appropriée. Le capteur ainsi produit est exposé à la solution contenant l'analyte à détecter ou à quantifier. L'analyte d'intérêt interagit alors avec la surface engendrant un déplacement de volume de la matrice se traduisant par un changement local d'indice de réfraction et donc de signal SPR. Par exemple, des biocapteurs SPR permettant la détection directe de pesticides dans l'alimentation furent développés pour atteindre des niveaux de détection concordant avec les standards imposés aux États-Unis.[28] La détection directe offre l'avantage d'être la plus simple des approches et souvent la plus rapide. Cette approche a donc été favorisée au cours des travaux présentés dans cet ouvrage.

Un second type d'essai SPR envisageable est l'essai **« sandwich »** qui permet d'amplifier le déplacement de volume à l'interface du capteur. Cette détection secondaire est effectuée subséquemment à la détection directe, à l'aide d'une seconde molécule de reconnaissance sélective pour l'analyte immobilisé à la surface du capteur. Ceci engendre un accroissement notable du signal SPR, particulièrement pour les petites molécules. Par exemple, les travaux de Jang et al. se basent sur l'exploitation de l'amplification du signal SPR dans un biocapteur à fibre optique pour détecter des biomarqueurs indicateurs de cancer de la prostate.[29]

Le troisième type d'essai SPR est l'essai **compétitif**. Au cours de cet essai, la molécule de reconnaissance immobilisée à la surface métallique est exposée à une première molécule interagissant avec la molécule de reconnaissance. Le capteur est ensuite exposé à l'analyte d'intérêt qui remplacera graduellement la première molécule présente sur la

molécule de reconnaissance. Ce type d'essai est particulièrement utile en pharmacologie pour déterminer les différences entre deux molécules d'intérêt pharmaceutique. Il est fréquent que la première molécule immobilisée à la surface soit attachée à une autre molécule volumineuse ce qui engendre un déplacement du signal SPR plus important lors du remplacement de cette première molécule par l'analyte. Ce type d'essai est employé pour détecter des quantités inférieures au partie par million (ppm) de benzo[a]pyrène, un composé toxique et cancérigène, dans les travaux de Miura et al.[30] Ces différents mode de détection en SPR sont représentés dans la Figure 1-7.

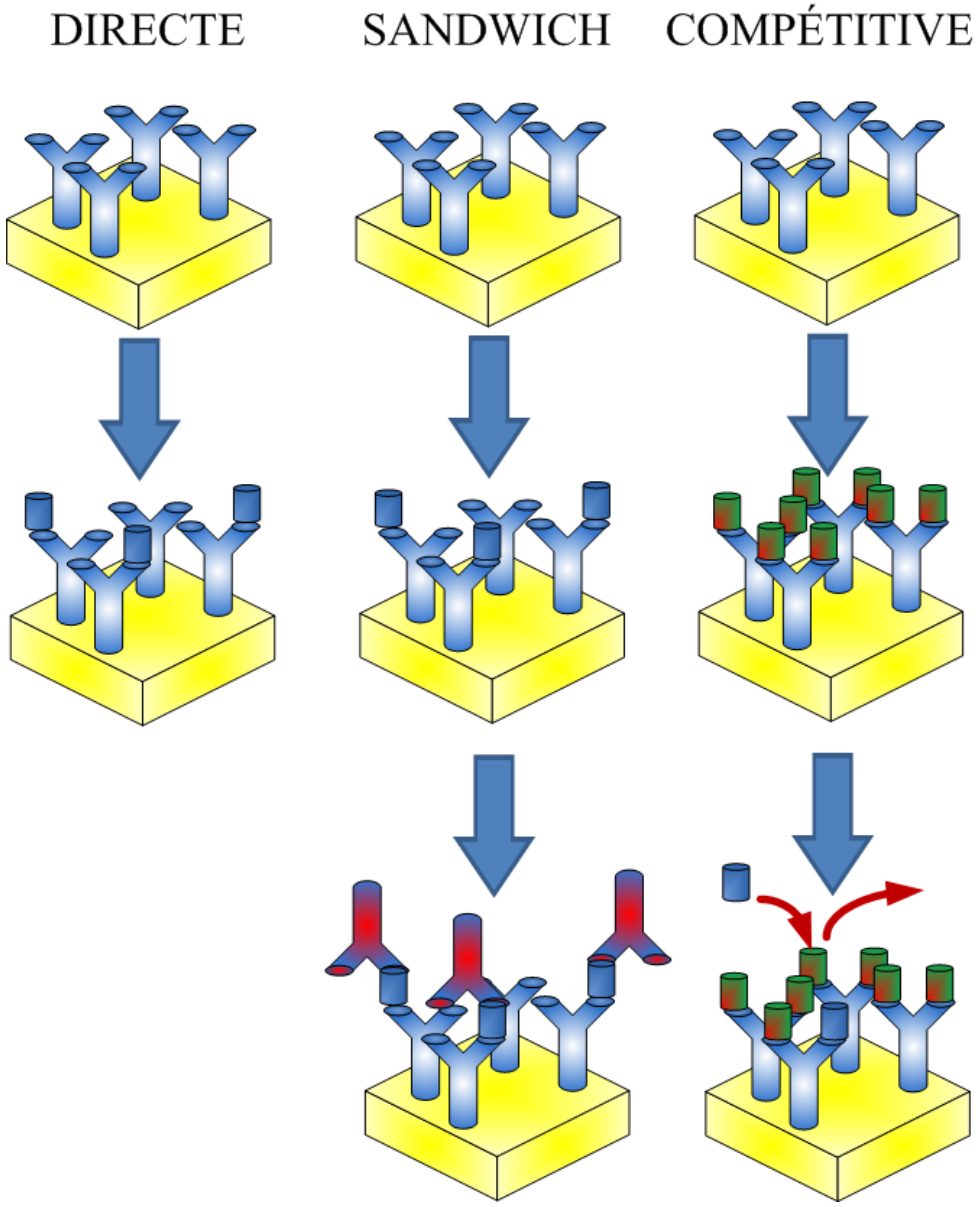

Figure 1-7. Exemples des modes de détections possibles en SPR pour des essais d'affinité antigène-anticorps.

1.2.4 Applications des biocapteurs SPR

Les applications principales des biocapteurs SPR résident dans les domaines de la biodétection et de l'identification d'analytes biologiques ainsi que dans l'analyse biophysique des interactions biomoléculaires.[18] Ce type d'analyse est relié à des domaines

en émergence au niveau des biocapteurs SPR, soit : les analyses alimentaires, la protéomique, l'immunologie/immunogénicité (développement de molécules engendrant des réponses immunitaires) et la découverte de médicaments.[31, 32] Les biocapteurs SPR sont complémentaires avec les études en protéomique puisqu'ils permettent de confirmer rapidement le déroulement d'interactions protéine-protéine lors de la recherche de partenaires protéiques.[33] Les biocapteurs SPR offrent l'avantage de pouvoir effectuer des mesures continues (chaque saisie d'un spectre dans le temps permet de déterminer le signal SPR à ce moment précis) dans différents milieux aqueux ce qui permet d'entrevoir des applications intéressantes en transformation agro-alimentaire. La SPR peut permettre d'effectuer des mesures sans avoir à ralentir la production ou encore à effectuer des prélèvements. Elle ne nécessite aucune technique de marquage ou d'ajout d'agents chimiques pour l'obtention de résultats.[34, 35] En immunogénicité, la SPR permet de mesurer l'efficacité des composés pharmaceutiques de nature protéique avant de passer aux essais cliniques pendant lesquels elle permettra d'effectuer le suivi des concentrations d'anticorps dans les systèmes biologiques d'intérêts.[36] La versatilité dans la conception de biocapteurs SPR permet l'immobilisation et la détection d'une grande variété de molécules telles que l'ADN, les enzymes ou encore les récepteurs moléculaires. Une grande variété de recherches visant le développement de nouvelles molécules actives peut donc bénéficier des avantages des biocapteurs SPR. Les biocapteurs SPR permettent d'effectuer un balayage rapide de candidats pour ne conserver que les composés les plus prometteurs pour procéder avec des phases plus avancées ou pour apporter des modifications aux molécules précédentes afin d'accélérer la découverte de la molécule à envoyer en étude clinique.[37]

1.2.5 Limites des biocapteurs SPR

Les biocapteurs SPR ont toutefois des limites. Expérimentalement, il est nécessaire d'effectuer des mesures dans des conditions de températures stables voire contrôlées. Puisque l'instrumentation SPR développée au cours de ces travaux était tout d'abord dépourvue de cellule fluidique, il était difficile d'effectuer des essais de biodétection à de faibles concentrations puisqu'une partie des variations SPR provenait des fluctuations de température de la solution. Pour une instrumentation SPR ayant une sensibilité de 2000nm/RIU, une variation de 1°C de la solution près de 25 °C signifie un déplacement de la bande SPR de 0,4 nm ce qui est de l'ordre des déplacements observés lors d'une biodétection. (En considérant que n_{eau} varie de ~0,0002 RIU/°C autour de 25°C pour la lumière visible[38])

Analytiquement, les techniques basées sur la SPR sont limitées par la migration des espèces en solution. Puisque le signal SPR est dû à un déplacement des espèces en solution vers la surface de reconnaissance, il faut tenir compte de la proximité de ces espèces avec la surface, ce qui en solution diluée implique une limite liée au transport de masse et à la migration des espèces en solution. Les travaux de Cui et al. dans le cas de la détection de la ferritine, une protéine de taille importante, 450 kDa, ont été limités à une LOD de l'ordre du µg/L à cause des conditions limitées par diffusion de la protéine.[39] Ce paramètre limite la LOD des biocapteurs SPR qui auraient détecté des concentrations très faibles, mais sur des périodes de temps de l'ordre du jour et davantage, ce qui n'est pas viable expérimentalement.

Une autre considération analytique majeure est que les techniques de détection basées sur la SPR ne fournissent par leur signal aucune information propre à la composition

d'une molécule ou encore ses propriétés chimiques comme le feraient les techniques spectrométriques ou spectroscopiques conventionnelles. La certitude qu'un changement de signal provient des interactions avec un analyte d'intérêt et non avec d'autres molécules d'une matrice complexe est donc strictement due à l'affinité de la molécule de reconnaissance immobilisée à la surface du biocapteur pour cet analyte. Cette considération importante en SPR explique donc l'importance capitale de produire des surfaces de reconnaissance qui soient aussi sélectives que possible pour l'analyte et qui interagissent au minimum avec les autres composants de la matrice (interférents) dits nonspécifiques. Par leur nature, l'efficacité des biocapteurs SPR provient donc directement de l'efficacité des molécules de reconnaissance immobilisées à leur surface. Une portion importante des recherches sur les biocapteurs SPR vise donc le développement de nouveaux types de molécules de reconnaissance qui soient plus performantes, telle que : les sondes basées sur l'ADN/ARN[40], les aptamères[41] ou encore les phages[42]. Toutefois, une partie importante des recherches dans le domaine des biocapteurs SPR implique l'utilisation de récepteurs moléculaires comme les anticorps biologiques ayant une grande affinité pour un analyte ciblé, ce qui a été le cas pour la majorité des travaux présentés dans cette thèse.

Puisque les biocapteurs SPR mesurent directement un déplacement de volume, leur LOD pour les molécules de faible taille (<1000 Da) demeure élevée en mode de détection directe. Toutefois, l'amplification du signal SPR à l'aide de matériaux nanostructurés ou de nanoparticules permet de pousser la LOD de ce type de biocapteur, tel que présenté dans les travaux de Mitchell et al.[43] Les travaux de Mitchell impliquent l'utilisation de nanoparticules de tailles variables au-dessus de biocapteurs SPR afin de détecter la

progestérone avec une LOD jusqu'à un ordre inférieur à celle observée en SPR conventionnelle.

1.3 Instrumentation SPR

1.3.1 Instrumentation SPR commercialement disponible

L'entreprise trônant au sommet du marché des instrumentations SPR avec une part de marché de près de 90% des instruments vendus en 2004 se nomme Biacore, nouvellement une division de GE Healthcare. Cette entreprise est la première entreprise à avoir commercialiser une instrumentation SPR et offre une variété d'instrumentation automatisée, disposant de systèmes fluidiques comparables aux autres systèmes analytiques conventionnels.[44] La technologie développée par cette entreprise repose généralement sur des instrumentations en configuration Kretschmann en mode de mesure angulaire bien que des instrumentations plus récentes exploitent des approches permettant l'amplification des signaux SPR. Toutefois, plusieurs entreprises technologiques dont Texas Instruments développent et mettent en marché de nouvelles instrumentations.[45] La grande majorité des laboratoires de recherche employant la SPR utilisent toutefois des instrumentations fabriquées maison répondant à leurs propres besoins surtout à cause du coût important relié à l'acquisition d'instrumentation SPR commerciale. C'est pourquoi une partie des travaux présentés dans cet ouvrage couvre la construction et la validation d'une nouvelle instrumentation SPR qui pourrait permettre la production de biocapteurs SPR complets à un coût très faible et utilisables par tous avec un minimum de formation. Des exemples d'instrumentations développées par Biacore sont montrés en Figure 1-8.

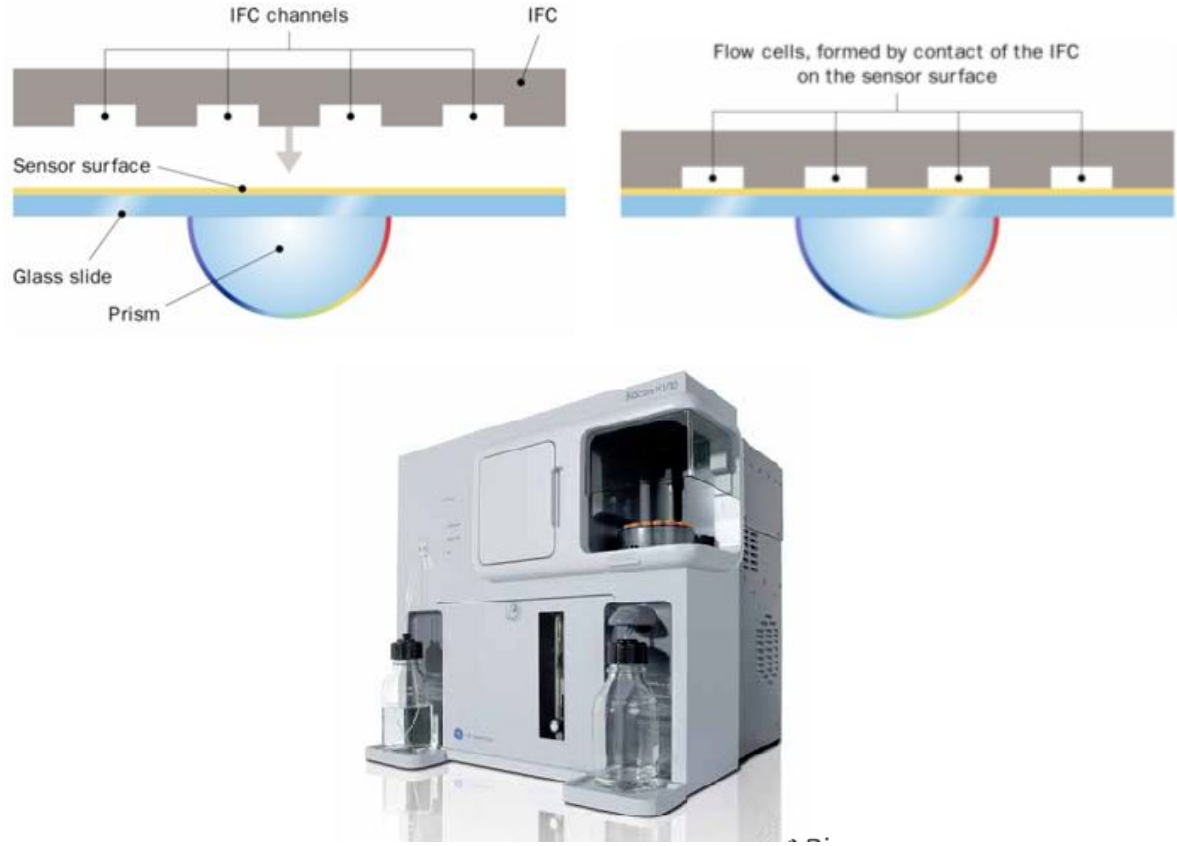

Figure 1-8. (Haut) Schéma simplifié d'un biocapteur SPR multicanaux produit par Biacore en configuration Kretschmann basé sur une technologie d'interrogation angulaire. IFC signifie canaux microfluidiques intégérés. (Bas) Instrument Biacore X-100. [44]

1.3.2 Développement actuellement en cours

Plusieurs recherches en cours visent à développer des biocapteurs SPR dont le signal est amplifié par des réseaux nano-structurés métalliques. Les réseaux métalliques ont pour effet de permettre le couplage de la lumière incidente avec les plasmons de surface, ce qui a pour effet de perturber la propagation des ondes évanescentes créant ainsi des plages d'énergies ne pouvant plus exciter les SP à l'interface. Ces plages créent des bandes minces dans le spectre de réflectance sensibles aux interactions ayant lieu à la surface. Le suivi de ces bandes permet d'augmenter la sensibilité par rapport aux

approches de SPR conventionnelles de multiples fois.[46] Le développement d'une instrumentation spectro-angulaire par un groupe de recherche montréalais permet le suivi de phénomènes analogues de manière à pouvoir effectuer le suivi d'interactions biomoléculaires à l'interface de ces biocapteurs.[47]

Des travaux de recherche ont permis de coupler la SPR avec divers autres techniques analytiques telles que l'électrochimie[48], la HPLC[49] et la spectrométrie de masse[50, 51]. Le couplage SPR-MS, parfois nommé « *biomolecular interaction analysis* » (BIA-MS), permet de pallier au manque d'information sur la nature de l'intéraction avec les biocapteurs tout en bénéficiant des capacités de quantifications de la SPR. Une instrumentation commerciale de ce type est d'ailleurs disponible via le Biacore 3000.[44]

Toutefois, la grande majorité des instruments faisant l'objet de recherches actuellement vise à obtenir davantage d'information ou à améliorer les signaux SPR obtenus. Les nouveaux systèmes qui sont le fruit de ces recherches sont donc plus complexes et dispendieux que les précédents. Peu de recherches visent à simplifier l'instrumentation SPR pour la rendre disponible à tous ou pour pouvoir développer des systèmes intégrés comme les biocapteurs. La SPR étant une technique émergente et l'instrumentation SPR étant encore trop peu disponible pour bien des chercheurs, il est important de développer une instrumentation plus simple et peu coûteuse. Les travaux de recherche présentés en Chapitre 2-3 visent à combler ce vide.

1.4 Réduction des interactions nonspécifiques (NSB)

1.4.1 Définition et compréhension des interactions nonspécifiques

Les sections précédentes montrent des exemples simples effectués dans des conditions contrôlées. Puisque le signal obtenu à l'aide des biocapteurs SPR ne dépend que de la sélectivité de la surface employée et ne fournit pas d'information exacte sur la nature des interactions mesurées, les essais en milieu plus complexes sont plus difficiles. L'utilisation des biocapteurs SPR pour effectuer des mesures dans les domaines environnemental et médical est directement limitée par le fait que les analytes sont alors contenus dans des matrices complexes contenant une multitude de composants divers souvent en concentrations nettement supérieures à l'analyte d'intérêt. Ces composants divers dits des interférents peuvent eux-aussi interagir avec la surface du biocapteur SPR ce qui engendre un signal de fond dû aux interactions nonspécifiques pouvant masquer le signal provenant des interactions avec l'analyte. La Figure 1-9 illustre schématiquement les interactions nonspécifiques et l'impact qu'elles ont sur les mesures SPR.

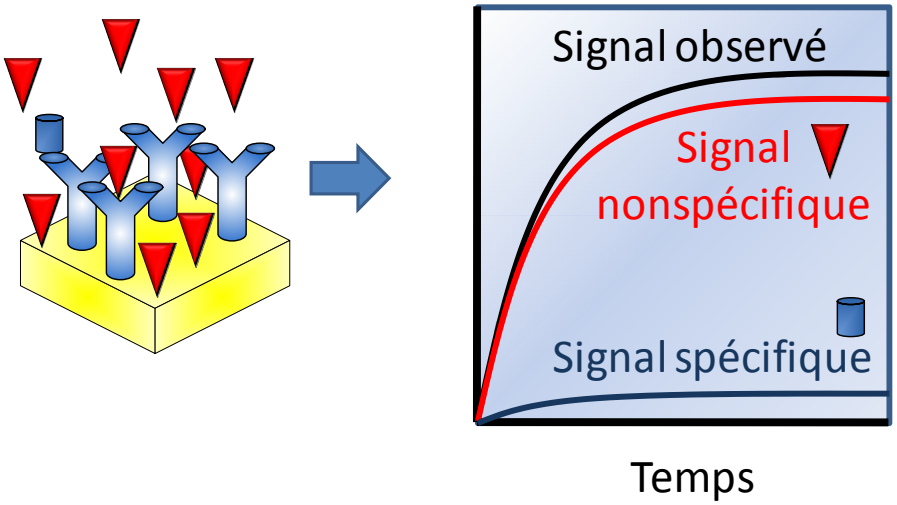

Figure 1-9. Représentation schématique des interactions nonspécifiques et de leurs effets sur les biocapteurs SPR. Les triangles rouges représentent une grande variété de composants nonspécifiques contenus dans la matrice. Les cylindres bleus représentent les analytes spécifiques aux molécules de reconnaissances représentées par les « Y » bleus.

La nature des molécules générant des interactions nonspécifiques dépend généralement du type de matrice complexe dans laquelle se déroulent les mesures. Dans le cadre de ces travaux, nous nous concentrons sur le sérum sanguin, puisque le sang est composé de plusieurs analytes d'intérêt médical dans le diagnostic de maladies diverses. Le sérum sanguin est le fluide provenant du sang centrifugé pour en retirer les globules rouges et blancs ainsi que les plaquettes. La centrifugation du sang est un processus rapide qui permet d'éliminer ces trois composants en préservant les protéines diverses dont la détection ou la quantification permet d'établir un diagnostic pour des pathologies diverses. Les différents types de surface de biocapteur développés ont alors été exposés au sérum bovin qui constitue un modèle très proche du sérum sanguin humain.

1.4.2 Approches développées pour réduire les interactions nonspécifiques

Plusieurs approches ont permis de limiter l'impact des interactions nonspécifiques à la surface des biocapteurs. L'approche la plus simple consiste encore à retirer complètement ou partiellement les interférents du milieu à analyser.[52, 53] Cette opération peut s'effectuer en plaçant une cartouche ayant de l'affinité pour les constituants de la matrice et positionnée avant le passage de la solution dans la cellule de détection. Une seconde approche emploie la préconcentration à l'aide de surfaces sélectives aux analytes se retrouvant dans la matrice complexe suivi d'un rinçage des interférents de la matrice avant de procéder à l'analyse finale des analytes retenues.[54] Ces approches offrent des performances acceptables, mais nécessitent des consommables souvent dispendieux et souvent d'utilisation unique. Une approche plus populaire consiste à passiver la surface des biocapteurs avec des tampons bloquants contenant souvent de l'albumine sanguine bovine (BSA) qui s'adsorbe nonspécifiquement à la surface non fonctionnalisée par la molécule de reconnaissance empêchant ainsi aux interférents de la matrice contenant l'analyte de s'y adsorber nonspécifiquement et donc de générer un signal de fond.[55] Cette approche, comme le confirment les travaux de Balcer et al. induit souvent une diminution du potentiel de détection des biocapteurs ainsi bloqués.[56]

1.4.3 Utilisation de monocouches organiques pour réduire les interactions nonspécifiques

Une approche souvent employée pour limiter les interactions nonspécifiques avec la surface des biocapteurs est celle impliquant la formation de minces couches organiques auto-assemblées[57] ou polymériques[58] engendrant le minimum possible d'interaction

nonspécifique avec les interférents de la matrice. Ces couches portent idéalement des groupements fonctionnels permettant l'immobilisation de la molécule de reconnaissance. Les composés les plus employés à cette fin sont formés de plusieurs unités éthylène glycol, le polyéthylène glycol (PEG), permettant de limiter les interactions nonspécifiques avec les interférents contenues dans le sérum sanguin de manière importante.[59-62] Cette approche est exploitée dans le cadre de cette étude, mais en employant des monocouches auto-assemblées de nature peptidique (Figure 1-10).

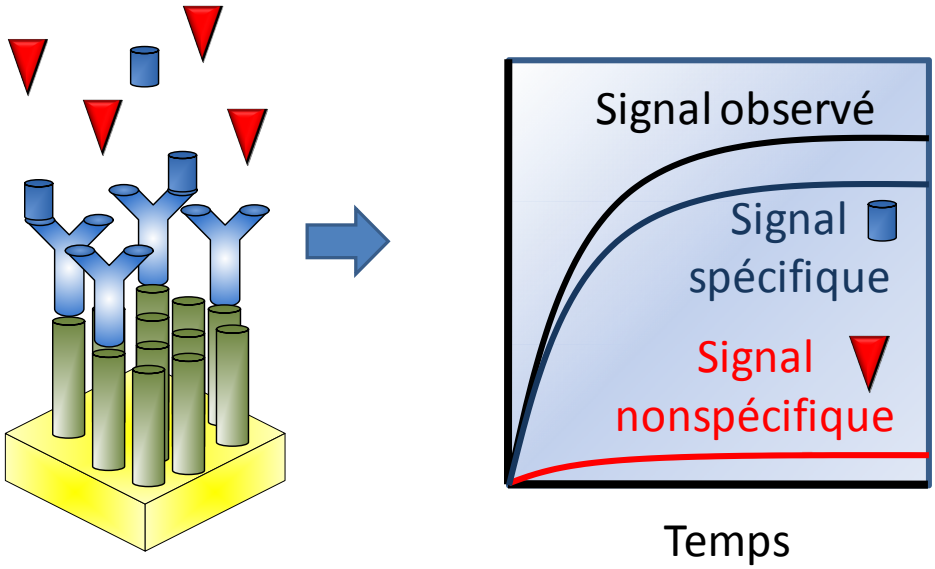

Figure 1-10. Utilisation de surfaces limitant les interactions avec les composants nonspécifiques au biocapteur contenus dans la matrice analytique complexe. Les triangles rouges représentent une grande variété de composants nonspécifiques contenus dans la matrice. Les cylindres bleus représentent les analytes spécifiques aux molécules de reconnaissances représentés par les « Y » bleus. Les cylindres verts représentent une monocouche résistante aux interactions avec les composants nonspécifiques.

L'utilisation de monocouches organiques limitant les interactions nonspécifiques est un enjeu de taille, non seulenment dans le domaine des biocapteurs, mais aussi en médecine où la biocompatibilité des implants est de toute première importance que ce soit pour des

prothèses dentaires ou pour des implants cardiaques.[63] Parmis les recherches impliquant l'utilisation de monocouches organiques, les travaux du groupe Whitesides comptent pour une portion impressionnante des réalisations dans ce domaine. Les travaux réalisés par Ostuni et al. ont permis de quantifier l'asdoprtion nonspécifique subie par des monocouches auto-assemblées terminées par 48 terminaisons différentes exposées au figrinogen.[64] Ces travaux mettent en lumière que des monocouches composés de groupements polaires ou ioniques permenttent de limiter l'adsorption nonspécifique du fibrinogen à ces surfaces. Les travaux de Sigal et al., au cours desquels des monocouches organiques à caractère amphiphiles, formées de détergents ont été exposées à des concentractions contrôlées des divers composantes du sérum sanguin ont montrés que la nature chimique de la monocouche en présence influençait le niveau des interactions avec les protéines en présence.[65] Chapman et al. ont développé des monocouches résistantes à un type particulier d'interaction entre les extrémités amine et acide carboxilique.[66] Les travaux de Holmin et al. ont montré que des monocouches à caractère zwitterionique limitent l'adsorption nonspécifiques des protéines contenues dans le sérum sanguin à un niveau faiblement supérieur à celui des surfaces composées d'unités éthylène glycol.[67]

Des couches de nature phospholipidiques ont été employées dans les travaux de Philips et al. permettant ainsi de retirer sélectivement les protéines adsorbées à la surface de la bicouche suite à une détection en milieu complexe, ne laissant que les analytes interagissant avec la molécule de reconnaissance immobilisée à la surface de manière covalente.[68] Elle a permis la détection de l'immunoglogulune-gamma (IgG) jusqu'à quelques femtomolaires. Cette étude est l'une des rares études se déroulant dans le sérum sanguin complet, puisqu'une pratique courante dans le domaine fait que ce type d'étude se

déroule en solution de concentration d'interférent prédéterminée et souvent inférieure à la concentration des protéines en milieu complexe complet.

1.5 Utilisation de surfaces peptidiques pour réduire les interactions nonspécifiques

1.5.1 Recherches précédentes incorporant des acides aminés

Certaines surfaces permettant de limiter les interactions nonspécifiques des protéines du sérum sanguin partiellement formées d'acides aminés ont été devéloppées. Les travaux de Statz et al.[69] ont mené au développement d'un composé peptidomimétique contenant des résidus lysine et des groupements méthoxyéthyle alternés limitant le niveau d'adsorption nonspécifique des protéines du sérum sanguin humain à quelques ng/cm^2. Cette performance impressionnante permet de penser que des surfaces composées entièrement d'acides aminés, soit des peptides pourraient limiter eux aussi les interactions nonspécifiques à la surface de biocapteurs. Cette constatation forme la base des travaux de recherche effectués sur les monocouches peptidiques présentés dans cette thèse.

1.5.2 Avantages des composés contenant des acides aminés

L'utilisation de surfaces peptides auto-assemblées dans la formation de biocapteurs laisse entrevoir de nombreux avantages expérimentaux. Les acides aminés physiologiques sont disponibles en abondance et offrent une grande variété de fonctions chimiques via leur chaîne latérale de nature variable. La chimie liée à leur polymérisation, soit la synthèse de peptide par la formation d'un lien amide est simple à effectuer, efficace et bien connue.[70-72] De plus, la présence naturelle des acides aminés dans l'environnement et dans les organismes vivants laisse entrevoir une biocompatibilité potentielle intéressante avec les molécules de reconnaissance à immobiliser. Puisque les polypeptides sont terminés par une

fonction amine et une fonction acide carboxylique à l'autre extrémité il est donc possible d'employer une chimie simple pour y attacher la molécule de reconnaissance essentiel à la fabrication des biocapteurs SPR.[69]

1.5.3 Approche analytique menant au développement de surfaces peptidiques résistantes aux interactions nonspécifiques

L'approche employée au fil des travaux présentés dans cette thèse utilise une méthode combinatoire en exminant la capacité des différentes monocouches produites à limiter les interactions avec les composants du sérum sanguin. Les propriétés des surfaces les plus performantes seraient préservées à l'étape suivante pour générer des surfaces encore plus performantes. Chaque chapitre traitant de ce sujet constitue une de ces étapes. Le passage vers une nouvelle génération de surface peptidique résistante aux intéractions nonspécifiques se fait donc en regard des résultats obtenus pour les composés de la génération précédente. Puisque les intéractions nonspécifiques entre les surfaces peptidiques développées et les différents composants de la matrice analytique sont complexes à modéliser, aucune simulation n'a été réalisée dans le cadre de ces travaux.

1.6 Applications des biocapteurs SPR en milieu pharmaceutique

Dans leur article publié dans Nature en 2005, Seeberger et Werz décrivent comment des vaccins basés sur les polysaccharides peuvent être développés, en une fraction du temps requis pour le faire à la main, en employant des synthétiseurs automatisés.[73] Ceci illustre bien comment les molécules pharmaceutiques d'aujourd'hui sont fabriquées. Des librairies importantes de molécules d'intérêt pharmaceutique sont générées en peu de temps après des exercices de modélisation permettant de choisir les molécules à synthétiser en fonction de

la cible. Il est toujours nécessaire néanmoins pouvoir déterminer quelle molécule est la plus performante et quelles modifications doivent y être apportées pour mener à la meilleure molécule qui sera ensuite envoyée en étude clinique. Les biocapteurs SPR visent à fournir une réponse satisfaisante à cette préoccupation en immobilisant et suivant directement les interactions entre la biomolécule cible et la molécule en développement.

Certains biocapteurs ont déjà été développés à cette fin pour divers types de pathologies. Les travaux de Lin et al. exploitent les biocapteurs SPR pour déterminer l'efficacité de médicaments potentiel se liant à l'ADN.[74] Les travaux de Hahauzit et al. profitent de la capacité d'immobiliser des récepteurs biomoléculaires pour développer de nouveaux médicaments de type hormonal.[75] Même les recherches sur des maladies incurables comme le sida bénéficient des biocapteurs SPR pour mieux comprendre leur mécanisme de fonctionnement et développer de nouveaux médicaments.[76]

Un exemple parmi tant d'autres, les interactions entre les ligands de type peptidique et le récepteur protéique CD36 fait l'objet de plusieurs recherches dont celles conduites par le groupe du professeur Huy Ong de l'Université de Montréal. Il a été démontré que certains ligands peptidiques ont des propriétés anti-athérosclérotiques lorsqu'ils interagissent avec le récepteur CD36. Le cas de la CD36 est un modèle idéal pour effectuer des développements dans ce domaine puisque la CD36 subit des changements conformationnels importants[77], mesurables en SPR, lors de ces interactions. Les biomolécules CD36 étant marquées par 6 résidus histidine consécutifs (Noté : H_6), il sera alors possible d'exploiter la présence de ce marqueur via une immobilisation sur une surface exposant des ions métalliques ce qui permet une immobilisation sélectivement réversible.

1.7 Amélioration des mécanismes de formation des monocouches auto-assemblées

L'utilisation de monocouches auto-assemblées dans les domaines liées aux biocapteurs SPR constitue une pratique fort courante. Néanmoins, les monocouches prennent plusieurs heures pour recouvrir les surfaces des biocapteurs et peuvent se dégrader ou voir leurs propriétés physico-chimiques altérées suite à une période d'entreposage prolongée. Même les surfaces constituées de polymères tout comme les surfaces constituées de groupements PEG se dégradent en quelques jours si les conditions d'entreposage ne sont pas minutieusement contrôlées.[78, 79] Le fait de pouvoir générer des monocouches rapidement et simplement immédiatement avant d'effectuer une analyse permet d'assurer la qualité de la surface, permettant des essais plus reproductibles et d'adapter facilement le biocapteur pour l'analyse à effectuer. L'électroformation oxydative selon la réaction 1-3 des monocouches permet de générer une monocouche simplement en appliquant une différence de potentiel précise à une interface d'Au baignant dans une solution contenant des composés thiolés pour former des monocouches complètes en quelques minutes.[80] La possibilité d'utiliser ce concept dans le cadre de la fabrication de biocapteurs SPR basés sur des monocouches peptidiques est investiguée en Chapitre 8. L'objectif est de déterminer les conditions de formation optimales de monocouches peptidiques résistantes aux interactions nonspécifiques.

1.8 Techniques analytiques employées pour caractériser les surfaces peptidiques

Les surfaces peptidiques recouvrant les biocapteurs SPR étudiées dans le cadre de ces travaux ont été caractérisées à l'aide de diverses techniques analytiques

conventionnelles. Le Tableau 1-1 résume les caractéristiques de chacune de ces méthodes ainsi que le type d'information qu'elles permettent d'acquérir.

Tableau 1-1. Description des méthodes analytiques conventionnelles employées dans le cadre du développement des biocapteurs SPR basés sur des monocouches peptidiques.

Fonctionnement	*Caractéristiques*	*Information fournie*
Spectroscopie GATR-FTIR [81-85]		
- Mesure les vibrations des liaisons chimiques	- Permet mesures localisées - Information caractéristique des liens chimiques	- Nature des liaisons des molécules immobilisées - Structure secondaire des composés peptidique
Dichroïsme circulaire (CD) [86-88]		
- Mesure l'absorption de la lumière polarisée circulairement	- Instrumentation entièrement automatisée - Analyse des résultats en comparant à des banques de données.	- Structure secondaire des composés peptidique
Spectrométrie de photoélectrons induits par rayons-X [81, 89, 90]		
- Mesure l'énergie cinétique des électrons de cœur	- Semi-quantitatif - Instrumentation coûteuse et peu courante - Information spectrale sous forme de minces bandes - Permet de sonder plusieurs profondeurs	- Nature des atomes en présence - Proportion des atomes en présence
Angle de contact [82, 91, 92]		
- Mesure de l'angle à l'interface liquide-solide pour un volume donné d'une solution donnée	- Instrumentation simple - Rapide à effectuer - Données relatives aux conditions expérimentales	- Hydrophobicité relative des surfaces lorsque comparées
Ampérométrie[93]		
- Mesure l'échange électronique à une interface due à une réaction à une interface liquide-solide	- Instrumentation simple et disponible - Nécessite référence	- Permet le suivi de réactions impliquant un échange d'électron en temps réel

Ces diverses techniques, souvent complémentaires, permettent d'obtenir de l'information sur les molécules chimiques immobilisées à l'interface des biocapteurs SPR développés. La spectroscopie GATR-FTIR ainsi que la XPS permettent d'obtenir de l'information sur la nature chimique des molécules à l'interface soit sur le type de liaisons chimiques en présence (GATR-FTIR) ou sur le type d'atomes composant ces molécules. Cela permet de confirmer l'immobilisation de molécules ou, dans le cas de la spectroscopie GATR-FTIR d'obtenir de l'information sur la structure secondaire des molécules immobilisées à la surface. Cette information peut être confirmée par des mesures en CD qui permettront d'obtenir, via la mesure d'absorption de lumière polarisée circulairement, une méthode efficace particulièrement dans le cas des peptides tel décrit dans *Nature* par Greenfield[94] L'utilisation de l'angle de contact permet d'obtenir rapidement de l'information sur l'hydrophobicité d'une surface. Un changement inattendu de cette propriété peut signifier un changement de configuration des protéines immobilisées à une surface ou encore l'altération de ces dernières. Cette technique est particulièrement simple à utiliser. L'ampérométrie permet le suivi de réactions impliquant l'échange d'électrons à une interface. Cette mesure peut s'effectuer en temps réel et la réponse est proportionnelle à la quantité de l'espèce effectuant cet échange et au nombre d'électron échangé par cette molécule. Toutes ces techniques ont été utilisées pour confirmer la chimie de surface développée au cours de ces travaux, pour confirmer la configuration des monocouches développées et pour tenter de déterminer les propriétés des surfaces les plus performante pour la fabrication de biocapteurs SPR afin d'orienter les prochains développements à effectuer.

1.9 Objectifs de la thèse

Les travaux de cette thèse visent le développement de trois composantes des biocapteurs SPR afin d'en améliorer les performances pour conduire ultimement vers l'élaboration de produits commerciaux. Des développements concernant l'instrumentation SPR, les interfaces chimiques ainsi que les protocoles expérimentaux y sont donc présentés.

Les développements instrumentaux visent à simplifier la manipulation des biocapteurs SPR tout en réduisant la quantité de composantes technologiques nécessaires à leur fabrication et à leur utilisation. La simplicité de l'instrumentation SPR ainsi développée doit donc en permettre l'utilisation par un personnel non-expert suite à des délais de formation d'à peine quelques heures. Cette étude est nécessaire pour rendre l'instrumentation SPR plus disponible, puisque les instruments commerciaux actuellement disponibles sont complexes et dispendieux. Ce sujet est traité aux Chapitres 2 et 3.

Les applications des biocapteurs SPR en milieu complexe sont actuellement limitées par les intéractions nonspécifiques, Ainsi, des surfaces furent développées afin de permettre la réduction significative des interactions nonspécifiques avec les interférents d'une matrice complexe, telle que le sérum sanguin. Ces surfaces doivent permettre d'y attacher des molécules de reconnaissance d'intérêt clinique, tels que des récepteurs sélectifs pour des biomolécules indiquant la présence de différentes pathologies, par exemple, le cancer. Ces surfaces doivent être caractérisées avant d'en investiguer les performances. L'utilisation de ces dernières doit donc permettre d'entrevoir des applications cliniques et pharmaceutiques découlant directement de leur intégration aux biocapteurs SPR. Ce sujet est traité aux Chapitres 4 à 7.

Un protocole de fabrication efficace de biocapteurs SPR basés sur ces technologies, en permettant la fabrication rapide, reproductible et peu coûteuse doit donc être élaboré dans ces travaux. Dans le cadre d'applications médicales, ces protocoles doivent permettre la fabrication de ce type de biocapteurs en quelques minutes ou moins afin de limiter les délais nécessaires à l'obtention d'un diagnostic qui pourra alors sauver des vies ou diminuer les délais précédant les traitements appropriés. Ces protocoles de fabrication doivent nécessiter un minimum de moyens pour en permettre l'utilisation en tout lieu et à tout moment impliquant ainsi une baisse des besoins en analyses conventionnelles pour obtenir des résultats de première ligne et ce après des délais souvent plus importants. L'emploi de l'électroformation de monocouches peptidiques auto-assemblées est décrit au Chapitre 8.

CHAPITRE 2 : Détails expérimentaux

Certaines expériences dont la partie expérimentale ne se trouve pas dans les chapitres subséquents sont détaillées dans ce chapitre.

2.1 Détails sur le fonctionnement de l'instrumentation SPR basée sur le prisme dove

2.1.1 Simplification de l'instrumentation SPR

Les instruments SPR à interrogation angulaire impliquent souvent l'utilisation de pièces mécaniques complexes et dispendieuses veillant l'alignement précis du faisceau incident. Toutefois, cette technique est généralement plus précise que l'interrogation par longueur d'onde puisque plusieurs propriétés optiques varient en fonction de λ. Puisque un système SPR compte plusieurs composantes optiques, la bande SPR observée est plus large en interrogation par λ que par θ. Toutefois, puisque la SPR vise le suivi du déplacement d'une bande plutôt que des variations d'intensité lumineuse (à l'exception du mode imagerie-SPR conventionnel), comme c'est le cas en fluorescence, l'utilisation de modélisation de la courbe SPR combiné avec des outils mathématiques appropriés permettent de limiter ces effets.

L'utilisation d'un prisme d'inversion (dove) permet, par un alignement simple d'obtenir un angle d'incidente permettant d'atteindre les conditions de réflexion totale interne pour un spectre lumineux dans le domaine visible. L'utilisation de la lumière blanche plutôt que'une lumière monochromatique n'implique pas l'utilisation de lasers ou de monochromateurs au niveau de la source. Elle permet l'utilisation de sources de type LED ou incandescente disponibles pour une infime fraction du prix d'un laser. Le spectre lumineux peut être analysé par un spectrophotomètre à barrette de diodes souvent compatible avec la majorité des ordinateurs portables qui permettent l'affichage des

résultats obtenus. Plusieurs itérations de cette instrumentation ont été effectuées dans le cadre de ces travaux de recherche menant au développement d'une instrumentation portable, tenant dans la main. Cette dernière itération (Figure 2-1) est dotée d'une cellule microfluidique d'une taille de 25 µL, de deux polariseurs respectivement de polarisation S et P, le tout relié par fibre optique à la source et au détecteur connecté à un ordinateur portable conventionnel.

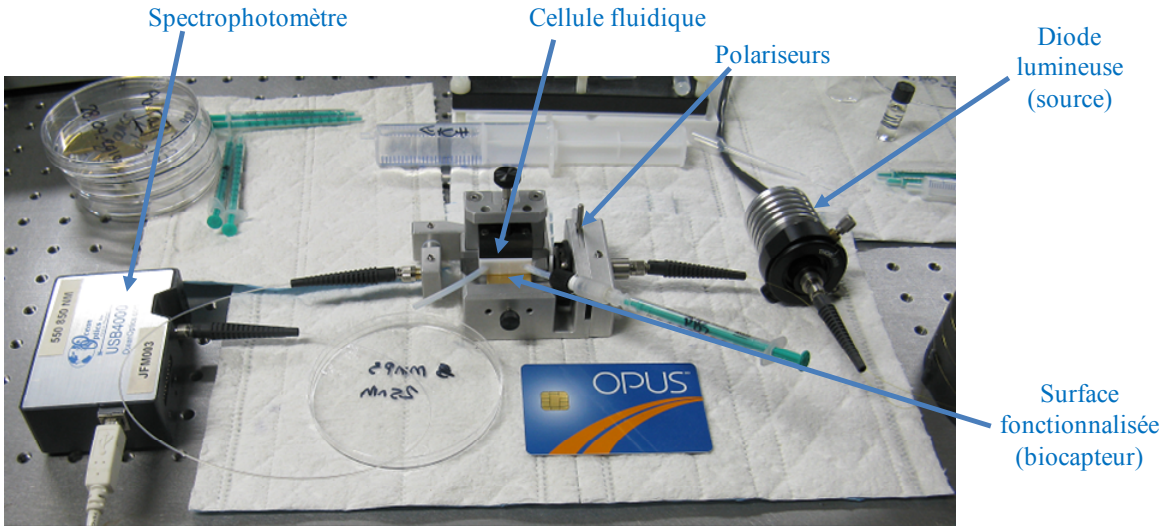

Figure 2-1. Instrumentation SPR à prisme dove (Version3 Révision1).

Cette version d'instrumentation a été employée au cours des travaux présentés au Chapitre 6 à 8 alors qu'une instrumentation faite à l'aide de pièces optiques commercialement disponibles (Figure 2-2) a été employée pour effectuer les travaux présentés en Chapitre 3 à 5.

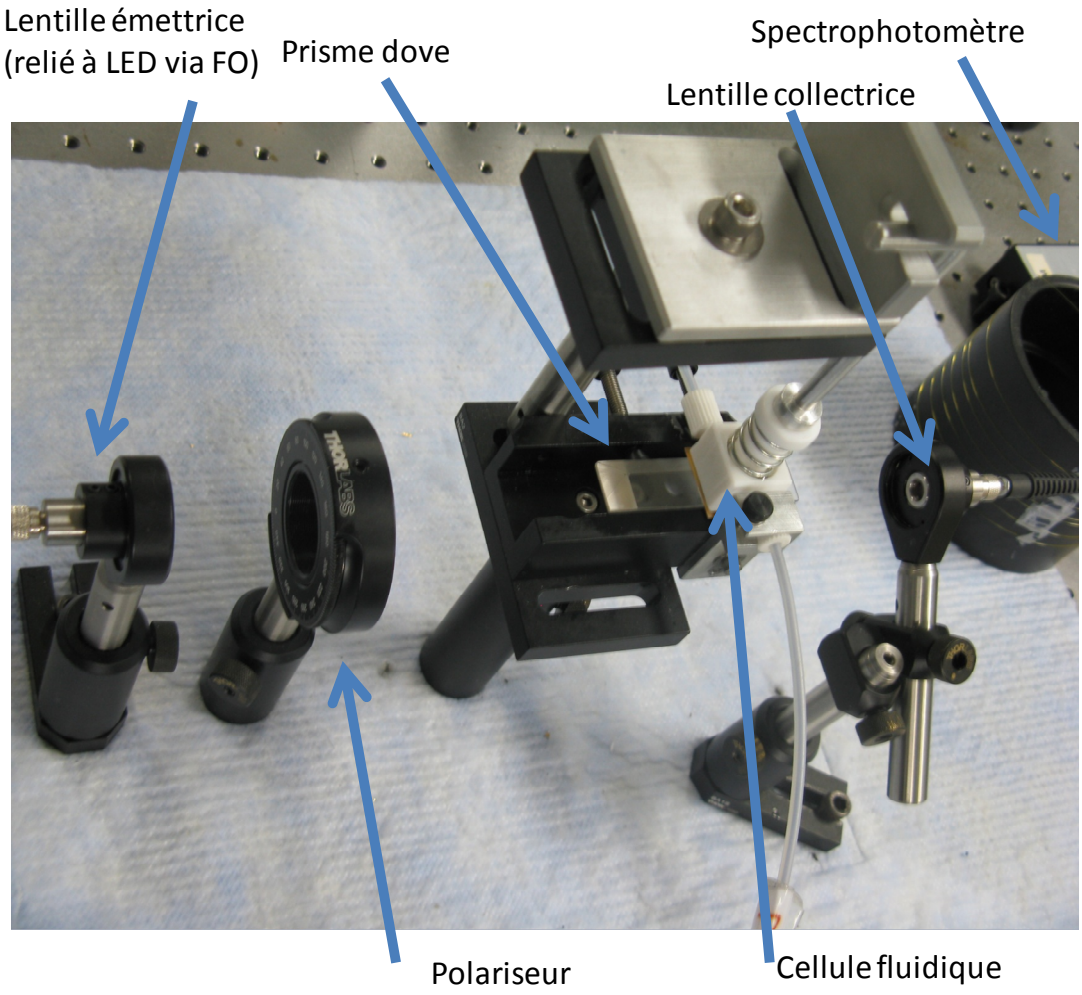

Figure 2-2. Instrumentation SPR à prisme dove (Version2 Révision2).

Ces instrumentations permettent l'acquisition de la lumière polarisée-S avant de procédés au suivi des interactions à la surface d'un biocapteur SPR en lumière polarisée-P. Des spectres types en lumière polarisée S et P obtenus à l'aide de cette instrumentation sont montrés en Figure 2-3.

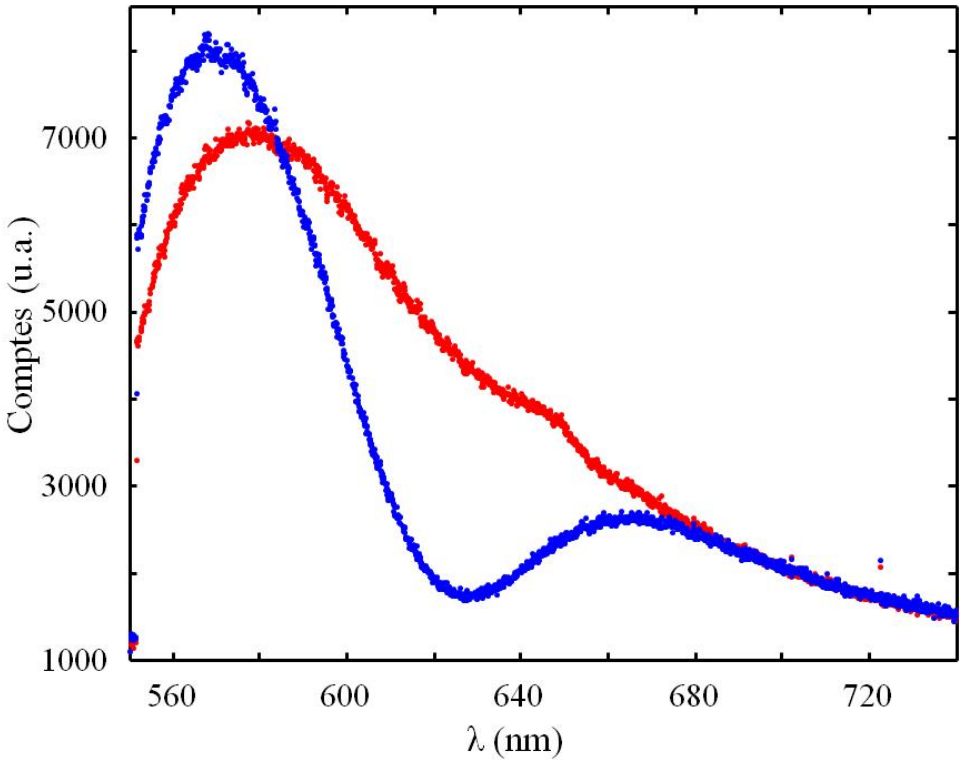

Figure 2-3. Spectres types obtenus à l'aide d'une instrumentation SPR à prisme dove en polarisation S (Rouge) et P (Bleu) obtenus pour une surface d'Au de 50 nm exposé à de l'eau Millipore.

Le spectre en polarisation P est alors mathématiquement divisé par le spectre de polarisation S à l'aide d'un logiciel de traitement de matrice, dans ce cas MatLAB pour obtenir un spectre SPR (Figure 2-4). Le signal SPR obtenu par l'utilisation du montage à prisme dove (aussi appelé prisme d'inversion inventé par Heinrich Wilhelm Dove 1803-1879) implique la prise d'une référence en lumière polarisée-S au début de la prise de données. La lumière polarisée-P est ensuite acquise en temps réel pour effectuer le suivi des interactions à la surface du capteur SPR. Le signal polarisé-P est ensuite divisé par le signal polarisé-S pour l'obtention du signal SPR brut, tel que montré en Figure 2-4. Les courbes SPR sont ensuite analysées mathématiquement pour déterminer la longueur d'onde

engendrant le maximum d'absorption (e.i., le minimim de transmittance) dû au phénomène de la résonance des plasmons de surface.

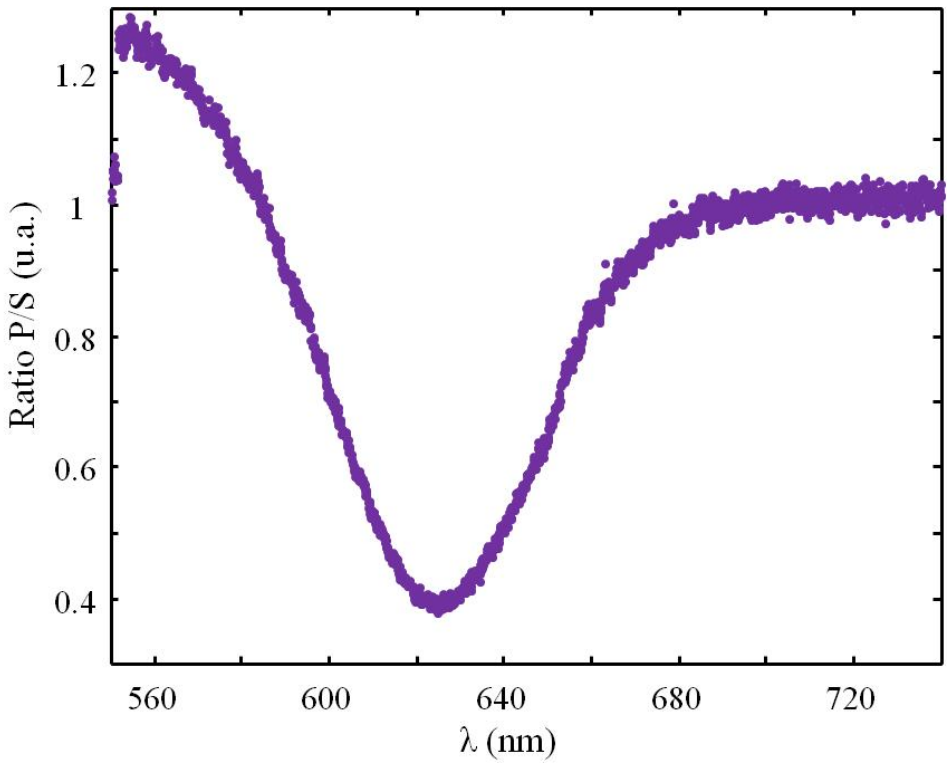

Figure 2-4. Spectre SPR obtenu pour un capteur SPR de 50 nm d'Au exposé à de l'eau Millipore

Un algorithme de programmation permet alors de modéliser la portion du spectre comprenant un minimum du ratio P/S par une fonction polynomiale, puis de calculer la longueur d'onde pour laquelle cette diminution est la plus importante, λ_{SPR}. Dans le cas montré en Figure 2-4, cette valeur est ~ 630 nm, ce qui est une valeur typique pour un film d'Au de 50 nm exposé à l'eau. Le suivi du déplacement de λ_{SPR} en temps réel permet d'obtenir le profil des interactions se déroulant à la surface du biocapteur SPR. L'exemple montré en Figure 2-5 montre la variation de λ_{SPR} lors de la détection de l'IgG à la surface d'un biocapteur fonctionnalisé avec un récepteur biologique anti-IgG.

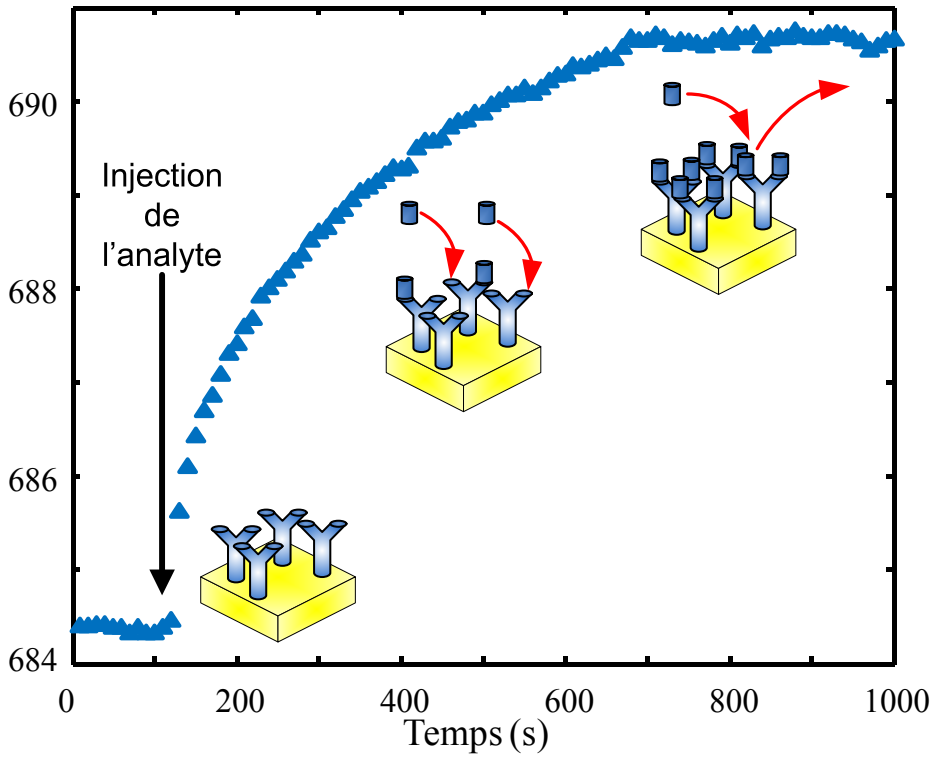

Figure 2-5. Détection d'IgG à l'aide d'un biocapteur SPR fonctionnalisé anti-IgG.

2.2 Élaboration d'un montage SPR auto-référencé

2.2.1 Motivation

Pour des raisons expérimentales, il est nécessaire de laisser les capteurs SPR reposer pour une période minimale de 5 minutes avant d'effectuer des mesures SPR sur une longue période de temps. Cela permet à l'huile optique de s'écouler jusqu'à ce que le capteur SPR adopte sa position d'équilibre générant ainsi un signal ne variant pas en intensité dans le temps dû à une variation du chemin optique engendré par de faibles mouvements du capteur SPR sur l'huile. Ceci implique donc que la référence en lumière polarisée-S pour les mesures prises en fin d'essais n'est pas exactement identique à celle acquise au départ engendrant ainsi des variations des ratios P/S menant à une variation de signal SPR suite à la détermination mathématique du minimum de réflexion. Ces

considérations n'auraient que peu d'importance si les spectres en lumière polarisée-S étaient acquis en temps réel en même temps que les spectres en lumière polarisée-P.

2.2.2 Amélioration apportée à l'instrumentation SPR

Plusieurs modifications de l'instrumentation SPR basée sur le prisme dove ont été envisagées afin de permettre l'acquisition simultanée des lumières polarisées S et P. Il serait possible d'inclure un second canal identique au premier et adjacent à ce premier permettant chacun l'acquisition d'une polarité. Cela nécessite néanmoins le dédoublement de tous les composants de l'instrument. Une autre solution envisageable aurait été de saisir les lumières S et P en alternance. Il serait alors nécessaire de pouvoir contrôler la polarité de la lumière incidente ou à la sortie du système ce qui n'était pas possible vu les moyens instrumentaux disponibles. L'approche favorisée a été de séparer le faisceau à la sortie du prisme dove à l'aide d'un prisme à 45° pour passer ensuite dans deux polariseurs de polarités différentes avant d'être détecté par deux spectrophotomètres différents, telle que représentée dans les plans de détails disponibles en Annexe A. Cette approche a été favorisée car elle ne nécessitait pas de modification importante des composantes en contact avec le capteur SPR.

2.2.3 Approche expérimentale

Afin de comparer les signaux obtenus par l'option avec référence en début d'essai et pour le système référencé en temps réel, un capteur SPR formé d'une surface nue de 50 nm d'Au a été exposée au sérum bovin complet. Le capteur a été rapidement installé sur l'instrumentation SPR avant la saisie de la référence en lumière polarisée-S pour fin de comparaison. La lumière polarisée-S a ensuite été saisie simultanément pour un essai exposant le capteur SPR 5 minutes au PBS, 20 minutes au sérum bovin et 5 minutes au

PBS. Les signaux obtenus en lumière polarisée-P ont été traités selon les deux méthodes, soit par rapport à la lumière polarisée-S acquise en début d'essais et par rapport à celle acquise en temps réel.

2.2.4 Comparaison des deux instruments

Les sensorgrammes superposés pour ces deux types d'instrumentations montrent bien qu'ils ne sont pas équivalents. Cela se reflète par une décroissance du signal SPR dans le cas d'une référence acquise avant les essais, tel que montré en Figure 2-6. La tendance attendue pour ce type d'essais est une courbe ascendante tout au long de l'exposition au sérum complet.[95] Il est à noter que suite à une période de stabilisation d'au moins 5 minutes, la différence de signal SPR observée en fin de mesure est de moins de 0,2nm entre les deux situations. Néanmoins, ce type d'instrument a été mis de côté pour les expérimentations qui suivirent en raison du coût élevé d'un spectrophotomètre supplémentaire pour réaliser ce montage afin d'éliminer l'attente de 5 minutes au préalable. Toutefois, un instrument permettant l'acquisition simultanée des lumières polarisées S et P seraient à considérer dans le cadre du développement d'instruments utilisables sur le terrain en cas d'urgence médicale, par exemple.

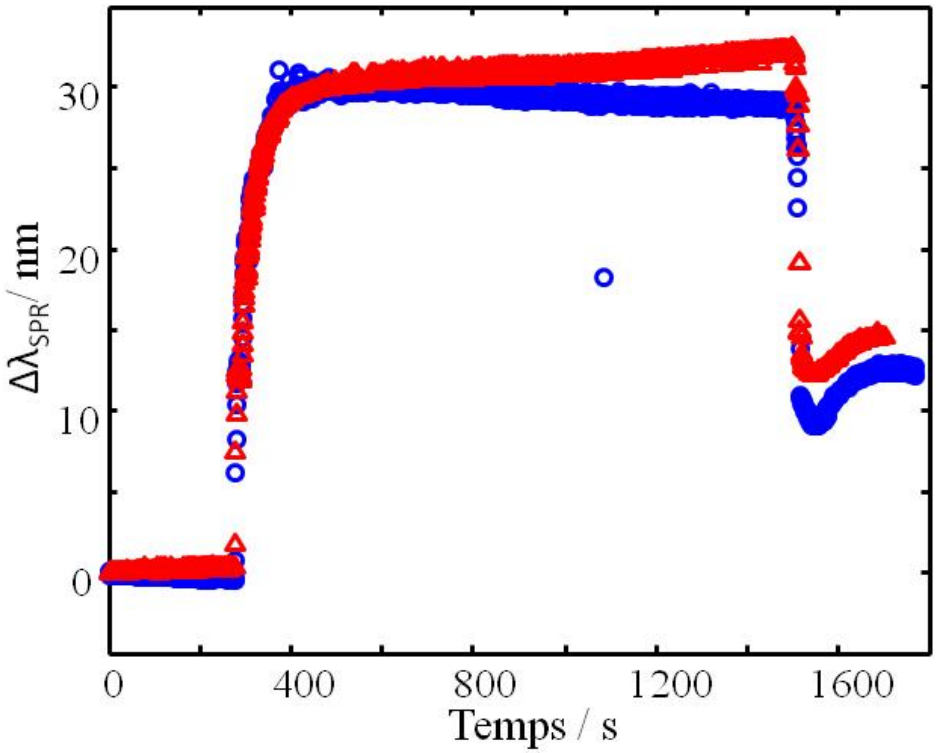

Figure 2-6. Sensorgrammes SPR montrant le suivi des interactions nonspécifiques entre les protéines du sérum sanguin bovin et une surface nue de 50nm d'Au. La courbe bleue est pour un système conventionnel alors que la courbe rouge montre la courbe pour la prise simultanée de la lumière polarisée S et P.

2.3 Formation de surfaces peptidiques à la surface du verre

2.3.1 Motivation

Plusieurs biocapteurs permettent la mesure d'interactions ayant lieu à des interfaces solide-liquide. Un cas particulier, repose sur un capteur dont la phase solide est faite de silice. Certaines de ces méthodes de détection permettent la mesure de la fluorescence directement ou suite à un transfert d'énergie par le biais des plasmons de surface [96]. Cette approche est aussi couramment utilisée en SERS où une coquille de verre est fonctionnalisée partiellement ou complètement de rapporteurs Raman.[97] Une portion importante de la chimie de surface du verre est basée sur des molécules de types

éthoxysilane (APTES) ou methoxysilane (APTMS) permettant l'attachement par trois liaisons avec l'oxyde de silicium composant le verre.[98-101] Les méthodes de détection employant ce type de surface sont elles aussi limitées par les interactions nonspécifiques avec les composants de la matrice complexe. Les surfaces peptidiques pourraient être employées pour moduler ces effets. Toutefois, la chimie basée sur les thiols n'est pas adaptée pour l'attachement de peptides au verre. De plus, il est difficile de synthétiser directement un peptide attaché à une molécule contenant des groupements fonctionnels éthoxysilane ou méthoxysilane, puisque ces derniers peuvent interagir avec les autres groupements fonctionnels des peptides en solution, tel que la terminaison acide carboxylique[102]. Ainsi, les molécules APTES ou APTMS contiennent une terminaison amine permettant l'attachement des molécules à immobiliser souvent via la chimie EDC/NHS permettant la formation d'un lien amide avec un groupement fonctionnel acide carboxylique. Toutefois, les peptides développés dans le cadre de ces travaux exposent l'extrémité N-terminal vers la surface et C-terminal en surface. Il est donc nécessaire d'employer une autre molécule servant d'intermédiaire pour lier les deux groupements fonctionnels amines. L'acide citrique ($C_6H_8O_7$) offre une alternative intéressante à l'accomplissement de cette tâche puisqu'il s'agit d'une molécule de faible taille offrant trois terminaisons acides carboxyliques.

2.3.2 Approche expérimentale

Un peptide de composition H_2N-GHHHDD-OH (704,24g/mol) a été synthétisé sur support solide selon le protocole décrit dans la littérature[103] sans toutefois l'attacher à une molécule thiolée. L'ajout d'un résidu glycine permet d'augmenter la mobilité du peptide à la surface tout en dégageant l'extrémité N-terminale qui se lie au citrate. Des lamelles de

verre 22x22mm furent préalablement nettoyées à l'aide d'une solution piranha suivi d'une solution eau/peroxyde/NH_4OH tel que présenté dans la littérature[104] afin d'augmenter la disponibilité des groupements silanols. Les plaques ont été immergées dans une solution 0,2% APTMS dans l'éthanol pour une période de 16 heures, puis rincées à l'éthanol. Des spectres GATR-FTIR ont été acquis afin de confirmer cette étape. Une solution 25mM de citrate de potassium dissout dans un tampon MES pH=5,00 a été produit. 3 équivalents NHS sont dissouts à cette solution suivi immédiatement de 6 équivalents EDC afin d'estérifier efficacement l'acide citrique avec NHS. Les plaques préalablement fonctionnalisées avec APTMS sont immergées dans cette solution pour 16 heures avant d'être rincées et d'acquérir des spectres GATR-FTIR pour confirmer l'attachement de l'acide citrique à la surface de verre. Les lamelles sont ensuite immergées pour 20 minutes dans une solution 50 mM/10mM EDC/NHS dans le tampon MES afin de réestérifier les extrémités libres du citrate à la surface avec NHS. Les lamelles de verre sont rapidement rincées à l'eau Millipore avant d'être immergées dans une solution 1mM du peptide H_2N-G-H_3-D_2-OH pour 16 heures avant un rinçage à l'eau Millipore suivi de la saisie d'un spectre GATR-FTIR.

2.3.3 Vérification des fonctionnalisations du verre par GATR-FTIR

Les spectres obtenus à chaque étape ont été normalisés et superposés afin de comparer les étapes subséquentes. L'attachement de la molécule APTMS est confirmé par les spectres montrés à la Figure 2-7 par la présence d'une forte bande à 1050 cm^{-1} représentant la présence de liaisons Si-C. La présence d'une bande d'absorption à 1190 cm^{-1} pour l'APTMS pur et à la surface correspond à des étirements des liaisons Si-O-C de l'APTMS. La présence d'une bande large centrée à 3450 cm^{-1} ainsi que d'une bande

d'intensité moyenne à 2840 cm^{-1} indique respectivement la présence d'étirements N-H et C-H de l'amine primaire essentiel à la confirmation de la fonctionnalisation.

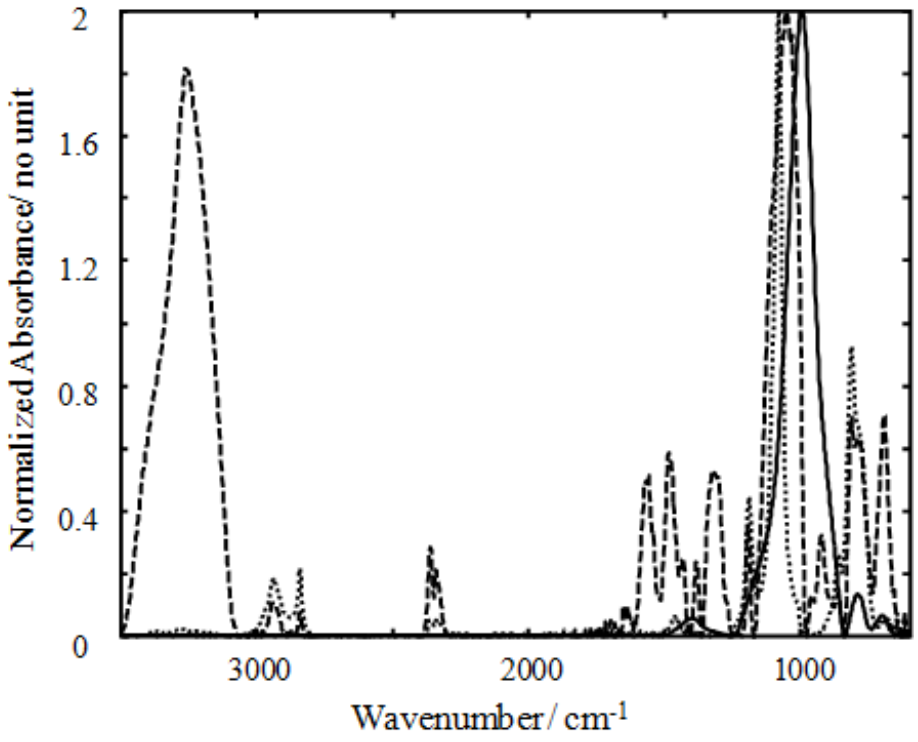

Figure 2-7. Confirmation par GATR-FTIR de la formation d'une couche d'APTMS sur du verre. (Trait plein) Verre, (Trait pointillé) APTMS pur et (Trait hachuré) Verre fonctionnalisé.

L'attachement du citrate est confirmé par la présence importante d'une bande à 1680 cm^{-1} correspondant aux étirements C=O des groupements acide carboxylique seulement visible pour la surface fonctionnalisée avec le citrate, tel que montré en Figure 2-8. La bande large à 3450 cm^{-1} subie un déplacement hypsochromique une fois fonctionnalisée avec le citrate. Cela est probablement dû à la présence d'étirements O-H des acides carboxyliques du citrate.

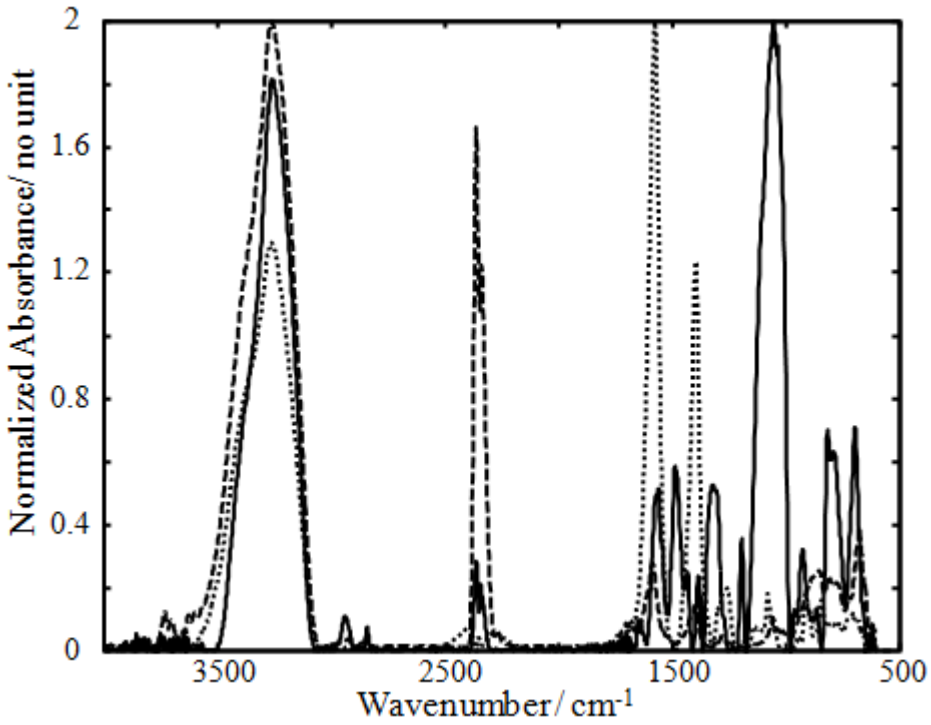

Figure 2-8. Vérification de l'attachement du citrate à la surface de l'APTMS. (Trait plein) Surface fonctionnalisée avec APTMS, (Trait pointillé) Citrate pur et (Trait hachuré) Surface fonctionnalisée avec le citrate.

L'attachement du peptide H_2N-GHHHDD-OH à la surface du verre est confirmé par un important accroissement de la bande amide I à 1645 cm^{-1} indiquant la présence possible d'un peptide en configuration hélice-α à la surface, tel que montré en Figure 2-9. La bande amide III due à la présence d'étirements C-N de la chaîne principale du peptide est visible à 1440 cm^{-1}. La présence d'une forte bande d'absorption à 1720 cm^{-1} indique la présence d'étirements C=O caractéristique des groupements acides carboxyliques à l'extrémité C-terminale des peptides.

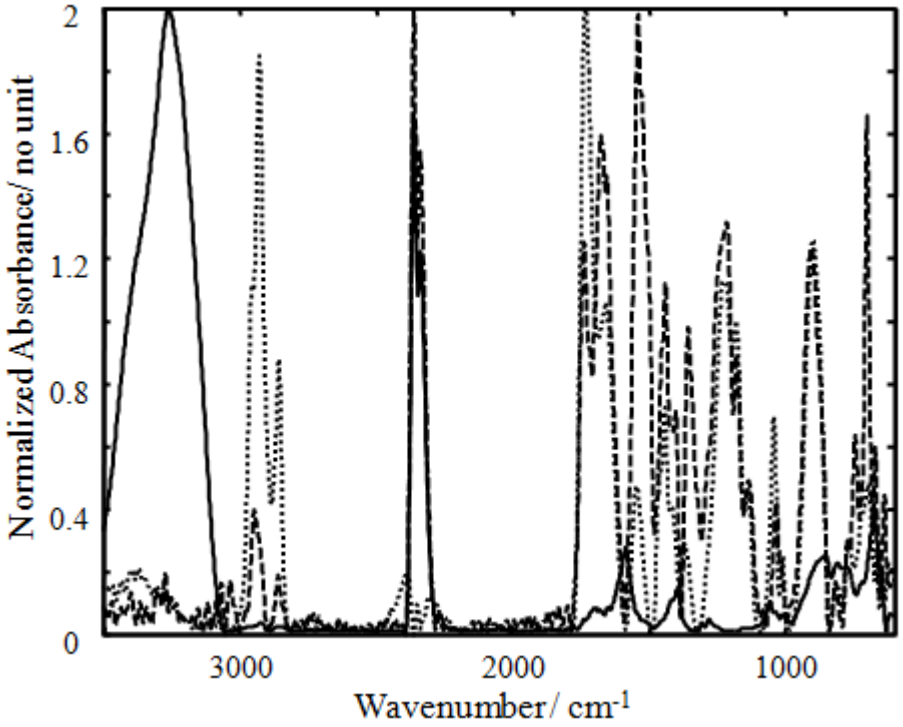

Figure 2-9. Vérification de l'attachement du peptide H_2N-G-H_3-D_2-OH à la surface du verre. (Trait plein) Surface fonctionnalisée avec le citrate, (Trait pointillé) H_2N-G-H_3-D_2-OH pur et (Trait hachuré) Surface fonctionnalisée avec H_2N-G-H_3-D_2-OH.

CHAPITRE 3 : High Resolution Surface Plasmon Resonance Sensors based on a Dove Prism [105]

Publié en tant que : Bolduc, O. R.; Live, L. S.; Masson, J.-F. *Talanta* **2009**, *77*, 1680-1687.

3.1 ABSTRACT

Wavelength interrogation surface plasmon resonance (SPR) spectroscopy using a dove prism combine simple and inexpensive optical design with high resolution refractive index monitoring and biosensing. The dove prism inverts the image with a total internal reflection angle of 72.8°, an angle active in SPR. Hence, a unique system can accomplish SPR biosensing using wavelength interrogation and also perform SPR imaging. This optical configuration advantageously uses a linear optical path between each optical component, simplifying the optical design of SPR instruments. Fluidics was also incorporated in the instrument design for efficient sample delivery. The SPR instrument is characterized in terms of refractive index (RI) sensitivity, RI resolution, and application for monitoring low concentration biological events. Data analysis methodologies are compared for improved resolution of the measured response. Raw data analyzed using the minima hunting procedure results in RI resolution in the 10^{-6} range, while pre-treating data with singular value decomposition improves resolution by one order of magnitude. Depending on the spectrophotometer employed, the RI range accessible can be tuned; examples with a 550 nm – 850 nm and a 550 nm – 1100 nm spectrophotometers are shown and results respectively in RI ranges of 1.32 – 1.39 RIU and 1.32 – 1.42 RIU. Monitoring of nM concentration of β-lactamase is performed using the wavelength interrogation configuration of the biosensor. Finally, a SPR image of a patterned-surface was obtained using the dove prism SPR with a band pass filter and a CCD camera. SPR using a dove prism configuration combines the advantages of portable SPR instruments, SPR imagers and research-grade SPR instruments in a single platform.

Index headings: Portable spectrophotometers, biosensing, refractometer, self-assembled monolayer, SPR imaging

3.2 INTRODUCTION

Surface plasmon resonance (SPR) sensing has become a widely utilized technique for the measurement of biomolecular interactions [106, 107], quantification of proteins [108, 109], and DNA [110]. Excellent reviews of the instrumentation [18], the technique [19] and recent advances in SPR spectroscopy [111] provide a general overview of SPR based sensors. The SPR phenomenon relies on the optical excitation of a charge-density oscillation existing at the interface of a thin metallic film and a dielectric. To achieve resonance conditions, the light must be in total internal reflection at a wavelength – angle couple matching the wavevector of the surface plamon (SP). Therefore, multiple optical configurations can possibly excite the SP. The most popular configuration uses monochromatic light to interrogate the angles in resonance with the SP, commonly known as the Kretschmann configuration [19]. Many instruments have been commercialized based on this technology such as the Biacore from GE Healthcare. However, this technology suffers from drawbacks limiting its application to biomedical problems. These SPR instruments are usually expensive to implement, non-deployable to the field and are not compatible with biological samples. Thus, in spite of the popularity of these types of SPR instruments, there is still a necessity to develop a SPR instrument combining the high resolution of Kretschmann configuration with the advantages of an inexpensive [112, 113] and portable instrument [114, 115]. Hence, a versatile and cost-effective technology could be implemented in many laboratories for low detection limits SPR sensing.

A SPR instrument using fiber optics as the sensing element is a cost effective alternative to research grade instrument, they are portable [116] and can be adapted to various applications such as salinity sensor [117], biosensor for wound healing [118], cardiac markers [119, 120] and staphylococcal enterotoxin B [121]. Sensitivity of fiber optic SPR can be improved using near infrared excitation of a micro prism located at the tip of the fiber optic [122]. However, the resolution achieved with this technique is limited by the numerical aperture (NA) of the optical fiber required to perform SPR on a fiber optic. A large numerical aperture (NA = 0.39) fiber is necessary to propagate the SPR-active angle – wavelength couples. However, due to a large number of angle – wavelength couples exciting the SPR surface, the spectrum broadens. To minimize this effect, low numerical aperture fiber optic (NA = 0.12) can be modified with a micro-prism at the distal end to improve the SPR spectrum [123] and increase the accessible range of refractive index of the sensor [124]. Using this configuration, the resolution is limited to 1.4×10^{-6} RIU. Further decrease of the numerical aperture of the fiber optic is necessary to achieve a resolution similar to the Kretschmann configuration (approx. 5×10^{-7} RIU). However, current manufacturing techniques do not allow such low numerical aperture.

A methodology to combine the advantages of the Kretschmann configuration and fiber optic SPR instrument could provide a SPR instrument that is portable, inexpensive and exhibiting high resolution to refractive index. Multiwavelength excitation of the SPR on a prism at a single angle using a combination of fiber optic light transmission and collection provides a simple optical design [125, 126]. Thus, compact fiber optic coupled with high resolution miniature spectrophotometer is providing high resolution measurement of

the refractive index. Spectral resolution achieved with the miniature spectrophotometer is a function of the grating resolution. In the case of the Kretschmann configuration, the resolution depends on scanning the incident angle (slow measurement and complex mechanical setup) or by focusing the incident light beam at the prism Au interface onto a linear array photodiode (lengthy optical path for high resolution). Hence, the Kretchmann configuration is not suitable for portability and for an inexpensive design of the SPR instrument. A current drawback of multiwavelength SPR instrument is the precise alignment of the optics [126] or the manufacture of a small sensing element [125]. To circumvent these drawbacks, the use of a dove prism is advantageous. The dove prism inverts an image, with a total internal reflection angle of 72.8°, active in SPR with an excitation wavelength between 600 nm and 1000 nm depending on the refractive index of the solution. Thus, since the dove prism inverts the image of a collimated light beam, a linear optical path is required to construct the SPR instrument, greatly simplifying the optical setup without loss of spatial or optical resolution. The sensing element is simply composed of a glass slide coated with Au and fluidics can be mounted on the sensor. This configuration combines the advantages of portable, inexpensive SPR instrument with the advantageous sensing from high resolution SPR instrument.

Increasingly, the need of multiplex arrays is arising for simultaneous analyte detection. The spatially resolved SPR measurements provide a technology for monitoring local changes of refractive index on a surface [127, 128]. Thus, the detection of biomolecular interactions is possible on a spatially resolved sensing array [129]. SPR imaging or SPR microscopy has been applied for high-throughput analyses of biomolecular binding event [106]. SPR imaging methodology has been modified with the improvement of the resolution

[130], optical coupling [131] and protein array formation [132]. However, no SPR measurement possesses the dual capability of measuring the conventional SPR response and the SPR image of a surface. The image inverting property of the dove prism allows the use of a single instrumental template for both conventional and SPR imaging techniques.

Therefore, the construction of a SPR instrument is demonstrated based on a compact optical setup using a dove prism coupled with fiber optics and a miniature spectrophotometer. Characterization of the dynamic range, the sensitivity, refractive index resolution, the reproducibility and biosensing for β-lactamase are reported in this article. Multiple data analysis strategies were previously developed to improve resolution of the SPR signal [133-136]. Minimum hunting (polynomial fit) and the algorithm (a-b)/(a+b) are investigated to improve resolution. Spectral denoising is also performed using singular value decomposition of the spectra to improve the signal to noise ratio and increase the resolution. Replacing the collection optics and miniature spectrophotometer with a bandpass filter and an imaging camera results in a SPR imager. An image of water droplets on a Au surface of the SPR sensor demonstrates the SPR imaging configuration.

3.3 EXPERIMENTAL SECTION

3.3.1 SPR sensor

Glass slides of 3" x 1" were cleaned using piranha solution (70% H_2SO_4 : 30% H_2O_2) at 80°C for 90 minutes. *Caution, piranha solution is highly corrosive!* The glass slides are then thoroughly rinsed with 18 MΩ water. Thereafter, the glass slides are reacted in a ultrasound bath with a 5 : 1 : 1 solution of H_2O : H_2O_2 : NH_4OH for 60 minutes. The glass slides are thoroughly rinsed with 18 MΩ water and stored in 18 MΩ water until use.

The slides are air dried undisturbed prior to metallization. Then, a 5 nm-thick adhesion layer of Cr followed with a 48 nm Au film are deposited to construct the SPR sensor.

3.3.2 SPR instrument

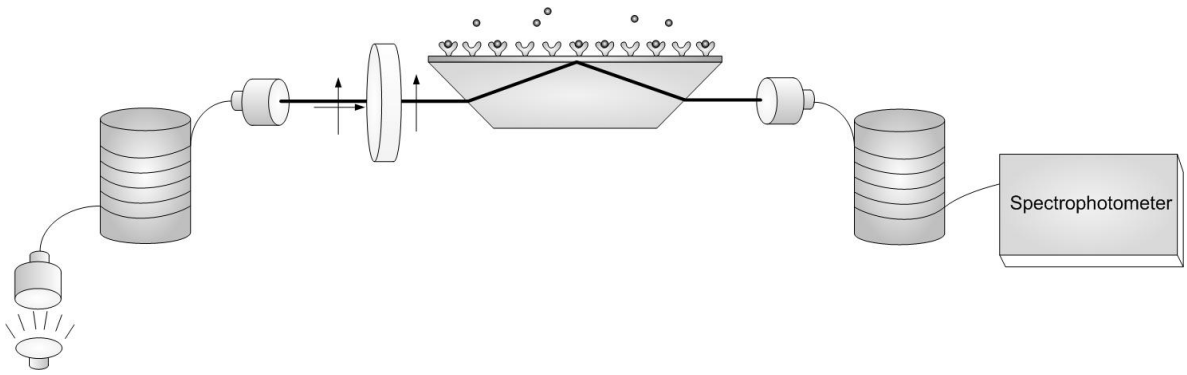

Figure 3-1. Schematic of a SPR instrument using a Dove prism. The optical path is linear between the excitation fiber and the collection fiber, resulting in a small-footprint instrument.

The SPR instrument was constructed based on a combination of wavelength-interrogation fiber optic SPR and total internal reflection in a dove prism (Figure 3-1). The light from a halogen lamp is focused in a 200 μm-diameter fiber optic (excitation fiber optic). Light exiting the excitation fiber optic is collimated (diameter about 3 mm), passed through a polarizer, the dove prism (BK7) with the SPR sensor contacted using refractive index matching oil, and collected into the collection fiber optic bundle (200 μm diameter) using an inverted fiber optic collimator. All these optical components are aligned in a single plane. The light exiting the collection fiber enters a miniature spectrophotometer. Depending on the RI range desired, a short range spectrophotometer (550 nm – 850 nm) covers from 1.33 to 1.39 RIU or a longer spectral range is obtained from a 550 nm – 1100 nm spectrophotometer and covers from 1.33 to 1.42 RIU. If the imaging configuration is used, the collection fiber optic is removed and replaced with a band pass filter (610 ± 10

nm). The collimated light exiting the band pass filter is analyzed using a CCD camera. A 50:50 beam splitter can be installed between the dove prism and the band pass filter for wavelength interrogation and imaging on a single platform.

The fluidic cell and syringe pumps were constructed in-house. The fluidic cell made of Teflon has a spade-shaped channel of 0.5 mm deep. The housing was designed to hold the dove prism, the SPR sensor and the fluidic cell in close contact. The dual channel syringe pump was designed for sample flow rates between 8 μL s^{-1} and 110 μL s^{-1}. A flow rate of 16 μL s^{-1} was typically used.

3.3.3 Calibration of the SPR sensor

Sucrose solutions with concentrations ranging from 0 % w/w to 50 % w/w were prepared in water. Thereafter, the solutions were successively exposed to the SPR sensors using the syringe pump and the flow cell. Data analysis was performed using two methodologies: minimum hunting [134] and the normalized difference (a-b)/(a+b) around the minimum reflectance of the SPR spectrum [136]. Singular value decomposition (SVD) of the SPR spectra and reconstruction of the SPR spectra using the first three components was performed to optimize signal to noise. With both data analysis methodologies, an ordinary linear least squares (OLLS) regression model is used to calibrate the SPR sensor.

3.4 RESULTS AND DISCUSSION

3.4.1 SPR using a dove prism

The excitation of SPR using a dove prism interface allows a compact and linear optical path between an excitation fiber optic and a collection fiber optic (Figure 3-1). Since collimated incident light is shone on the prism, a single angle of 72.8° propagates

in total internal reflection through a BK7 prism. This angle permits excitation of the surface plasmon on a 48-nm Au film, with an excitation wavelength of approx. 610 nm with aqueous solutions (Figure 3-2). Therefore, the instrument must combine multi-wavelength excitation with a spectrophotometer to observe a full SPR spectrum. To accomplish this, fiber optic bundles and small portable spectrophotometer result in a small footprint instrument, of 17 cm length by 6.5 cm width and 17 cm height. The SPR instrument consist of a broadband halogen light source, an excitation fiber (VIS-NIR fiber optic bundle of 200 μm diameter) with a collimating lens terminating the fiber, a polarizer, a dove prism, and a collection fiber identical to the excitation fiber. The excitation fiber is introduced in a small portable spectrophotometer with a wavelength range of 550 nm to 850 nm for a short range of accessible refractive index (1.32 to 1.39 RIU) or a spectrophotometer with a range from 550 nm to 1100 nm for a broader range of refractive index accessible to the SPR sensor (1.32 to 1.42). This instrument has the advantage of simultaneous acquisition of all wavelength of the SPR spectrum, hence allowing for fast acquisition of the spectra. Typically, the data reported here is acquired at a rate of 50 Hz, the accumulation of 50 spectrum composed one data point (1 s time resolution). In comparison, an instrument scanning the angles cannot achieve such temporal resolution. Otherwise, focusing a beam on the SPR prism requires a lengthy optical path to achieve better spectral resolution. Hence, using the dove prism configuration, it is possible to achieve a compact design without compromising the spectral resolution. The alignment is also much simpler compared to a SPR instrument interrogating multiple angles simultaneously. The dove prism simply requires a linear alignment of the optical component, light must be focused at a precise angle using an instrument interrogating multiple angles.

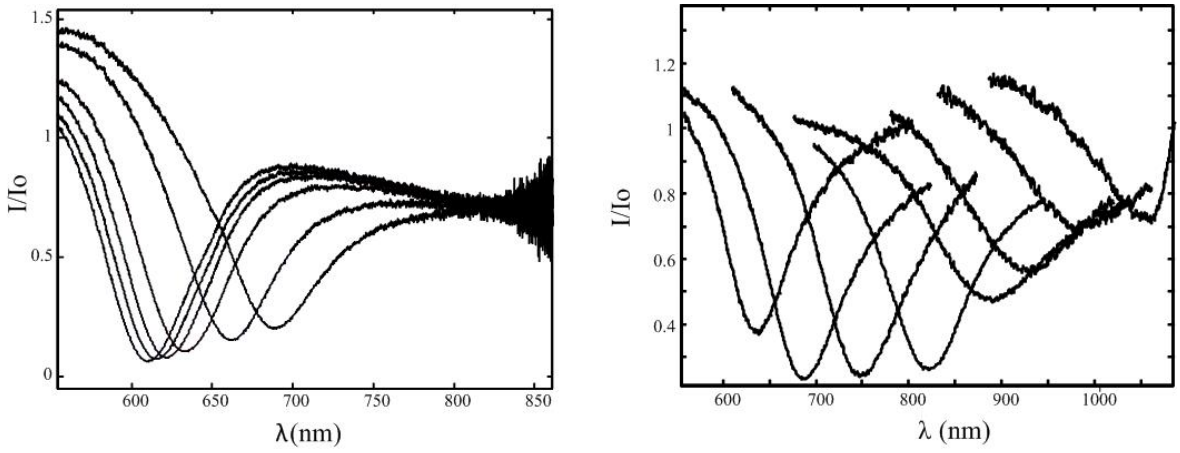

Figure 3-2. SPR spectra are shown for the sucrose solutions with refractive index varying between 1.33 – 1.36 RIU (short range configuration) on the left and between 1.33 and 1.42 RIU in the long range configuration.

A tunable of the spectral range is beneficial for different applications. Some applications require high spectral resolution for monitoring the SPR response of low concentration of an analyte with high resolution (i.e. biosensor for a low protein concentration), while other application require a large spectral range to monitor changes in refractive index from bulk composition of the solution. In this case, the spectral range of the SPR instrument depends on the grating utilized in the spectrophotometer. Hence, a grating with a larger number of grooves per mm will result in a larger spectral resolution, but a smaller refractive index range accessible to the instrument. In a first configuration presented here, a spectrophotometer with a spectral range between 550 nm and 850 nm is connected to the collection fiber. This spectrophotometer results in a refractive index range of the SPR instrument between 1.33 and 1.39 RIU and is adequate for most applications in aqueous solutions, such as biosensing (Figure 3-2). The noise observed on the spectra at wavelengths > 750 nm is due to the use of a narrow spectral range LED, emitting between 550 nm and 700 nm. The high power LED (Philips lumiled) is advantageous, resulting in

short integration time (20 ms) for a single acquisition, such that multiple acquisitions are accumulated to compose a single spectrum with a reduced noise on the signal. Hence, kinetic data can be obtained at a fast acquisition rate, with a low noise on the measured spectra. In another configuration presented here, the SPR spectra are shown using a spectrophotometer sensitive between 550 nm and 1100 nm (Figure 3-2). This longer spectral range results in SPR sensitivity between 1.33 and 1.42 RIU. Thus, the range of refractive index accessible to the SPR instrument is tunable with different spectrophotometers. This instrumental configuration results in a single template applicable to different experiments.

The SPR sensor is calibrated to determine the sensitivity for refractive index in the biological region. The measurement of the SPR response from solutions of varying refractive index calibrates the SPR sensor for bulk refractive index changes. Figure 3-2 shows the SPR spectra for both configurations with sucrose solutions of increasing concentration, thus of increasing refractive index. A refractometer with an accuracy of 1 x 10^{-5} RIU accurately measures the refractive index of the sucrose solutions. Sucrose solutions are a good model for refractive index calibration, as sucrose does not interact with the Au surface of SPR sensors [134]. Hence, the response measured with the SPR sensor results uniquely from the refractive index for the bulk solution and no contribution is observed from the accumulation of molecules at the surface. The sensitivity with the SPR using the dove prism was measured at 1765 ± 100 nm/RIU. However, the calibration curve for the refractive index sensitivity of SPR sensors is non linear, as the refractive index sensitivity increases for solutions of higher refractive index. Therefore, the sensitivity reported here, is only valid for the biologically relevant range of refractive indices between

1.33 and 1.35 RIU. The error reported here is for two standard deviations, calculated using ordinary linear least squares regression.

3.4.2 Data analysis methodologies

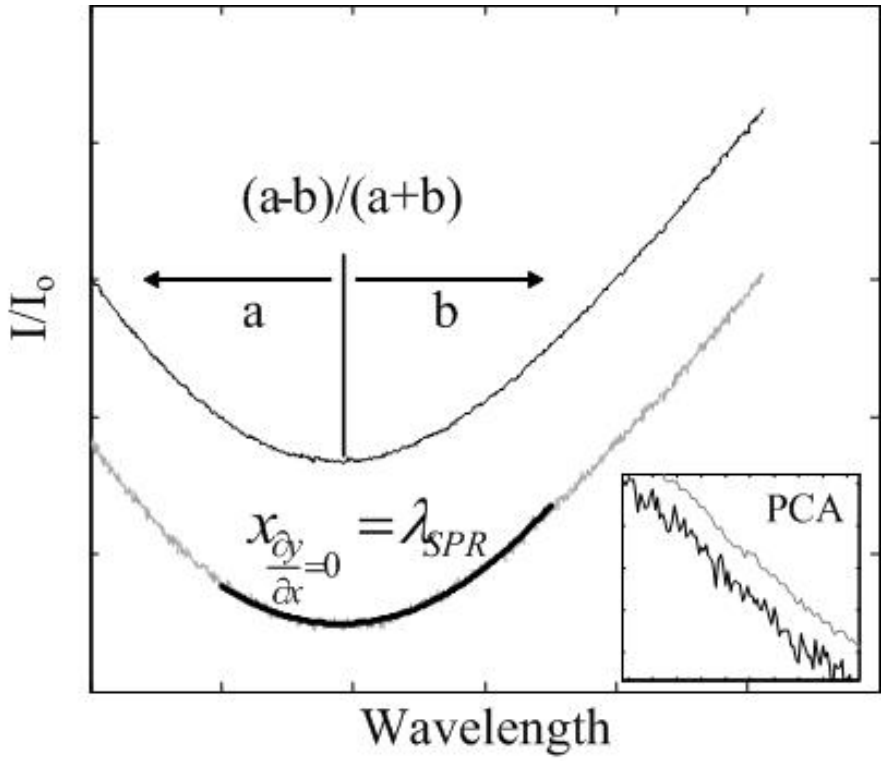

Figure 3-3. Data analysis of SPR spectra using minimum hunting (λ_{SPR}) and the normalized difference method. PCA is used to decompose and reconstitute the spectra with the components containing the chemical information to reduce the noise on the spectra.

SPR sensors respond to refractive index with a change of the matching wavelength. Therefore, the methodology used for the determination of the change of refractive index must be accurate and sensitive to small changes of refractive index. The noise level of the measured response must also be minimized. Traditionally, a minimum intensity finding algorithm mathematically fits a second order polynomial to the SPR spectra and determines the minimum from the zero of the derivative of the second order polynomial (Figure 3-3).

Alternatively, an algorithm calculating the difference between the intensity of the branches around a constant wavelength (λ_o), divided by the sum of the intensity for both branches results in a measurement of the position of the SPR response (Figure 3-3). Hence, the algorithm *(a-b)/(a+b)*, where *a* is the sum of the branch for $\lambda < \lambda_o$, while b is the sum of the branch for $\lambda > \lambda_o$, is sensitive to minute changes of the position of the SPR response. This algorithm also accurately measures the topography with an atomic force microscope. In order to decrease the noise on the SPR spectra, a singular value decomposition of the SPR spectra into principal components, followed by the reconstitution of the spectrum with the first components containing the chemical information reduces the noise. Reconstitution of the SPR spectra with the first three principal components results in no loss of chemical information.

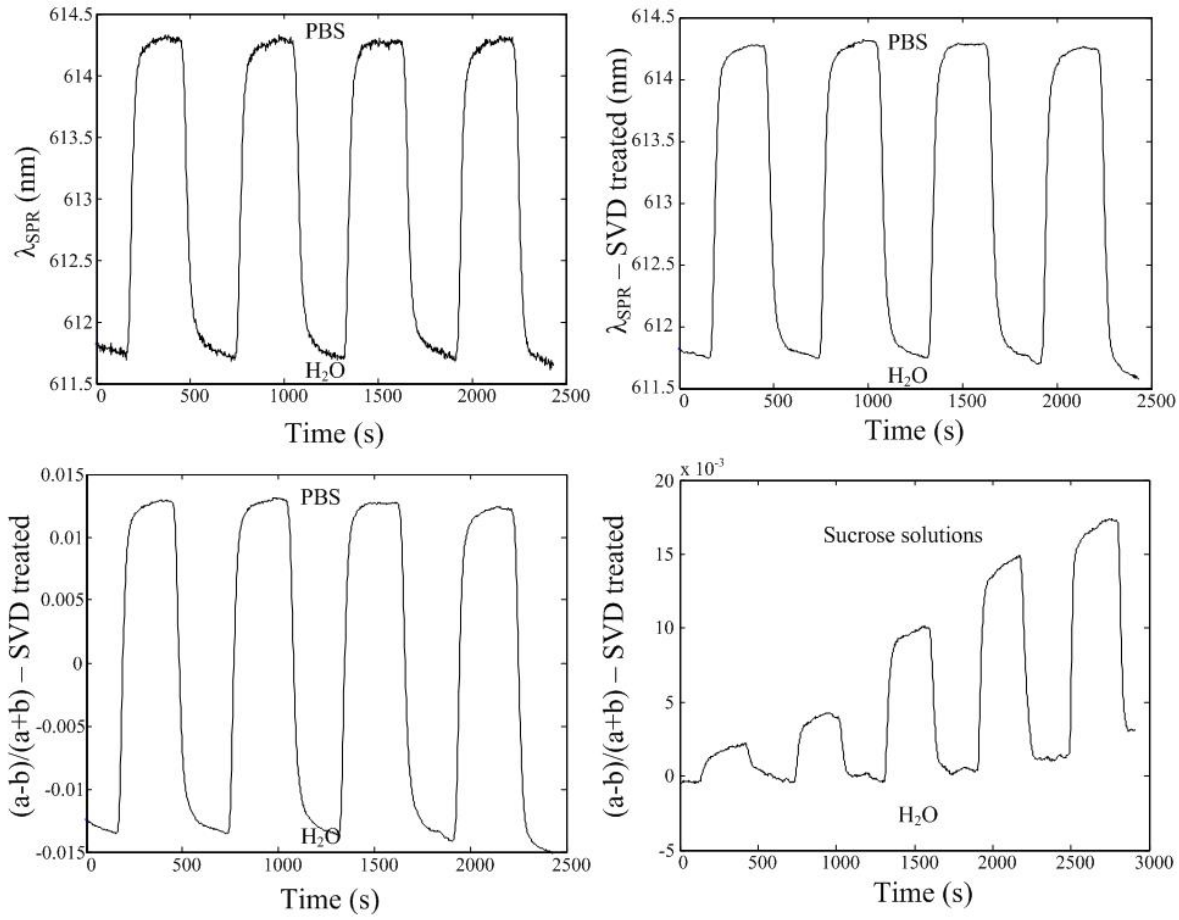

Figure 3-4. (Top Left) Repeated measurement of phosphate saline buffer (PBS, 1.34xxx RIU) and water (1.33287 RIU). Data analysis using the minimum hunting procedure (Top right) PCA decomposition of the SPR spectra, reconstitution using the first three components followed by the minimum hunting procedure. (Bottom left) Identical PCA treatment as top right, however using the normalized difference method. (Bottom right) Calibration curve for sucrose solutions (RI ranges between 1.333 RIU and 1.334 RIU) using the flow cell, PCA treatment and the normalized difference.

A flow cell was designed to deliver the samples to the SPR sensor using a syringe pump. The syringe pump has variable flow rate between 0.5 mL/min (8.3 µL/s) to 6.5 mL/min (108 µL/s). The results thereafter were obtained at 16 µL/s. The SPR sensor is consecutively exposed for 5 minutes to 18 MΩ water and PBS for four cycles (Figure 3-4). The SPR response is reproducible at a wavelength shift of 2.470 ± 0.011 nm between PBS

(RI = 1.33498 at 20.00°C) and water (RI = 1.33316 at 20.00°C) using the minima hunting data analysis. Singular value decomposition of the raw SPR spectra and reconstituting of the SPR spectra with the first three components results in a wavelength shift of 2.482 ± 0.021 nm. Thus, it is observed that the denoising SPR spectra with singular value decomposition do not alter the SPR response. Using the algorithm (a-b)/(a+b) and singular value decomposition denoising yields a response of 0.0257 ± 0.0002 (unitless). The reproductibility of the flow cell is better than 1% variation (n = 4) with each data analysis methodologies.

Table 3-1. Comparison of data analysis methodologies for flow cell stability and β-lactamase biosensing

	Minimum hunting	**(a-b)/(a+b)**
Refractive index resolution		
raw data	3×10^{-6} RIU	9×10^{-7} RIU
SVD	1×10^{-6} RIU	1.5×10^{-7} RIU
β-lactamase response (700 nM)		
raw data	0.17 ± 0.03 nm	$6.4 \pm 0.8 \times 10^{-4}$
SVD	0.127 ± 0.005 nm	$4.05 \pm 0.15 \times 10^{-4}$

A significant decrease of the noise on the SPR response is observed from denoising the raw SPR spectra with singular value decomposition. A further decrease of the noise observed on the SPR spectra is observed for data processing using the (a-b)/(a+b) algorithm. The continuous measurement of the SPR response for a water sample is used to calculate the resolution for each data analysis methodologies (Table 3-1). Two standard deviation on the measurement of the SPR response during a 2-minute exposition to water at

a flow rate of 16 μL/s and dividing this value by the sensitivity calculates the resolution. Using minima hunting without singular value decomposition, the resolution on the refractive index measured is 3 x 10^{-6} RIU. Denoising the raw spectrum improves the resolution to 1 x 10^{-6} RIU. Therefore, an improvement by a factor of 3 is observed for denoising the data using singular value decomposition. In comparison, the algorithm (a-b)/(a+b) significantly improves the resolution compared to the minimum hunting algorithm. A resolution of 9 x 10^{-7} RIU and 1.5 x 10^{-7} RIU are respectively observed for data processing using (a-b)/(a+b) without denoising and with singular value decomposition denoising. Therefore, a greater improvement is observed by denoising the data prior to processing with (a-b)/(a+b) compared with the minimum hunting algorithm. This greater improvement on the resolution observed for denoising (a-b)/(a+b) is due to the methodology of data processing. The main factor limiting the resolution for the minimum hunting procedure is the accuracy of the polynomial fit of the SPR minimum. However, the random noise on the SPR spectra does not significantly change the shape of the spectra. Thus, the fit of the second order polynomial for minimum hunting is only slightly improved by denoising. For the (a-b)/(a+b) algorithm, the resolution is mainly limited by the random noise on the measurement. However, the reduction of the noise from random fluctuations on the spectrum significantly impacts the resolution of the SPR response using the (a-b)/(a+b) algorithm. This results in a greater reduction of the noise and improves resolution of the SPR instrument. Resolution in the 10^{-7} RIU range rivals with the best SPR instruments and is adequate for high resolution SPR biosensing. The resolution were respectively reported for angular interrogation SPR at 5 x 10^{-7} RIU [19], at 1.4 x 10^{-6} RIU for

fiber optic SPR [116], at approx. 10^{-5} RIU for wavelength interrogation SPR [19, 125], and at 5 x 10^{-5} RIU for intensity measurement SPR (SPR imaging).

To exhibit the potential to measure solutions with a small refractive index difference, a calibration curve was constructed for sucrose solutions with a refractive index between 1.333 and 1.334 (Figure 3-4). Therefore, the difference in refractive index between each step is $< 2 \times 10^{-4}$ RIU. The signal to noise ratio on the SPR response does not approach the limit of detection. The SPR signal measured with (a-b)/(a+b) shows a linear response to refractive index, due to the short range of the calibration curve. The non-linearity of the SPR calibration occurs for refractive index calibration spanning over differences of > 0.02 RIU. The sensitivity to refractive index was measured at 12.5 RIU^{-1} with the (a-b)/(a+b) algorithm. The response measured with this data processing algorithm is unitless.

3.4.3 β-lactamase biosensing

The SPR instrument is characterized for biosensing with a model biological system. A bioassay for β-lactamase is performed with the immobilization of anti-β-lactamase on a monolayer of N-hydroxysuccinimide ester of 16-mercaptohexadecanoic acid (NHS-MHA). Immobilization of antibodies to a NHS-MHA monolayer has been demonstrated to maximize sensitivity in a direct bioassay format [137]. Resistance to traditional antibiotics is common in patients. The presence of β-lactamase is one of the most common factor in antibiotic resistance [138]. However, the detection technique for antibiotics resistance still relies on standard microbiological methodologies, limiting the time required to perform the assay and the throughput of the assay for antibiotics resistance.

Hence, detection of β-lactamase using SPR biosensors would offer improved methodology to quantify β-lactamase compared to actual detection techniques [139].

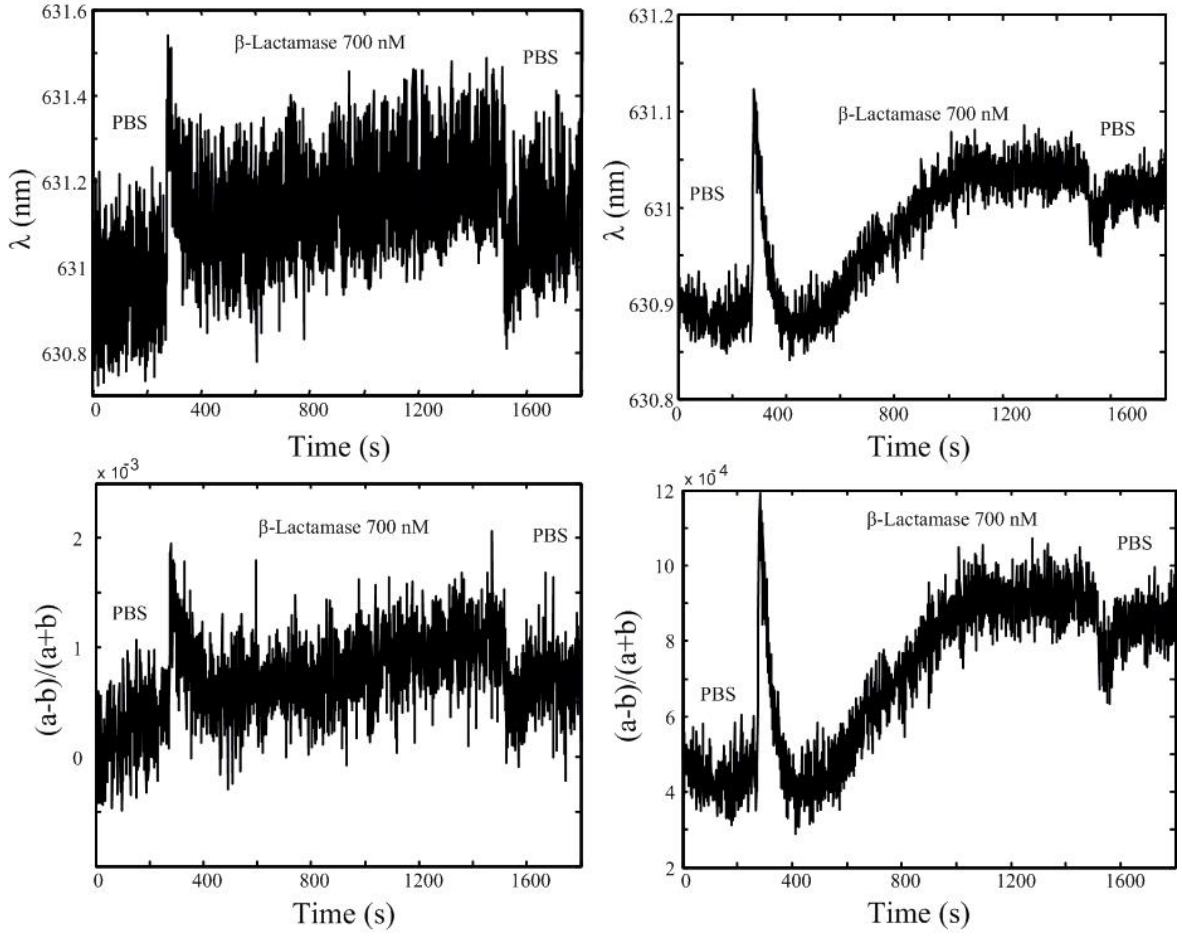

Figure 3-5. Measurement of β-lactamase in PBS at nM levels using the dove prism SPR: (top left) minimum hunting algorithm (relative error = 21%), (top right) minimum hunting algorithm with singular value decomposition (relative error = 3.9%) and (bottom left) (a-b)/(a+b) algorithm (relative error = 13%) (bottom right) (a-b)/(a+b) algorithm with singular value decomposition (relative error = 3.7%).

The detection of β-lactamase was performed in a phosphate buffer saline (PBS) solution at nM concentration (Figure 3-5). β-lactamase was measured without the flow cell, in a diffusion limited regime. Each data analysis methodologies were used to process data. A significant improvement of the noise level is observed in the response of the β-lactamase

biosensor. The binding event of β-lactamase is undistinguishable using the minimum hunting procedure. The change of the SPR response between the PBS measured after β-lactamase binding and from the baseline prior to binding of β-lactamase is 0.17 ± 0.03 nm. The error represents two standard deviations on the mean and a relative error of 21 %. Denoising data with singular value decomposition significantly improves the signal to noise ratio. The β-lactamase binding curve is clearly observed following denoising. The change of the SPR response is then 0.127 ± 0.005 nm, resulting in a reduced relative error at 3.9%. The algorithm (a-b)/(a+b) reduces also the noise level on the binding curve of β-lactamase compared to the minimum hunting procedure. The response measured is $6.4 \pm 0.8 \times 10^{-4}$ (unitless) with (a-b)/(a+b). Hence, the relative error is 13%, less than with the minimum hunting procedure. However, this is still too large to observe the binding curve for β-lactamase. Denoising the data with singular value decomposition reduces the noise to a level equivalent to minimum hunting. The response measured for β-lactamase binding is $4.05 \pm 0.15 \times 10^{-4}$ (unitless). Hence, denoising the data also improves the signal to noise of the binding curve with (a-b)/(a+b) with a relative error of 3.7%. Measurement of a dynamic process results in a similar relative error between minimum hunting and the (a-b)/(a+b) algorithms. The error is mainly due to the accuracy of the measurement.

3.4.4 SPR imaging

SPR imaging increases in popularity due to the multiplex array format allowing for the analysis of multiple molecules simultaneously in a single sample. The SPR instrument based on the dove prism can be readily modified to an imaging configuration with the replacement of the collection fiber – spectrophotometer with a bandpass filter and an imaging camera. Thus, a 610 ± 10 nm bandpass filter was mounted between the dove

prism and an imaging CCD camera. The collimated light entering the dove prism is inverted through the prism with retention of spatial information. Hence, an image of the SPR surface can be obtained with this configuration of the instrument. As an example, the SPR image of individual water droplets on the Au surface of the SPR sensor was acquired with this configuration of the SPR instrument (Figure 3-6). The image represents an area of approx. 1 cm². The spatial resolution of the image can be improved using telescopic lenses to zoom on the surface. The absorbance measured for each of the six droplets is constant at 0.0317 ± 0.0012 absorbance units. Denoising the raw data with singular value decomposition reduces significantly the noise on the SPR image. Reconstitution of the SPR image required the use of the first five components to avoid loss of chemical information. With typical SPR spectra (Figure 3-2 and 3-3), the first three components adequately reconstitute the spectra without loss of chemical information. However, the higher degree of complexity of the SPR image requires a larger number of components to adequately reconstitute the image.

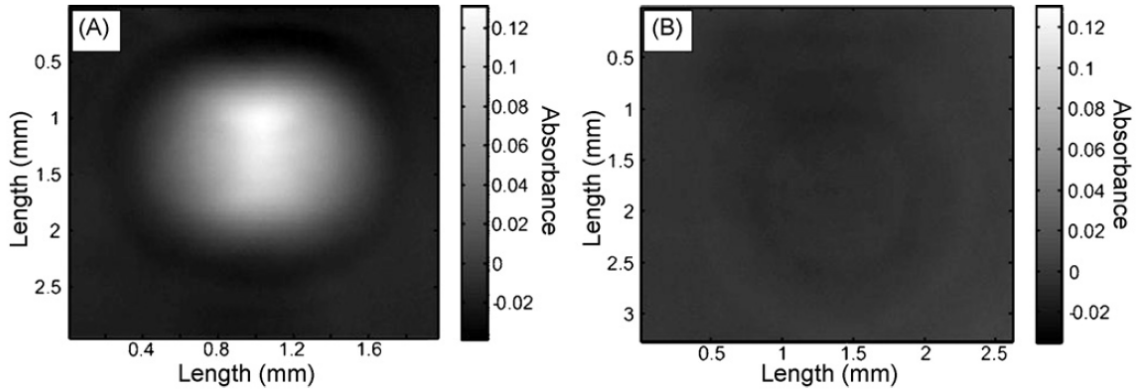

Figure 3-6. (A) SPR image of a water droplet on a Au film and (B) total internal reflection image of a water droplet on a glass slide.

3.5 CONCLUSIONS

A versatile SPR instrument was designed to perform biosensing with the wavelength interrogation and imaging configurations. The SPR instrument combines low cost and off-the-shelf components with high resolution of the measured response. Depending on the data analysis methodology employed to process raw SPR spectra, the resolution varies between 3 x 10^{-6} RIU and 1.5 x 10^{-7} RIU. Fitting a second-order polynomial to the SPR spectra results in a resolution lower than using the (a-b)/(a+b) algorithm. Denoising the data with singular value decomposition and reconstitution with the components containing the chemical information improves the resolution by approx. one order of magnitude. Therefore, the combination of (a-b)/(a+b) and denoising with singular value decomposition increases the resolution. Depending on the spectrophotometer employed, the refractive index accessible ranges from 1.33 to 1.39 RIU with a 550-850 nm spectrophotometer and from 1.33 to 1.42 RIU with a 550-1100 nm spectrophotometer. The measurement of repetitive injection of PBS is demonstrated with a custom-built flow cell. The reproducibility of the measurement is < 1 % with the dove prism SPR instrument. A β-lactamase sensor was constructed with anti-β-lactamase immobilized on a NHS-MHA monolayer. Detection of nM β-lactamase was performed in saline solution. Finally, the SPR instrument was modified to measure the SPR image of water droplets. It could be ultimately envisioned to locate a beam splitter between the dove prism and collection optics to select on a single platform either the conventional SPR spectroscopy or the SPR imager. Hence, the SPR instrument has the versatility of accomplishing traditional and imaging SPR measurements with high resolution using a single instrumental template.

3.6 ACKNOWLEDGEMENTS

The authors thank Martin Lambert, Louis Beaumont and Yves Teasdale for technical support with construction of element from the SPR instrument. Financial support was provided by the Université de Montréal, the Fonds Québécois de la Recherche sur la Nature et les Technologies (FQRNT) and the Canadian Foundation for Innovation (CFI).

CHAPITRE 4 : Monolayers of 3-mercaptopropyl – amino acid to reduce nonspecific adsorption of serum proteins on the surface of biosensors[104]

Publié en tant que : Bolduc, O. R.; Masson, J.-F. *Langmuir* **2008**, *24*, 12085-12091.

4.1 ABSTRACT

Monolayers prepared with polar or ionic amino acids with short side chains have reduced nonspecific adsorption of serum proteins compared to hydrophobic amino acids and organic monolayers immobilized on the gold surface of surface plasmon resonance (SPR) biosensor. Proteins contained in biological samples adsorb on most surfaces, which in the case of biosensors causes a nonspecific response hindering the quantification of biomarkers in these biological samples. To circumvent this problem, self-assembled monolayers (SAM) of N-3-mercaptopropyl amino acids (3-MPA-amino acids) were prepared from 19 natural amino acids. These SAM were investigated to limit nonspecific adsorption of proteins contained in biological fluids and to immobilize molecular receptors (e.g. antibodies) necessary in the construction of biosensors. SPR and Ge attenuated total reflection (GATR) FTIR spectroscopy were employed to characterize the formation of the amino acid SAMs. Monolayers of 3-MPA-amino acids are densely packed on the surface of the SPR biosensors with a surface concentration of approx. 10^{15} molecules/cm². SPR also quantifies the surface concentration of serum proteins nonspecifically adsorbed on 3-MPA-amino acids following exposition of the biosensor to undiluted bovine serum. The concentration of nonspecifically bound proteins ranges from approximately 400 ng/cm² with polar and ionic amino acids to 800 ng/cm² with amino acids of increased hydrophobicity. Nonspecific adsorption of serum proteins on the 3-MPA-amino acids increases with the following order: Asp - Asn - Ser - Met - Glu - Gln - Thr - Gly - His - Cys - Arg - Phe - Trp - Val - Pro - Ile - Leu - Ala - Tyr. Analysis of the adsorption and desorption curves for serum proteins on the SPR sensorgram has demonstrated a strong irreversibility of the protein adsorption on each surfaces. The effective hydrophilicity of the

SAMs was measured from the contact angle with a saline buffer and demonstrated a predictability of the resilience to the adsorption of serum proteins for the 3-MPA-amino acid SAMs. The antibody for β-lactamase was immobilized on a 3-MPA-glycine SAM and β-lactamase was detected in nM range. The presence of β-lactamase is an indicator of antibiotic resistance.

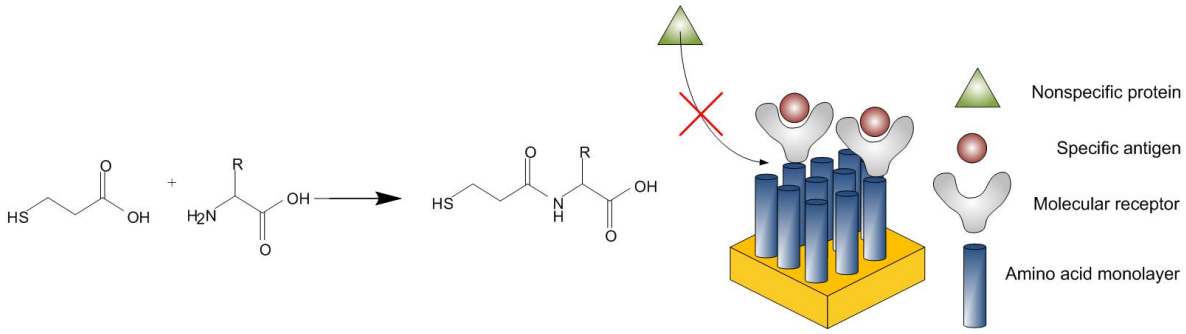

Figure 4-1. Schematic representation of 3-mercaptopropyl – amino acid reducing nonspecific adsorption of serum proteins

4.2 INTRODUCTION

Surface plasmon resonance (SPR) is a promising detection technique to fulfill current needs in the healthcare industry for rapid, inexpensive and diagnostic measurement of biomarkers present in biological samples [18, 19, 140]. SPR measures biomarkers (e.g. antigens, DNA, RNA or enzymes) at concentrations in the order of pM or nM in saline solutions. However, biological samples typically consist of a relatively complex mixture of compounds, including a high concentration of non-specific proteins, e.g. cell culture media contains 1-10 mg/mL of proteins [118] and serum contains 40-80 mg/mL of proteins [119]. Moreover, proteins contained in biological samples tend to adsorb nonspecifically to surfaces [141, 142], a process initiating a cascade of phenomenon leading to rejection of foreign object in human body, such as prosthesis. This problem is not only confined to prosthesis or

implants rejection, but also limits the use of many biosensing platforms for analyses in biological samples. The onus of this problem is due to adsorption of proteins on the surface of biosensors leading to a nonspecific response of the biosensor, which is undistinguishable from the response resulting from the binding of a specific biomarker. In the case of SPR biosensors, the molecular receptor immobilized on the surface of the SPR biosensor recognizes a unique unlabeled biomarker in the solution. Binding of the biomarker to the molecular receptor changes the refractive index of the solution near the biosensor; resulting in a measurable change of the optical response with SPR. This RI change is recorded in real-time to monitor specific binding of the biomarker and to determine the concentration of biomarkers in solutions. However, the adsorption of non-specific proteins contained in biological samples is also causing a change of refractive index, masking the response from the biomarker [143]. This effect has currently limited SPR biosensing and other biosensing technologies to mostly saline solutions or relatively diluted biological solutions [119]. Dilution of biological samples is usually not an option in bioanalysis, due to a relatively low concentration of biomarkers in the biological solutions. Therefore, the reduction of protein adsorption on metallic surfaces is an important stake for many medical applications, especially to extend the life of prosthesis and to improve the utility of biosensors with biological samples.

SPR biosensors are constructed with a gold thin film immobilized on a dielectric material. Thiol chemistry forms a stable chemical linker on Au surfaces and it is typically used to immobilize an antibody on the Au film [26, 144, 145]. Several approaches have been designed to immobilize antibodies to surfaces including but not limited to: immobilization on a thiol [146], on a polymer derived with a thiol [147, 148], on a polysaccharide immobilized to

a thiol [149], or using streptavidin immobilized to a thiol [150]. With each methodologies utilized to immobilize the antibody, the chemical layer serves a dual function on the surface; it must immobilize a maximal concentration of antibodies to increase the signal of the biomarker and it must eliminate non-specific adsorption of proteins. Many SAMs have been successfully developed for each purpose individually. However, there is no unique monolayer exhibiting satisfactory functionality for both purposes simultaneously. As an example, a 3-dimensional matrix of CM-dextran exhibits a large response from biomarkers, due to the immobilization of a large concentration of antibodies to the CM-dextran matrix [149]. However, CM-dextran does not perform well in complex solutions[147]. Otherwise, various approaches were exploited in order to reduce nonspecific protein adsorption, with the most promising one using poly(ethylene oxide) (PEO) to coat surfaces [151-153]. Among the strategies explored, Whitesides et al. used zwitterionic [67] molecules and explored a vast library of functional groups as terminal groups at the surface of biosensors [64]. They found that hydrophilic monolayers with hydrogen bond donors and no hydrogen bound acceptors, and neutral monolayers exhibited improved reduction of nonspecific adsorption of fibrinogen and lysozyme [64, 65, 154-156]. It was also proposed to use alkanethiols of different lengths to limit the effect of serum protein on SPR biosensors [137]. A membrane cloaking methodology was recently developed to remove nonspecific adsorption after a sample was exposed to biological fluid, without disrupting the biomarker bound to the molecular receptor [68]. In spite of these results, the mechanism of protein adsorption is not clearly understood [63]. It is suggested that different proteins consecutively adsorbs at surfaces, starting with the most prominent protein in serum, albumin, followed by larger proteins such as IgG and fibrinogen [141, 142]. This proteins cascade at the surface is the first step

towards cell adhesion on surfaces. This plenitude of species contributing to nonspecific adsorption requires a model system with protein content similar to human serum. Therefore, the nonspecific adsorption of serum protein must be investigated using undiluted serum, such that nonspecific adsorption is measured in condition similar to biological samples.

A novel approach uses biological building blocks to build monolayers and has been the focus of research in mitigating the nonspecific adsorption from proteins contained in biological samples. Of particular interest, Statz and al. synthesized peptidomimetic polymers of alternating L-3,4-dihydroxyphenylalanine (DOPA) and lysine residues to minimize cell adhesion [157]. Thereby, they have shown a reduction of cell adhesion by two orders of magnitude compared to current state-of-the-art methodologies. Otherwise, it was demonstrated that a pentapeptide inhibits aggregation of gold nanoparticles and it also serves as a chemical layer to build a biosensor [158, 159]. Hence, amino acids or peptides monolayers have great potential for biosensing: they are biocompatible, a wide selection of functional groups is available, such that they have tunable chemical properties and they can be utilized in the construction of biosensors with the immobilization of antibodies on the terminal carboxylic acid of amino acids or short peptides. Natural amino acids have a broad range of structural and chemical properties, with amino acids having either short or long side chains, hydrophobic or polar side chains and neutral or ionic side chains. These properties of amino acids make them highly suitable candidates for the determination of chemical structure-nonspecific adsorption investigations and they possess the chemical characteristics necessary for biosensing purposes. An amino acid monolayer may improve activity retention of immobilized molecular receptors, by providing a “protein-like”

environment at the surface. These characteristics are essential for the development of functional biosensors in real biological samples. However, no study has demonstrated the efficacy of amino acids monolayers to reduce nonspecific binding from serum proteins and to immobilize an antibody for the measurement of a biomarker.

This article demonstrates that polar or ionic amino acids attached to 3-mercaptopropionic acid significantly limit nonspecific adsorption from serum proteins. The hydrophilic properties of each SAM were measured using contact angle, which demonstrated that the SAM with larger hydrophilic character reduces the nonspecific response from bovine serum. The potential of such SAMs for SPR biosensing is demonstrated with an affinity biosensor using an antibody specific to β-lactamase attached to a 3-MPA-Gly monolayer. The presence of β-lactamase is one of the most common factor in antibiotic resistance [138]. Standard detection techniques for β-lactamase involve cellular culture which makes these tests unsuitable for the analysis of a large amount of samples and to obtain a rapid response of the β-lactamase concentration. Therefore, it is imperative to develop improved detection techniques of β-lactamase to reduce the response time of medical personnel for patients exhibiting resistance to traditional antibiotics. Detection of this enzyme directly into blood or blood-borne samples using SPR biosensors would offer improved methodology to quantify β-lactamase compare to actual detection techniques [139].

4.3 EXPERIMENTAL SECTION

4.3.1 Preparation of 3-MPA-amino acids

Glu, Asp, Asn and Gln were purchased in the acidic form and reacted to form the methylester on the free carboxylic acids using thionyl chloride ($SOCl_2$, Fluka purity > 99%)

in methanol (Fisher Sientific) [160]. This operation was necessary to avoid polymerization of the amino acids. 3-mercaptopropionic acid (3-MPA) was purchased from Sigma-Aldrich with a purity exceeding 99% and used without further purification. Careful handling of 3-MPA must be taken when brought to solution since this liquid is stenchful. A solution containing 2.4 mmol of 3-MPA was quickly prepared with 7.5 mL of N,N-dimethylformamide (DMF, EMD). Another solution containing 1.2 equivalent (2.9 mmol) of 4-(dimethylamino)pyridine (DMAP, Fluka purity > 98%) and 1.1 equivalent (2.6 mmol) of N,N'-dicyclohexylcarbodiimide (DCC, Sigma-Aldrich purity > 99%), 1.1 equivalent (2.6 mmol) of the amino acid were then dissolved with 7.5 mL of DMF [161]. A sonification bath was used to dissolve the reaction mixture. The amino acids used as methylester hydrochloride (Sigma-Aldrich or Fluka), requiring the use of > 1 equivalent of DMAP to neutralize the hydrochloride and to catalyze the reaction. The 3-MPA and DMAP-DCC-amino acid solutions were mixed at a ration of 1:1 and thereafter stored at room temperature, away from excessive light and without agitation for an overnight period. Each reaction mixture was thereafter filtered to remove the DCC-urea precipitated during the reaction. The solution was then evaporated to obtain a white solid with a creamy texture. The FTIR spectrum for each 3-MPA-amino acid was acquired using a FT-IR with Ge attenuated total reflection (GATR) (Bruker optics) to insure the completeness of the reaction.

4.3.2 Preparation of 3-MPA-amino acid monolayer

Solutions of 5 mM of 3-MPA-amino acid were prepared in absolute ethanol to form a monolayer on microscope slides (BK7, 22x22 mm, Fisher Scientific) coated with a 5 nm Cr adhesion layer and 48nm of Au (ESPI metals) using a Cressington 208HR sputter

coater. Each amino acid was tested with 4 replicates. The solution of 3-MPA-amino acid was reacted for at least 16 hours to form a well-ordered monolayer [148]. Thereafter, each sample was rinsed with Millipore water and was submerged in a 0.01 M HCl solution for two hours to hydrolyze the methylester and result in the unprotected carboxylic acid on the surface of the SAM. Absolute ethanol was then used to wash each sample. The reaction was followed using SPR spectroscopy and FTIR-GATR to insure completeness.

4.3.3 SPR and contact angle measurements

The advancing contact angle was measured for each sample with a contact angle instrument built in-house. The contact angle was obtained from 300 μL of PBS (CellGro, Mediatech inc.). PBS was used to measure the contact angle in a solution of salinity and pH similar to serum or other biological samples. The slides were then mounted on a custom-made SPR instrument constructed with a modified prism-based geometry using wavelength interrogation. The SPR sensors were stabilized in PBS buffer for 5 minutes before the spectral reference in s-polarization was acquired. Real-time measurement then started in p-polarization for 5 minutes before replacing the PBS buffer with bovine serum (Sigma) containing 76 mg/mL of protein for 20 minutes. The serum was then replaced with PBS for another 5 minutes to be able to quantify the amount of protein still attached to the surface of the SAM. Raw data were then processed with MatLab. This procedure was repeated for each of the 19 natural amino acids, in order to obtain at least three experimental curves for each amino acid.

4.3.4 Measurement of bovine serum protein desorption with high salinity PBS

In order to obtain information about the nature of the interaction between 3-MPA-amino acid and serum protein, the irreversibly adsorbed proteins immobilized on 3-MPA-Ser were exposed to a PBS enriched with 1 M sodium chloride (Sigma-Aldrich, purity > 99.5%). Increasing the ionic strength may remove adsorbed proteins [64]. This experiment was conducted on a 3-MPA-Ser that was exposed to the bovine serum using the same conditions as described above. After 5 minutes in unspiked PBS, the solution was replaced with the NaCl-enriched PBS for 5 minutes and then exposed again with unspiked PBS for another 5 minutes to obtain the amount of protein desorbed.

4.3.5 Immobilization of anti-β-lactamase

The antibody specific for β-lactamase (QED Bioscience inc.) was immobilized on 3-MPA-Gly to demonstrate the use of 3-MPA-amino acid SAMs for the construction of a biosensing layer. β-lactamase was prepared according to Pelletier et al. [162, 163]. The 3-MPA-Gly samples (four replicates) were prepared as described above. Two different approaches were used to immobilize the antibody, both based on the reaction of 3-MPA-Gly with N-hydroxysuccinimide (NHS, Sigma-Aldrich purity > 98%) chemistry [164-166]. This results in activation of the free carboxylic acid of 3-MPA-Gly, in the form of 3-MPA-Gly-NHS. The first approach allowed 3-MPA-Gly to react for 20 minutes in an aqueous solution composed of 25 mM NHS and 25 mM N-Ethyl-N'-(3-dimethylaminopropyl)carbodiimide (EDC, Fluka purity > 97%) [167]. The second approach involved the reaction of 3-MPA-Gly with 75 mM of DCC and 75 mM of NHS overnight. NHS and EDC or DCC were all used in large excesses compared to 3-MPA-Gly to insure

an optimal number of binding sites would be available for antibody attachment. Thereafter, the antibody specific to β-lactamase was diluted in sterile PBS to a concentration of 37 µg/mL and reacted overnight with 3-MPA-Gly-NHS on samples previously rinsed with PBS. Each step involving the antibody or an antibody-derived sample were accomplished in a refrigerated laboratory at 4°C, unless otherwise indicated [168]. Thereafter, the samples were rinsed with PBS and reacted for 10 minutes in a 1 M aqueous solution of ethanolamine hydrochloride (Sigma-Aldrich) adjusted at a pH of 8.5 with 10 M NaOH (Fluka purity > 98%). This step deactivates unreacted NHS remaining on the surface after antibody immobilization [169]. The slides are stored in PBS at 4°C for at least 60 minutes prior to use.

4.3.6 Detection of β-lactamase

A solution at 909 nM of β-lactamase was prepared in PBS at 4°C by the dilution of a stock solution. This solution is kept at 4°C until 20 minutes prior to use, then equilibrated at room temperature. A sample with the β-lactamase specific monolayer was mounted on the SPR instrument and room temperature PBS was placed on the sample for 10 minutes, in order to stabilize the sensor. A spectral reference (s-polarized light) was acquired immediately before the real-time measurement started. PBS was measured for 5 minutes to acquire the baseline response and was thereafter replaced with the β-lactamase solution for 20 minutes. Finally, the sensor was placed again in PBS for 5 minutes verifying if the binding between the anti-β-lactamase and β-lactamase was reversible.

4.4 RESULTS AND DISCUSSION

4.4.1 FTIR characterization of the 3-MPA-amino acids SAM

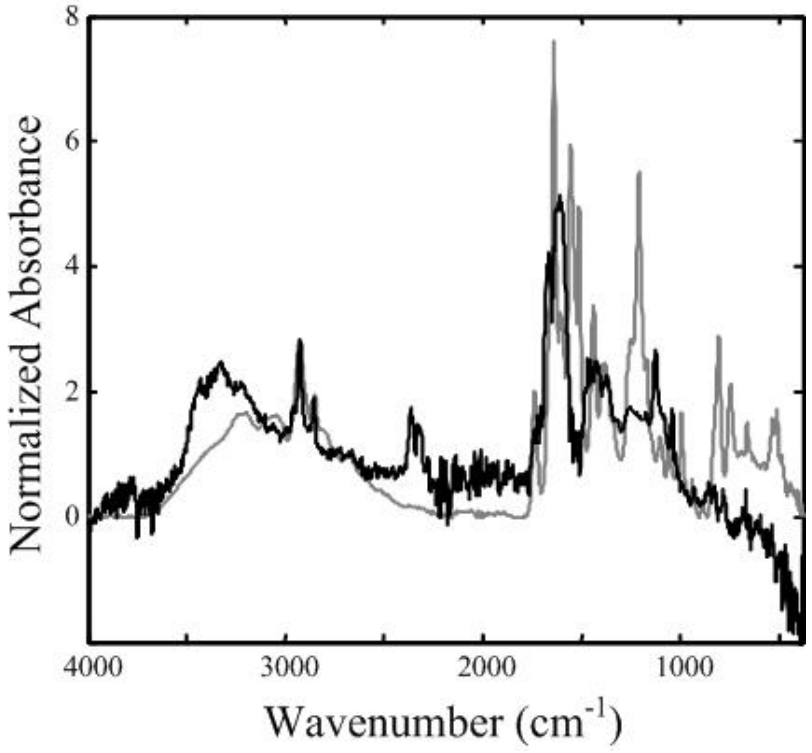

Figure 4-2. GATR FT-IR obtained for a complex 3-MPA-Tyr in solution (thin line) and on a microscope slide coated with 48 nm of gold (thick line).

The preparation of 3-MPA-amino acids was performed in a DMF solution using DCC coupling and DMAP catalysis. DMAP was added at greater than 1 equivalent; the first equivalent serves to neutralize the hydrochloride of the methylester-amino acid and the small excess catalyzes the reaction. The reaction is performed with the methylester of the amino acid to avoid formation of an oligopeptide. However, lysine has yielded a mixed oligopeptide and it will not be included in these experiments. The synthesis of 3-MPA-amino acids resulted in excellent yields (> 90%). The IR spectra for the product of the reaction between 3-MPA and the amino acid were obtained to confirm the formation of 3-

MPA-amino acids. The carbonyl band was the focus of the FTIR analysis, as it clearly shows the formation of an amide bond (typically 1630-1680 cm^{-1}) from the carboxylic acid of 3-MPA (typically 1740-1800 cm^{-1}). The C=O stretching band originally at 1720 cm^{-1} for the carboxylic acid shifted to 1640 cm^{-1}, confirming the formation of the amide bond expected for the 3-MPA-amino acids. A C=O band is also observed at 1740 cm^{-1}, corresponding to the methylester form of the amino acid (typically 1730-1750 cm^{-1}). Since every IR spectra were confirmatory for the preparation of 3-MPA-amino acid in the methylester form, a monolayer was formed for each of these products on the Au surface of SPR biosensors. The formation of each monolayer was also confirmed by GATR FTIR. The spectra were acquired directly on the Au slide covered with the SAMs using GATR FTIR. Figure 4-2 shows the spectra obtained for 3-MPA-Tyr in the methylester form in solution and for the monolayer. Both spectra overlay well, with the bands at 1740 cm^{-1} and 1640 cm^{-1} being present in both spectra, confirming the formation of the 3-MPA-Tyr monolayer. The relative intensity of each band usually vary between a FTIR spectrum acquired in solution compared to the FTIR spectrum acquired in the solid phase of a monolayer, as observed in this case. The absorbance signal around 2400 cm^{-1} was a characteristic of CO_2 present during the measurement. The noise present in the spectrum of a 3-MPA-Tyr in the methylester form of the monolayer is mainly due to water absorption. Lastly, the spectrum of the 3-MPA-amino acid following hydrolysis was acquired as a monolayer on Au to confirm completeness of the reaction of the 3-MPA-amino acid in the methylester form with HCl. The CH_3 stretching band at 2852 cm^{-1} observed in Figure 4-2 is characteristic of a CH_3 attached to an oxygen atom such as in the methylester form of 3-MPA-amino acid. Following the reaction with HCl, this band is no longer present

confirming the hydrolysis of the methylester to the carboxylic acid form. Thereby, the FTIR spectra are confirming the presence of each 3-MPA-amino acid on the Au surface of SPR biosensors.

4.4.2 SPR characterization of 3-MPA-amino acids SAM

The SPR response ($\Delta\lambda_{SPR}$) during binding of the 3-MPA-amino acids is a measure of the surface coverage of the SAM. The SPR response is calculated from the SPR response in PBS of a bare gold surface and the SPR response in PBS from the 3-MPA-amino acids SAM. The difference in these measurements results in $\Delta\lambda_{SPR}$. To obtain the surface concentration (Γ) for each SAM from the change in SPR wavelength, the equation from Jung and al. was employed [147, 170].

$$\Gamma = \rho\left(\frac{-l_d}{2}\right) ln\left(1 - \frac{\Delta\lambda_{SPR}}{m(\eta_{SAM} - \eta_{PBS})}\right) \qquad (4\text{-}1)$$

The sensibility (m) of the current SPR biosensor was measured at 1765 ± 100 nm/RIU using sucrose solutions. The refractive index of PBS buffer (η_{PBS}) was experimentally measured at 1.33476 ± 0.00002 RIU with a high resolution refractometer. The penetration depth of plasmons (l_d) is approximately 230 nm (use 2.3 x 10^{-5} cm in eq. 3-1) at the experimental SPR wavelength (λ = 630 nm), the refractive index of thiols (n_{SAM}) is 1.45 RIU and their density (ρ) is 0.9 g/cm³ [26]. The surface concentration for each 3-MPA-amino acid is obtained in ng/cm² and it is thereafter converted in molecules/cm² with the molar mass and the Avogadro number (Table 4-1). The surface concentration of 3-MPA-amino acid SAM varies between 0.18 – 1.80 x 10^{15} molecules/cm², indicating that dense monolayers are formed on the surface of the SPR biosensors. In general, small aliphatic

amino acids, aromatic amino acids capable of hydrogen bonding, glutamic acid and glutamine form denser layers. Alcohols, sulfur-containing and basic amino acids form lesser dense layers.

Table 4-1. Surface concentration of 3-MPA-amino acids on the SPR biosensors

	Amino Acid	Γ_{SAM} (10^{15}molecules/cm²)		Amino acid	Γ_{SAM} (10^{15}molecules/cm²)
Hydrophobic	Gly	1.39	**Polar**	Met	0.63
Aliphatic and Aromatics	Ala	1.80	Alcohols, sulfur-containing and amides	Cys	0.35
	Val	1.00		Ser	0.29
	Leu	0.79		Thr	0.18
	Ile	0.68		Gln	1.47
	Pro	0.58		Asn	0.72
	Phe	0.52	**Ionic**	Asp	0.61
	Tyr	1.12	Acids and bases	Glu	1.05
	Trp	1.25		His	0.34
				Arg	0.19

Aliphatic amino acids form denser layers with shorter side chains. The steric hindrance prohibits larger side chains to form well-packed monolayers. Therefore, it follows the expected order of Gly > Val > Leu > Ile > Pro, with the exception of Ala which forms the densest monolayer of every amino acids, while having the second shortest chain to Gly. Steric hindrance of the phenyl group on Phe results in the smallest monolayer density of the aromatic amino acids. Although Tyr (1.12 x 10^{15} molecules/cm²) and Trp (1.25 x 10^{15} molecules/cm²) should have greater steric hindrance and form lesser dense

monolayers than Phe (0.52 x 10^{15} molecules/cm²), the SAMs are denser due to hydrogen bonding between the side chains, facilitating the packing of 3-MPA-Tyr and 3-MPA-Trp at the surface. Alcohols and sulfur containing SAM forms most of the lesser dense monolayers. In the case of Cys, the possibility of forming two Au-S bond result in a poor packing at the surface. The amides forms denser monolayers than their corresponding acids (Gln > Glu and Asn > Asp), while basic monolayers do not form well-packed monolayers. The side chains of His and Arg are long and bulky, limiting the packing of these monolayers on the surface of SPR biosensors.

4.4.3 Nonspecific adsorption of serum proteins on surfaces

Adsorption of serum proteins to surfaces is a critical problem to solve, in order to develop biosensors working in biological fluids. The model system used in this study is bovine serum as previously reported elsewhere [137, 147]. Bovine serum has a total protein concentration (76 mg/mL) near human serum with a protein composition similar to human serum, therefore providing a good model system for use of biosensor in human biological fluid. Thus, adsorption of bovine serum protein was measured for each 3-MPA-amino acid monolayer and with 16-mercaptohexadecanoic acid (MHA). MHA will serve as a comparison point with previous studies. MHA had previously exhibited low nonspecific adsorption [137].

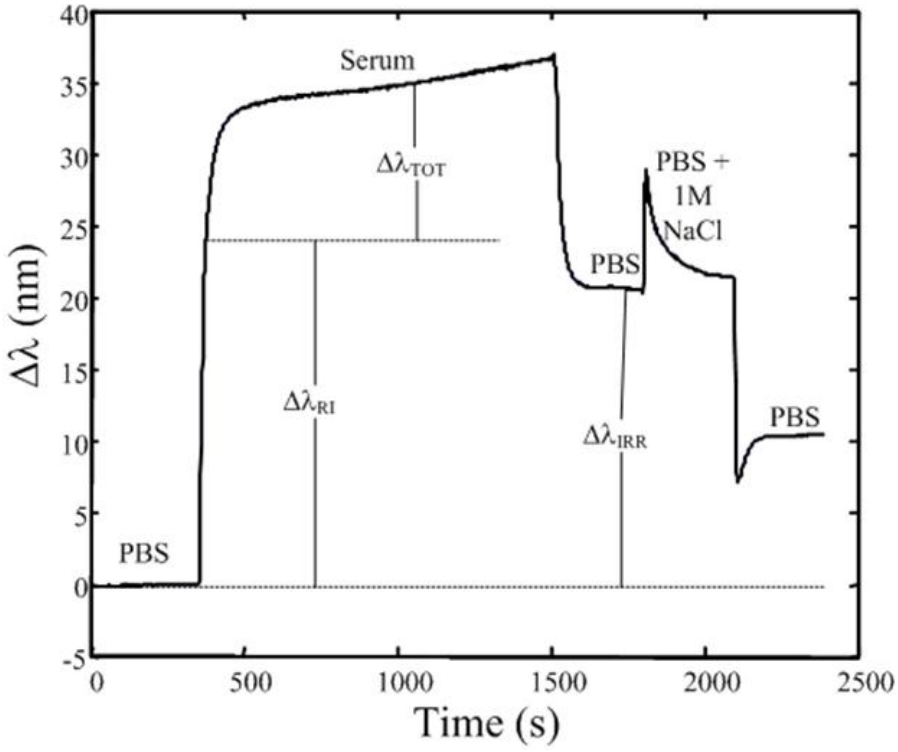

Figure 4-3. Kinetic curve obtained for a 20 minutes exposure of bovine serum followed by a 5 minutes exposure of enriched PBS buffer on a 3-MPA-Ser SAM.

The surface concentration for the total protein concentration (Γ_{TOT}) bound to each surface, the fraction irreversibly (Γ_{IRR}) bound to each surface and the fraction reversibly (Γ_{REV}) bound were extracted from the SPR kinetic curves (Figure 4-3). These values are obtained from the change in SPR wavelength. The difference between $\Delta\lambda_{TOT}$ and $\Delta\lambda_{IRR}$ results in $\Delta\lambda_{REV}$. The shift $\Delta\lambda_{RI}$ was due to the refractive index difference of PBS and bovine serum. The parameters to calculate the surface coverage of an adsorbed protein layer are (see equation 1 above): refractive index of proteins ($n_{protein}$) is 1.57 RIU and their density (ρ) is 1.3 g/mL [170].

4.4.4 Adsorption of serum protein – Hydrophobic amino acids

Table 4-2. Nonspecific binding of bovine serum proteins and advancing contact angle on 3-MPA-AAs

	Amino acid	$\Delta\Gamma_{total}$ (ng/cm^2)	$\theta_{c\_advancing}$ (°)		Amino acid	$\Delta\Gamma_{total}$ (ng/cm^2)	$\theta_{c\_advancing}$ (°)
Hydrophobic	Gly	473 ± 133	52 ± 3	**Polar**	Met	422 ± 76	43 ± 2
Aliphatic and Aromatics	Ala	740 ± 75	60 ± 1	Alcohols, sulfur-containing and amides	Cys	515 ± 146	46 ± 1
	Val	614 ± 95	56 ± 3		Ser	419 ± 33	38 ± 4
	Leu	706 ± 19	63 ± 1		Thr	462 ± 135	42 ± 3
	Ile	703 ± 57	58 ± 2		Gln	442 ± 70	53 ± 5
	Pro	702 ± 92	61 ± 4		Asn	417 ± 39	40 ± 4
	Phe	575 ± 202	67 ± 3	**Ionic**	Asp	416 ± 121	32 ± 2
	Tyr	808 ± 51	55 ± 3	Acids and bases	Glu	431 ± 24	38 ± 2
	Trp	588 ± 91	65 ± 2		His	486 ± 149	37,3 ± 0.3
					Arg	563 ± 140	33 ± 2

The chemical composition of the side chain of each amino acid greatly influences the properties of the monolayer immobilized on the SPR biosensors. The hydrophobic amino acids are comprised of the aliphatic and aromatic sub-groups. The side chain of hydrophobic amino acid immobilized at the surface of the SPR biosensor greatly influences the amount of serum proteins adsorbed (Table 4-2). The results are reported for 4 replicate measurements and the error indicates two standard deviations about the mean (95% confidence interval). The surface concentration of protein varies from 473 ng/cm^2 for glycine to 808 ng/cm^2 for tyrosine. Glycine is the simplest of amino acids, with side chain consisting of a hydrogen atom, has the lowest total surface concentration of nonspecifically

bound protein of aliphatic amino acids with 473 ± 133 ng/cm². Tyrosine has a bulkier phenolic side chain, has the largest surface concentration of bound serum protein with 808 ± 51 ng/cm². The series of aliphatic amino acids, Gly – Ala – Val – Leu – Ile – Pro, has a side chain of increasing size. The total surface concentration of bound proteins also increases with the series, except for Ala, which has the largest surface concentration of nonspecifically bound proteins. Also, it was noted above that Ala has the densest monolayer of the series, while the density decreases for other aliphatic amino acids with increasing side chain length. Thus, a combination of the steric hindrance and hydrophobicity of the side chain influence the nonspecific adsorption of proteins, but other factors may also be contributing to the process. The advancing contact angle is comprised between 52° and 63° for each of the aliphatic 3-MPA-amino acid monolayer. It was measured in PBS to evaluate the hydrophilicity of the monolayers in biological buffer, an environment similar to biological fluids. Hence, it is to be noted that the contact angle is relatively low, due to the rather polar character of each amino acid. This is explained with 3-MPA-amino acids having a carboxylic acid in their terminal position. Therefore, it is expected that the contact angle would be similar, with the small differences due to the change of the side chain composition.

In the case of aromatic amino acids, Phe and Trp exhibited similar resistance to nonspecific adsorption of serum proteins, with 575 and 588 ng/cm² of bound proteins at the surface. Tyr has the worst resistance to nonspecific adsorption of all amino acid tried, with 808 ng/cm² of bound proteins. The side chain of each aromatic amino acid has a different ionic character. Phe and Trp are neutral aromatic compounds while Tyr will be slightly negatively charged at physiological pH, from the phenolic side chain. The contact angle

suggests that Tyr is more polar that Phe and Trp, with a contact angle of 55° compared to 67° and 65° for Phe and Trp respectively. Thus, these observations indicate that the polarity of the side chain may also influence the resistance to nonspecific adsorption of serum proteins. A greater hydrophobicity of the side chain on the amino acids offered less resistance to the proteins adsorption. In the case of aromatic amino acids, the packing density of monolayers does not seem to have a strong influence, as Tyr and Trp exhibited similar monolayer density and they have a significantly different resistance to non-specific interactions.

4.4.5 Adsorption of serum protein – Polar amino acids

Polar amino acids are comprised of 3-MPA-amino acids with either alcohol, sulfur-containing or amide side chains. Ser and Thr differ by a methyl group, similarly to Asn and Gln. Met is a thioester and cyteine is a thiol. In the case of cysteine, three orientations of the monolayer are possible and probably found on the SPR biosensor; the thiol of 3-MPA may bind to Au, the thiol on the side chain may bind to Au, and a fraction may have both thiol bound to the surface. The small surface concentration of 3-MPA-Cys may have contributed to result in the worst nonspecific adsorption of proteins for polar amino acids, with 515 ng/cm² of nonspecifically bound proteins. Otherwise, 3-MPA-amino acid with a polar side chain exhibited good resistance to nonspecifically bound proteins. The surface concentration of the nonspecifically bound serum proteins for other polar 3-MPA-amino acids ranged from 417 ng/cm² to 462 ng/cm². This group of amino acids has relatively homogeneous resistance to nonspecific adsorption. However, it is to be noted that a *t-test* statistically confirms ($p<0.10$) that Ser has better nonspecific adsorption properties than Thr. Similarly, Asn has better resistance to nonspecific adsorption of serum protein than

Gln. Thr has a longer side chain and a worse monolayer density than Ser, while Gln also has a longer side chain but a better packing density than Asn. Contact angle measurements shows the same trend for Ser ($\theta_{c\_advancing}$ = 38°) compared to Thr ($\theta_{c\_advancing}$ = 42°) and for Asn ($\theta_{c\_advancing}$ = 40°) compared to Gln ($\theta_{c\_advancing}$ = 53°). Hence, the hydrophobicity is increased with a longer chain length. This supports the observation that the side chain length influences the nonspecific properties mostly due to the hydrophobicity of the chain length, with a greater importance than the packing density of the monolayer. This observation shows that in some cases, multiple factors contribute simultaneously to the nonspecific properties of 3-MPA-amino acids.

4.4.6 Adsorption of serum protein – Ionic amino acids

This group of amino acids contains the acidic and basic side chains of the 3-MPA-amino acids. Lys could not be synthesized and is not included in these results. Synthesis on resins using better protective groups may solve this problem. Similarly to polar amino acids, Asp (Γ_{TOT} = 416 ng/cm²) seems to result in greater resistance to nonspecific adsorption than Glu (Γ_{TOT} = 431 ng/cm²), although the error on the measurement cannot statistically confirm this. However, the difference in bound proteins between Asp and Glu seems to follow the same trend as previously observed with hydrophobic and polar side chains. Increasing the chain length by one methyl group increases the surface concentration of nonspecifically bound serum proteins on 3-MPA-amino acids, even if the packing density of Glu is greater than for Asp. The contact angle for Asp and Glu are 32° and 38°, indicating a slight increase in hydrophobicity with Glu. The basic side chains respectively have 486 ng/cm² and 563 ng/cm² of nonspecifically bound proteins. These surface concentrations of nonspecific serum proteins are greater than for the acidic and for most

polar side chains. Thus, it is observed that acidic and polar, with short side chains demonstrates improved performance in resisting proteins adsorption from serum.

4.4.7 Reversibility of the protein interaction

The chemical nature of the interactions between nonspecifically bound proteins and the surface may be interpreted from the reversibility or irreversibility of the nonspecific adsorption. The reversible adsorption of serum protein occurs with interaction at equilibrium in saline buffers, such as hydrogen bonding. Otherwise, the irreversible interactions occur from bonds that are more stable in aqueous environment, such as Van der Waals interactions or ionic attraction (if ionic strength is constant). Most interactions occurring on 3-MPA-amino acids monolayer are irreversible with 95% of nonspecifically bound proteins due to the irreversible interactions. This value is obtained from the average response for every 3-MPA-amino acid and no trend in the data was observed between amino acids. Increasing the ionic strength of PBS exposed to the 3-MPA-amino acids with the irreversibly bound proteins has provided insight on the nature of the irreversible interactions. A significant fraction (approx. 50%) of the irreversibly adsorbed proteins is removed from a highly ionic solution consisting of PBS spiked with 1 M NaCl. The proteins removed from high ionic strength are most likely to be bound with ionic interactions to the surface, while the proteins bound with Van der Waals interactions will remain adsorbed to the surface. Most proteins have hydrophobic, polar, and ionic regions, each contributing to the nonspecific adsorption phenomena. Therefore, an efficient monolayer to resist nonspecific adsorption of serum proteins must balance these interactions to a minimum.

4.4.8 Venn diagram of nonspecific adsorption

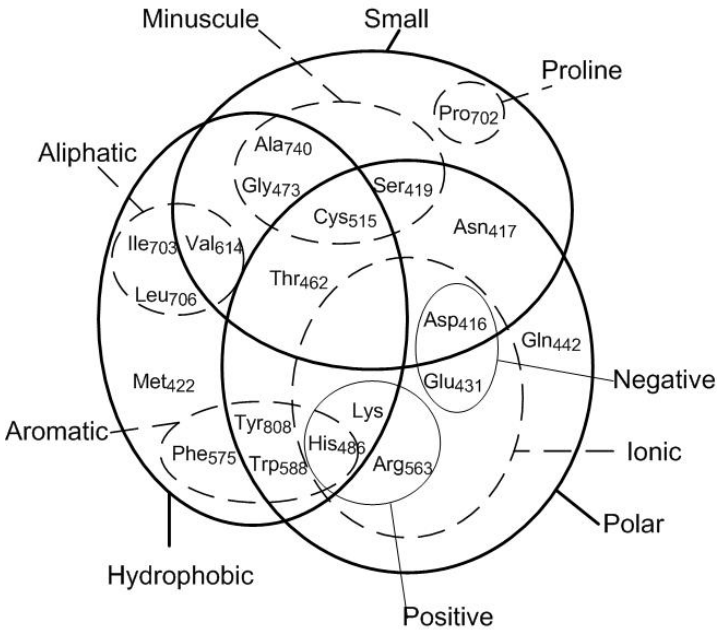

Figure 4-4. Venn's diagram representing nonspecific adsorption of serum proteins on 3-MPA-amino acids. The numbers associated with each amino acid represent the surface coverage induced by bovine serum proteins.

The relationship between the chemical groups on the side chain of the 3-MPA-amino acids and the resistance to proteins adsorption from serum is represented using a Venn's diagram of the chemical properties from natural amino acids (Figure 4-4). A Venn diagram uses the set theory to graphically show all the relationships between sets. Therefore, in the case of amino acids, it regroups various physical and chemical properties in sets with different levels of inclusion. The amino acids are regrouped in three main primary sets: small, hydrophobic and polar. The small set includes a minuscule and the proline sets. The hydrophobic primary set includes the aliphatic and aromatic secondary sets. The polar includes the ionic secondary set, which is composed of the positively and negatively charged ternary sets. Primary, secondary and ternary sets overlap with other sets.

The representation of the Venn diagram for amino acids shown in Figure 4-4 is according to Livingstone et al. [171].

Each 3-MPA-amino acid exhibiting improved resistance to nonspecific protein adsorption is clustered around a few physical and chemical properties. As discussed previously, smaller side chains on the amino acids performed better in resisting adsorption of serum proteins. An increased polarity also improves the resistance to nonspecific adsorption, especially for negatively charged ionic side chains and smaller polar side chains. It was noted that small molecules offer better performances then large or aromatic molecules. A few exceptions arise with the Venn diagram. Glycine, although it is considered hydrophobic by the Venn diagram classification, also offers a good resistance to nonspecific protein adsorption due to the smallness of the side chain. Met is another exception in the hydrophobic set according to the Venn diagram, which is among the best 3-MPA-amino acids to resists nonspecific adsorption of serum proteins. The contact angle is low for Met, indicating that the surface is more hydrophilic than hydrophobic. Therefore, Met is classified with the polar compounds in Table 4-1, within the sulfur containing group.

4.4.9 Advancing contact angle relationship with nonspecific adsorption

The advancing contact angles vary depending on the chemical composition of the side chain. With the measurement of contact angle in PBS, the values reported are an indication of the effective hydrophilicity of the surface. Lower contact angles indicate a surface with higher hydrophilicity. Therefore, polar 3-MPA-amino acids have lower contact angles in PBS than hydrophobic amino acids. A lower contact angle was also observed for side chain with identical chemical groups, but with shorter chain length. Hence, Figure 4-5

shows that amino acid with lower contact angles (more hydrophilic) are more efficiently resisting nonspecific adsorption. This observation is similar to the conclusions of Xu and Siedlecki [172]. The co-linearity of the contact angle measured in PBS and of the surface concentration of nonspecifically bound proteins indicates that the contact angle must be minimized in order to develop a 3-MPA amino acid surface that will resist nonspecific adsorption. The contact angle may be used as a quick measurement to predict the resistance of nonspecific adsorption.

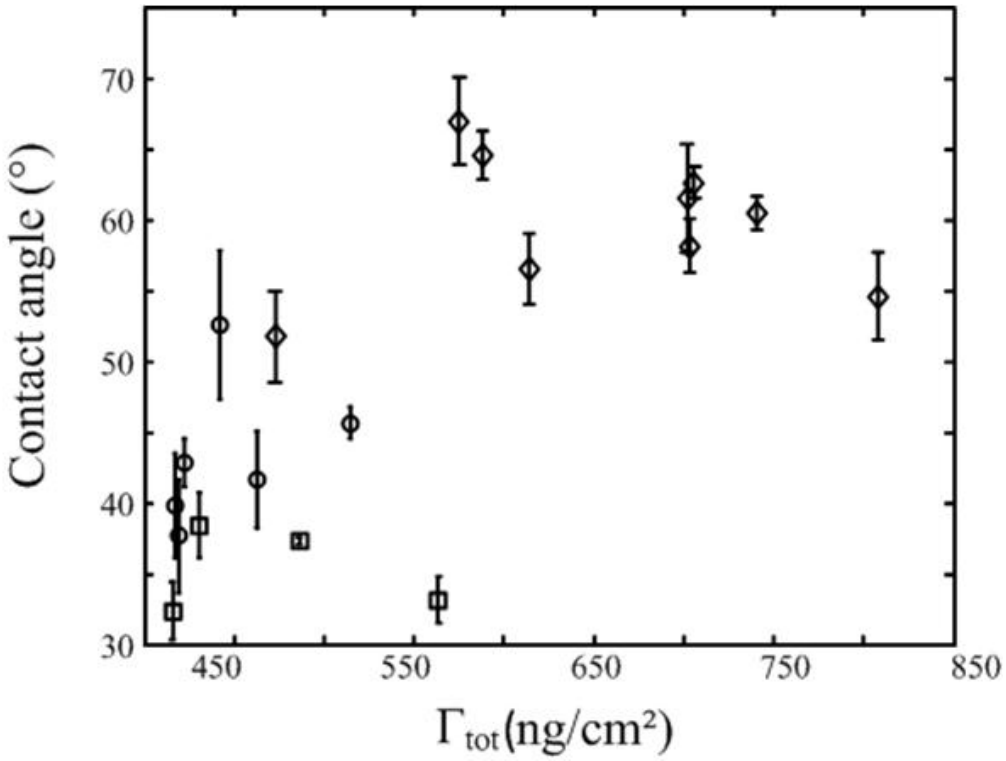

Figure 4-5. Relationship between surface coverage and the advancing angles of amino acids, hydrophobic (diamonds), polar (circles) and ionic (squares) amino acids are represented.

4.4.10 Non specific adsorption of 16-mercaptohexadecanoic acid

Previous studies reported an improved resistance to the adsorption of bovine serum proteins for a SPR biosensors using 16-mercaptohexyldecanoic acid (MHA) [137, 173]. MHA has been used for its ability to reduce nonspecific protein adsorption. Thus, MHA is a comparison point between previously reported work and the results reported herein [154, 174]. A level of nonspecific adsorption equal or below the level of MHA would indicate that 3-MPA-amino acids are performing well in relation to other strategies. By forming a SAM of MHA, the surface concentration of bound serum proteins is 428 ± 16 ng/cm^2. This demonstrates that the best 3-MPA-amino acids have the same biofouling capabilities than MHA, since their surface concentrations of bound proteins are similar. One interesting characteristic of MHA is the value of its advancing contact angle with PBS tending towards zero. In fact, the PBS buffer added on the surface of this SAM immediately formed a film on the surface. This confirms once again that improved resistance to nonspecific adsorption tends to be on surfaces of increased hydrophilicity.

4.4.11 Immunoassay for β-lactamase using 3-MPA-Gly

To demonstrate the possibility of using 3-MPA-amino acids SAM as a chemical linker for antibodies, a biosensor for β-lactamase was constructed with the immobilization of anti-β-lactamase on the free carboxylic acid of 3-MPA-Gly. Both approaches (using EDC or DCC coupling of NHS) produced efficient biosensors, which resulted in a signal to β-lactamase when exposed to a solution containing 909 ηM of this antigen. Figure 4-6 shows a typical sensorgram obtained from antibody immobilization using the optimal EDC conditions. This demonstrates that 3-MPA-amino acids are not only reducing nonspecific adsorption, but can immobilize large amount of antibodies for sensitive biosensing.

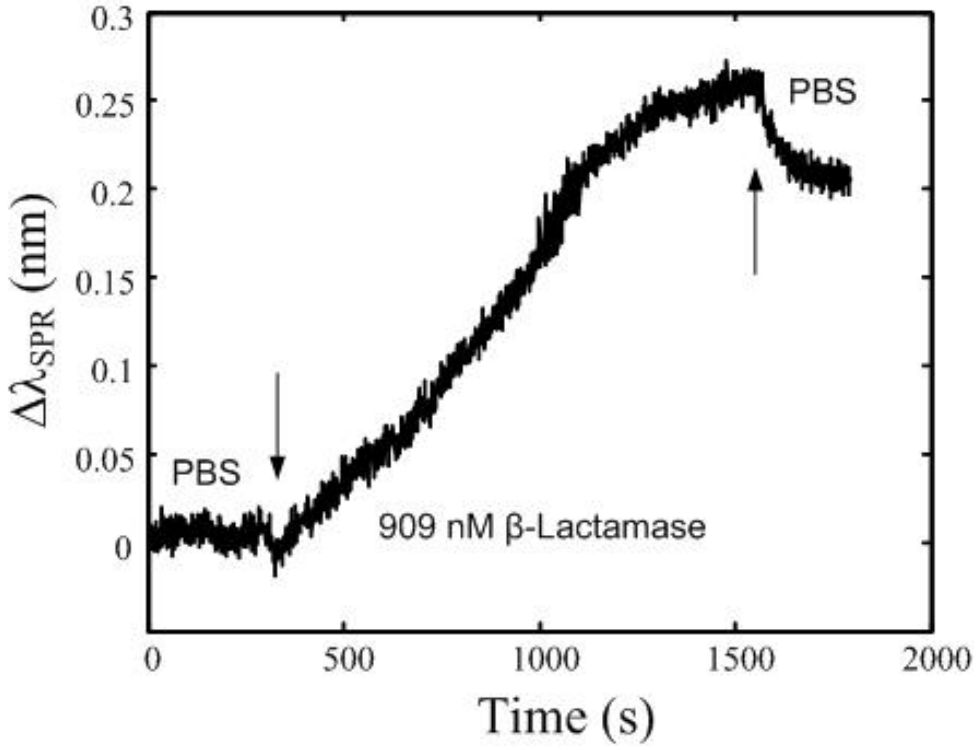

Figure 4-6. Response resulting from the binding of 909 ηM β-lactamase on SPR biosensor specific for β-lactamase, monolayer of 3-MPA-Gly with anti-β-lactamase. The arrows are showing when PBS was replaced with β-lactamase and when PBS was contacted with the SPR biosensor following β-lactamase exposition.

4.5 CONCLUSIONS

This article presented the use of amino acid monolayers based on 3-mercaptopropyl-amino acid for improved resistance of nonspecific adsorption. The chemical preparation and the characterization using FITR, SPR and contact angle are reported for these monolayers. FTIR studies demonstrate that monolayer of 3-MPA-amino acids form on the Au surface of SPR biosensors and confirmed that the deprotection of the methylester on the SAM is complete. The SAMs are generally densely-packed on the Au surface, with varying degrees of surface concentration between 0.18 – 1.80 x 10^{15} molecules/cm². Aliphatic

amino acids with a short side chain length, aromatic amino acids, glutamine and glutamic acid are forming denser monolayers. The study of 19 natural amino acids has determined the characteristics for improved efficiency in limiting the nonspecific protein adsorption from bovine serum. Monolayers with polar and ionic amino acids, with the shortest chain length were the most effective in reducing nonspecific adsorption, regardless of packing density of the SAMs. It has also been showed that there is a relationship between the hydrophilicity of a surface, as measured with advancing contact angle, and its ability to reduce nonspecific binding. These 3-MPA-amino acids exhibit a reduction of the nonspecific adsorption of proteins from serum samples, to a level matching the best organic monolayers. Moreover, the possibility of using 3-mercaptopropylamino acid as an immobilization layer for antibodies was demonstrated by an immunoassay carried out with β-lactamase. The 3-MPA-amino acid monolayers are a very interesting option to develop monolayers that combine good resistance to nonspecific binding and also immobilizes large amount of antibodies for biosensing, as demonstrated with a low adsorption of serum proteins and nanomolar sensitivity for β-lactamase.

4.6 ACKNOWLEDGMENT

The authors thank Joelle Pelletier for providing β-lactamase and Christian Pellerin for granting access to a GATR FTIR. Financial support was provided by the Université de Montréal, the Canadian Foundation for Innovation (CFI) and the Fonds Québécois de la Recherche sur la Nature et les Technologies (FQRNT).

CHAPITRE 5 : Peptide self-assembled monolayers for label-free and unamplified SPR biosensing in crude cell lysate [103]

Publié entant que : Bolduc, O. R.; Clouthier, C. M.; Pelletier, J. N.; Masson, J.-F. Analytical Chemistry 2009, 81, 6779-6788.

5.1 ABSTRACT

Short peptides, composed of polar or ionic amino acids, derived with a short organic thiol significantly reduce nonspecific adsorption of proteins in complex biological matrices such as serum and crude cell lysate which have 76 and 30-60 mg/mL of nonspecific proteins respectively. Minimizing these nonspecific interactions has allowed rapid and direct quantification of β-lactamase in a crude cell lysate using a surface plasmon resonance (SPR) biosensor. A library of short peptides with varying chain length and amino acid composition were synthesized using a solid-phase approach. A 3-mercaptopropionic acid (3-MPA) linker was covalently attached to the amino terminus of the peptides to subsequently form a monolayer on gold in the form of 3-MPA-$(AA)_n$-OH, where n = 2-5 is the length of the amino acid chain. Leu, Phe, Ser, Asp, and His were selected to investigate the effect on nonspecific adsorption with different physico-chemical properties of side-chains; aliphatic, aromatic, polar, acid and base. Advancing contact angles measured the hydrophobicity of each peptidic SAM and showed that hydrophilicity of the gold surface improves with increasing chain length of polar or ionic peptides, while aromatic and aliphatic peptides decreased the hydrophilicity with increasing chain length. The nonspecific adsorption of undiluted bovine serum on SPR sensors prepared with the library of 3-MPA-$(AA)_n$-OH showed that the lowest nonspecific adsorption occurred with polar or ionic amino acids with a chain length where n = 5. We demonstrate that a monolayer composed of 3-MPA-$(Ser)_5$-OH has significant advantages including: 1) minimization of nonspecific adsorption in undiluted bovine serum, 2) provides increased surface concentration of immobilized antibodies, 3) shows a great retention of activity for the antibodies, 4) improved the response from β-lactamase by approximately one order of

magnitude compared to previous experiments, and 5) allows direct quantification of nanomolar β-lactamase concentration in a crude cell lysate with 30-60 mg/mL of nonspecific proteins. The use of this peptide based monolayer offers great advantages for quantitative SPR biosensing in complex biological media.

5.2 INTRODUCTION

Numerous biosensing techniques rely on the measurement of chemical or biological processes occurring on surfaces to detect molecules. In particular, affinity biosensors provide a measurable signal triggered by the binding of a molecule to a surface-immobilized receptor. Multiple physico-chemical phenomena can be utilized to measure molecules with affinity biosensors, such as the change in mass, impedance, current, optical output or wavelength, or a change in refractive index among others [175]. The latter is especially interesting in the case of measuring proteins, antibodies or enzymes, as these molecules have a large molecular weight and high refractive index resulting in a sensitive response using a refractive index sensor. To measure this response, surface plasmon resonance (SPR) is a label-free analytical technique that allows real-time measurements of small changes of refractive index caused by the binding of a molecule with a molecular receptor such as DNA, enzymes, or antibodies [18, 19, 176]. The SPR effect occurs when a thin metallic film deposited on a dielectric material is excited in total internal reflection. SPR is sensitive to within 200-300 nm over the metallic surface, usually gold or silver. Thereby, any molecule migrating within this sensing volume with a refractive index different from the solution will cause a change in the SPR response. This results in SPR being sensitive to numerous categories of molecules, such as DNA or proteins. The broad sensitivity to many important classes of molecules makes SPR an interesting bioanalytical technology, but at

the same time greatly limits its application with real biological samples due to nonspecific adsorption. Previous studies have demonstrated the ability of SPR affinity biosensors to efficiently detect or quantify specific biological markers in solutions such as buffers or strongly diluted biological matrices.[177] It is imperative to extend this technique to more complex matrices such as cellular lysate, blood serum, urine and blood.[147, 148] However, for complex matrices containing high concentrations of proteins that have the potential to interact with the surface of the SPR biosensors, the greater potential for nonspecific responses which can mask the analytical signal has limited the scope of SPR to solutions that are pure or contain few impurities.[141, 142] In order to extend SPR to more complex matrices, an efficient method of reducing nonspecific interactions is required. The need to reduce nonspecific interactions in biological matrices is common to many analytical techniques such as electrochemical biosensors[178], surface acoustic wave biosensors[179], or SPR biosensors[137, 180]. Nonspecific adsorption is also a major cause for prosthesis and implant rejection.[181] Hence, the design of chemical layers capable of protecting the surface of SPR sensors or other surfaces against nonspecific adsorption is an important challenge to overcome for the development of biosensors capable of measuring molecules directly in biological samples and for improved biocompatibility of surfaces.

In the case of SPR biosensors, proteins contained in the biological solution are the major source of nonspecific adsorption. Proteins are present in the millimolar range in most biological fluids while the analytes of interest are in the nanomolar range or less. Nonspecific adsorption of proteins can be reduced by modifying the surface chemistry of the SPR biosensor with organic self-assembled monolayers (SAMs)[26]. When designing a SPR biosensor, such monolayers must excel at limiting nonspecific adsorption while also

serving as the linker to the molecular receptor used for the specific analyte detection [182]. To this end, the use of polymers such as poly(ethyleneglycol) (PEG)[151-153, 183] is the most commonly used approach. Alkanethiols also provide low nonspecific adsorption of proteins on a gold surface while allowing the immobilization of molecular receptors for SPR biosensing [137]. A further approach used to enhance the signal to noise ratio for the detection of lectin in presence of nonspecific serum proteins uses carbohydrate-tri(ethyleneglycol)-alkanethiol co-adsorbed monolayers.[184] In this case, the monolayer incorporated elements of organic monolayer and biological components.

Recent studies have suggested that monolayers based on biological building blocks, especially amino acids and peptides, could mitigate the nonspecific adsorption of proteins in biological matrices and provide an appropriate template for the immobilization of molecular receptors [69, 185-187]. In particular, the use of peptidomimetic polymers containing lysine residues has demonstrated excellent resistance to cell adhesion [69, 185]. Moreover, the use of PEG-lysine copolymer dendrons improves the signal to noise ratio in a solution containing bovine serum albumin [186]. Previous work conducted within our lab showed the potential of SAMs based on amino acids to reduce nonspecific adsorption of bovine serum proteins on SPR biosensors [187]. In that study, polar or ionic amino acids with short side chains reduced nonspecific adsorption of bovine serum proteins more efficiently than hydrophobic amino acids with longer side chains. These monolayers reached a level of nonspecific adsorption similar to previously investigated organic antibiofouling agents. To further investigate the properties and potential applications of amino-acid-based monolayers in biosensing, we extend that study to peptide-based SAMs. The investigation

of peptides of differing lengths and compositions is required to determine their resistance to nonspecific adsorption and their sensitivity in bioassays.

In order for peptides to be used as monolayers, they must possess an amino-terminal thiol for immobilization on the gold surface of the SPR biosensor. This leaves the carboxyl terminus free for various chemistries to immobilize molecular receptors toward specific detection of a molecule. Peptides with an amino-terminal cysteine are capable of forming self-assembled monolayers on gold [158, 188, 189]. When immobilized on gold nanoparticles, they can control aggregation of the nanoparticles [159]. Surfaces have also been modified using sulfide or disulfide conjugates of peptides [190-192], or with alkanethiol derived peptides [193]. Thus, metallic particles or gold surfaces have been capped with a 3-mercaptopropionic derivatized peptide [194, 195] or proteins [196]. These peptides carried C-terminal amide functions, not allowing the immobilization of molecular receptors. Peptides with an amino-terminal thiol linker are not commercially available but they can be readily synthesized using Fmoc protected amino acids coupled to a phenoxy resin [197, 198], followed by reaction with a carboxylic acid thiol. These peptide conjugates should form monolayers on gold which can then be reacted with a desired molecular receptor to construct a biosensor. To date, no study has yet established the resistance of these types of monolayers to nonspecific adsorption and their application as a chemical linker for a biosensor.

Herein, we present an application of peptide-conjugated gold monolayers for the detection of β-lactamase, an enzyme that is central to clinically-relevant drug resistances. Due to their well-recognized importance in bacterial drug-resistance to commonly-prescribed penicillins and cephalosporins, a host of methods have been developed for the detection of β-lactamases. Methods for phenotypic detection include direct detection of β-

lactamase activity using colorimetric compounds, which frequently rely on expensive, non-clinically-relevant substrates such as nitrocefin. Most commonly used in clinical settings are bacteriological growth tests in liquid or solid media in presence of various antibiotics. However, diagnostic times range from hours to days and reproducibility using such microbiological assays is not trivial [199]. A more rapid means for detection of β-lactamase in biological samples is urgently required as the number of β-lactamase variants continues to increase. Molecular detection of β-lactamase-encoding genes by PCR is a faster alternative to phenotypic detection but is not yet a common practise in clinical settings [200]. Immunoassays can also be performed but they provide multi-component, indirect detection [201]. It would be advantageous to establish a more rapid, direct, sensitive and economical method for detection of β-lactamase in biological fluids.

We previously demonstrated that SAMs with single amino acids successfully immobilized an anti-β-lactamase antibody to the surface of SPR biosensor, providing nanomolar range detection of purified TEM1 β-lactamase [187]. Here, we demonstrate the efficiency of short peptides as SAMs resisting the nonspecific adsorption of biological fluids, while promoting the immobilization of highly active molecular receptors on SPR biosensors. A library of peptides from 2 to 5 amino acids in length was synthesized using five chemically diverse amino acids to investigate the resistance of each of these peptides to nonspecific adsorption in bovine serum. Immobilization of a β-lactamase-specific antibody at the surface of a 3-MPA-$(Ser)_5$-NHS SAM allowed quantification of this antibiotic resistance indicator. A calibration of β-lactamase in phosphate-buffered saline solution (PBS) allowed nanomolar detection in cellular lysate, a complex analytical matrix. Hence,

both the resistance to nonspecific adsorption and the specific response from a bioassay are established with these peptide-based SAMs.

5.3 EXPERIMENTAL SECTION

5.3.1 Synthesis of 3-MPA-$(AA)_n$-OH

Amino acids were bought from Novabiochem (distributed by EMD biochemicals, Ville Mont-Royal, QC) with the amine and side chain protected (Fmoc-Phe-OH, Fmoc-Leu-OH, Fmoc-His(Trt)-OH, Fmoc-Asp(OtBu)-OH, Fmoc-Ser(tBu)-OH) to avoid multiple couplings and side reactions during the solid phase synthesis. Polystyrene SynPhase lanterns [197, 198] (A-Series, Mimotopes, Australia) exposing a hydroxymethylphenoxy linker were first immersed in dichloromethane (DCM) twice for 30 minutes to prepare the linker for the coupling of a first amino acid to the phenoxy groups of the lantern. A solution containing 6 equivalents of amino acid mixed with 3 equivalents of diisopropylcarbodiimide (Sigma-Aldrich, Milwaukee, WI) was prepared in N,N-dimethylformamide (DMF) for immersion of the lanterns. Thereafter, a DMF solution containing a catalytic amount of 4-(dimethylamino)pyridine (DMAP, Fluka, Milwaukee, WI) was quickly mixed with the previous solution. The reaction mixture was stored overnight, at room temperature and away from excessive light. The lanterns were then rinsed three times with DMF, three times with methanol and three times with DCM, for 3 minutes at each rinse. This rinsing method was used after each of the following steps. Two pieces of the lanterns were cut to determine coupling efficiency. The first piece of lantern was used to perform a Kaiser test[202, 203] in order to verify that the coupling was complete. The second piece of the lantern was immersed in a 20 : 80 piperidine (Sigma-Aldrich, Milwaukee, WI) : DMF solution for 30 minutes to remove the N-terminal Fmoc protecting

group, for peptide growth. The Kaiser test was repeated with the deprotected lantern to verify the completion of the deprotection reaction. The subsequent coupling reactions were performed with 3 equivalents of the amino acid, 3 equivalents of 2-(1H-Benzotriazole-1-yl)-1,1,3,3-tetramethyluronium (HBTU, Novabiochem) and 9 equivalents of N-ethyldiisopropylamine (DIEA) in DMF for two hours. The final coupling was accomplished with one equivalent of *N*-3-mercaptopropionic acid (3-MPA, Sigma-Aldrich) instead of 3 equivalents of amino acid. Thereafter, a one hour reaction in a solution of 95% trifluoroacetic acid (TFA, EMD biochemicals), 2.5% triethylsilane (TES, Alfa Aesar, Ward Hill, MA) and 2.5% water cleaved the peptide from the lantern to yield the 3-MPA-$(AA)_n$-OH, with n corresponding to the number of amino acids in the peptide. TFA was evaporated and the peptide was precipitated in diethyl ether to recover the pure 3-MPA-$(AA)_n$-OH. The composition of each peptide was verified using LC-ESI-MS. The yield varied between 35% and 85% depending on the amino acid. Thereby, 3-MPA-$(AA)_n$-OH peptides were synthesized with n = 1, 2, 3, 4, and 5 for AA = Leu, Phe, Ser, Asp, His, and with n = 8, 10 for Ser.

5.3.2 Preparation of peptidic monolayers

Microscope slides (BK7, 22 x 22mm) were coated with a 3 nm Ti adhesion layer and a 50 nm Au layer (purity 99.99%, ESPI metals) using a Cressington 308R sputter coater. These Au coated SPR slides were immersed for at least 16 h in a 5 mM peptide solution in absolute ethanol to form a well-ordered monolayer [148]. Four replicates were prepared for each 3-MPA-$(AA)_n$-OH. Each sample was rinsed with absolute ethanol to wash away unbound peptides. Slides used to bind biological receptors were immersed in a 0.01 M HCl solution for 2 h to ensure that the C-terminal extremities were available [187].

5.3.3 SPR and contact angle measurements

The surface coverage for each monolayer was measured according to the change in response of the SPR sensor in PBS for the bare Au surface relative to the peptide-coated Au surface. To measure the formation of the monolayers, each SPR sensor was mounted on a custom-made SPR instrument based on a dove prism with wavelength interrogation as previously described [105]. The advancing contact angles were measured for SAMs with 300 µL of PBS (CellGro, Mediatech Inc.) with a custom built contact angle instrument. PBS has similar pH and salinity as biological samples, i.e. bovine serum. Once mounted on the SPR instrument, the sensors were stabilized 5 min in PBS before the acquisition of the s-polarized reference. The p-polarized real-time measurement was initiated by monitoring the baseline for 5 min in PBS, which was replaced with undiluted bovine serum for 20 min (Sigma-Aldrich) containing 76 mg/mL proteins. The serum was replaced for 5 min by PBS to quantify nonspecifically bound proteins. Raw data were processed with Matlab. This procedure was repeated at least four times for each of the 3-MPA-$(AA)_n$-OH prepared with n = 1 to 5 residues.

5.3.4 Immobilization of anti-IgG and anti-MMP3

3-MPA-H_3-D_2-OH was selected for its optimal performance in limiting nonspecific protein adsorption to construct SPR biosensors. The SAM was formed as described above before it the device is placed in the SPR spectrometer equipped with a fluidic cell for at least 5 minutes of stabilization in Millipore water. Each solution necessary to the building of a SPR affinity biosensor was flown over before the injection of the solution containing the analyte. The measurement starts with 2 minutes of reference in Millipore water. Then an aqueous solution composed of 25 mM N-ethyl-N'-(3-dimethylaminopropyl)-

carbodiimide (EDC, Fluka) and 5 mM of N-hydroxysuccinimide (NHS, Sigma-Aldrich) if flown for 2 minutes followed by a rinsing with PBS adjusted at a pH of 4.5 water for 2 more minutes. A solution made of 25ug/mL of the antiboby in regular PBS then replaced the preceding solution for 15 minutes. The excess of antibody is rinsed Each SPR biosensor was then rinsed with 18 MΩ water followed by PBS and placed in a Teflon reaction vessel designed to seal the biosensors from the external environment limiting the evaporation of the anti-β-lactamase solution during the overnight reaction with the activated monolayer on the SPR sensor. Each step involving an antibody or an antibody-derived SPR sensor was accomplished in a refrigerated laboratory and the sensors were kept at 4^0C until use [168]. The antibody specific for TEM-1 β-lactamase (QED Bioscience Inc.) was diluted to a concentration of 37 μg/mL and 250 μL of this solution were reacted with the activated 3-MPA-$(Ser)_5$-OH surfaces. The samples were rinsed with PBS and reacted for 10 min in 1 M ethanolamine hydrochloride (Sigma-Aldrich) adjusted to pH 8.5 with 10 M NaOH (Fluka) to inactivate the unreacted NHS after the antibody immobilization.[169] The biosensors were rinsed and stored in PBS for at least 60 min prior to use.

5.3.5 β-lactamase expression and purification

Wild-type TEM-1 was overexpressed in *Escherichia coli* as previously described [204]. Cells were pelleted by centrifugation (30 min, 5000×g, 4ºC) and resuspended in 20 mL of 10 mM Tris-HCl buffer pH 7.0 for lysis on ice using a Branson sonicator (four pulses at 200 W for 30 s with a tapered micro-tip). Cellular debris was pelleted by centrifugation (50 min, 20000×g, 4ºC) and the supernatant was filtered through a 0.2 μm filter, yielding crude lysate. The purification was performed according to a 2-step purification protocol using an

Äkta FPLC (GE Healthcare). The first step was as previously described [204], using a linear gradient of 10-200 mM Tris-HCl pH 7.0 to elute the enzyme. Fractions containing β-lactamase were identified by qualitative nitrocefin (Calbiochem, Mississauga, ON)) hydrolysis assay and confirmed by SDS-polyacrylamide (SDS-PAGE) gel electrophoresis (15% (w/v) with Coomassie Brilliant Blue staining. For the second step, fractions containing β-lactamase were pooled (20 mL) and concentrated to 1.5 mL using an Amicon concentrator (MCWO 10000, Millipore, Billerica, MA) for injection on a Superose12 column (1.6 × 55 cm). The sample was eluted with 50 mM Tris-HCl, pH 7.0, at a flowrate of 1.0 mL/min. Fractions containing β-lactamase were identified as described above. Enzyme purity was evaluated using separation by SDS-PAGE stained with Coomassie Brilliant Blue and the public domain image analysis software Scion Image (NIH, rsb.info.nih.gov/nih-image). Protein concentration was quantified using Bradford assay [205] (Biorad, Hercules, CA), with bovine serum albumin as the standard. Pooled fractions of purified β-lactamase were concentrated to 1 mg/mL (33 μM), as above.

5.3.6 Determination of β-lactamase enzyme concentration

β-lactamase activity for crude and purified TEM-1, as well as crude lysate from the host strain that does not overexpress TEM-1 (*E. coli* XL1-Blue), were determined by measuring the initial rate of CENTA (CalBioChem, Mississauga, ON) hydrolysis at 405 nm ($\Delta\varepsilon_{405}$ = 6400 $M^{-1}cm^{-1}$) at 25ºC in 50 mM sodium phosphate buffer pH 7.0 under saturated enzyme conditions (700 μM CENTA) [206, 207] with a Cary 100 Bio UV-visible spectrophotometer (Varian Canada Inc., Montréal, QC). Concentration of β-lactamase was determined using the equation [E] = V_{max}/k_{cat} using reported k_{cat} [206, 207] and experimentally determined V_{max}.

5.3.7 Calibration of TEM-1 β-lactamase in PBS

Solutions of different concentrations of TEM-1 β-lactamase (700, 350, 175, 88 and 44 nM) were prepared in PBS from an aliquot of the concentrated solution, prepared as described above. These solutions were kept at 4^0C until 20 min prior to use. The SPR biosensors specific for TEM-1 β-lactamase were then mounted on the SPR instrument equipped with the fluidic cell. A delay of 10 min prior to the initial experiment was necessary for the biosensor to stabilize before acquiring the s-polarized reference. Immediately after, the real-time measurement in p-polarized light was undertaken for 5 min in PBS. The solution was then replaced with β-lactamase solution for 20 min. Finally, PBS was monitored to verify whether the binding of β-lactamase was reversible.

5.3.8 Detection of TEM-1 β-lactamase in crude cell lysate

The 3-MPA-$(Ser)_5$-OH based biosensors were exposed for 12.5 min to a cellular lysate without TEM-1 β-lactamase (blank cell lysate) after a stabilizing period of 5 min in PBS. This lysate was then replaced with the lysate containing TEM-1 β-lactamase for 12.5 min for the specific detection of TEM-1 β-lactamase. The concentration of TEM-1 β-lactamase in crude lysate is high, such that saturation of the SPR biosensor was expected. Thus, the β-lactamase cell lysate was diluted with PBS by a factor of 2 and 4. Blank runs with TEM-1 β-lactamase-free crude cell lysate were accomplished with a 3-MPA-$(Ser)_5$-OH and with a 16-mercaptohexadecanoic acid based biosensor which had previously been reacted with anti-β-lactamase.

A 3-MPA-$(Ser)_5$-OH SAM with immobilized anti-β-lactamase was stabilized for 5 minutes in PBS prior to injection of blank cellular lysate over a 12.5 minutes period to saturate the remaining sites on the biosensor with nonspecifically adsorbed proteins. The

blank lysate was then replaced with a crude cell lysate overexpressing TEM-1 β-lactamase diluted 100-fold with the blank cell lysate. The SPR response induced by this replacement allowed the quantification of the amount of β-lactamase in the crude cell lysate by using the equation obtained with the calibration using pure β-lactamase in PBS.

5.4 RESULTS AND DISCUSSION

5.4.1 Synthesis and characterization of 3-MPA-(AA)$_n$-OH

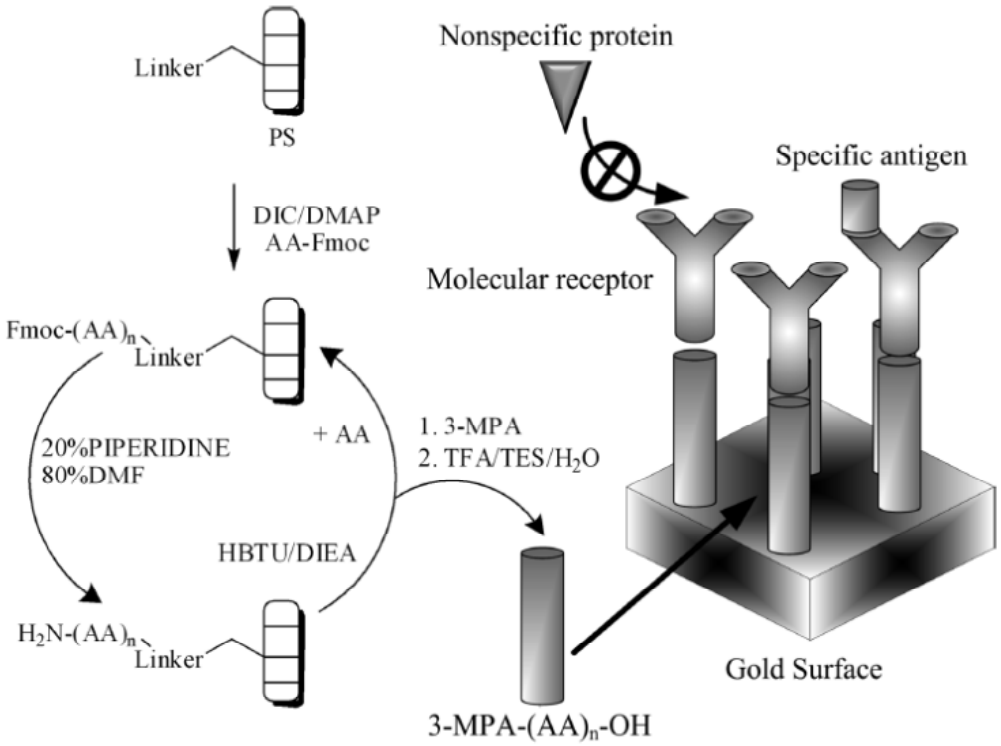

Figure 5-1. Synthesis of 3-MPA-(AA)n-OH, where n is the number of reaction cycles prior to the termination of the reaction by grafting 3-MPA. The formation of monolayers on gold with these compounds is investigated for reduction of nonspecific adsorption. AA refers to amino acid, specifically to Leu, Phe, Ser, Asp, and His in this study.

Using a combinatorial approach, a library of 22 SAMs was synthesized using a solid-phase strategy where homopeptides of varying lengths were synthesized from the carboxyl to the amino terminus with covalent attachment of a 3-mercaptopropionic acid to

the N-terminal amine (Figure 5-1). Cleaving the final compound from the solid support produced peptides carrying thiol groups in the form of 3-MPA-$(AA)_n$-OH. Usual tests for solid-phase peptide synthesis confirmed the completeness of the reactions and the formation of the desired molecules. Kaiser tests conducted after each amino acid coupling step confirmed that the coupling reaction was successful and the terminal amine of the peptide could be deprotected from FMOC. Larger scale syntheses were conducted for each amino acid: Leu, Phe, Ser, Asp, and His. After each coupling step, a proportion was set aside for reaction with 3-MPA to obtain 3-MPA-$(AA)_n$-OH, with n = 2-5. The results from n = 1 are from a previous investigation by Bolduc and Masson [187]. Following the cleavage of 3-MPA-$(AA)_n$-OH from the solid-phase, most of the resulting compounds were analyzed using LC-MS with the exception of 3-MPA-$(Phe)_n$-OH which did not elute from the HPLC column due to its hydrophobic nature. The HPLC purity was measured and the MS confirmed the synthesis of 3-MPA-$(AA)_n$-OH with the presence of one or more of the following: the molecular ion, the molecular ion suffering one or more water losses or from the disulfide complex of the peptide. The disulfide compound from 3-MPA-$(AA)_n$-OH was visible in the mass spectrum confirming the presence of the thiol. The coupling reaction using HBTU/DIEA was very efficient as assessed by the fact that only traces of shorter peptides were observed upon LC-MS analysis of 3-MPA-$(AA)_5$-OH. Thereby, the 3-MPA-$(AA)_n$-OH were synthesized with n = 2-5 for Phe, Leu, Asp, and His and with n = 2-5, 8, and 10 for Ser.

5.4.2 Characterization of 3-MPA-$(AA)_n$-OH SAMs

SPR was used to quantify the surface coverage of the 3-MPA-$(AA)_n$-OH SAMs. Immediately after coating a BK7 glass slide with 50 nm of Au, the SPR response was

recorded in PBS to determine the SPR wavelength (λ_{SPR}). Following the formation of the SAM, the SPR response was measured in PBS to calculate the change in the SPR response ($\Delta\lambda_{SPR}$) caused by the formation of the SAM on the SPR sensor. The change in SPR response was used with the equation from Jung et al. to calculate the surface concentration (Γ) of the SAMs prepared with 3-MPA-$(AA)_n$-OH [170, 208]:

$$\Gamma = \rho\,(-0.5 l_d)\,\ln(1 - (\Delta\lambda_{SPR}\, m^{-1}(\eta_{SAM} - \eta_{PBS})^{-1})) \qquad (5\text{-}1)$$

where the sensitivity (m) of the SPR instrument was measured with sucrose solutions at 1765 nm/RI. The refractive index of PBS (η_{PBS}) was determined experimentally with a high resolution refractometer at 1.33476 ± 0.00002 RIU and the refractive index related to the SAMs was approximated to be 1.45 RIU. The penetration depth of the plasmons (l_d) is 230 nm (2.3 x 10^{-5} cm in eq. 5-1). The density of the molecules forming the SAMs is 0.9 g/cm^3.[26] The molecular weight of each peptide allowed the calculation of the surface coverage in molecules/cm². The surface concentration of 3-MPA-$(AA)_n$-OH SAMs varies depending on the chain length of the peptide used. The average surface coverage for the homopeptides with identical chain length decreases significantly from n = 1 to 2, and from n = 2 to 3. Thereafter, the decrease is minimal from n = 3 to 4 and 5. The longest peptides with n = 5 (Γ = 1.4 x 10^{14} molecules/cm²) have a surface coverage of nearly 4 times less than with n = 1 (Γ = 5.1 x 10^{14} molecules/cm²) (see Table 5-1). The lower surface concentration of the longer 3-MPA-$(AA)_n$-OH SAMs implies a less dense monolayer. This could be explained by the ternary structure of the amino acids with longer chain length. Straight chain alkanethiols usually have a high surface density of nearly 10 x 10^{14} molecules/cm². This corresponds to a densely packed monolayer. 3-MPA-$(AA)_n$-OH with small n likely have a surface conformation similar to straight chain

alkanethiols. However, peptides tend to adopt ternary structures in solution, such as helices and sheets. It was reported in a previous study that polylysine on a gold surface forms β-sheets for n = 4 and 10, while it formed α-helices for n = 30 [209]. Thus, it is possible that from the lower surface concentration for n = 3, 4, and 5 for 3-MPA-$(AA)_n$-OH that a β-sheet could be favoured and explain the less dense monolayer compared to n = 1 and 2.

Table 5-1. Surface concentration of 3-MPA-$(AA)_n$-OH SAMs immobilized on the gold surface of SPR biosensor, reported as 10^{14} molecules/cm²

n	Leu	Phe	Ser	Asp	His	*Average*
1	7.9	5.2	2.9	6.1	3.4	*5.1*
2	3.0	2.4	4.9	2.6	2.0	*3.0*
3	3.1	1.3	1.6	1.3	1.5	*1.8*
4	3.1	1.3	1.6	2.3	2.8	*2.2*
5	1.5	1.9	0.98	1.4	1.3	*1.4*

Data for n = 1 are from Bolduc and Masson [187]. Measurements in triplicate.

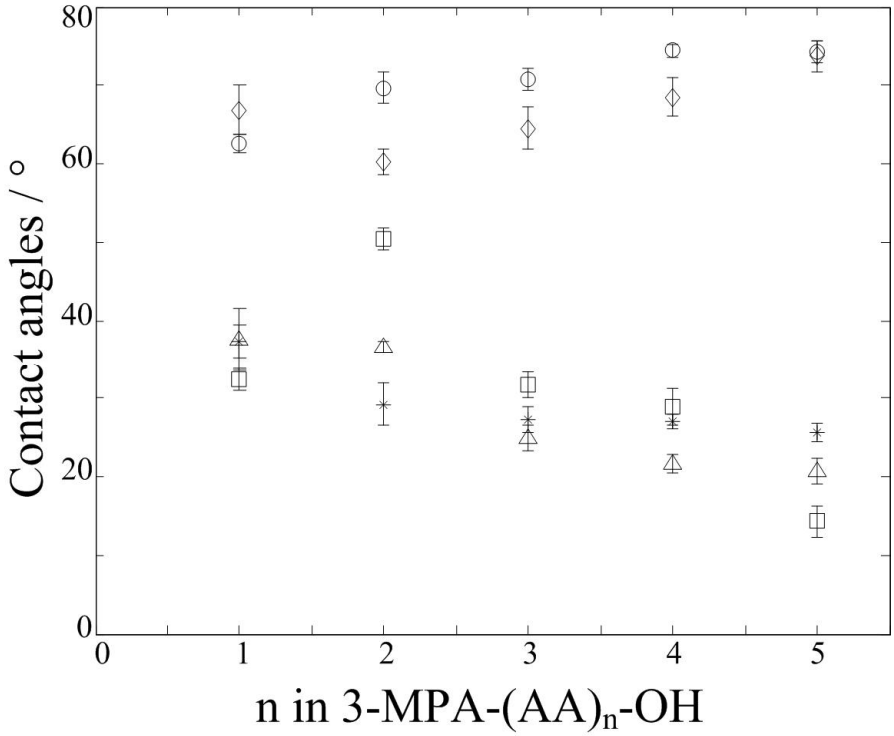

Figure 5-2. Changes in contact angle of the 3-MPA-$(AA)_n$-OH with increasing chain length of the peptide (n = 3 measurements). The symbols refer to: leucine (○), phenylalanine (◊), histidine (*), serine (Δ) and aspartic acid (□).

The advancing contact angle of PBS for different chain length of 3-MPA-$(AA)_n$-OH SAMs are an indication of the hydrophobicity of the surface, hence the physico-chemical properties of the SAMs. The advancing contact angles indicate that 3-MPA-$(Leu)_n$-OH are generally the most hydrophobic layers tested (Figure 5-2). Moreover, the hydrophobicity of 3-MPA-$(Leu)_n$-OH and 3-MPA-$(Phe)_n$-OH increases with the chain length of the peptide. These peptides are composed of hydrophobic aliphatic and aromatic side chains, respectively. The observed increase in contact angle with chain length indicates an increased contribution of the side chain physico-chemical property toward the overall properties of the monolayer. This tendency was similar for the SAMs prepared with Ser,

Asp and His, as the contact angle decreased with increasing chain lengths for those hydrophilic peptides, indicating increased hydrophilicity of the SAMs.

5.4.3 Adsorption of bovine serum proteins on 3-MPA-peptide SAMs

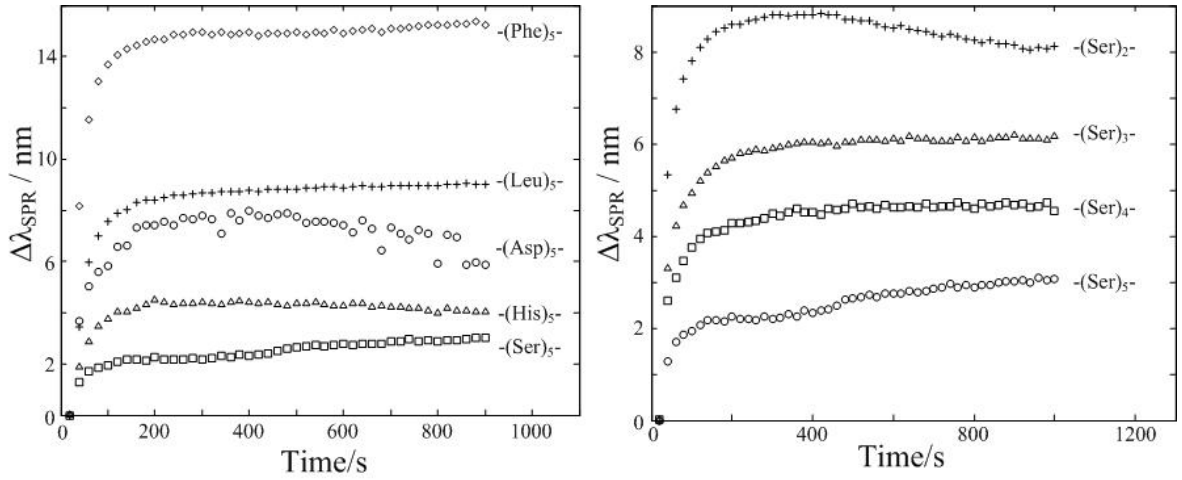

Figure 5-3. Sensorgrams of nonspecific adsorption of bovine serum protein, (left) for five 3-MPA-$(AA)_5$-OH prepared with different amino acids, (right) for different number of Ser in the peptide chain.

Determining the surface coverage of nonspecifically bound proteins with a standard solution is essential in assessing the potential use of monolayers as a chemical template for a bioassay in complex biological fluids. In the case of SPR biosensors, these nonspecifically-bound proteins resulted in a response that cannot be distinguished from the response of interest, such that few studies have been reported of detection in relevant biological media. To determine the resistance of the 3-MPA-$(AA)_n$-OH SAMs to nonspecific adsorption, the monolayers on Au were exposed to undiluted bovine serum. Bovine serum contains proteins similar to human serum while being slightly more concentrated than human serum, providing a perfect test for the monolayers. Each 3-MPA-$(AA)_n$-OH monolayer was exposed successively to PBS for 5 minutes, to bovine serum for

20 minutes and to PBS for a further 5 minutes. An overlay of typical kinetic curves expressing the bovine serum protein adsorption (Figure 5-3) for each 3-MPA-$(AA)_5$-OH shows notable differences in nonspecific protein adsorption with the type of amino acid present. Polar and ionic amino acids tend to perform better than hydrophobic ones as noted from smaller changes in the SPR responses with these peptides. A second overlay of typical kinetic curves shows that nonspecific adsorption of proteins depends on the length of the peptide present. Monolayers prepared with increasing chain length of 3-MPA-$(Ser)_n$-OH showed a marked decrease in the SPR response with bovine serum, corresponding to lower nonspecific protein adsorption on the surface of the SPR sensor. This corresponds to an improved performance of the monolayer in complex biological fluids.

Table 5-2. Surface coverage due to nonspecific adsorption of undiluted bovine serum with increasing chain length of different 3-MPA-$(AA)_n$-OH on the gold surface of SPR biosensor, reported in ng/cm^2

n	Leu	Phe	Ser	Asp	His
1	706 ± 19	575 ± 202	419 ± 33	416 ± 121	486 ± 149
2	598 ± 84	328 ± 67	302 ± 20	430 ± 54	329 ± 75
3	488 ± 122	388 ± 117	226 ± 20	337 ± 54	213 ± 38
4	404 ± 112	369 ± 96	165 ± 10	291 ± 122	185 ± 30
5	345 ± 78	619 ± 66	132 ± 33	290 ± 22	188 ± 71
8			246 ± 111		
10			259 ± 33		

Data for n = 1 are from Bolduc and Masson [187]. Measurements in triplicate and the error represents two standard deviations on the mean.

The comparison of each 3-MPA-$(AA)_n$-OH with increasing chain length shows interesting trends. Firstly, the surface concentration of proteins adsorbed on each SAM was obtained from the sensorgrams as in Figure 5-3 and is reported in ng of nonspecifically bound proteins/cm^2 using equation 1. In calculating the surface coverage of nonspecifically bound proteins, the parameters of equation 1 are identical with the exception of the density of proteins being 1.3 g/cm^3 and the refractive index being equal to 1.57 RIU. Nonspecific adsorption generally decreased with increasing chain length of the 3-MPA-$(AA)_n$-OH in presence of bovine serum, with the exception of 3-MPA-$(Phe)_5$-OH that increased considerably in comparison to the other 3-MPA-$(Phe)_n$-OH (Table 5-2). Otherwise, this reduced nonspecific adsorption was notable in the case of 3-MPA-$(Ser)_n$-OH, which showed an approximate 4-fold decrease with the longer chains compared to the already excellent properties of 3-MPA-$(Ser)_1$-OH (Figure 5-4). Overall, the results generally indicate that increasing the chain length resulted in more "peptide-like" monolayers possessing significantly improved performance towards nonspecifically adsorbed proteins from bovine serum. Further increasing the chain length of 3-MPA-$(Ser)_n$-OH to n = 8 and 10 resulted in a decreased performance of the monolayer with the surface coverage of nonspecifically adsorbed proteins increasing to approximately 250 ng/cm^2 for n = 8 and 10 versus 132 ng/cm^2 when n = 5. Thus, the performance of 3-MPA-$(Ser)_n$-OH seems to be optimal at n = 5.

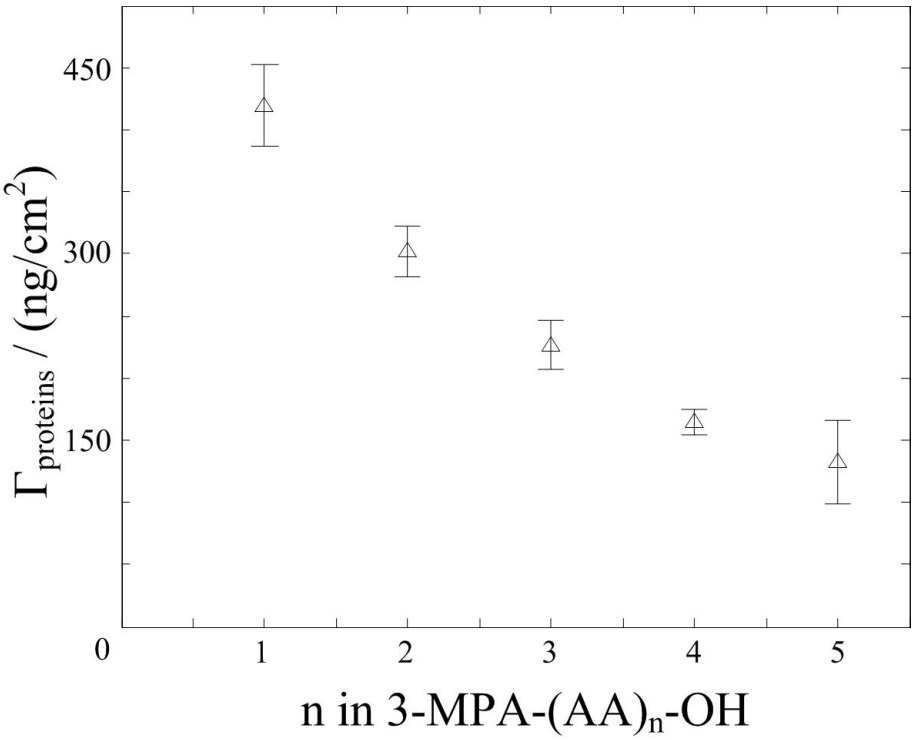

Figure 5-4. Decrease of the surface coverage due to nonspecific adsorption of undiluted bovine serum with increasing chain length of different 3-MPA-$(Ser)_n$-OH, where n = 1 to 5, measurements in triplicate.

Among the 3-MPA-$(AA)_n$-OH tested, the 3-MPA-$(Phe)_n$-OH and 3-MPA-$(Leu)_n$-OH were found to be the worst since these hydrophobic monolayers adsorbed a significantly greater amount of serum proteins. Comparatively, 3-MPA-$(Leu)_n$-OH formed SAMs resulting in greater nonspecific adsorption at shorter chain lengths while 3-MPA-$(Phe)_n$-OH resulted in poor results at longer chain lengths. The performance of the other peptides improved upon testing of the 3-MPA-$(Asp)_n$-OH, 3-MPA-$(His)_n$-OH, and 3-MPA-$(Ser)_n$-OH with the latter exhibiting the best resistance to nonspecific adsorption of bovine serum proteins. It should be noted that both the 3-MPA-$(His)_n$-OH and 3-MPA-$(Ser)_n$-OH showed improved resistance to nonspecific adsorption by at least a factor of 2 compared to

the other 3-MPA-$(AA)_n$-OH. Thus, it appears that the more polar and ionic peptides SAMs are the most efficient at reducing nonspecific interactions at the surface of biosensors, in good agreement with our previous study using short (n =1) monolayers and from other SAM monolayers [187],[64]. Based on these results, 3-MPA-$(Ser)_5$-OH was selected for the further validation of a bioassay using a 3-MPA-$(AA)_n$-OH SAM to immobilize a target molecular receptor and to minimize nonspecific adsorption in a complex biological fluid.

5.4.4 Calibration of β-lactamase in PBS

In order to validate the use of 3-MPA-$(Ser)_5$-OH monolayers, a β-lactamase model system was used to demonstrate the efficiency of SPR biosensors in complex biological medium with these types of monolayers. No commercial biosensor is currently available to quantify β-lactamase. This enzyme constitutes a logical choice for a test system both due to its clinical importance and because it is a well characterized 'bench-mark' protein. Anti-TEM-1 β-lactamase was purchased from a commercial source. No information on the affinity constant for this antibody with β-lactamase is currently available. The molecular weight of anti-TEM-1 β-lactamase is approximately 155 kDa. The immobilization of anti-β-lactamase from a 37 μg/mL solution in PBS resulted in a change of the SPR response of 8.25 nm from multiple measurements (n = 3 measurements). Equation 1 provides an estimate of the surface coverage of the antibody on the SPR sensor. Using standard parameters for proteins, the surface concentration of anti-β-lactamase is 0.86 pmol/cm², or 5.6×10^{11} molecules/cm². The maximum surface coverage for a molecule of 160 kDa should be approximately 2×10^{12} molecules/cm², assuming a diameter of 7 nm for the molecule [210, 211]. Thus, it is observed here that approximately 25% of the available binding sites are occupied with anti-β-lactamase. Improving the surface concentration of antibody

would further improve the sensitivity of SPR biosensor, although this fraction of approx. 25% of occupied sites is typical for protein coverage on a monolayer using NHS chemistry.

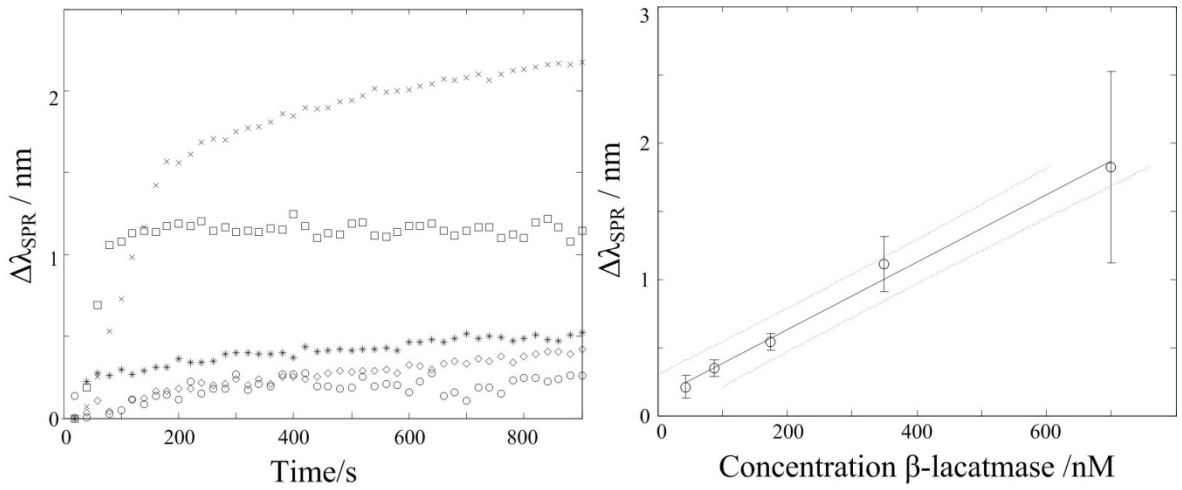

Figure 5-5. (Left) Sensorgrams of β-lactamase in PBS for different concentration solutions using a SPR affinity biosensor prepared with 3-MPA-$(Ser)_5$-(anti-β-lactamase). The β-lactamase concentration of the solutions is 700 nM (×), 350 nM (□), 175 nM (*), 88 nM (◊) and 44 nM (○). (Right) Calibration of β-lactamase in PBS with the SPR sensor. The error bars represent two standard deviations on the mean (n = 3 measurements), while the light gray line represents two standard deviation on the regression. The equation of the linear regression is $\Delta\lambda_{SPR}$ = 0.0025 nm nM^{-1}*[β-lactamase] + 0.13 nm and R^2 = 0,991.

β-lactamase was purified to approximately 90% from *E. coli* overexpressing TEM-1 β-lactamase and concentrated to 1.0 mg/mL as determined according to the catalytic activity toward the chromogenic substrate CENTA. The concentrated enzyme solution was diluted with PBS and injected manually over a β-lactamase-specific SPR biosensor using a fluidic cell built in-house. The fluidic cell was very useful in reducing the impact of the experimental conditions on the analytical signal, especially the change of temperature. Hence, minimal drift due to temperature changes were observed on the sensorgrams, allowing the observation of smaller changes due to specific interactions. An overlay of typical kinetic curves obtained for solutions containing nanomolar concentrations of this

enzyme clearly shows that this type of biosensor is sensitive to the concentration of the analyte in solution (Figure 5-5). The sensitivity of the SPR biosensor is limited to nanomolar concentrations by the poor affinity of the anti-β-lactamase antibody. No highly specific antibodies are commercially available for this biological system. Triplicate measurements of each concentration allowed the calibration of the system to quantify the amount of β-lactamase in more complex solutions (Figure 5-5). The limit of detection was determined to be near 10 nM for β-lactamase. The calibration curve for the SPR response induced by β-lactamase in PBS is linear, but the linear regression does not cross the origin which suggests that there is a nonlinear domain for superior concentrations. This is usual with site limited surface techniques such as SPR biosensors, where the signal is only linear for a limited concentration range. Using a Langmuir calibration isotherm allows for the compensation of these variations and also to extrapolate important thermodynamic information on anti-β-lactamase as demonstrated with equation 5-2:

$$\Delta\lambda_{SPR}^{-1} = (KC\Delta\lambda_{SPRmax})^{-1} + \lambda_{SPRmax}^{-1} \qquad (5\text{-}2)$$

where K is the affinity constant of the antibody for the antigen, $\Delta\lambda_{SPR}$ is the change of the SPR response for a concentration C and $\Delta\lambda_{SPRmax}$ is the change of the SPR response at saturation of the antibody. Thus, by plotting the inverse x and y axis of figure 5-5, an affinity constant of 2.5×10^6 M^{-1} is obtained, which is significantly lower than for many antibodies. Antibodies with affinity constant in the range of 10^8 and 10^9 M^{-1} are regularly employed with SPR biosensors to obtain lower detection limits. Hence, the detection limit and linearity range could be improved with an antibody engineered to have a higher affinity constant. The $\Delta\lambda_{SPRmax}$ for this sensor is 2.7 nm, which corresponds to a surface concentration of 1.5 pmol/cm² or 9.0×10^{11} molecules/cm². This signifies that at saturation,

a ratio of β-lactamase : antibody of 1.7 : 1 is achieved. Thus, multiple binding per antibody occurs with this system, consistent with antibodies having 2 binding sites per molecule. It also indicates that the fraction of active antibody is 87%, a very high fraction for covalently bound antibody to a Au surface. Typically, the fraction of active antibodies bound to the surface of sensors is closer to 70-80% [118, 211]. This result suggests a greater retention of activity for the antibody immobilized on 3-MPA-$(Ser)_5$-OH. This peptide-like surface may minimize conformational changes after immobilization of the antibody.

The SAM based on 3-MPA-$(Ser)_5$-OH not only provides improved resistance to nonspecific adsorption in serum and greater retention of activity at the surface, but also yields a greater antibody density immobilized onto the surface of the SPR biosensor. The average $\Delta\lambda_{SPR}$ induced by the immobilization of TEM-1 anti-β-lactamase on a NHS-MHA is 2.15 nm according to our previous studies [105]. However, with 3-MPA-$(Ser)_5$-OH based SAMs, the average SPR response induced by the immobilization of anti-β-lactamase is 8.35 nm, a 4-fold improvement relative to NHS-MHA. This demonstrates that 3-MPA-$(Ser)_5$-OH SAMs present a significant number of available –COOH groups at the surface and thus increase the amount of biological receptors attached to the SPR surface. Coupled to the increased retention of activity, this significantly improves the performance of the SPR sensor. An improvement of approximately one order of magnitude is observed in the response obtained with either a 700 nM β-lactamase solution using NHS-MHA ($\Delta\lambda_{SPR}$ = 0.13 nm) [105] or a 909 nM β-lactamase solution using a 3-MPA-Gly-OH SAM ($\Delta\lambda_{SPR}$ = 0.25 nm) [187] relative to 700 nM β-lactamase solution using 3-MPA-$(Ser)_5$-OH ($\Delta\lambda_{SPR}$ = 1.8 nm). These responses were obtained using the identical experimental conditions while using the different SAMs to immobilize anti-β-lactamase. This significant improvement is explained

with the improved retention of activity and the greater density of immobilized antibody molecules on the 3-MPA-$(Ser)_5$-OH SAM.

5.4.5 Improved specificity with 3-MPA-$(Ser)_5$-OH based SPR biosensors

The analytical response is significantly improved for β-lactamase using a 3-MPA-$(Ser)_5$-OH SAM and a minimized nonspecific adsorption is obtained in serum relative to 16-MHA SAM. A more stringent test for performance of the biosensors is to measure the concentration of TEM-1 β-lactamase in a crude cell lysate. The crude cell lysate generated here contained 30 – 60 mg/mL of nonspecific proteins compared to 76 mg/mL for bovine serum, thus constituting a good system for comparison. Thus, in order to validate the performance of the SPR sensor in crude cell lysate, a measurement of the blank cell lysate was performed on the SPR sensor with 3-MPA-$(Ser)_5$-anti-β-lactamase or with 16-MHA-anti-β-lactamase. The sensorgrams were compared to a measurement with crude cell lysate overexpressing TEM-1 β-lactamase (Figure 5-6). Nonspecific adsorption was much more significant with 16-MHA-anti-β-lactamase compared to 3-MPA-$(Ser)_5$-anti-β-lactamase. To verify reproducibility and rule out any physical effect from the replacement of a solution in the fluidic cell, a second portion of the blank cell lysate was applied to both SAMs. For 3-MPA-$(Ser)_5$-anti-β-lactamase, there was no change in signal showing that no more nonspecific interaction occurs after a 12.5 min exposure to cell lysate, while for 16-MHA-anti-β-lactamase SAMs, nonspecific adsorption continued to occur at a steady rate.

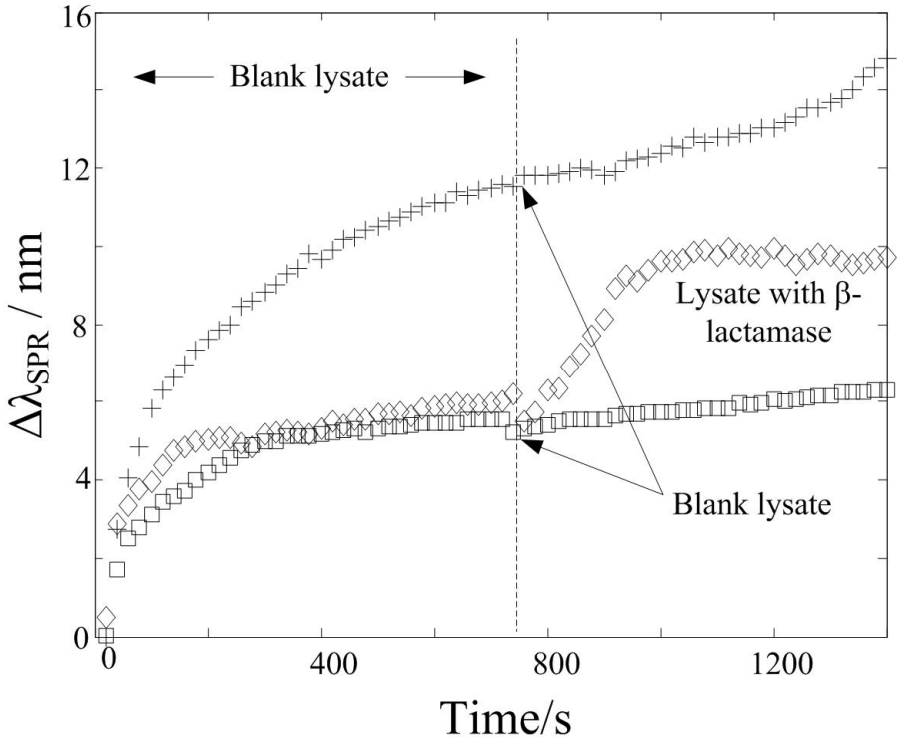

Figure 5-6. Detection of β-lactamase in crude cell lysate (◊) and blank measurements for two different SAMs: 16-MHA (+) and 3-MPA-$(Ser)_5$-OH (□). The dashed line represents the replacement of blank crude cell lysate with a second sample of blank lysate for 16-MHA-anti-β-lactamase (+) and 3-MPA-$(Ser)_5$-anti-β-lactamase (□) or with crude cell lysate containing β-lactamase in case of detection measurement with 3-MPA-$(Ser)_5$-anti-β-lactamase. Nonspecific adsorption reached a maximal value after approx. 400s for 3-MPA-$(Ser)_5$-OH allowing detection of β-lactamase in the crude cell lysate, while nonspecific adsorption was more important and occurred over a longer period for 16-MHA.

Following the conditioning of the sensor with the blank cell lysate on 3-MPA-$(Ser)_5$-anti-β-lactamase, the cell lysate with β-lactamase was injected. As shown in figure 5-6, the kinetic curve demonstrated an important shift of λ_{SPR}, illustrating the excellent specificity of 3-MPA-$(Ser)_5$-OH based SPR biosensors. Comparing the kinetic measurement using 16-MHA performed in the same experimental conditions demonstrated that serine based SAMs reduce nonspecific interactions by a factor of 2 relative to 16-MHA. Thus, a direct measurement is possible with 3-MPA-$(Ser)_5$-anti-β-lactamase

following a short conditioning of the sensor with the biological fluid in which the analyte is dissolved.

5.4.6 Quantification of β-lactamase in crude cell lysate

In order to demonstrate the efficiency of the 3-MPA-$(Ser)_5$-OH monolayer on a SPR biosensor, an experimental procedure was designed for the quantification of β-lactamase in crude cell lysate. Controls using the blank cell lysate are required to correct for background signal, as *E. coli* strains naturally express β-lactamases at very low levels. Thus, TEM-1 cells overexpressing β-lactamase were lysed. The β-lactamase activity assay and the Bradford assay [205] of the complex solution determined a β-lactamase concentration of 0.39 mg/mL (12.8 μM) and a total protein concentration of the primary lysate of approximately 30 – 60 mg/mL. To validate the biosensor, the crude cell lysate containing β-lactamase was diluted 100-fold with blank cell lysate, as a μM concentration of β-lactamase is within the saturation range of the SPR sensor. The blank cell lysate provided a good blank measurement and an appropriate medium to dilute the overexpressed β-lactamase sample without changing the composition of the solution. The diluted β-lactamase sample was injected using the same procedure as the solutions prepared in PBS, such that the concentration of the overexpressed β-lactamase sample could be determined. The nonspecific interactions reached its maximum within the first few minutes of exposure of the biosensor to the crude cellular lysate. The linear regression equation obtained by the previous calibration of β-lactamase in PBS results in a 56 μM concentration in the undiluted cell lysate, which is in good agreement with the values obtained by measurement of the enzyme activity (12.8 μM). Hence, the actual concentration measured in the solution is within the nM range, taking into account the 100-fold dilution into blank cell lysate. This

indicates that the SPR sensor can detect nM concentrations of β-lactamase in a relevant, biologically complex solution.

5.5 CONCLUSIONS

This article reports the use of 3-MPA-$(AA)_n$-OH based SAMs to reduce nonspecific protein adsorption on SPR biosensors. The synthesis of SAMs with n = 2-5 amino acids attached to 3-mercaptopropionic acid (3-MPA) was accomplished using a solid phase approach on phenoxy resin lanterns allowing combinatorial type synthesis. The molecules synthesized were characterized by LC-MS before forming a SAM on thin glass slides coated with a thin film of Au. The surface concentration of the SAMs on Au varied between 98×10^{12} molecules/cm^2 and 486×10^{12} molecules/cm^2 with longer peptide chains forming less dense monolayers. The advancing contact angles showed that longer peptidic chains on the SAM enhanced the hydrophobic or the hydrophilic properties of the SPR surface depending on the peptide. 3-MPA-$(AA)_n$-OH prepared with the polar and ionic amino acids Ser, His and Asp, showed better performances in limiting the nonspecific signal induced by bovine serum proteins by a factor of 2 to 3 in comparison to the 3-MPA-$(AA)_n$-OH prepared from the more hydrophobic amino acids Leu and Phe. The attachment of a biological receptor to 3-MPA-$(Ser)_5$-OH using N-hydroxysuccinimide ester chemistry allowed the calibration of TEM-1 β-lactamase in PBS that led to the quantification of nM concentration of this enzyme in crude cell lysate. 3-MPA-$(Ser)_5$-OH increased the amount of antibodies available at the surface of a SPR biosensor and provided a greater retention of activity and a lower nonspecific signal induced by proteins from crude bacterial lysate. This increased the analytical signal observed by a factor of nearly 10 compared to the results obtained for alkanethiol or 3-MPA-amino acid based biosensors. Thus, these 3-MPA-

$(AA)_n$-OH SAMs exhibited numerous advantages for SPR biosensing in complex biological fluids.

5.6 ACKNOWLEDGMENTS

The authors thank William D. Lubell, Luisa Ronga, and Caroline Proulx for assistance with the synthesis of 3-MPA-$(AA)_n$-OH compounds. Financial support was provided by the Université de Montréal, the Canadian Foundation for Innovation (CFI), National Sciences and Engineering Research Council of Canada (NSERC), and the Fonds Québécois de la Recherche sur la Nature et les Technologies (FQRNT).

CHAPITRE 6 : SPR Biosensing in Crude Serum Using Ultralow Fouling Binary Patterned Peptide SAM [21]

Publié entant que : Bolduc, O. R.; Pelletier, J. N.; Masson, J.-F. *Analytical Chemistry* **2010**, *82*, 3699-3706.

Informations supplémentaires en Annexe B

6.1 ABSTRACT

Near-zero fouling monolayers based on binary patterned peptides allow low nanomolar detection of the matrix metalloproteinase-3 (MMP-3) directly in crude bovine serum, without sample pretreatment, secondary antibody detection or signal amplification. The peptide 3-MPAHHHDD-OH (3-MPA, 3-mercaptopropionic acid) was found optimal compared to other binary patterned peptides based on 3-MPA-Ax-By-OH, where $0 \leq x, y \leq 5$, and $x + y = 5$, and compared to PEG. In this study, amino acid A was His, Asp, Ser, or Leu, and amino acid B was His, Asp, or Ser. Zwitterionic peptides and other peptides exhibited excellent resistance to nonspecific adsorption. Binary patterned peptides were capped with 3-MPA on the N-terminus providing a monolayer with the C-terminus carboxylic acid available to subsequently immobilize antibodies. Thereby, an IgG biosensor demonstrated the efficiency of binary patterned peptides in SPR biosensing with a detection limit of 1-10 pM in PBS, similar to other optical or electrochemical techniques. This protocol was applied to establish a calibration curve for MMP-3, an analyte of clinical interest for many pathologies and a potential indicator of cancer. The LOD for MMP-3 was 0.14 nM in PBS, with a linearity of up to 50 nM. With the use of PBS calibration, MMP-3 was quantified at low nanomolar in undiluted bovine serum. The SPR response in serum was statistically the same as in PBS. A sensor exposed to blank serum exhibited negligible nonspecific adsorption. Hence, binary patterned peptides are suitable for biosensing directly in complex biological matrixes.

6.2 INTRODUCTION

Surface plasmon resonance (SPR) has evolved into a useful bioanalytical tool to detect proteins, DNA, enzymes and other biomolecules [19]. The excellent sensitivity of SPR

for detecting proteins explains the increasing popularity of SPR. However, biomolecule detection in complex matrices (such as cell lysate, serum and blood) is greatly limited due to nonspecific interactions on SPR biosensors. Nonspecific proteins interact with the surface of biosensors creating a false positive response, hindering the detection of analytes in crude biological fluids. Thus, it is necessary to reduce nonspecific interactions in order to allow the use of biosensors for direct monitoring of biomolecules in biological fluids, eliminating the need of cleaning steps, signal amplification, labeling or indirect detection of the analyte.

Immobilized molecular receptors on self-assembled monolayers are used to specifically detect biomolecules with SPR sensors [182]. Ideally, the monolayer should protect the SPR surface from nonspecific adsorption and provide an anchoring point for the molecular receptor to the SPR surface. Hence, extensive research in surface chemistry has been undertaken in the past decade to overcome nonspecific adsorption. In fact, the high sensitivity of SPR to protein adsorption also makes it an excellent tool to monitor nonspecific adsorption on self-assembled monolayers [154]. Dextran polymers have been extensively used in SPR biosensing, with mitigated results in complex biological fluids. The higher molecular weight dextrans, which are essential for the sensitive detection of analytes, fail to protect the SPR surface [147, 212]. Structure-property studies revealed that thiol monolayers with polar head groups were especially efficient in resisting nonspecific adsorption [64, 66, 213]. Among layers investigated in those studies, polyethyleneglycol (PEG), also known as polyethylene oxide (PEO), offered optimal performances in limiting nonspecific adsorption [64]. Numerous variants of PEG monolayers have been investigated for nonspecific adsorption [214-217]. Although PEG monolayers have been used for detection

of proteins in serum [218], they exhibit limitations including non-zero fouling, oxidative damage and the need of carboxylic acid functionalization of PEG in order to immobilize the molecular receptor.

Hybrid materials have been designed to improve on the properties of PEG. As examples, PEG copolymers of maleimide-PEG monolayers [219, 220], polypropylene sulfide-PEG [221] and poly(lysine)-PEG [222] were all successful in resisting nonspecific adsorption. The later combines the properties of peptides with PEG. This approach was further developed by the group of Messersmith, which successfully developed a peptidomimetic polymer with ethylene glycol brushes [69, 185]. This surface limited nonspecific adsorption from cells on a metallic surface. Similarly, a poly(aspartic acid) peptide with ethylene glycol (EG)-biotin brushes exhibited low nonspecific adsorption and could provide immobilization of molecules *via* biotin-streptavidin modified EG and biotinylated antibodies [223, 224].

The idea of using peptide monolayers to minimize nonspecific adsorption of biological media to SPR surfaces is attractive. The varied physico-chemical properties of the side chains provide prospects for tuning the surface properties, while the *N*-terminal amino acid is well suited to bind to a carboxy-terminated thiol, exposing the terminal carboxylic acid of the peptide to the solution for specific protein immobilization. To this end, we have previously studied the structure-property relationships of amino acid monolayers resistant to nonspecific adsorption [187]. This allowed selection of amino acids with optimal properties: small, polar and ionic, in accordance with previous results obtained for organic monolayers [64, 213]. Peptide monolayers were also demonstrated to reduce nonspecific adsorption to a level equivalent to PEG according to previous work, sufficient

for biomolecule detection in complex matrices such as crude cell lysate [103, 225]. Ultralow fouling was recently reported based on zwitterionic monolayers [67, 226, 227], allowing protein detection in blood plasma [228]. Here, the capacity of zwitterionic and non-zwitterionic peptides in achieving ultralow fouling, immobilization of recognition biomolecules and low level detection of proteins in serum will be investigated.

Matrix metalloproteinase-3 (MMP-3) is an enzyme involved in important pathologies including atherosclerotic plaques [229, 230], circulatory malfunctions [231, 232], arthritis [233], chronic liver diseases [234] and different types of cancer [233, 235-243]. MMP-3 is a proteinase involved in the degradation of the extracellular matrix, therefore potentially playing an important role in metastasis development during the early stage of invasive cancers [239, 240]. In those and other pathologies, it has been shown that the serum concentration of MMP-3 is upregulated up to four times relative to its normal abundance[229, 235, 238-240]. Depending on the experimental conditions used for the recovery of the media containing MMP-3 and the analytical techniques used to quantify this analyte, the normal concentration of MMP-3 (for healthy subjects) in serum varies from 0.7 nM [230] to 7 nM [234, 235]. Unamplified SPR biosensing typically reaches a limit of detection (LOD) in the low nM or pM range. Therefore, MMP-3 concentrations are within the range of detection by SPR. Although MMP-3 quantification alone could not be used to give a clear diagnostic for the pathologies listed before, it is a marker of great clinical importance. Because the variation in serum MMP-3 concentration in the above-mentioned diseases is modest, high-precision analytical detection is essential. Moreover, its low abundance in biological fluids makes it an ideal model for demonstrating the potential of mixed peptide SAMs for a direct detection assay in complex biological matrices.

6.3 EXPERIMENTAL SECTION

6.3.1 Preparation of 3-MPA-peptide-OH

Short thiolated binary patterned peptides were synthesized according to the procedure previously published for the synthesis of short homopeptides.[103] A minor difference is that the solid-phase synthesis support was replaced with a hydroxymethyl polystyrene resin. This precludes any change in the experimental conditions previously developed for hydroxymethylphenoxy polystyrene lanterns and allows a cost-effective and larger scale synthesis.[244] Numerous peptides were synthesized based on the general structure of 3-MPA-A_x-B_y-OH, where A is either Leu, Asp, His or Ser, B is either Asp, His or Ser, with $0 \leq x, y \leq 5$, and $x + y = 5$. LC-MS coupled with electrospray ionization validated the new approach and confirmed the mass of each final product. The overall yield varied between 15% and 70% depending on the peptide sequence. (See Annexe B for detailed procedure)

6.3.2 Preparation and characterization of monolayers

Peptide-based SAMs were prepared overnight in DMF solutions as stated previously [103, 187]. Monitoring of each SAM was accomplished on a Kretchmann SPR setup based on a dove prism [245]. Advancing contact angles with PBS were acquired with a home-built instrument. Peptide-based SAMs were also characterized using Ge-attenuated total reflection (ATR-FTIR). Quantification of nonspecifically adsorbed proteins on each surface was accomplished by exposing to PBS for baseline monitoring, followed by undiluted bovine serum then PBS to monitor the baseline after nonspecific adsorption. (See Supporting Information section for detailed procedure) CM-Dextran was prepared according to a previously reported procedure [120, 148].

6.3.3 Fabrication of SPR biosensors and detection of biomolecules

IgG and MMP-3 specific biosensors were built using the EDC/NHS chemistry on the free carboxylic acid of the peptide [149, 246-248]. Sensors fabricated as described above were mounted on the SPR instrument equipped with a fluidic cell and the signal was stabilized for at least 5 min in 18 MΩ water. The solutions required for fabrication of a SPR affinity biosensor were sequentially injected to chemically derive the surface with an antibody monolayer, procuring the specificity to the SPR sensor. The measurement began with 2 min of reference in 18 MΩ water. Then, an aqueous solution composed of 100 mM N-ethyl-N'-(3-dimethylaminopropyl)-carbodiimide (EDC, Fluka) and 20 mM of N-hydroxysuccinimide (NHS, Sigma-Aldrich) was injected for 2 min followed by a rinsing step with PBS (pH 4.5) for 2 more min. A solution of 25 µg/mL antibody (anti-human IgG, Cedarlane laboratories ltd, Burlington, ON, or anti-human MMP-3, GeneTex, Irvine, CA according to the experiments described below) in PBS (pH 7.4) was injected for 15 min to derivatize the surface with antibody. The excess antibody was rinsed with PBS for 2 min before a 5-min exposition to a 1 M ethanolamine solution adjusted to pH 8.5. The SPR sensor was rinsed again for 5 min in PBS before injection of the analyte of interest. The detection assay was performed for 10 min with a PBS solution of IgG or MMP-3 (according to the antibody immobilized) and was followed by a 5-min baseline measurement in PBS.

6.3.4 Quantification of MMP-3 in bovine serum

The SPR biosensors were used for direct detection of biomolecules in serum and diluted serum. Biosensors were prepared as described above. In this experiment, a 2-min exposition to bovine serum verified occurrence of nonspecific interaction on these

biosensors. Thereafter, bovine serum spiked with human MMP-3 to a concentration of 25 nM was injected on the SPR sensor. A blank serum measurement verified whether the SPR response monitored for MMP-3 was due to specific interactions and not to nonspecific adsorption. As a further control, the spiked serum was diluted by a factor of two to 12.5 nM with PBS or with bovine serum to verify that the signal was proportional to the analyte concentration. Statistical analysis was performed to validate the response.

6.4 RESULTS AND DISCUSSION

6.4.1 Synthesis of peptides

The peptide synthesis protocol was adapted from previous work based on SynPhase^{TM} lanterns, to the hydroxymethyl polystyrene resin used here [103]. The modifications were necessary to reduce the production cost of the peptides with minimal optimization of the preparation steps. This approach allowed the production of the various peptides involved in this study. To confirm that the SynPhase^{TM} lanterns protocol was valid for the hydroxymethyl polystyrene resin, the synthesis of a thiolated peptide was confirmed after each step using LC-MS. For example, prior to coupling of H_2N-HHHDD-OH with 3-MPA, the molecular ion was clearly visible at m/z = 660.2 indicating that the synthesis of the peptide was successful. The mass spectrum for the corresponding final product 3-MPA-HHHDD-OH showed a major signal at m/z = 748.7 corresponding to the expected mass molecular ion. It was revealed by LC-MS that significant fraction of the peptides formed disulfide bonds. For 3-MPA-HHHDD-OH, this was observed from a molecular ion at m/z = 1494.5; the final product adopted the disulfide form to a proportion of nearly 10%. It was also noticed that every product with His showed a yellow color in TFA, in accordance with prior observations for other His-containing peptidomimetic

structures [249]. This color disappeared after complete evaporation of the solvent leaving a white to grey precipitate similar to other peptides. The overall synthetic yield varied from 15% to 70% depending on the sequence of the peptide.

6.4.2 Effect of block length in binary patterned peptide SAMs

The combination of materials into hybrid materials yields properties that are not a linear combination of the properties of the individual materials. As an example, zwitterionic monolayers exhibit significantly decreased nonspecific adsorption [250-252]. This was observed for polymers of poly-L-lysine with poly-styrene sulfonate [253], where a mixed copolymer significantly decreased nonspecific adsorption. This approach is investigated here with block peptides, peptides constituted of a block of one amino acid at the N-terminus and a block of another amino acid at the C-terminus, exposed to the solution. In a first study, the optimal composition of the block length for a binary patterned pentapeptide was determined with a series of peptides with the general composition 3-MPA-H_x-D_y-OH, where $0 \leq x, y \leq 5$, and $x + y = 5$. The optimal length of peptide monolayer was previously determined to be five residues long for maximal reduction of nonspecific interactions [103], hence all peptides in this study are of that length. The peptides were synthesized with His at the N-terminus (in the base) to leave the Asp block, rich in COOH, surface-exposed for later reaction in immobilizing molecular receptors. Each block was varied from 0 to 5 to investigate all possible combinations of a His/Asp diblock pentapeptide.

Nonspecific adsorption of proteins contained in biological media has greatly limited the use of many biosensors by producing a false positive response. Therefore, measuring the nonspecific adsorption of binary patterned peptides on Au surfaces is essential in assessing the potential of these monolayers in biosensing templates. The surface coverage

for nonspecific adsorption of proteins on binary patterned peptide SAMs was obtained from the equations of Jung *et al*. [170, 208] and the parameters previously published [103]. Figure 6-1 shows a sensorgram obtained for 3-MPA-HHHDD-OH. A 5 min period in PBS allowed the system to stabilize before PBS was replaced with bovine serum containing 76 mg/mL of proteins. The protein concentration in bovine serum is similar to human serum making this model relevant. An important portion of the shift of signal observed during this replacement was due to the bulk change of refractive index between PBS and serum. The SPR response to nonspecific adsorption was obtained at least four times for every peptide.

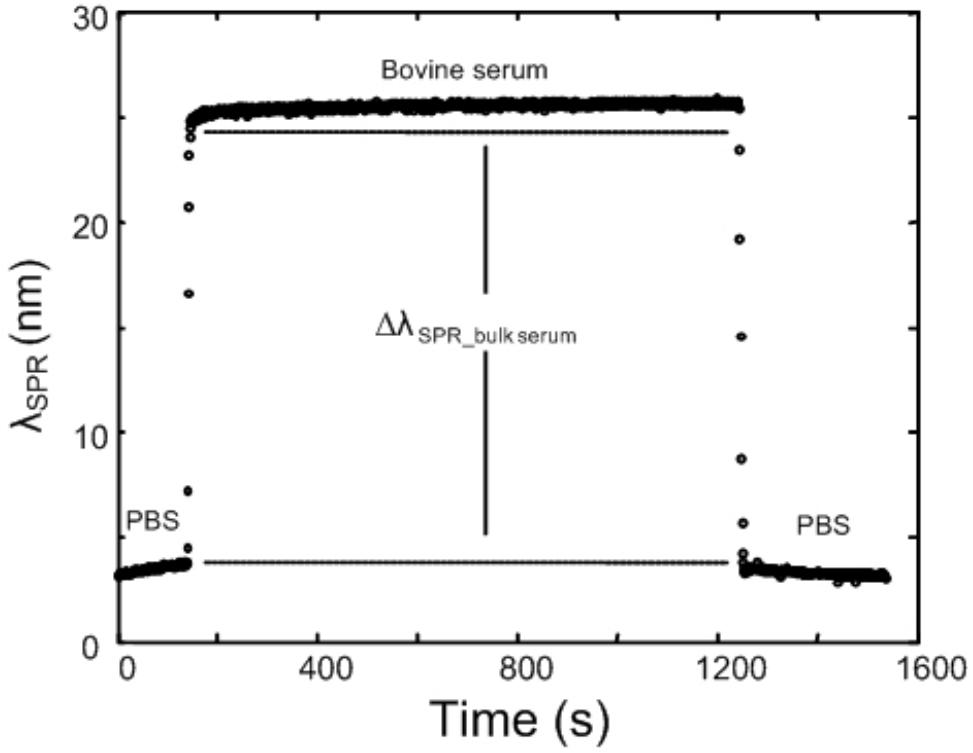

Figure 6-1. Sensorgram demonstrating low nonspecific adsorption of bovine serum proteins on a SAM of 3-MPA-HHHDD-OH.

Nonspecific adsorption was greatly decreased using binary patterned peptides (Figure 6-2, left panel). Homopeptides 3-MPA-HHHHH-OH and 3-MPA-DDDDD-OH

showed relatively high nonspecific adsorption at nearly 200-300 ng/cm². However, binary patterned peptides with these same two amino acids arranged in blocks decreased nonspecific interaction by one order of magnitude. Nonspecific adsorption of serum decreased for peptides with increasing block length of either of the two different amino acids. Nonspecific adsorption decreased to a minimum (32 ng/cm²) for a peptide with the composition 3-MPA-HHHDD-OH. This is significantly lower than PEG, which exhibits approximately 100 ng/cm² of nonspecific adsorption [103], and CM-Dextran (829 ± 46 ng/cm²) using an identical experimental setup and solutions. This signifies that binary patterned peptides significantly improve nonspecific adsorption compared to the homopeptides and to state-of-the-art PEG. Similarly, a decrease of one order of magnitude for mixed monolayers compared to pure components has been observed with poly-L-lysine and poly-styrene sulfonate [253]. To extend these results to a variety of peptide compositions, further binary patterned peptides with the same 3-MPA-AAABB-OH configuration were also investigated (*vide infra*).

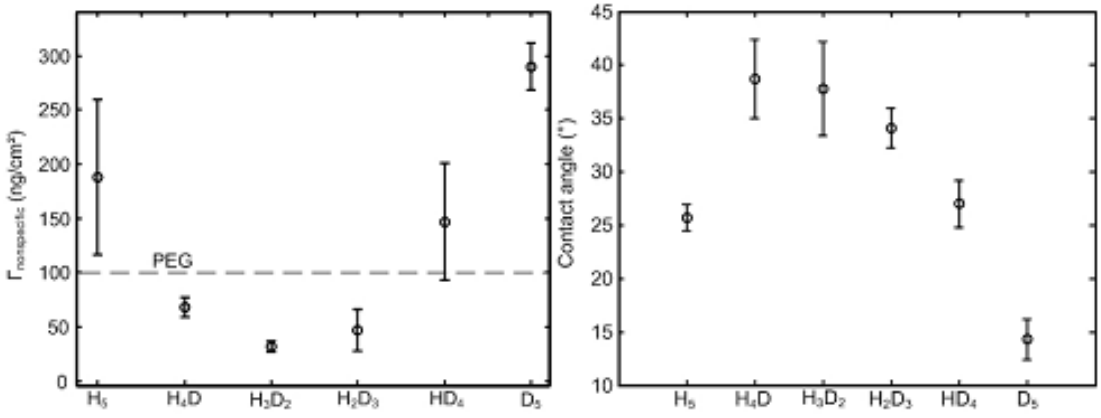

Figure 6-2. (Left) Reduction of nonspecific adsorption with binary patterned peptides. (Right) Contact angle with binary patterned peptides. The peptides are identified as: H5 for 3-MPA-HHHHH-OH, H4D for 3-MPA-HHHHD-OH, H3D2 for 3-MPA-HHHDD-OH,

H2D3 for 3-MPA-HHDDD-OH, HD4 for 3-MPA-HDDDD-OH, and D5 for 3-MPA-DDDDD-OH. The error bars represent two standard deviations of the mean.

6.4.3 Characterization of the peptides with contact angle, FTIR and capillary electrophoresis

To better understand the physico-chemical effects involved in the decrease of the nonspecific adsorption to these binary patterned peptide surfaces, several studies were undertaken. Contact angle measurements are related to the hydrophilicity of the monolayers. In the case of binary patterned peptides, contact angle increased upon combining blocks of Asp and His to reach a maximum plateau of approx. 35° for 3-MPA-HHDDD-OH, 3-MPA-HHHDD-OH and 3-MPA-HHHHD-OH (Figure 6-2, right panel), roughly correlating with decreased nonspecific adsorption. Highly charged surfaces (*e.g.* CM-dextran) were previously found to increase nonspecific adsorption [147]. Hence, it is possible that the decrease of nonspecific adsorption is related to the zwitterionic character of these binary patterned peptides, as observed with several polymers [227, 253]. In order to verify if this difference in nonspecific adsorption is due to the global charge of the peptide, capillary electrophoresis was accomplished for the peptides providing the greatest decrease in nonspecific adsorption. Calibration runs were accomplished demonstrating that the difference in global charge between 3-MPA-HHDDD-OH, 3-MPA-HHHDD-OH and 3-MPA-HHHHD-OH was almost negligible. Their global charge was approximately -1 as determined by capillary electrophoresis, indicating that the peptides carry one more carboxylate anion than iminium cation. Hence, it appears that the binary patterned peptide surfaces with lowest nonspecific adsorption exhibit a strong zwitterionic character.

Peptides in solution exhibit structures which are essential for their biological functions. However, it is well known that antibodies are denatured to some extent when immobilized directly on Au. It was thus of interest to observe whether the peptide monolayer on the Au surface adopted any significant secondary structure, to provide insight on the potential formation of a "biologically compatible monolayer". The secondary structure of peptides on a surface is generally monitored *via* the amide I and II bands visible by mid-IR (Figure 6-3) [209]. Peptides adopting an α-helical configuration show a strong amide I band at 1645 cm^{-1}, while peptides auto-assembling in the extended configuration lead to a shifted amide I at 1675 cm^{-1} [209, 254]. Interestingly, all peptides investigated here adopted an α-helical configuration except for 3-MPA-HHHDD-OH. These results indicate that the peptides adopt a secondary structure on the surface and are not "quenched" by the Au surface. The conformation of 3-MPA-HHHDD-OH and 3-MPA-LLLDD-OH was also assessed in PBS using circular dichroism. In accordance with mid-IR results, 3-MPA-HHHDD-OH adopted an extended conformation in PBS, while 3-MPA-LLLDD-OH exhibited an α-helical conformation. The interpretation of circular dichroism data was performed according to Doneux *et al* [255]. However, the high performance of 3-MPA-HHHDD-OH in decreasing nonspecific adsorption cannot be correlated with adoption of the extended configuration, as other peptides exhibited similar nonspecific adsorption while adopting an α-helical configuration.

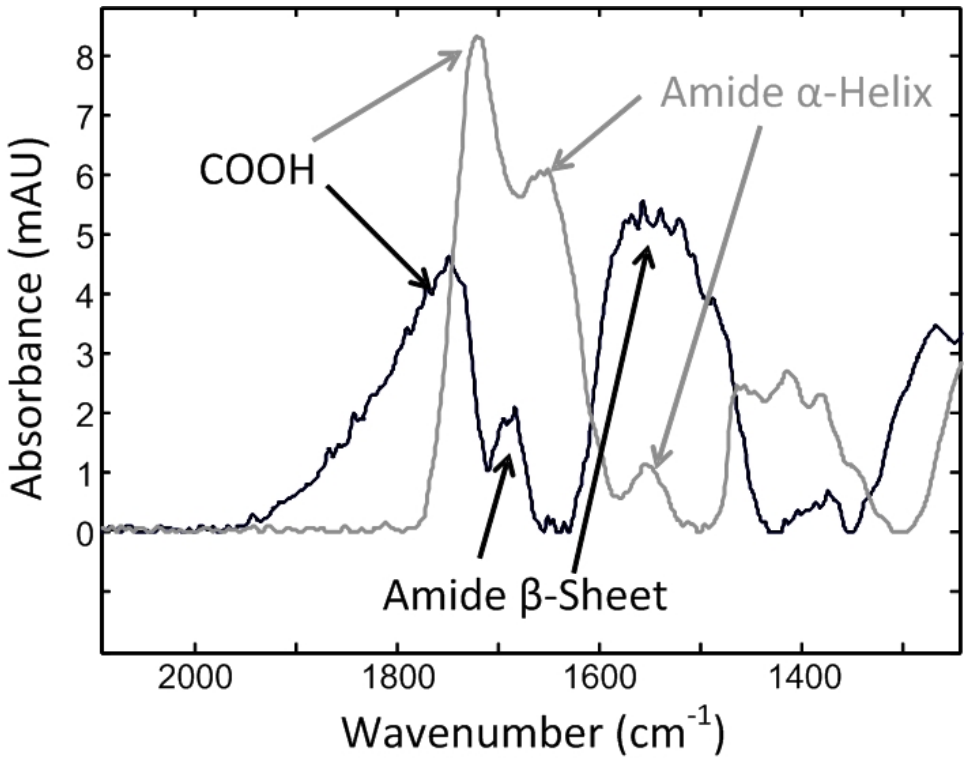

Figure 6-3. Determination of the extended or α-helix configuration of a binary patterned peptide SAM using FT-IR. The gray line is for 3-MPA-LLLDD-OH and is representative of the signal observed for all other binary patterned peptides except for 3-MPA-HHHDD-OH which is represented by the black line.

6.4.4 Effect of the physico-chemical properties of the different blocks in mixed peptides

In order to test if a further decrease in nonspecific adsorption could be obtained with binary patterned peptides, every possible combination of the form 3-MPA-AAABB-OH was synthesized, where A is either His, Asp, Ser or Leu and B is His, Asp or Ser. The resulting peptides tested the four major physico-chemical properties for the N-terminal block: hydrophobic (Leu), polar (Ser), acidic (Asp) and basic (His), where Leu was introduced to investigate the influence of a hydrophobic block on nonspecific interactions in complex biological matrices. The C-terminal block was always constituted of

hydrophilic residues, either neutral or charged. By those means, generalities on the influence of the peptide physico-chemical properties could be observed.

Table 6-1. Characterization of block peptide SAMs immobilized on the gold surface of a SPR biosensor

Sequence	$\Delta\Gamma_{nonspecific}$ (ng/cm^2)
3-MPA-SSSDD-OH	23 ± 10
3-MPA-HHHDD-OH	32 ± 5
3-MPA-LLLDD-OH	35 ± 23
3-MPA-LLLSS-OH	39 ± 13
3-MPA-LLLHH-OH	45 ± 11
3-MPA-HHHSS-OH	48 ± 18
3-MPA-DDDHH-OH	56 ± 22
3-MPA-DDDSS-OH	69 ± 40
3-MPA-SSSHH-OH	79 ± 50

The error represents two standard deviations.

The different peptide monolayers were classified from the most to the least resistant to nonspecific adsorption of serum proteins (Table 1), highlighting the relationship between the peptide sequence and their performance in limiting nonspecific adsorption. Two distinct trends were observed. Firstly, the three monolayers displaying the least nonspecific interactions with bovine serum had Asp as the C-terminal block. These monolayers present the dual advantage of improved resistance to nonspecific interactions and potentially improving bioreagent immobilization, since the free carboxylates should be available for attachment of a recognition molecule (antibody, enzyme, DNA, aptamer or others) through NHS-ester chemistry. While 3-MPA-SSSDD-OH offered slightly better performance, its synthetic yield was four times lower than 3-MPA-HHHDD-OH, hindering its use in

practical applications. This led to the selection of 3-MPA-HHHDD-OH for subsequent experiments.

Interestingly, each binary patterned peptide maintained excellent resistance to nonspecific adsorption, where adsorption of nonspecific proteins ranged from 23 ng/cm^2 to 79 ng/cm² (Table 6-1). These values are extremely low, as the resistance to nonspecific interactions from bovine serum typically ranges between 100 to 1000 ng/cm² [137, 147, 187, 256]. Specifically, these values are inferior by roughly one order of magnitude with most monolayers and by up to a factor of 4 compared to state-of-the-art PEG monolayers [103]. Also providing low nonspecific adsorption, monolayers including a Leu base offered the 3rd to 5th best performances among the binary patterned peptides tested. These results show that a zwitterionic monolayer is not essential for ultralow fouling. It suggests that the combination of different physico-chemical properties within a single monolayer such as charge for zwitterionic monolayers or hydrophobicity/hydrophilicity in others is a condition for ultralow fouling. As we demonstrate below, this improvement allowed direct detection assays in complex matrices.

6.4.5 SPR biosensors with binary patterned peptide SAMs: 3-MPA-HHHDD-OH

In order to demonstrate the efficiency of binary patterned peptide SAMs to immobilize biorecognition molecules such as antibodies in the construction of an affinity biosensor, an IgG biosensor was demonstrated. IgG detection is commonplace in biosensing and provides an excellent comparison point with other techniques and approaches. To fabricate this biosensor, a series of chemical reactions were performed on the binary patterned peptide monolayer, as demonstrated in Figure 6-4 (left panel). The

interaction between IgG and anti-IgG is strong, as observed from the slow return to the initial baseline during the last exposition to PBS of the IgG biosensor (longer than the data acquisition). This is expected as IgG and anti-IgG has a large binding constant. Hence, the 3-MPA-HHHDD-OH is suitable for biosensor construction. A control was performed with the unreacted 3-MPA-HHHDD-OH surface. 1 μM IgG was injected on the sensor, which showed no response to IgG, unless the antibody was immobilized to the peptide monolayer (positive control).

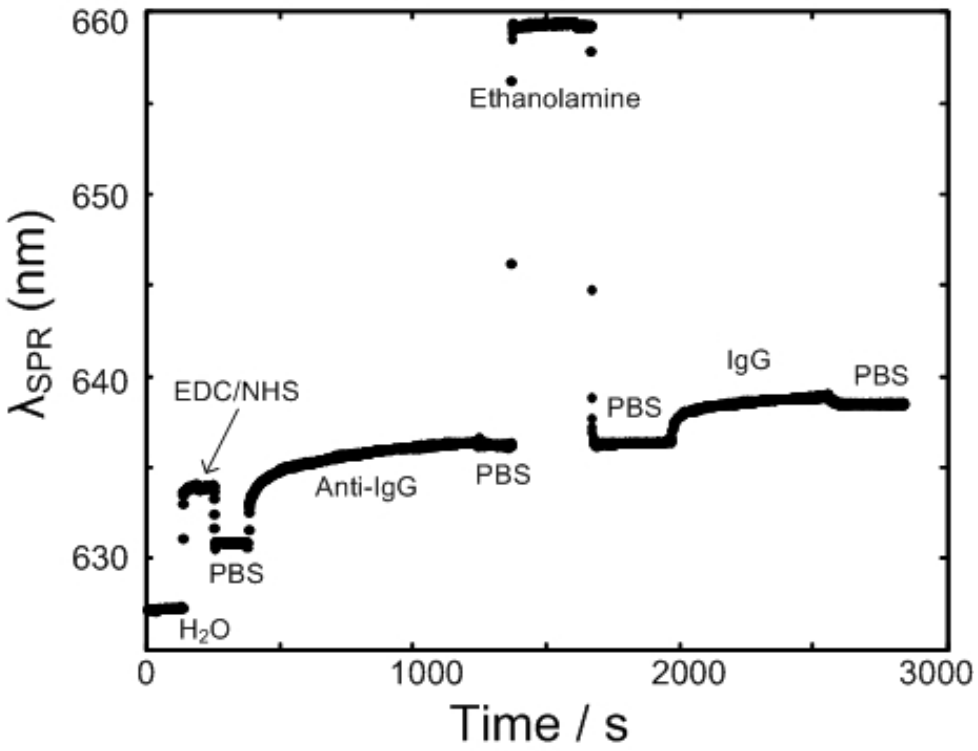

Figure 6-4. Sensorgram for the fabrication of an IgG specific biosensor. This SPR sensor held a 3-MPA-HHHDD-OH monolayer.

The calibration curve of IgG using a SPR sensor derived with 3-MPA-HHHDD-OH and anti-IgG, showed the expected behavior of a Langmuir isotherm (Figure 6-5 – left). The binding constant of IgG/anti-IgG measured on peptide monolayer is 2.6×10^{7} M^{-1}. This

is consistent with the anti-IgG/IgG affinity constant published elsewhere, which was as high as 3.2 x 10^7 M^{-1} [257]. A linear domain of SPR response was observed within the nM concentration range (from 0 to 3 in the logarithmic concentration scale). This domain delimits the concentration of interest that could be determined with high sensitivity using this SPR biosensor. The SPR response observed outside this domain was saturated at higher concentrations and exhibited low sensitivity at lower concentrations. An apparent detection limit of 0.11 nM was obtained from this high sensitivity domain, which is typically used for the determination of LOD in SPR. This LOD is calculated with 3 times the noise on the SPR sensorgram (3σ = 0.03 nm), with the slope of the highly sensitive region. Among others, SPR imaging sensors exhibited a detection limit of 3.7 nM for direct detection of IgG [257]. In our work, the lower LOD by one order of magnitude is explained by the wavelength interrogation method being more accurate than the intensity measurement [19]. However, the low-sensitivity region of the calibration curve still exhibited a response proportional to concentration and greater than the limit of detection. We conclude that the actual limit of detection for IgG would be between 1-10 pM, similar or better than that reported for other biosensors. Due to the low sensitivity of this region, an exact LOD is not reported. Lower detection limits have been obtained with sandwich immunoassays using SERS (19 pM) [258], SPR (6.7 pM) [259], chemiluminescence (3 pM) [260], anodic stripping voltammetry (3 pM) [261], and LSPR with Ag nanoparticles (9 pM) [262]. However, these methods require multi-step detection schemes.

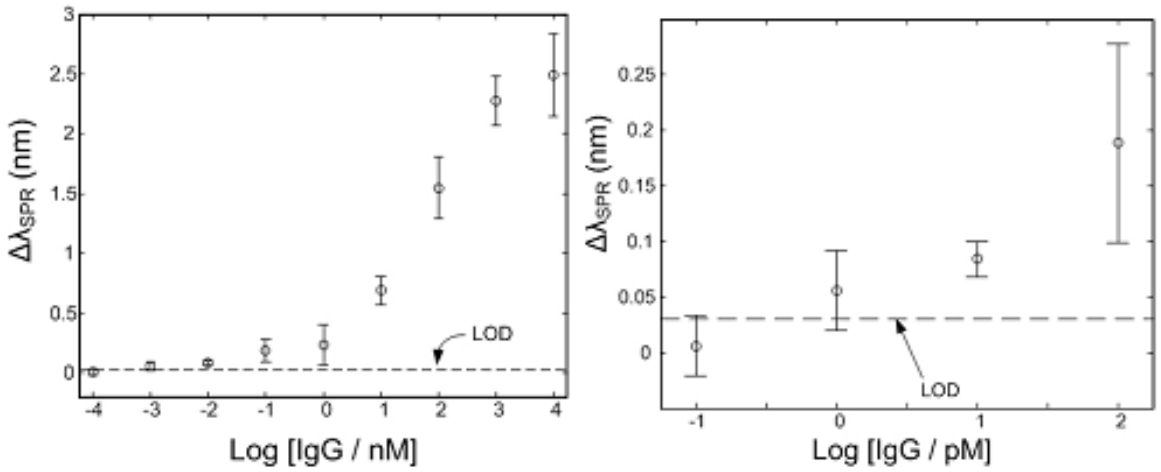

Figure 6-5. (Left) Calibration curve of IgG in PBS. The concentration of IgG is given in a logarithmic scale in nM. (Right) Low-sensitivity response of IgG in the pM range, with a LOD of 3 pM.

6.4.6 Calibration of MMP-3 in PBS

The possibility of substituting antibodies for other biologically relevant problems is an important advantage of SPR biosensors. MMP-3 is an important biomarker to monitor various diseases. Hence, a SPR sensor was prepared as for IgG, with the exception of anti-human MMP-3 acting as the recognition biomolecule for human MMP-3. The sensorgrams for different concentrations of MMP-3 showed increasing intensity of the SPR responses to increasing concentration of MMP-3 in PBS (Figure 6-6 - left). The correlation coefficient (R^2) for this calibration curve is 0.96 indicating a strong linear relationship between the SPR response from MMP-3 and the concentration of MMP-3. The slight deviation from unity of the regression coefficient could be explained by the non-linearity at high concentration of the Langmuir isotherm. The calibration allows the quantification of MMP-3 over a targeted domain of concentrations comprised between 0.5 and 50 nM, with a detection limit at 0.14 nM. Moreover, addition of PBS led to a nearly complete return of the

SPR response to initial value prior to MMP-3 binding (data not shown), suggesting that MMP-3 binding to anti-MMP-3 was rapidly reversible.

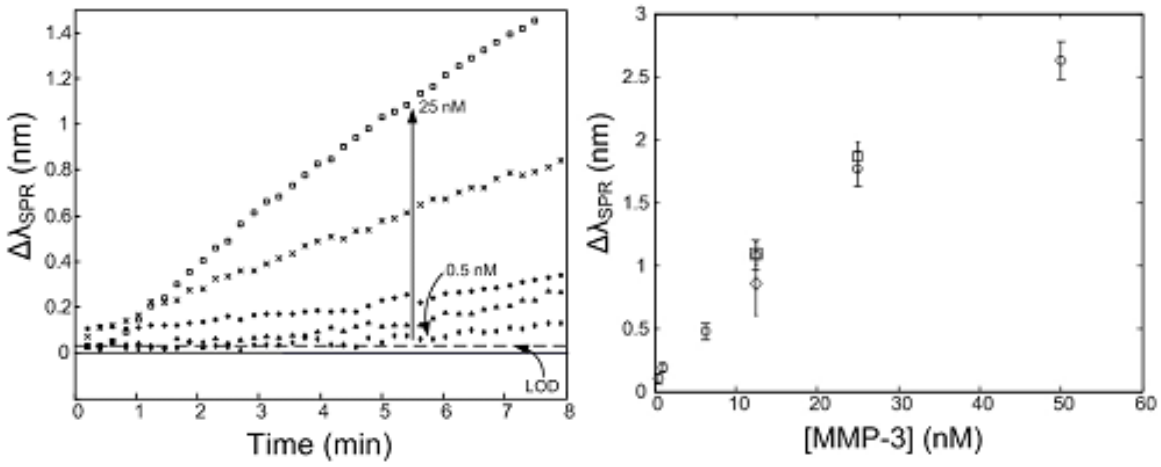

Figure 6-6. (Left) Overlay of sensorgrams for the detection of different concentrations of MMP-3 in PBS. The concentrations detected are 0.5, 1, 6, 12.5 and 25 nM. (Right) Calibration curve of MMP-3 in PBS ('o'; n=3: number of replicate measurements at each concentration). Quantification of MMP-3 in complex matrices: '□' show the detection of 12.5 and 25 nM MMP-3 in full bovine serum; '◊' shows the detection of 12.5 nM MMP-3 in 1:1 bovine serum / PBS.

6.4.7 Detection and quantification of MMP-3 in bovine serum

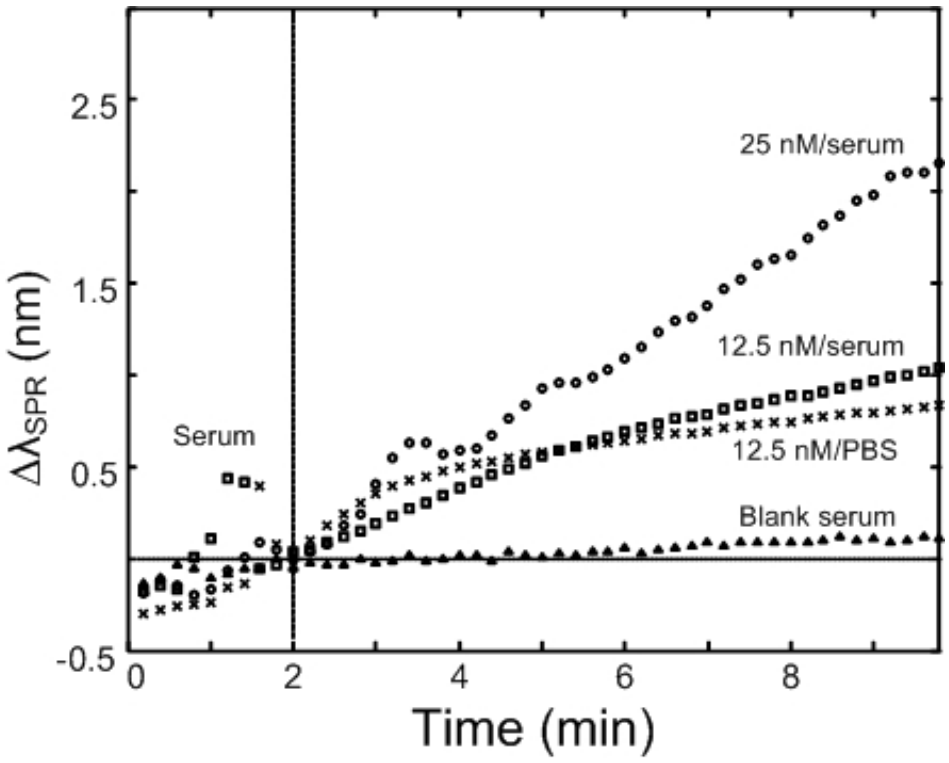

Figure 6-7. Detection of human MMP-3 in complex matrices. MMP-3 was spiked into bovine serum (exempt of human MMP-3) at 25 nM ('o'). A 1:1 dilution with bovine serum ('□') and with PBS ('x'), decreased this concentration to 12.5 nM. The blank ('Δ') demonstrates that the SPR response observed for the three other sensorgrams is due to specific interactions of MMP-3 with anti-MMP-3.

In order to demonstrate the efficiency of 3-MPA-HHHDD-OH in reducing the level of nonspecific interactions with the surface of a biosensor, detection of MMP-3 was performed in undiluted bovine serum. The two-minute pre-exposition of the SPR sensor to serum exempt of MMP-3 showed little response due to nonspecific interactions (Figure 6-7). This further demonstrates that the peptide-derived SPR biosensor is very stable in undiluted serum. Figure 6-7 shows the SPR response of 25 nM MMP-3 in serum, which was significantly different than the response of a blank serum sample. As highlighted in figure 6-6, the detection of 25 nM MMP-3 in bovine serum resulted in a SPR response

statistically identical to the detection of 25 nM MMP-3 in PBS. The predicted concentration for the detection of 25 nM in PBS using the linear calibration model in PBS results is 30 ± 2 nM. The deviation between the predicted and actual concentration is due to the slight deviations from linearity observed with the Langmuir model. Detecting the same concentration in undiluted serum resulted in a predicted concentration of 32 ± 2 nM. This indicates that the serum does not influence the detection of MMP-3 in a complex biological matrix and that the response is identical to the one measured in saline solution.

Dilution of the MMP-3 serum sample with serum or PBS provided a comparative study to evaluate the influence of serum on the detection of MMP-3 in complex matrices. The dilution of MMP-3 to 12.5 nM with PBS or serum resulted in a proportional decrease of the SPR response (Figure 6-7). The similar SPR response with 12.5 nM MMP-3 in serum (predicted concentration of 17 ± 1 nM) and 1:1 PBS/serum (predicted concentration of 12 ± 4 nM) suggests that nonspecific protein adsorption in undiluted serum has a minimal influence on the measured SPR response. This is very similar to the predicted concentration of 12.5 nM MMP-3 measured in PBS (predicted concentration of 17 ± 2 nM). These assays demonstrated the efficacy of binary patterned peptide SAMs immobilized on the SPR biosensors for detection assays in complex analytical matrices. Lastly, a direct detection assay, without flowing blank bulk bovine serum over the biosensor before injecting the serum containing 25 nM of MMP-3, led to similar results although the shift observed was overestimated by 15 % due to previously observed minimal nonspecific adsorption still taking place. This could easily be taken into account in calibration models. Therefore, binary patterned peptide monolayers are suitable for detection of low nM levels of MMP-3 in serum, without sample pre-treatment or signal amplification.

6.5 CONCLUSION

This article demonstrates the efficacy of binary patterned peptide self-assembled monolayers (SAMs) to reduce nonspecific interactions caused by bulk proteins in complex analytical matrixes to a level allowing the quantification of a biological molecule of clinical interest in undiluted serum. Various studies revealed that the decrease in nonspecific adsorption provided by binary patterned peptides or other ultralow fouling monolayers is unrestricted to the zwitterionic character and also includes monolayers combining mixed physicochemical properties. Various peptide compositions, including 3-MPA-HHHDD-OH, exhibited ultralow fouling properties. The calibration of IgG using SPR biosensors, based on the binary patterned peptide 3-MPA-HHHDD-OH, verified the potential of such SAMs for building SPR biosensors, with an excellent detection limit of 1-10 pM. MMP-3, an upregulated marker in cancer, was quantified by applying the same protocol leading to a quantification of low nanomolar amount of this analyte in undiluted bovine serum. The detection limit for the MMP-3 biosensor was 0.14 nM. These two examples of biosensing with binary patterned peptide monolayers demonstrate the strong potential of this methodology for SPR sensors.

6.6 ACKNOWLEDGMENTS

The authors would like to thank William Lubell and Caroline Proulx from Université de Montréal, for technical assistance in synthesizing the peptides. Financial support was provided by NanoQuébec, the Canadian Space Agency, the Canada Foundation for Innovation (CFI), the National Sciences and Engineering Research Council of Canada (NSERC), the Fonds Québécois de la Recherche sur la Nature et les Technologies (FQRNT).

CHAPITRE 7 : Modified peptide monolayer binding His-tagged biomolecules for small ligand screening with SPR biosensors[263]

Publié entant que : Bolduc, O. R.; Lambert-Lanteigne, P.; Colin, D. Y.; Zhao, S. S.; Proulx, C.; Boeglin, D.; Lubell, W. D.; Pelletier, J. N.; Fethiere, J.; Ong, H.; Masson, J.-F. Analyst 2011, 136, 3142-3148.

Informations supplémentaires en Annexe C

7.1 ABSTRACT

A peptide self-assembled monolayer (SAM) was designed to bind His-tagged biomolecules for surface plasmon resonance (SPR) bioanalysis, which was applied for the determination of K_d for small ligand screening against CD36. Nonspecific adsorption could be minimized using penta- and hexa-peptides monolayers. In particular, monolayers consisting of 3-mercaptopropionyl-leucinyl-histidinyl-aspartyl-leucinyl-histidinyl-aspartic acid (3-MPA-LHDLHD) exhibited little (12 ng/cm^2) nonspecific adsorption in crude serum. Modification of this peptide monolayer with Nα,Nα-bis(carboxymethyl)-L-lysine gave a surface competent for binding His-tagged proteins, as demonstrated using enzyme (human dihydrofolate reductase), protein/antibody and receptor (CD36) examples. Immobilization featured chelation of copper and the His-tagged protein by the peptide monolayer, which could be recycled by removing the copper using imidazole washes prior to reuse.

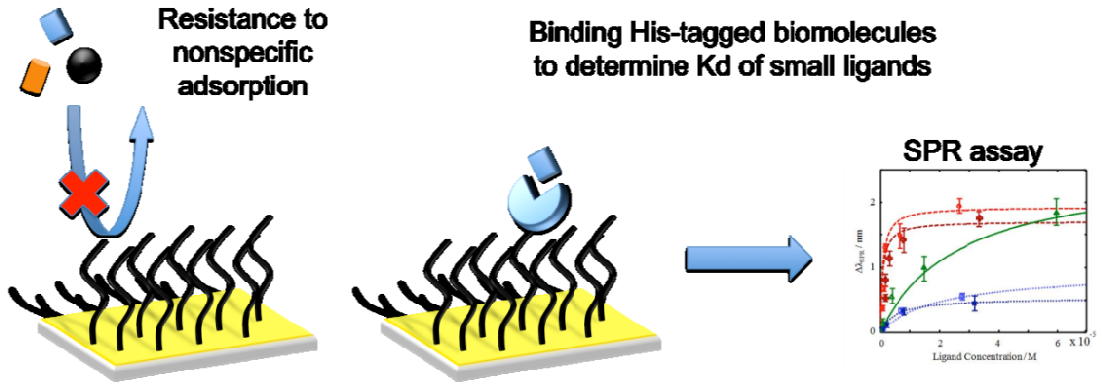

Figure 7-1. A peptide monolayer was designed to resist nonspecific adsorption of crude serum and to bind histidine-tagged biomolecules for SPR assays.

7.2 INTRODUCTION

Biosensors based on optical and acoustic wave technologies are promising analytical tools for many applications including clinical diagnostics, as well as environmental, food and water analysis [2, 264-267]. Appropriate surface chemistry is important for optical sensor development because interactions are monitored at the interface of a recognition layer and an optical medium [268]. The ideal chemical layer should provide abundant immobilization sites and maintain the activity of the recognition element without eliciting nonspecific interactions with other elements of the analytical media. Many surfaces have been investigated to fulfill these requirements, including CM-Dextran, polymers and organic self-assembled monolayers (SAM) [64, 147, 269, 270]. However, most strategies have yet to achieve analytical sensitivity when measuring analytes in biological fluids. Self-assembled monolayers (SAM) based on thiolated short peptides immobilized on gold-coated surfaces have been recently introduced as surface plasmon resonance (SPR) sensors [103, 187, 271, 272]. These peptide monolayers have demonstrated little nonspecific interaction with complex biological media such as cell lysate and crude serum, decreasing nonspecific adsorption to nearly 20-40 ng/cm^2, in contrast to commonly used PEG, which typically adsorbed 100 ng/cm2 of proteins. Such peptides have also been used to efficiently immobilize active antibodies for specific detection of proteins at nM levels and IgG at pM levels. In addition, the matrix metalloproteinase-3 (MMP-3) cancer marker was detected in crude serum using this approach [271]. Although peptide monolayers have performed well in bio-analyses by minimizing nonspecific adsorption, relatively few peptide architectures, mostly binary sequences have been employed and the effects of more complex sequences has yet to be studied to achieve even lower nonspecific adsorption in complex samples.

Sensor efficiency may be greatly influenced by immobilization chemistry. Standard chemical reactions for immobilizing biomolecules employ often coupling procedures using EDC/NHS (N-ethyl-N'-(3-dimethylaminopropyl)-carbodiimide / N-hydroxy-succinimide) to attach surface accessible free amines on the biomolecule to carboxylic acids in the peptide monolayer. Although biocompatible, such couplings may influence the environment of the immobilized biomolecule. For example, immobilization of human dihydrofolate reductase (hDHFR) using standard EDC/NHS coupling onto various peptide and organic monolayers failed to yield active enzyme, likely due to modification of the amine side chains of lysine residues proximal to the enzyme active site (vide infra). Because many cancer treatments are based on competitively inhibiting the activity of hDHFR [273, 274] and clinical follow-up may require quantifying circulating levels of such anticancer agents, alternative approaches for effective immobilization of hDHFR on SPR sensors in active form were needed. Exploring other surface chemistry using peptide monolayers, we have pioneered an approach for immobilization of active hDHFR, with general utility for anchoring fragile biomolecules.

Recombinant proteins are frequently expressed with a histidine tag for purification by forming complexes with Cu or Ni immobilized on a solid support. In this approach, the protein is modified with a stretch of histidine residues (most commonly 6-His) at the N- or -C terminus, which is usually distant from the functional region of the enzyme. Biological activity may thus be unaffected by the histidine-tag, as demonstrated recently using His-tagged proteins immobilized on biosensors containing self-assembled monolayers of nitrilotriacetic acid (NTA) analogs [275-278]. Similarly, PEGylated and CM-dextran modified NTA surfaces have been used in commercial SPR chips for anchoring His-tagged

protein[268, 269, 277]. Employing the inherent advantages of peptide monolayers with respect to nonspecific adsorption compared to CM-dextran and PEG surfaces, we have now developed novel surfaces for anchoring His-tagged biomolecules (Figure 7-2). In addition, the binding chemistry of our new surfaces has been particularly useful for preserving the activity of hDHFR and determining the K_d of other sensitive proteins such as CD36 immobilized on SPR sensors.

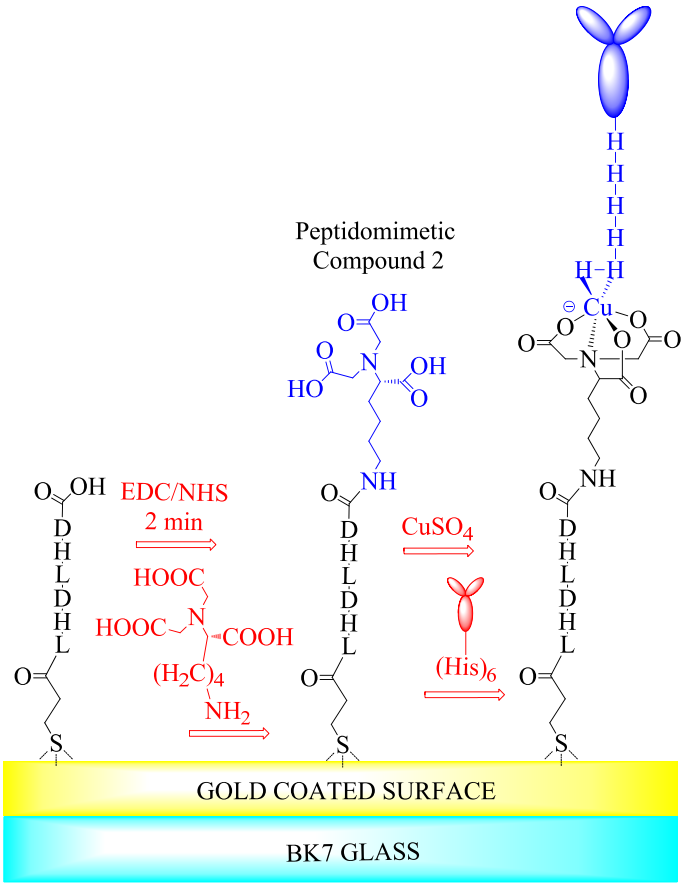

Figure 7-2. Schematic representation of the modified peptide layer binding His-tagged biomolecules.

7.3 EXPERIMENTAL SECTION

7.3.1 Materials

Microscope slides (BK7, 22×22 mm), anhydrous methanol and imidazole were bought from Fisher Scientific. Sterile filtered adult bovine serum, L-histidine, N-ethyl-N'-(3-dimethylamino-propyl)-carbodiimide (EDC), N-hydroxysuccinimide (NHS), ethylene diaminetetraacetic acid (EDTA) and Nα,Nα-bis(carboxymethyl)-L-lysine hydrate were purchased from Sigma-Aldrich. Gold (purity of 99.99%) and chromium were acquired from ESPI Metals. Dimethylformamide (DMF, ACS grade) was bought from EMD chemicals. Phosphate buffered saline 1x (PBS), pH = 7.4 was prepared by Cellgro from Mediatech.

7.3.2 Synthesis and characterization of peptide-based self-assembled monolayers

The peptides were synthesized and attached to gold surfaces according to a previously described protocol [271] (more details in Annexe C - ESI). EDC/NHS chemistry was used to attach Nα,Nα-bis(carboxymethyl)-L-lysine hydrate to the carboxylic acids of the immobilized modified peptide layer SAM available on the surface. The carboxylic acid donor could be either the C-termini or the aspartic acid side chain. The final step was a 10-minute exposition to 100 mM CuSO4, during which Cu2+ binds to the modified peptide layer. Mid-infrared spectroscopy (mid-IR) and x-ray photoelectron spectroscopy (XPS) were used to ensure the presence of Cu2+ on the SPR sensors (details in ESI).

7.3.3 SPR measurements

The real-time monitoring of the SPR sensorgram was accomplished using a miniature dove prism SPR instrument in the Kretschmann configuration [245]. An Ocean Optics USB4000 fibre optic spectrometer ranging from 550 to 850 nm was used to acquire

the spectral information, processed with Matlab to obtain the SPR sensorgram. A 25 μL Teflon fluidic cell positioned on top of the SPR sensors was used to inject the solutions required to functionalize with the recognition element and detect the analytes of interest. The SPR response was acquired at a frequency of 1 Hz. The s-polarized reference was acquired in PBS buffer before monitoring a 5-minute baseline in p-polarization. PBS was replaced with crude bovine serum (76 mg/mL protein) for 20 minutes and rinsed with PBS for 5 minutes to quantify the amount of non-specifically adsorbed proteins.

7.3.4 Real-time monitoring of the hDHFR enzymatic reaction

The modified peptide layer binding His-tagged biomolecules was exposed for a period of 15 minutes to a 50 μg/mL solution of His-tagged hDHFR in PBS and rinsed with PBS. The SPR sensor with His-tagged hDHFR was placed in a UV/Vis cuvette for monitoring enzyme activity, similar to a method developed by Xu et al. [279]. His-tagged hDHFR was obtained as previously reported [280]. A negative control, consisting of the peptidomimetic-modified SPR sensor without hDHFR, was exposed to buffer and rinsed to verify that the observed change in absorbance was due to immobilized His-tagged hDHFR and not to the surface itself. The SPR sensors were immersed in a solution of 100 μM NADPH (cofactor) and 100 μM dihydrofolate (DHF, substrate) in 10 mM Tris buffer, pH = 8.0, for 1 hour. The activity of the enzyme was measured by following the time course of the absorption ($\Delta A(t)$) at λ = 340 nm due to consumption of NADPH and DHF, by subtracting the blank signal (Ablank(t)) and the initial absorbance of the solution (A(0)). Therefore, the activity of the immobilized hDHFR induced a decrease of absorbance due to the consumption of its natural substrate, DHF and its cofactor NADPH. The activity was confirmed for each sample of His-tagged hDHFR on the SPR sensor. 1 U of enzyme

activity corresponds to the conversion of 1 μmol substrate to product per min. Absorption spectra were recorded with a Cary 100 Bio UV/Vis spectrophotometer equipped with a liquid temperature control system running at 35˚C to be in the optimal condition for the enzymatic reaction to take place. After monitoring the activity, the SPR sensors were rinsed with buffer, 18.2 MΩ water and the His-tagged hDHFR was removed from the surface with a 0.5 M imidazole solution for 10 minutes. The abundantly rinsed surfaces were tested again for enzyme activity at 340 nm to show that no His-tagged hDHFR remained on the SPR sensor. Another rinse was performed with 18.2 MΩ water, followed by 10 minutes in 100 mM CuSO4, then with His-tagged hDHFR to regenerate the surface. The enzymatic reaction was monitored to demonstrate the reusability of this immobilization strategy.

7.3.5 Monitoring of antibody-antigen interactions

Analyzing antibody-antigen interaction as a model system for comparison assessed performance of the SPR sensor. A 2-minute baseline was acquired in PBS. A 300 μg/mL solution of a His-tagged maltose binding protein (MBP) fusion protein (70 kDa) specific to IgG (150 kDa) prepared in HEPES-NaCl with 10-20% glycerol, was diluted to the specified concentration with PBS and was injected for 10 minutes to allow the immobilization of the His-tagged protein antigen on the SPR sensor. This system was analyzed to compare the performance of the SPR sensor with a known biological system and correlated to other techniques. The excess of antigen was rinsed with PBS before acquiring a 5-minute baseline in PBS. Binding of specific IgG was detected by flowing increasing concentrations (5 nM to 1 mM) of the antibody solution with an analysis time of 5 minutes for each concentration. A final rinsing step with PBS was accomplished. A 10-minute exposition to a saturated EDTA solution followed by a 10-minute period in a 100 mM copper sulfate

solution was used for a complete regeneration of the sensor, demonstrated by performing two detection cycles for IgG on the same SPR sensor.

7.3.6 CD36 peptide ligands screening

The SPR sensors for screening small peptide ligand binding to a recombinant soluble His-tagged CD36 functionalized surface were prepared as described above. Nine ligands were investigated: EP80317, CP-2A(v), CP-2B(i), CP-2B(v), CP-3(ii), CP-3(iv), CP-1A(iv), DBG-178(27) and GHRP-6 with concentrations ranging from 100 nM to 30 μM except for EP80317. The latter was used for optimizing the system with solutions ranging from 100 nM to 1 mM. EP80317 and GHRP-6 are positive controls of known activity, CP-2B(i) and CP-3(ii) are negative controls, and CP-3(iv), CP-2A(v), CP-2B(v), CP-1A(iv) and DBG-178(27) are novel ligands synthesized by C. Proulx and D. Boeglin (manuscript in preparation). Another negative control was made by exposing the His-tagged hDHFR functionalized surface to the same concentration of CD36 peptidic ligand. Two different approaches were used to remove the (His-tagged CD36)-Cu complex from the SPR sensors: concentrated histidine solution or saturated EDTA solution. The Langmuir isotherm (Equation 7-1) allowed the determination of K and ΔλSPR for the CD36-ligand system.

$$\Delta\lambda_{SPR} = (K[ligand])\Delta\lambda_{SPRmax}(1 + K[ligand])^{-1} \quad (7-1)$$

where $K = 1/K_d$. The measured K_d's were correlated to the EC50 values obtained in the activated src-kinase activation assay following CD36 receptor activation by the tested peptides.

7.4 RESULTS AND DISCUSSION

7.4.1 Properties of peptide SAMs

Peptide SAMs show a significant decrease in nonspecific adsorption of serum proteins [103, 187, 271]. To the best of our knowledge, only simple peptide architectures based on homopeptide and binary sequences and a single complex peptide have been previously investigated as monolayers. In this study, a series of seven peptides were investigated for their potential to serve as monolayers with the general structures: 3-Mpa-XXYYZZ, 3-Mpa-XYXYX, 3-Mpa-$(XYZ)_2$ and 3-Mpa-X_4Y, in which 3-Mpa was 3-mercaptopropionic acid, and X, Y and Z were different amino acids. Nonspecific adsorption to the peptide monolayer surface of the SPR sensors was quantified using the equation from Jung et al. [208] (Table 7-1). Certain peptide monolayers exhibited significant nonspecific adsorption, with protein coverage greater than >100 ng/cm^2: i.e., 3-Mpa-XXYYZZ, 3-Mpa-DHDHD and 3-Mpa-GGGGD. Peptides with binary sequences formed SAMs with lower nonspecific adsorption (23 ± 10 ng/cm²), which was improved to 12 to 17 ng/cm^2 by using sequences of the form 3-Mpa-$(XYZ)_2$. Moreover, 3-Mpa-LHDLHD afforded the lowest nonspecific adsorption of the peptide sequences studied with a value approaching the detection limit of SPR (nearly 1 ng/cm^2). In light of its lack of nonspecific interactions, 3-Mpa-LHDLHD was selected for further investigation.

Table 7-1. Nonspecific adsorption from bovine serum ($\Delta\Gamma_{nonspecific}$) on peptides SAM and secondary structure determined by mid-IR and circular dichroism

Sequence	$\Delta\Gamma_{nonspecific}$ (ng/cm^2)	Secondary Structure mid-IR (SAM)	Secondary Structure CD (solution)
3-MPA-LLHHDD-OH	174 ± 120	α	α
3-MPA-GGHHDD-OH	149 ± 100	α	α
3-MPA-DHDHD-OH	274 ± 109	α	α
3-MPA-DSDSD-OH	34 ± 31	extended	extended
3-MPA-LHDLHD-OH	12 ± 11	α	α
3-MPA-SHDSHD-OH	17 ± 14	α	extended
3-MPA-GGGGD-OH	218 ± 65	α	α

The activity of peptides is usually contingent on their conformation, which may be studied in solution using NMR or circular dichroism (CD) spectroscopy; however, peptides on a surface may be more effectively analyzed using mid-IR spectroscopy [209, 254]. Generally, the mid-IR spectra of the amide bands of the peptide surfaces correlated with their CD spectra, except for 3-Mpa-SHDSHD, which exhibited FTIR and CD spectra corresponding to α-helical and extended conformations, respectively. As previously observed [103, 271], most peptides in the monolayers adopted an α-helical conformation (Table 7-1), which has been suggested to exhibit less nonspecific adsorption [272]. In exception, 3-Mpa-DSDSD adopted an extended conformation and little nonspecific adsorption. Highly hydrophilic peptides generally gave more nonspecific adsorption. Preservation of enzyme activity with immobilized His-tagged hDHFR

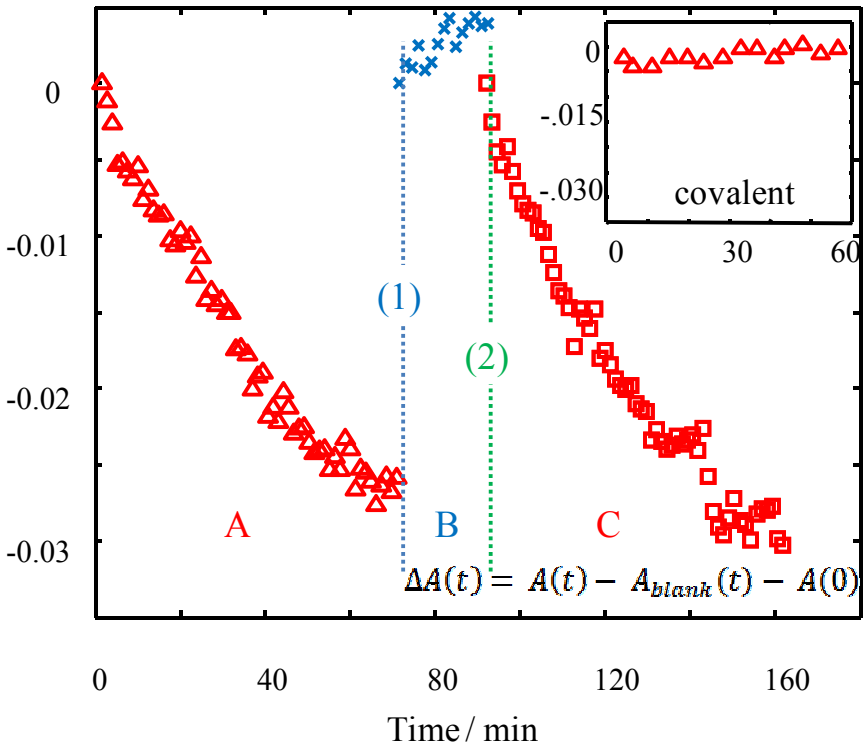

Figure 7-3. Real-time monitoring of the enzymatic reaction for His-tagged hDHFR-immobilized on the modified peptide layer. First, the measurement of the enzyme activity (step A) showed a decrease in absorbance due to the consumption of the reactants. Washing away the enzyme (step 1) from the surface resulted in absence of enzymatic activity, rate -4.0*10^{-4} Abs/min (step B). The regeneration of the surface (step 2) was followed by the second measurement of the enzyme activity, rate: -5.7*10^{-4} Abs/min (step C). Inset: hDHFR covalently immobilized on SPR sensors using EDC/NHS chemistry showed no activity. Each data point represents the average of five.

As mentioned for hDHFR, coupling of monolayer peptide carboxylates with accessible amines on the protein may occur indiscriminately and result in loss of biological activity on the SPR sensor. Measurement of activity by UV/Vis spectroscopy at 340 nm indicated no substrate turnover using immobilized hDHFR anchored by EDC/NHS chemistry onto the SPR surface by way of 16-mercaptohexadecanoic acid (16-MHA) nor peptide monolayer spacers (Figure 7-3 - inset). In contrast, His-tagged hDHFR immobilized on the modified peptide monolayer (Figure 7-2) retained activity as observed

by a decrease in absorbance at λ = 340 nm indicating substrate (NADPH and DHF) consumption (Figure 7-3). Accounting for the specific activity of His-tagged hDHFR in presence of saturating reactants (8.5 U/mg), the absorption coefficient (Δε = 12.8 mM-1 cm-1), and measured slope in C (-5.7*10-4 Abs/min), the activity measured for hHDFR immobilized to the SPR sensor corresponded to an activity of 4.4 ± 0.8*10-5 U, equivalent to 5 ± 0.9 ng (n = 4) of fully active enzyme in solution. In the absence of hDHFR, the modified peptide layer SPR sensor exhibited no significant absorbance fluctuations. Although hDHFR was active when immobilized on the modified peptide layer using the His-tagged approach, the fraction of active enzyme on the surface could not be determined, because immobilized enzyme activity is a factor of the activity of the enzyme in solution, the time required for reactant diffusion on the surface (hemispherical diffusion for immobilized hDHFR and spherical for hDHFR in solution), and product diffusion in the light beam of the UV-Vis (which is not a factor for the enzyme in solution).

Recycling of the active surface was another advantage of the His-tag chemistry. The SPR sensors were regenerated with similar results (n = 4 for each solution) by displacing Cu using solutions of either 0.5 M imidazole, concentrated EDTA or 1 M histidine, followed by hDHFR removal by surface washing until no activity was observed by UV-Vis monitoring (Figure 7-3). Upon between 50-75 ng/cm^2 active enzyme after each immobilization cycle. No activity was measured without enzyme, and the average variation of the absorbance over 60 minutes for four sensors regenerated with imidazole was determined to be –(4.4*10-4 ± 0.6*10-4) Abs/min (n = 8) demonstrating consistent recycling without alteration of the surface properties. This observation is supported by the fact that two on four sensors offered slightly greater rate after the regeneration of the sensor

while two on four offered slightly inferior rate. The combination of appropriate peptide chemistry and metal-based affinity provided a low-background, reusable surface for immobilization of biomolecules.

7.4.2 Applicability of the modified peptide binding His-tagged biomolecules to protein/antibody

The His-tag approach was next demonstrated to be effective for making antibody biosensors by measuring the dissociation constant (K_d) of a fusion protein-IgG system (Figure 7-4). Multiple measurement cycles per sensor were effectively achieved by functionalization, detection, regeneration and detection of a His-tagged Ag/Ab system. Extensive rinsing was achieved using concentrated histidine, imidazole or EDTA solutions at a volume 100 times greater than that held by the fluidic cell. The SPR shifts were consistent after the first and second detection cycles and the K_d was determined to be (9.6 ± 0.3) × 10-9 M, which correlated with values obtained by other techniques for antigen-IgG interactions [281-284].

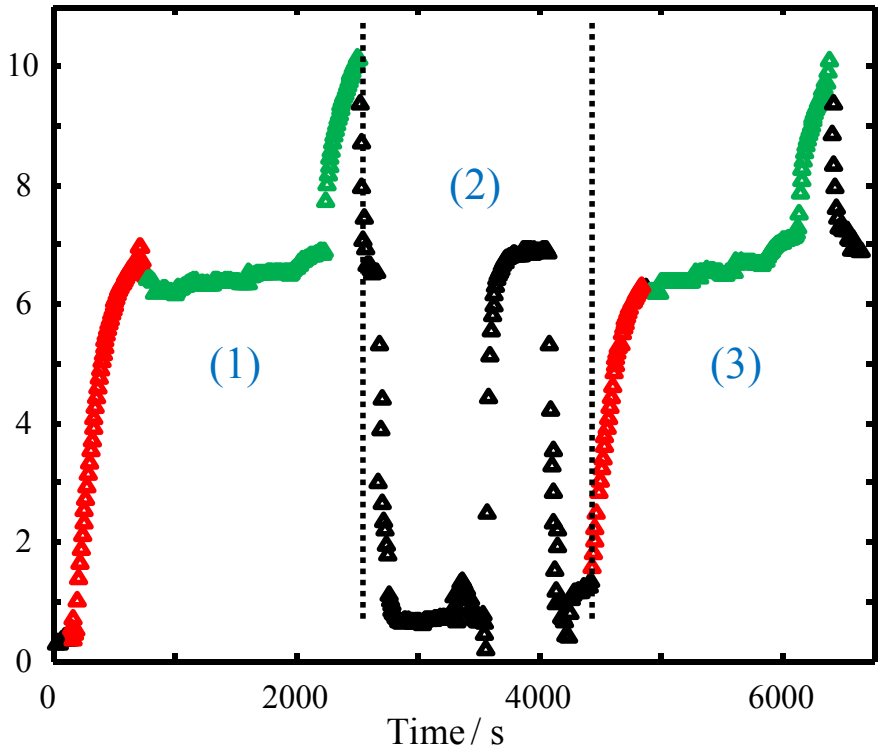

Figure 7-4. SPR sensorgram of two quantifications (steps 1 & 3) of IgG with a His-tagged fusion protein immobilized to the SPR sensor. Online regeneration of the sensor (step 2) was performed using a concentrated EDTA solution.

7.4.3 SPR characterization of CD36 ligands as potential therapeutic agents

The use of optical sensing techniques is of growing interest in the pharmaceutical industry as primary drug screening techniques, as a result of their high performance in real-time, label-free, and automation possibilities [285-289]. Recombinant receptor targets for many drugs are often expressed and purified with a His-tag. Their immobilization close to the SPR surface using modified peptide monolayers would thus be advantageous for maintaining activity and achieving sensitivity.

Table 7-2. EC_{50} values for CD36-peptidic ligands (of given molecular weight, MW) obtained using common techniques and corresponding K_d values determined by SPR sensors using modified peptide layers. $\Delta\lambda_{SPR}$ indicates the maximum change of SPR signal for each ligand.

Ligands	Sequence	MW	SPR		SRC-kinase cellular assay
		(g/mol)	K_d (10^{-6}M)	$\Delta\lambda_{SPR}$ (nm)	EC50 (10^{-6}M)
CP-3(ii)	His-D-Trp-Ala-AzaPhe-D-Ala-Lys-NH_2	758.87	67 ± 6	0.33	>> 10 000
CP-2B(i)	His-D-Trp-AzaLeu-Trp-D-Phe-Ala-NH_2	858,98	31 ± 1	0.54	>> 10 000
CP-1A(iv)	Ala-AzaPhe-Ala-Trp-D-Phe-Lys-NH_2	768,90	10.2 ± 0.1	2.17	3.74
CP-2B(v)	Ala-D-Trp-AzaLeu-Trp-D-Phe-Lys-NH_2	850.02	4.7 ± 0.2	2.19	5.02
CP-2A(v)	Ala-D-Trp-AzaGly-Trp-D-Phe-Lys-NH_2	793.91	2.86 ± 0.09	1.92	0.026
EP80317	Haic-D-2_MeTrp-D-Lys-Trp-D-Phe-Lys-NH_2	1035.20	2.75 ± 0.08	2.64	0.026
DBG-$178_{(27)}$	His-D-Trp-Ala-AzaTyr-D-Phe-Lys-NH_2	850.97	0.77 ± 0.02	2.22	0.063
CP-3(iv)	Ala-D-Trp-Ala-AzaPhe-D-Phe-Lys-NH_2	768.90	0.72 ± 0.01	2.10	0.044
GHRP-6	His-D-Trp-Ala-Trp-D-Phe-Lys-NH_2	873.01	25.6 ± 0.9	2.13	NA

NA: data not available

A His-tagged variant of the type B scavenger receptor CD36 (CD36: Cluster of Differenciation 36) was similarly immobilized onto the peptide monolayer and used for screening of growth hormone-releasing peptides (GHRPs) [290, 291], such as EP80317, which exhibits anti-atherosclerotic activity mediated by CD36 [292, 293] and interferes with the binding of oxidized low-density lipoprotein (oxLDL) to the scavenger receptor expressed on macrophages [293]. Novel GHRP analogs (CP and DBG series) were also examined with this sensitive SPR screening technique to the determine dissociation constants (K_d, n = 4). The relative binding affinity of the peptide analogs correlated with the EC50 for CD36-dependent phosphorylation of src kinase (Lyn/Fyn) in CD36 expressing J774 macrophage. For the src-kinase cellular assay and SPR, the rank order potency for the tested peptides (in decreasing order) was as follows: EP80317 [1, 3] > CP-2A(v) [2, 4] > CP-3(iv) [3, 1] > DBG-178(27) [4, 2] > CP-1A(iv) [5, 6] > CP-2B(v) [6, 5] > CP-2B(i) [7, 7] ≈ CP-3(ii) [8, 8] (Table 7-2). The numbers in brackets indicate the rank order of the [src kinase, SPR] assays. It is important to show the results in terms of rank order, because SPR measures $K_{d\text{-}app}$ and src-kinase measures an EC50 value. Although high $K_{d\text{-}app}$ may typically lead to a high EC50 (a r2 of 0.83 is obtained for the linear regression of the Log-Log plot of $K_{d\text{-}app}$ and EC50), the magnitude of the response may differ between these measurements due to the inherent difference in the assays. The SPR assay is performed with approximately 3.2 pmol of CD36 immobilized on the active sensor area. With a sample volume of 25 μL, a total of 2.5 to 800 pmol of ligand is available to bind CD36. Thus, the assay is performed with limiting ligand concentrations, especially at lower concentrations, and results in an overestimation of the $K_{d\text{-}app}$ estimated in the submicromolar range. However, performing the analysis with lower concentration of CD36 receptor on the SPR surface to achieve an

excess of ligand concentration for binding, would provide a SPR signal too weak for detection, while injecting a greater volume of sample will consume a greater amount of ligands, exceeding the total amount available to us and lead to long analysis time due to longer time required by the ligand to diffuse to the surface of the SPR sensor.

Controls were performed to validate the SPR assay. GHRP-6 is a positive control known to be less selective than EP80317. As expected, the SPR assay showed GHRP-6 to be a weaker binder than EP80317. The negative controls CP-3(ii) and CP-2B(i) exhibited the lowest binding affinity to CD36 (Figure 7-5). For the specific CD36-peptide ligands, a correlation appears between the affinity for CD36 as determined by SPR and their efficiency to produce a cellular response in the src kinase assay. The src kinase assay, which required several days to perform in order to obtain dose-response curves for each ligand, is a lengthy procedure. In contrast, the SPR measurements were made in approximately 1 hour and could be used as a high throughput screening method. The simplicity of the SPR assay allowed straightforward and less time-consuming screening of the ligands for the CD36 receptor.

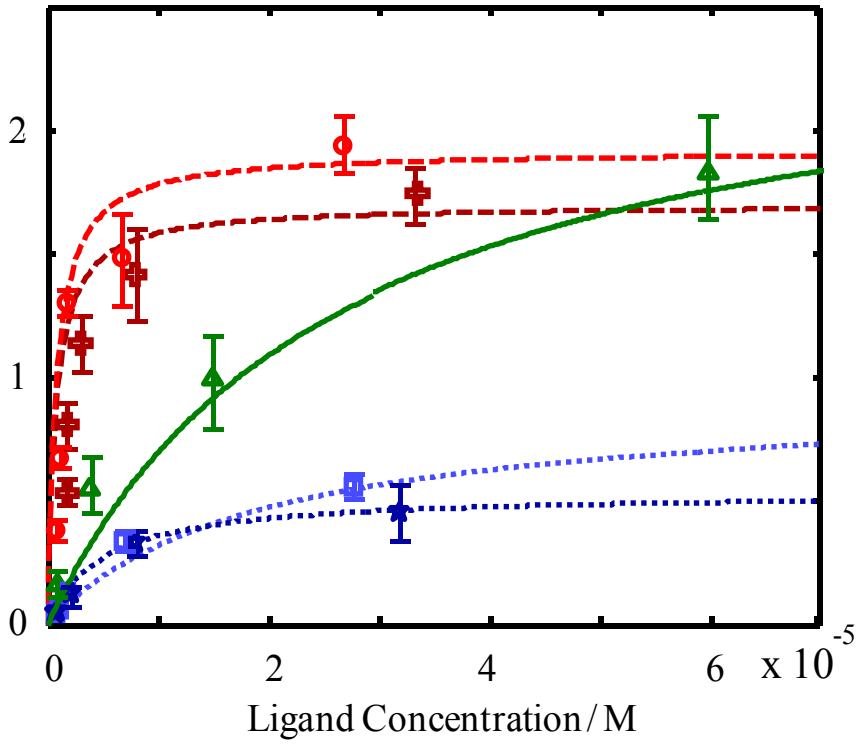

Figure 7-5. Determination of K_d and $\Delta\lambda_{SPR}$ using the Langmuir equation (equation 1) for DBG-178$_{(27)}$ (circles), CP-3(iv) (crosses), GHRP-6 (triangles), CP-3(ii) (squares) and CP-2B(i) (stars). Doted, solid and dashed lines represent best iterations generated by Matlab's curve fitting tool. Error bars represent two standard deviations. The negative controls in blue show low binding affinity for CD36.

Notably, the binding of the small peptides (MW 800 to 1000 g/mol) to the CD36 receptor would be close to the limits of detection, because unamplified SPR techniques do not yield large response for molecules of less than 1000 g/mol. The magnitude of the SPR response at saturation varied according to the small peptide ligand assayed with the negative controls exhibiting low SPR responses 0.3 to 0.5 nm in sharp contrast to the nearly 2 nm response from specific ligands and positive controls (Table 7-2).[294] The large shift in the signal when exposing a CD36-His-tag-functionalized surface to small peptide ligands (Figure 7-6 – Upper trace) may be a consequence of a conformational change of the receptor upon ligand binding, thus amplifying the signal. Conformational changes on ligand

binding have been suggested to influence the biological activity of the CD36 receptor.[77] No significant change of signal for hDHFR-His-tag functionalized sensors were observed when exposed to the same peptides as controls (Figure 7-6, Lower trace) indicating that the signal observed with the CD36 surface is specific to receptor-ligand interactions. Without conformational changes, the SPR response at saturation would be expected to reach the same λ_{SPRmax} for positive and negative controls at their respective concentrations for receptor saturation. In addition to the dissociation constants (K_d), the influence of ligand on the conformation of the CD36 receptor appears to modulate λ_{SPRmax}.

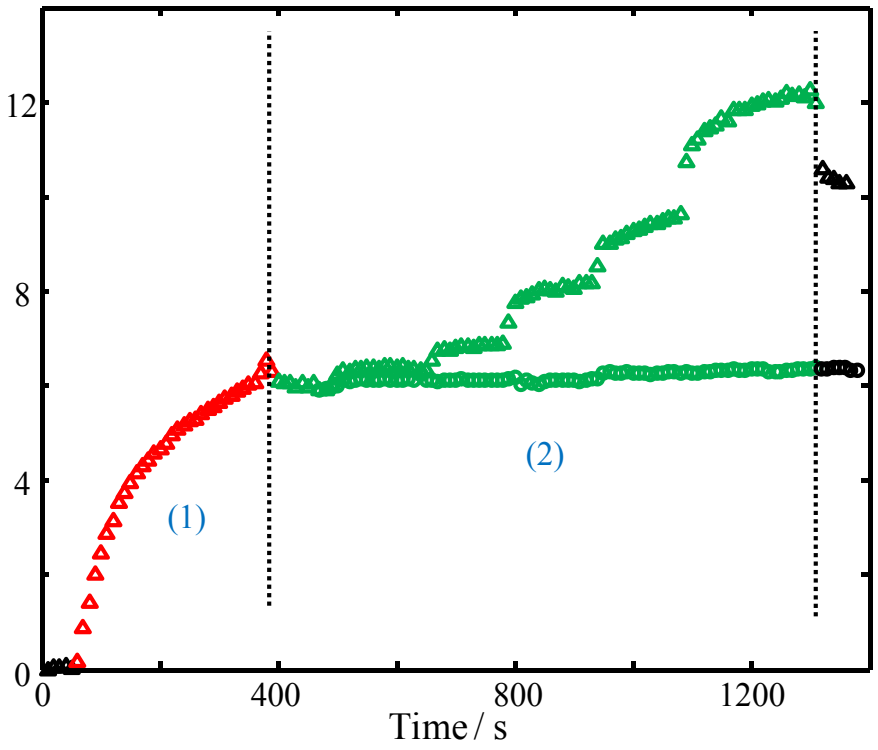

Figure 7-6. (Upper trace) SPR sensorgram of CD36 functionalized (step 1) sensor exposed to increasing concentrations of EP80317 (step 2). (Lower trace) SPR sensorgram of hDHFR functionalized sensor (nonspecific to peptidic ligand) exposed to increasing concentrations of EP80317.

7.5 CONCLUSIONS

Peptide monolayers have been tailored for the immobilization of His-tagged biomolecules on an ultralow fouling surface. A third generation of complex peptides was demonstrated to decrease nonspecific adsorption from serum to nearly 10 ng/cm². Peptide-based surfaces functionalized with NTA-type molecules demonstrated potential for immobilizing active proteins and enzymes labelled with His-tags. In particular, hDHFR-His-tag sensors maintained activity, which was lost using conventional coupling chemistry. The K_d of a protein/antibody system was efficiently measured. Moreover, ligands were screened effectively for affinity to the CD36 receptor. Considering the prevalence of His-tagged proteins and the ease of synthesis of the peptide monolayer, this novel immobilization approach should find practical use for the development of effective SPR sensors.

7.6 ACKNOWLEDGMENTS

Financial support was provided by NanoQuébec, the Canadian Space Agency, the Canada Foundation for Innovation (CFI), the National Sciences and Engineering Research Council of Canada (NSERC), the Fonds Québécois de la Recherche sur la Nature et les Technologies (FQRNT) and the Centre for self-assembled chemical structures (CSACS).

CHAPITRE 8 : Electroformation of peptide based self-assembled layers on surface plasmon resonance sensors

Accepté entant que : Bolduc, O. R.; Masson, J.-F. Langmuir, la-2011-03493v, (accepté : 19/10/2011).

8.1 ABSTRACT

The application of a potential to deposit a peptide monolayer, 3-MPA-HHHDD-OH, controls the density and molecular structure of the monolayer, which results in different wettability of the surface, surface density, orientation of the molecule and nonspecific adsorption of serum proteins. 3-MPA-HHHDD-OH must be deposited at 200 mV to maintain an extended configuration, which promoted in this case ultralow biofouling properties.

KEYWORDS: Peptide, Monolayers, Electroformation, Potentiostatic, Surface Plasmon Resonance, SPR, Nonspecific interaction, Biosensors.

8.2 INTRODUCTION

Peptide based monolayers are suited for reducing nonspecific interactions with serum proteins.[103, 295, 296] The level of nonspecific interaction is decreased to a few ng/cm² on Au substrates for surface plasmon resonance (SPR) biosensing. This ultralow level of nonspecific interaction is comparable to other surfaces, such as polycarboxybetaine[297], and lower than PEG[216, 298]. Peptides also offer the advantages of simple synthetic methods and the use of a "real" peptide coupling reaction to graft proteins, enzymes or antibodies or his-tag binding chemistry on a modified peptide monolayer.

While peptide present many advantages as a chemical layer on SPR sensors, it requires overnight deposition to attain monolayer formation and achieve good protein resistance to nonspecific adsorption. Alternative methods for the deposition of the peptide monolayer must be investigated. For example, electrochemical deposition provides control on the orientation and surface coverage of thiolated molecules, while increasing the

deposition rate on the order of minutes instead of hours. Terrill *et al*. employed the control of the resistivity between the interfaces to form monolayer of thiol compounds on Au.[299, 300] Other groups investigated the possibility to influence the kinetic of formation of chemical layers of thiolated molecules by applying an electric potential at the solid-liquid interface, where the monolayer is intended to be deposited.[80, 301, 302]

The control of the monolayer formation is of great interest from a biosensor conception point of view. It could provide a fast, reliable and inexpensive way to obtain large area of functionalized surfaces on request to conduct specific assays. By modifying the deposition conditions, surfaces demonstrating different properties can be fabricated, allowing the production of more adapted surfaces depending on their final applications. For example, applying difference of potential (ΔE) at the liquid-solid interface of an already formed monolayer can modulate the conformation of the organic molecule immobilized depending on their chemical properties.[255] In some cases, this change of conformation could be exploited to deploy or hide the detection element or a marker from the solution to be analyzed.[303] Therefore, it is important to verify that the application of a ΔE while forming a monolayer does not alter the desired properties observed for a regular self-assembled monolayer, in this case the nonbiofouling properties.

This paper investigates the influence of the potential applied to a SPR sensor modified with a peptide monolayer and the influence of deposition potential on the formation of the monolayer. The formation of monolayers of 3-MPA-HHHDD-OH (where 3-MPA: 3-mercaptopropionic acid, H: histidine, D: aspartic acid) on SPR biosensors, a monolayer previously shown to minimize nonspecific adsorption, is a suited model system

for the investigation of the deposition potential by monitoring in real-time the process with SPR sensing. The ability of the resulting SPR biosensors to reduce nonspecific interactions with blood serum proteins is important. As it was previously observed for other type of organic monolayers that nonspecific adsorption is a function of surface density [304], the nonspecific adsorption of bovine serum protein on peptide monolayers of different density need to be monitored to evaluate the non biofouling properties of electrochemically-deposited peptide monolayers.

8.3 EXPERIMENTAL

8.3.1 Electrochemical-SPR instrumentation

An electrochemical-SPR combining a dove prism based SPR instrumentation[105] with a custom 1 mL electrochemical cell and a Biologic SP-150 potentiostat was constructed to allow the simultaneous and real-time monitoring of electrochemical formation of the peptide monolayer. Bare SPR sensors consisting of gold coated glass slides were prepared as previously published[295] before being mounted on the instrumentation. The sensitivity of the SPR instrumentation around the refractive index of 1M KOH solution in ethanol (n=1.3726) was determined using sucrose solutions ranging from 1.365 to 1.380 at (4400 ± 100) nm/RIU. Thin copper strips covered with electrolyte glue assured the electrical connection with the gold surface used as the working electrode. A freshly cleaned Pt counter-electrode and a freshly prepared Ag/AgCl reference electrode were employed for every run to avoid any alteration of the electrodes due to 3-MPA-H_3D_2-OH.

8.3.2 Real-time measurement of potentiostatic formation of 3-MPA-H_3D_2-OH layers

3-MPA-HHHDD-OH was synthesized according to a previously published procedure.[295] A 10 mM solution of 3-MPA-HHHDD-OH in 1 M KOH ethanol solution was freshly prepared before every run and nitrogen was bubbled in every solution before being introduced into the electrochemical cell. A volume of 0.50 mL of 1 M KOH in ethanol solution was injected in the electrochemical cell to acquire the s-polarized light used as reference for SPR measurements. A constant ΔE was applied in amperometric monitoring mode immediately before acquiring p-polarized light (SPR active) The SPR and amperometric signals were both acquired at a 1 Hz for 90 minutes. Optical measurements were acquired after applying the potential difference to avoid a change of SPR signal due to the influence of the application of the electrical potential as previously observed while applying oscillating potential on the SPR sensors.[305] Following the application of a potential difference to the surface for 30 s, 0.50 mL of 10 mM 3-MPA-HHHDD-OH was injected in the electrochemical cell to monitor the formation of the 3-MPA-HHHDD-OH layer. Data was generated in triplicate for each potential investigated.

8.3.3 Characterization of the 3-MPA-H_3D_2-OH layers

SPR measurements provided the information about the density of the layer formed. Contact angle measurements were acquired by depositing 300 μL of 1X phosphate buffer saline (PBS) on the surfaces. A photograph of the PBS droplet was acquired and processed with Image J (NIH freeware). The mid-IR spectrum was obtained using a Ge-attenuated total reflection (ATR-FTIR) instrument. Some monolayers electroformed at different potential were exposed to bovine serum to measure the amount of nonspecifically bound

proteins. The SPR sensors were exposed 5 min to PBS for monitoring a stable baseline, 20 min to crude bovine serum and 5 min to PBS. The amount of nonspecifically adsorbed proteins was calculated using the Jung *et al*. equation[208] as previously published.[104]

8.4 RESULTS AND DISCUSSION

8.4.1 Real-time measurement of potentiostatic formation of 3-MPA-HHHDD-OH layers

SPR and amperometric measurements are complementary techniques. SPR provides information about the reaction kinetic and surface density for the monolayer deposition at the solid-liquid interface, while amperometry provides information about the density of the layer formed at this interface. The formation of 3-MPA-HHHDD-OH monolayer for applied potentials of 0, 200 and 400 mV shows distinct behaviors (Figure 8-1). Surface density identical to a self-assembled monolayer deposited overnight at open circuit potential is obtained by applying from 0 to 200 mV to the SPR sensor, while the formation occurs faster by increasing the potential from 0 to 200 mV (Table 8-1). The surface density achieved by overnight deposition and electroformation at potentials below 200 mV varies slightly between 0.21 and 0.24 x 10^{15} molecules/cm^2. This value is close to the one expected for a fully standing peptide monolayer assuming a standard 0.8 nm pitch of the α-helix conformation, which result in 0.2 x 10^{15} molecules/cm^2. For applied potentials higher than 200 mV the surface density of 3-MPA-HHHDD-OH exceeded the surface coverage a full monolayer (Table 8-1). This could be explained by the formation of multilayers made possible by ΔE values higher than the one required forming a single layer of a 3-MPA-HHHDD-OH. The shape of the SPR curves for sensorgrams of the formation of a monolayer at applied potentials of 250 to 400 mV suggests a different mechanism of

immobilization. By applying a potential greater than 200 mV to the surface, it takes a slightly longer time to reach equilibrium than at 200 mV, but the surface concentration stabilizes over a short period of time near the full monolayer surface concentration, before rapidly increasing beyond a full monolayer until the end of the run. While SPR provides a good measure of the surface concentration, it is also influenced by the orientation of the molecules at the surface. For example, phase transitions where the self-assembled molecules of an alkylthiol chain melts by becoming disorganized with gauche defects, creates a thinner monolayer, which results in larger SPR shifts [306].

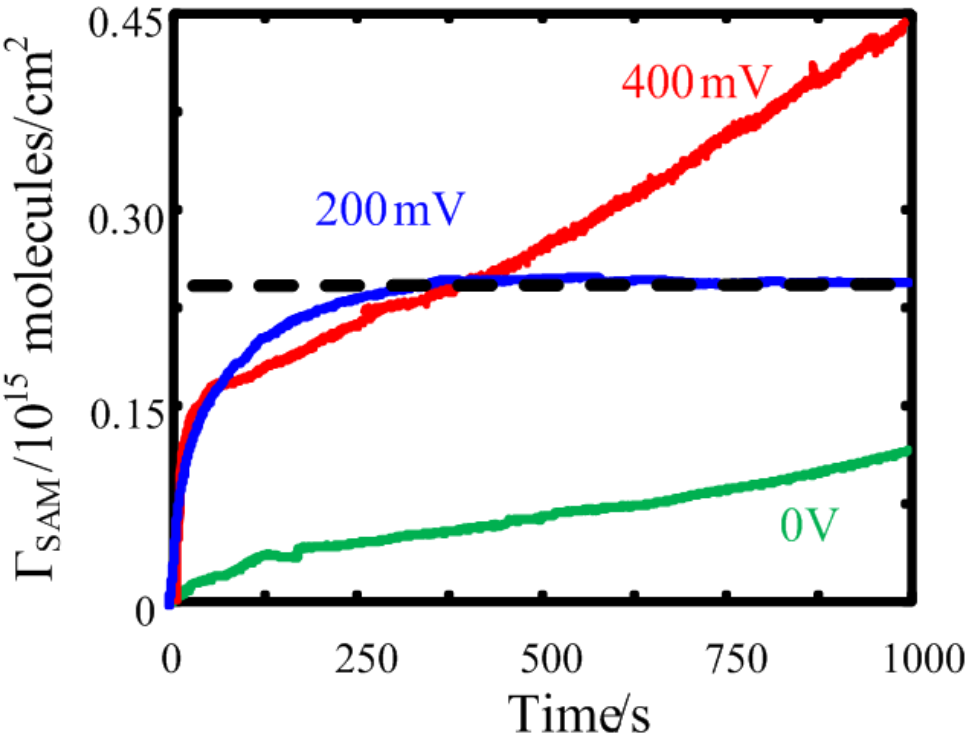

Figure 8-1. Overlay of the SPR sensorgrams for the formation of a 3-MPA-H_3D_2-OH layer for ΔE vs Ag/AgCl from 0 mV, 200 mV and 400 mV;. The dashed line represents the density for a monolayer self-assembled overnight in ethanol at open circuit potential. A complete version of this figure is available in Annexe D in Figure D-1.

Table 8-1. Preparation of electroformed 3-MPA-H_3D_2-OH layers over 90 minutes.

$\Delta E_{applied}$ / mV	Time to reach Γ_{SAM} /10^3s	Γ reached after 90 min / (10^{15}molecules/cm²)
0	3.2 ± 0.2	0.22 ± 0.03
50	2.4 ± 0.1	0.21 ± 0.05
100	2.1 ± 0.1	0.23 ± 0.02
150	1.3 ± 0.1	0.22 ± 0.05
200	0.35 ± 0.05	0.24 ± 0.04
250	0.67 ± 0.03	0.31 ± 0.03
300	0.66 ± 0.03	0.32 ± 0.08
350	0.37 ± 0.04	0.38 ± 0.07
400	0.38 ± 0.02	0.5 ± 0.1
Overnight preparation	16 hours	Γ_{SAM} = (0.23 ± 0.04)

Measurements in triplicate and the error represent two standard deviations on the mean.

The electrochemical adsorption of molecules can be observed from the current measured during the formation of the monolayer. Figure 8-2 shows that increased ΔE induces faster immobilization of a 3-MPA-HHHDD-OH to the surface of the SPR sensor, visible by the increased values of initial current (i(t)) and by the time required to reach a current near 0. For example, the time required to form a monolayer at 0 mV lead to a monolayer coverage in about 3200 s, while it is less than 6 minutes at 200 mV. This result is in agreement with the one observed by Lennox's group for alkanethiols.[80] The amperometric curves suggests that the initial value of i(t) is nearly proportional to the ΔE applied at the interface of the sensors within the range investigated in this study. The shape of the i(t) curves also suggest that the adsorption of 3-MPA-HHHDD-OH goes through a

rapid adsorption phase. This result contrasts with the SPR data, which keeps increasing at longer deposition times.

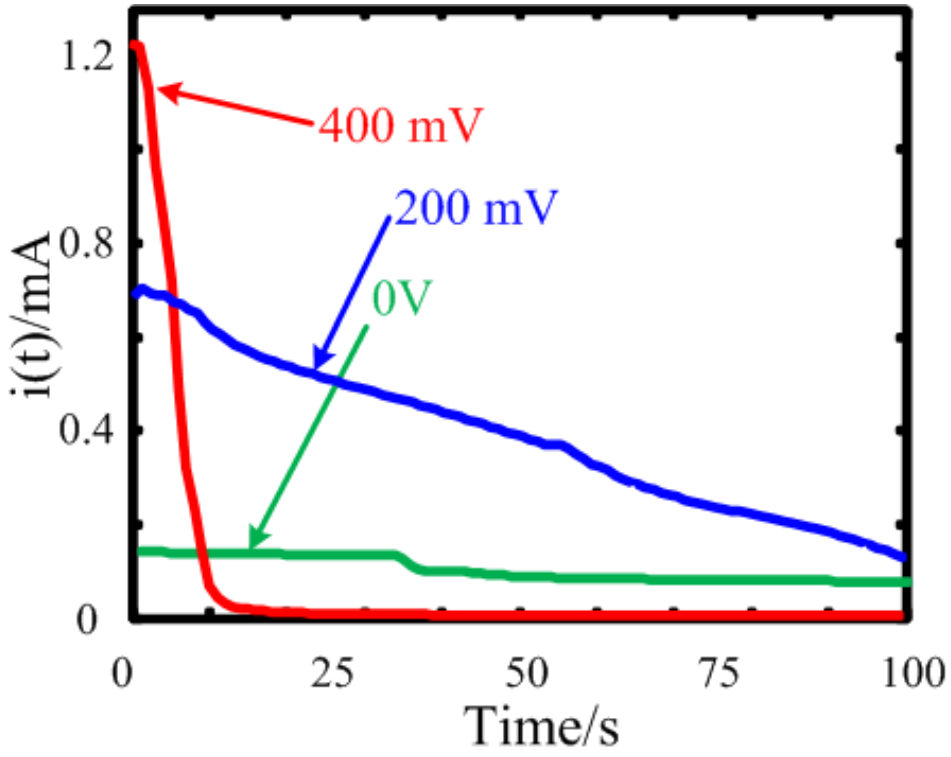

Figure 8-2. Amperometric measurements for the formation of a 3-MPA-HHHDD-OH layer for ΔE vs Ag/AgCl of 0, 200 mV and 400 mV. A complete version of this figure is available in Annexe D in Figure D-2.

The difference in behavior of the SPR and amperometric data can be explained by the organization of the monolayer at the surface. Electroformation is performed in ethanol solutions of KOH, such that 3-MPA-HHHDD-OH is negatively charged. At high potentials, the carboxylate anion at the end of the peptide further away from the surface is strongly attracted to the cathode (SPR sensor). This attraction may be sufficient to induce a phase transition in the monolayer, from a well-oriented to a disordered monolayer. This phase transition occurs at potentials greater than 200 mV, such that this potential is optimal

for deposition of 3-MPA-HHHDD-OH. While these results strongly suggest that a phase transition occurs at high potentials, strong evidences will be provided by other techniques such as cyclic voltammetry, molecular spectroscopy and scanning tunneling microscopy.

8.4.2 Characterization of the 3-MPA-HHHDD-OH layers and investigation of their non biofouling properties

Cyclic voltammetry was used to characterize oxido-reduction processes at the interface of the electrode while depositing the peptide. A broad peak that reaches a maximum current at 300 to 400 mV is observed on the anodic sweep, which correlated with the deposition of the peptide monolayer on the SPR sensor. In addition, for 3-MPA-HHHDD-OH monolayers exposed to potentials greater than the phase transition, it was observed that a second oxidation peak appears at a reductive potential of -130 mV (Figure 8-3). This same peak was observed for potentiostatic conditions for monolayers deposited at 200 mV for 30 minutes. The peak observed at -130 mV is quite unusual, as it displays a very sharp oxidation peak, uncharacteristic of oxidation/reduction reactions. This suggests a change of conformation in layers partially or completely formed exposed to a potential of -130 mV. At this cathodic potential, charge repulsion may occur with the carboxylate anion, resulting in a phase transition of the monolayer. The peak observed at -1 V is due to the reduction of the S-Au, leading to desorption of 3-MPA-HHHDD-OH from the surface of the sensor. The absence of this peak in the blank run indicates that capacitive current dominates the response, and that this transition is not due to artifact from the SPR sensor's surface but to the presence of a layer of 3-MPA-HHHDD-OH at the liquid-solid interface (Figure 8-3). These results strongly suggest that the monolayer undergoes a reversible phase transition depending on the potential applied to the SPR sensor.

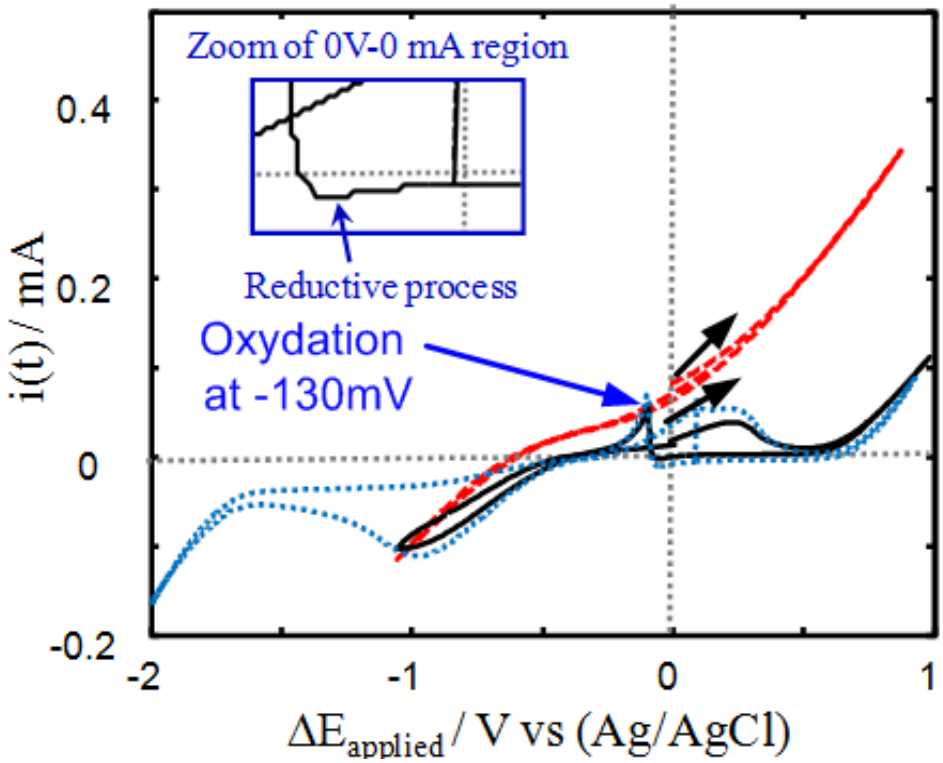

Figure 8-3. Cyclic voltammogram (CV) showing the electroformation of 3-MPA-H_3D_2-OH layer for $\Delta E_{applied}$ sweep from -2 to 0.8 V starting at 0 V at a rate of 10 mV/s. Dashed red line represents blank run in absence of 3-MPA-H_3D_2-OH. The dotted blue line represents a CV accomplished for larger range ΔE allowing the reductive desorption of 3-MPA-H_3D_2-OH. Black arrows represent the starting point of each run. (Inset) Zoom of the 0V-0mA region showing a reductive process preceding the oxidation process at -130 mV.

Mid-IR spectra obtained for 3-MPA-HHHDD-OH deposited at potentials between 0 and 200 mV agrees with the extended conformation observed for layers prepared overnight presented in our previous work.[295] This was confirmed by the spectra exhibiting the amide I band at 1675 cm^{-1} (Figure 8-4). The spectrum obtained for layers prepared at 300 mV contains Amide I band shifted to 1648 cm^{-1} and an Amide II band shifted to 1554 cm^{-1}. These shifts close to the values observed for peptide layers adopting the α-helix configuration, were attributed to disorder in the layer formed and were confirmed

elsewhere by using grazing-incidence x-ray diffraction (GIXD).[307] This also agrees with the results obtained for organic monolayers exposed to higher values of ΔE in the work of Sek *et al*.[27] This result clearly demonstrates that the monolayer undergoes a phase transition at high potential. It also correlates with the apparent reduction in monolayer thickness observed in the SPR data, due to electrostatic attraction of the carboxylate end of the monolayer to the anode. This transition induces disorder in the monolayer.

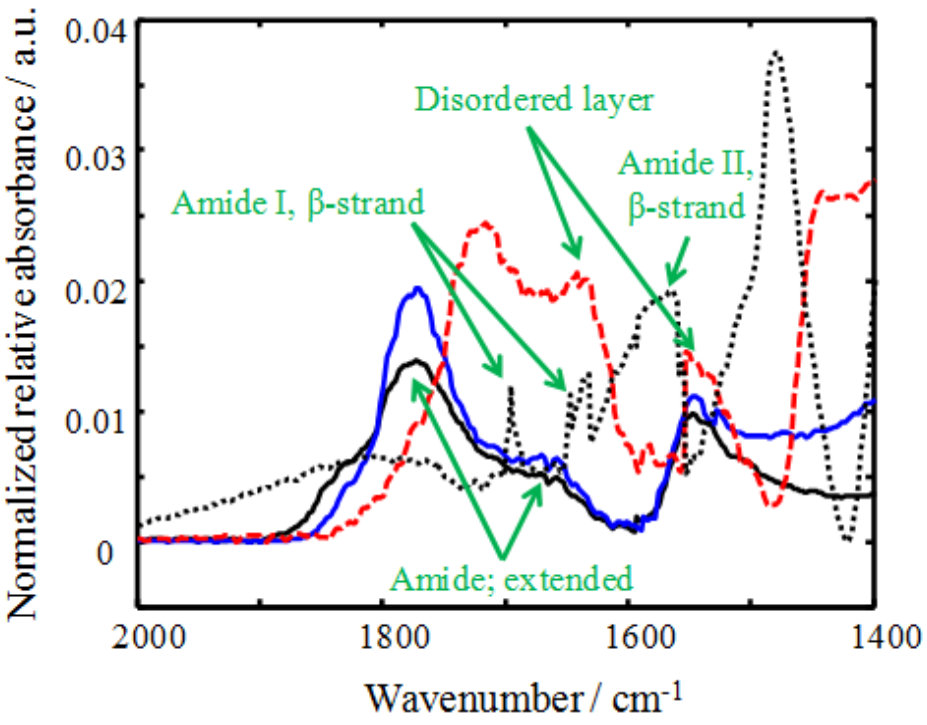

Figure 8-4. GATR-FTIR spectra of electroformed 3-MPA-HHHDD-OH layers. Spectrum of electroformed 3-MPA-HHHDD-OH layer at a ΔE vs Ag/AgCl of 0 V (Black-solid line), 200 mV (Blue-solid line), 300 mV (Red-dashed line) and -130 mV (Black-dotted line).

In the case of surfaces prepared at -130 mV, the mid-IR spectrum demonstrated that the peptide adopts a β-strand conformation at the surface. Rappaport *et al*. previously demonstrated that β-strand peptide layers could sit flat on surfaces. According to their results the presence of Amide I bands at 1627 cm^{-1} and 1689 cm^{-1} as shown in Figure 8-4 – (Black-dotted line) could indicate that the peptide lies in this configuration. In addition, Fenter *et al*. demonstrated that alkanethiol are lying down on the surface at low surface coverage of the molecule.[308] The reductive potential applied to the electrode guarantees that the surface coverage of the monolayer remains low, for short deposition times. Thus, a lying down conformation is likely for monolayers prepared at -130 mV.

Advancing contact angles (θ_c) provides a relative measure of the hydrophilicity or the hydrophobicity of different surfaces. Partially formed layers of 3-MPA-HHHDD-OH for 0 and 100 mV were more hydrophobic in comparison to monolayers deposited at 200 mV and at open circuit potential overnight , which were both statistically identical (Table 8-2). For monolayers deposited at higher potentials (400 mV), the hydrophilicity of the surface remains statistically identical to the layer deposited at 200 mV. The layer electroformed at -130 mV is significantly hydrophilic, also in agreement with a different conformation of the monolayer.

In order to verify that electroformed peptide monolayers could be used as biofouling resistant surfaces for biosensing in crude blood serum, electrodeposited monolayers were exposed to crude bovine serum. SPR monitors the amount of nonspecifically adsorbed proteins at the interface. Partially formed monolayers of 3-MPA-HHHDD-OH provide poorer resistance to nonspecific adsorption of serum proteins (Table 8-2). Indeed, monolayers deposited at 0 and 100 mV nonspecifically adsorbed respectively 174 ± 38 and

132 ± 19 ng/cm² of proteins, far from the performance of the monolayer deposited at open circuit potential, which adsorbed 32 ± 5 ng/cm². The layer electroformed at 200 mV for 30 minutes adsorbed 25 ± 14 ng/cm² of nonspecific interactions a value statistically equivalent to the level observed for a surface prepared by overnight incubation. Interestingly, the disordered surface resulting from deposition at 300 mV was significantly less performing with 96 ± 36 ng/cm² of serum proteins adsorbing. This indicated that the ordering and density of the peptide monolayers influences the nonspecific adsorption properties of SPR biosensors exposed to crude blood serum. It is thus very important to control the conditions of formation of chemically or electrochemically adsorbed layers to maximize the performances of the system in use and to avoid any undesired variation influencing the reproducibility of the method used.

Table 8-2. Hydrophilicity and non biofouling properties of electroformed peptide based layers built over a period of 30 minutes.

$\Delta E_{applied}$ / mV	θ_c /degrees	Γ_{NSB}/ (ng/cm²)
-130	< 10	105 ± 21
0	43 ± 4	174 ± 38
100	41 ± 2	132 ± 19
200	32 ± 3	25 ± 14
300	28 ± 5	96 ± 36
Overnight preparation	35 ± 4	32 ± 5

Measurements in triplicate; error represents two standard deviations on the mean.

8.5 CONCLUSION

This study showed that electroformation of 3-MPA-HHHDD-OH monolayers reduces significantly the preparation time required to obtain a monolayer offering the same properties than a layer self-assembled by overnight incubation. The optimal applied difference of potential was determined to be 200 mV leading to a monolayer in less than 6 minutes. It was shown that changes of conformation of the layer could take place for high anodic or low cathodic potentials, which influenced the ultralow biofouling properties of the monolayer. Advancing contact angles, mid-IR and SPR measurements showed that electroformation of peptide based layers could lead to different types of surfaces using the same molecule by varying the difference of potential applied.

8.6 ACKNOWLEDGMENT

Financial support was provided by NanoQuébec, the Canadian Space Agency, the Canada Foundation for Innovation (CFI), the National Sciences and Engineering Research Council of Canada (NSERC), the Fonds Québécois de la Recherche sur la Nature et les Technologies (FQRNT) and the Centre for self-assembled chemical structures (CSACS).

CHAPITRE 9 : Conclusions générales

Conclusions

Les biocapteurs sont des outils technologiques complexes dans une enveloppe extrêmement pratique. Ils permettent d'effectuer des mesures rapidement, en tout lieu avec un minimum de moyens. Les biocapteurs optiques basés sur la SPR permettent l'obtention de résultats en temps réel sans avoir à recourir à des techniques de marquage, et sans nécessiter d'instrumentation complexe et dispendieuse.

L'objectif principal de ces travaux fut de développer les applications des biocapteurs SPR. Pour ce faire, il était nécessaire de développer un nouvel instrument qui soit robuste, simple d'utilisation et peu dispendieux afin d'en permettre l'utilisation en toutes conditions par un personnel ne requérant que peu de formation tout en améliorant l'accès à cette technologie. Il était aussi nécessaire de développer une méthode donnant accès un nouveau type de chimie de surface permettant de limiter les effets des molécules nonspécifiques de la matrice analytique complexe sur le signal SPR observé lors de mesures en milieux complexes d'intérêt médical réel, tel que le lysat cellulaire ou le sérum sanguin. Il fallait aussi étendre les applications de ces biocapteurs à des domaines pouvant exploiter pleinement les informations disponibles par le biais de la SPR tels que les domaines pharmaceutique et pharmacologique. L'amélioration des techniques de fabrication de ces biocapteurs devait elle aussi être optimisée pour limiter les moyens et le temps nécessaire à leur production tout en demeurant reproductible au niveau de leur capacité de détection.

Ces travaux ont conduit à l'élaboration d'un instrument SPR versatile et peu coûteux basé sur l'utilisation d'un prisme d'inversion (dove) – Chapitre 3. La résolution de

cet instrument combinée avec l'utilisation des algorithmes de traitement de données appropriés varie entre $3x10^{-6}$ et $1,5x10^{-7}$ RIU selon la méthode de traitement de données utilisée. Cette résolution demeure supérieure d'environ un ordre de grandeur à celle des instrumentations commerciales développée par Biacore, mais à un coût de plusieurs ordres de grandeur inférieur et ce avec une instrumentation nettement plus simple.[45] L'ajout de composantes fluidiques appropriées a permis un remplacement efficace de la solution analysée sans toutefois interrompre les mesures en cours, en limitant l'influence des variation de conditions expérimentales. La possibilité d'employer cet instrument pour développer des biocapteurs SPR a été démontrée par la production d'un biocapteur SPR pour détecter la β-lactamase sur une couche organique typiquement employée en biodétection SPR. L'utilisation d'une caméra CCD d'imagerie a permis de démontrer que ce type d'instrument peut être employé en mode imagerie, un mode généralement employé pour le multiplexage des biodétections. Ceci est difficile à réaliser à l'aide d'une instrumentation commerciale (Biacore) qui n'est pas aussi versatile que la technologie développée ici ne nécessitant que peu d'alignement pour passer d'un mode à l'autre (imagerie ↔ canaux désignés).

Une méthode efficace pour investiguer le potentiel des composés peptidiques à limiter les interactions nonspécifiques avec les divers composants d'une matrice biologique complexe a été mise au point. Tout d'abord, des composés organiques thiolés exposant 19 des 20 acides aminés naturels à la surface de biocapteurs SPR ont été développés pour déterminer lesquels de ces acides aminés limitent les interactions nonspécifiques et quelles sont leurs propriétés physico-chimiques – Chapitre 4. Ces surfaces ont été analysées en employant les techniques FTIR, SPR et la mesure des angles de contact pour en déterminer

les propriétés. Des monocouches auto-assemblées de densités variables allant de $0{,}18 \times 10^{15}$ à $1{,}80 \times 10^{15}$ molécules/cm^2 ont été observées. L'élaboration de biocapteurs permettant la détection de la β-lactamase a permis de démontrer la possibilité d'utiliser ces surfaces pour bâtir des biocapteurs SPR efficaces.

L'élaboration de peptides de type 3-MPA-$(X)_n$-OH à l'aide de synthèse sur support solide a permis l'amélioration des performances des composés de première génération – Chapitre 5. L'utilisation de 5 acides aminés, 3 ayant démontrés leur potentiel à limiter les interactions non spécifiques en milieu complexe, a permis de réduire de 2 à 3 fois la quantité d'adsorption non spécifique subie par des surfaces de ce type faites avec des acides aminés moins performants. Le niveau de l'adsorption non spécifique subie par 3-MPA-$(Ser)_5$-OH est inférieur d'un ordre de grandeur à celui des surfaces organiques les plus performantes en SPR. La comparaison des résultats obtenus à l'aide de ces surfaces avec ceux de la génération précédente de composés montre que ce type de surface non seulement limite les interactions non spécifiques, mais permet une meilleure immobilisation et rétention de l'activité des molécules de reconnaissance immobilisés.

Une deuxième génération de surfaces formées de peptides binaires a permis de réduire davantage le niveau d'adsorption non spécifique à la surface des biocapteurs SPR – Chapitre 6. Des monocouches à caractère zwitterionique ont démontré une forte résistance aux interactions non spécifiques dans le sérum sanguin complet. Les surfaces constituées de 3-MPA-HHHDD-OH ont montré de très faibles niveaux d'interactions non spécifiques. La limite de détection de l'IgG obtenue à l'aide de ces biocapteurs a été déterminée entre 1-10 pM alors que pour la MMP-3, un biomarqueur surexprimé en cas de cancer, elle a été déterminée à 0,14 nM. Suite à la publication de l'étude sur les monocouches basés sur les

acides aminés, quelques groupes dont celui de Jiang, University of Washington, se sont eux aussi intéressé aux surfaces peptidiques pour leur résistance aux interactions nonspécifiques,[226] Il est toutefois difficile de comparer les niveaux d'adsorption nonspécifique observés pour les monocouches actuellement sous investigation, car ces surfaces sont majoritairment exposées à des solutions de complexité diverses. L'utilisation de solutions contrôlées ne contenant seulement que de l'albimune et/ou du fibrinogen et/ou de l'IgG, les trois composantes principales du sérum sanguin, est une pratique courante qui ne reflète que peu la réalité de l'adsorption nonspécifique. Les travaux de Rabe et al.[309], Green et al.[142] and Masson et al.[137] révèlent que l'adsoption nonspécifique est davantage une cascade d'évènement impliquant tous les composants du sérum sanguin. Ceci suggère que la résistance aux intéractions nonspécifique doit être mesurée dans la matrice complexe complète et non diluée, autant que possible, tel que proposés dans cette thèse.

Afin d'élargir les applications de ce type de surface, une troisième génération de composés peptidiques a été élaborée pour immobiliser des biomolécules d'intérêt pharmacologiques marquées par un tag hexahistidine (H_6) – Chapitre 7. Cette nouvelle génération de surface permet d'atteindre un niveau d'adsorption non spécifique de près de 10 ng/cm^2 dans le sérum sanguin complet. L'immobilisation de biomolécules-H_6 se fait via l'attachement de molécule de type NTA en terminaison de chaîne du peptide. Cette méthode d'immobilisation offre l'avantage d'être simple, sélective du lieu d'attache selon la position du groupement H_6 et réversible permettant la régénération des biocapteurs à l'aide de méthodes simples. Différents ligands du récepteur CD36, une cible d'importance pharmacologique ont été testés pour en déterminer leur valeur respective de K_d. Cette approche a aussi permis de maintenir l'activité de l'enzyme hDHFR qui, immobilisée de

manière covalente, perd toute activité. Les travaux de Fischer et al. ont récement montré l'efficacité de ce type d'immobilisation de molécule de reconaissance par rapport à une approche covalente,[310] Biacore ont eux-aussi recemment lancer une série de biocapteurs intégrant cette technologie basée sur des alcanethiols qui sont démontré dans les travaux de Rich et al.[311]

Les conditions d'électroformation de monocouches peptidiques ont été déterminées afin de réduire considérablement le temps requis à la préparation de ce type de surface et d'offrir des conditions de formations contrôlées – Chapitre 8. La différence de potentiel appliquée optimale pour la formation d'une monocouche de 3-MPA-HHHDD-OH a été déterminée à 200 mV vs Ag/AgCl. Cela permet la formation de surfaces résistantes aux interactions nonspécifiques en moins de 6 minutes, ce qui est conforme aux résultats obtenus (~5min) par le groupe de Lennox pour ces monocouches basées sur les alcanesthiolés.[80] La possibilité de faire varier l'arrangement de ces surfaces selon le potentiel appliqué a aussi été démontré. La formation de couches de 3-MPA-HHHDD-OH de densité variable a permis de déterminer que la densité de couches de même composant, mais de densité variable influence la résistance à l'adsorption nonspécifique. Ce type de changement de conformation a été caractérisé par Lioubimov et al. dans le cas de biomolécules immobilisées à la surface d'une couche métallique.[305]

Les perspectives de recherche qui suivront ces travaux sont nombreuses. Il est maintenant nécessaire d'intégrer les surfaces peptidiques aux matériaux micro et nanostructurés pour effectuer des essais de routine en bénificiant d'une amplification des signaux SPR. Il est essentiel d'effectuer le lien entre la résistance aux interactions nonspécifiques de certains types de peptides en particulier par rapport à leurs propriétés

physico-chimiques. Cela peut s'effectuer en couplant la SPR avec d'autres techniques analytiques telles que la spectrométrie de masse ou la spectroscopie de fluorescence afin de déterminer la nature exacte de ce qui est adsorbé à la surface des biocapteurs SPR formés de monocouches peptidiques. L'approche employée au cours du développement des monocouches peptidiques résistantes aux intéractions nonspécifiques peut être transposée à d'autres matrices, par exemple, le lait, l'urine ou le sang, afin d'étendre les applications de ce types de surface dans le domaine des biocapteurs SPR. La méthode dévelopée pour mesurer la performance des ligands d'intérêts pharmaceutique permettra de poursuivre les trasvaux basés sur le récepteur CD36, afin de déterminer le ligand qui soit le plus performant. D'autres cibles d'intérêts prarmacologiques pourront aussi bénificier de cette approche, suite à quelques travaux d'optimisation.

L'instrument développé au cours de ces travaux a permis de rendre la SPR plus accessible et efficace, et d'élargir son spectre d'activité afin que la communauté scientifique puisse davantage exploiter son potentiel. La méthode de développement et de fabrication de surfaces peptidiques permet de générer des surfaces qui sont mieux adaptées aux mesures dans des milieux complexes à analyser. Ceci apporte une contribution importante au domaine des biocapteurs SPR, afin que de nouvelles applications et de nouveaux produits basés sur cette technologie soient développés.

Sources documentaires

(1) Cooper, J.; Cass, T. *Biosensors : A practical Approach, 2nd edition* **2004**, *Oxford University Press*, 256 pages.

(2) Ligler, F. S. *Analytical Chemistry* **2009**, *81*, 519-526.

(3) Wang, J. *Chemical Reviews* **2008**, *108*, 814-825.

(4) Odenthal, K. J.; Gooding, J. J. *Analyst* **2007**, *132*, 603-610.

(5) Ivnitski, D.; Abdel-Hamid, I.; Atanasov, P.; Wilkins, E.; Stricker, S. *Electroanalysis* **2000**, *12*, 317-325.

(6) Erdem, A.; Ozsoz, M. *Electroanalysis* **2002**, *14*, 965-974.

(7) Shah, J.; Wilkins, E. *Electroanalysis* **2003**, *15*, 157-167.

(8) Trojanowicz, M. *Electroanalysis* **2002**, *14*, 1311-1328.

(9) Bunde, R. L.; Jarvi, E. J.; Rosentreter, J. J. *Talanta* **1998**, *46*, 1223-1236.

(10) Janshoff, A.; Galla, H. J.; Steinem, C. *Angewandte Chemie-International Edition* **2000**, *39*, 4004-4032.

(11) Jin, G.; Tengvall, P.; Lundstrom, I.; Arwin, H. *Anal. Biochem.* **1995**, *232*, 69-72.

(12) Demchenko, A. P. *Anal. Biochem.* **2005**, *343*, 1-22.

(13) Taitt, C. R.; Anderson, G. P.; Ligler, F. S. *Biosens. Bioelectron.* **2005**, *20*, 2470-2487.

(14) Popa, A. M.; Wenger, B.; Scolan, E.; Voirin, G.; Heinzelmann, H.; Pugin, R. *Appl. Surf. Sci.* **2009**, *256*, S12-S17.

(15) Rainina, E. I.; Efremenco, E. N.; Varfolomeyev, S. D.; Simonian, A. L.; Wild, J. R. *Biosensors and Bioelectronics* **1996**, *11*, 991-1000.

(16) Lacorte, S.; Barcelo, D. *Analytical Chemistry* **1996**, *68*, 2464-2470.

(17) Tulej, M.; Iakovleva, M.; Leya, I.; Wurz, P. *Analytical and Bioanalytical Chemistry* **2011**, *399*, 2185-2200.

(18) Homola, J. *Analytical and Bioanalytical Chemistry* **2003**, *377*, 528-539.

(19) Homola, J.; Yee, S. S.; Gauglitz, G. *Sensors and Actuators B-Chemical* **1999**, *54*, 3-15.

(20) Schasfoort, R.; Tudos, A. *Handbook of Surface Plasmon Resonance* **1998**, *RSC Publishing*, 426 pages.

(21) Live, L. S.; **Bolduc, O. R.**; Masson, J. F. *Analytical Chemistry* **2010**, *82*, 3780-3787.

(22) Nuster, R.; Paltauf, G.; Burgholzer, P. *Opt. Express* **2007**, *15*, 6087-6095.

(23) Abbas, A.; Linman, M. J.; Cheng, Q. *Biosensors and Bioelectronics* **2011**, *26*, 1815-1824.

(24) Jain, P. K.; Huang, X.; El-Sayed, I. H.; El-Sayad, M. A. *Plasmonics* **2007**, *2*, 107-118.

(25) Chowdhury, M. H.; Ray, K.; Gray, S. K.; Pond, J.; Lakowicz, J. R. *Analytical Chemistry* **2009**, *81*, 1397-1403.

(26) Bain, C. D.; Troughton, E. B.; Tao, Y. T.; Evall, J.; Whitesides, G. M.; Nuzzo, R. G. *Journal of the American Chemical Society* **1989**, *111*, 321-335.

(27) Sek, S. *Langmuir* **2009**, *25*, 13488-13492.

(28) Yang, G.; Cho, N. H. *Food Sci. Biotechnol.* **2008**, *17*, 1038-1046.

(29) Jang, H. S.; Park, K. N.; Kang, C. D.; Kim, J. P.; Sim, S. J.; Lee, K. S. *Optics Communications* **2009**, *282*, 2827-2830.

(30) Miura, N.; Sasaki, M.; Gobi, K. V.; Kataoka, C.; Shoyama, Y. *Biosens. Bioelectron.* **2003**, *18*, 953-959.

(31) Karlsson, R. *Journal of Molecular Recognition* **2004**, *17*, 151-161.

(32) Rich, R. L.; Myszka, D. G. *Journal of Molecular Recognition* **2002**, *15*, 352-376.

(33) Wilson, S.; Howell, S. *Biochemical Society Transactions* **2002**, *30*, 794-797.

(34) Bokken, G.; Corbee, R. J.; van Knapen, F.; Bergwerff, A. A. *Fems Microbiology Letters* **2003**, *222*, 75-82.

(35) de Waard, R.; Claassen, E.; Bokken, G.; Buiting, B.; Garssen, J.; Vos, J. G. *Clinical and Diagnostic Laboratory Immunology* **2003**, *10*, 59-65.

(36) Carnahan, J.; Wang, P.; Kendall, R.; Chen, C.; Hu, S.; Boone, T.; Juan, T.; Talvenheimo, J.; Montestruque, S.; Sun, J. L.; Elliott, G.; Thomas, J.; Ferbas, J.; Kern, B.; Briddell, R.; Leonard, J. P.; Cesano, A. *Clinical Cancer Research* **2003**, *9*, 3982S-3990S.

(37) Deinum, J.; Gustavsson, L.; Gyzander, E.; Kullman-Magnusson, M.; Edstrom, A.; Karlsson, R. *Anal. Biochem.* **2002**, *300*, 152-162.

(38) Hawkes, J. B.; Astheimer, R. W. *J. Opt. Soc. Am.* **1948**, *38*, 804-805.

(39) Cui, X. Q.; Sha, Y. F.; Yang, F.; Yu, P.; Li, J. N.; Yang, X. R. *Chinese Journal of Analytical Chemistry* **2005**, *33*, 1639-1642.

(40) Bally, M.; Halter, M.; Voeroes, J.; Grandin, H. M. *Surface and Interface Analysis* **2006**, *38*, 1442-1458.

(41) Wang, Z.; Wilkop, T.; Xu, D.; Dong, Y.; Ma, G.; Cheng, Q. *Analytical and Bioanalytical Chemistry* **2007**, *389*, 819-825.

(42) Balasubramanian, S.; Sorokulova, I. B.; Vodyanoy, V. J.; Simonian, A. L. *Biosens. Bioelectron.* **2007**, *22*, 948-955.

(43) Mitchell, J. S.; Wu, Y. Q.; Cook, C. J.; Main, L. *Anal. Biochem.* **2005**, *343*, 125-135.

(44) *Site internet:* http://www.biacore.com/ **Page consultée 17/04/2011**.

(45) Baird, C. L.; Myszka, D. G. *Journal of Molecular Recognition* **2001**, *14*, 261-268.

(46) Hoa, X. D.; Kirk, A. G.; Tabrizian, M. *Biosensors and Bioelectronics* **2009**, *24*, 3043-3048.

(47) Alleyne, C. J.; Roche, P. J. R.; Filion-Cote, S.; Kirk, A. G. *Opt. Lett.* **2011**, *36*, 46-48.

(48) Wang, S.; Huang, X.; Shan, X.; Foley, K. J.; Tao, N. *Analytical Chemistry* **2010**, *82*, 935-941.

(49) Du, M.; Zhou, F. *Analytical Chemistry* **2008**, *80*, 4225-4230.

(50) Borch, J.; Roepstorff, P. *Methods in molecular biology (Clifton, N.J.)* **2010**, *627*, 269-281.

(51) Nedelkov, D. *Methods in molecular biology (Clifton, N.J.)* **2010**, *627*, 261-268.

(52) Ahmed, N.; Barker, G.; Oliva, K.; Garfin, D.; Talmadge, K.; Georgiou, H.; Quinn, M.; Rice, G. *Proteomics* **2003**, *3*, 1980-1987.

(53) Bellei, E.; Bergamini, S.; Monari, E.; Fantoni, L. I.; Cuoghi, A.; Ozben, T.; Tomasi, A. *Amino Acids* **2011**, *40*, 145-156.

(54) Nguyen, T. H.; Pei, R.; Stojanovic, M.; Landry, D.; Lin, Q., 21-25 June 2009 2009; 1822-1825.

(55) Ryan, M. R.; Lowry, J. P.; Oneill, R. D. *Analyst* **1997**, *122*, 1419-1424.

(56) Balcer, H. I.; Spiker, J. O.; Kang, K. A. In *Oxygen Transport to Tissue Xxiv*; Dunn, J. F. S. H. M., Ed., 2003; Vol. 530, pp 133-141.

(57) Masson, J.-F.; Battaglia, T. M.; Khairallah, P.; Beaudoin, S.; Booksh, K. S. *Analytical Chemistry* **2007**, *79*, 612-619.

(58) Frisch, B.; Carriere, M.; Largeau, C.; Mathey, F.; Masson, C.; Schuber, F.; Scherman, D.; Escriou, V. *Bioconjugate Chemistry* **2004**, *15*, 754-764.

(59) Banerjee, I.; Pangule, R. C.; Kane, R. S. *Advanced Materials* **2011**, *23*, 690-718.

(60) Jon, S. Y.; Seong, J. H.; Khademhosseini, A.; Tran, T. N. T.; Laibinis, P. E.; Langer, R. *Langmuir* **2003**, *19*, 9989-9993.

(61) Konradi, R.; Pidhatika, B.; Muehlebach, A.; Textort, M. *Langmuir* **2008**, *24*, 613-616.

(62) Shin, B. C.; Wisniewski, N.; Reichert, W. M. *Journal of Biomaterials Science-Polymer Edition* **2001**, *12*, 467-477.

(63) Ostuni, E.; Yan, L.; Whitesides, G. M. *Colloids and Surfaces B-Biointerfaces* **1999**, *15*, 3-30.

(64) Ostuni, E.; Chapman, R. G.; Holmlin, R. E.; Takayama, S.; Whitesides, G. M. *Langmuir* **2001**, *17*, 5605-5620.

(65) Sigal, G. B.; Mrksich, M.; Whitesides, G. M. *Journal of the American Chemical Society* **1998**, *120*, 3464-3473.

(66) Chapman, R. G.; Ostuni, E.; Yan, L.; Whitesides, G. M. *Langmuir* **2000**, *16*, 6927-6936.

(67) Holmlin, R. E.; Chen, X. X.; Chapman, R. G.; Takayama, S.; Whitesides, G. M. *Langmuir* **2001**, *17*, 2841-2850.

(68) Phillips, K. S.; Han, J. H.; Cheng, Q. *Analytical Chemistry* **2007**, *79*, 899-907.

(69) Statz, A. R.; Meagher, R. J.; Barron, A. E.; Messersmith, P. B. *Journal of the American Chemical Society* **2005**, *127*, 7972-7973.

(70) Dudash, J.; Jiang, J. J.; Mayer, S. C.; Joullie, M. M. *Synth. Commun.* **1993**, *23*, 349-356.

(71) Nakajima, N.; Ikada, Y. *Bioconjugate Chemistry* **1995**, *6*, 123-130.

(72) Zhang, R. S. *Polymer* **2005**, *46*, 2443-2451.

(73) Seeberger, P. H.; Werz, D. B. *Nature Reviews Drug Discovery* **2005**, *4*, 751-763.

(74) Lin, L.-P.; Huang, L.-S.; Lin, C.-W.; Lee, C.-K.; Chen, J.-L.; Hsu, S.-M.; Lin, S. *Current drug targets. Immune, endocrine and metabolic disorders* **2005**, *5*, 61-72.

(75) Habauzit, D.; Chopineau, J.; Roig, B. *Analytical and Bioanalytical Chemistry* **2007**, *387*, 1215-1223.

(76) Rich, R. L.; Myszka, D. G. *Trends in Microbiology* **2003**, *11*, 124-133.

(77) Boutard, N.; Jamieson, A. G.; Ong, H.; Lubell, W. D. *Chem. Biol. Drug Des.*, *75*, 40-50.

(78) Qin, G.; Cai, C. *Chemical Communications* **2009**, 5112-5114.

(79) Reiche, J.; Kratz, K.; Hofmann, D.; Lendlein, A. *International Journal of Artificial Organs* **2011**, *34*, 123-128.

(80) Ma, F. Y.; Lennox, R. B. *Langmuir* **2000**, *16*, 6188-6190.

(81) Motta, A.; Condorelli, G. G.; Pellegrino, G.; Cornia, A.; Fragala, I. L. *Journal of Physical Chemistry C* **2010**, *114*, 20696-20701.

(82) Liu, Y. J.; Navasero, N. M.; Yu, H. Z. *Langmuir* **2004**, *20*, 4039-4050.

(83) Kimura, F.; Umemura, J.; Takenaka, T. *Langmuir* **1986**, *2*, 96-101.

(84) Cheng, S. S.; Chittur, K. K.; Sukenik, C. N.; Culp, L. A.; Lewandowska, K. *Journal of Colloid and Interface Science* **1994**, *162*, 135-143.

(85) Ahn, D. J.; Franses, E. I. *Journal of Physical Chemistry* **1992**, *96*, 9952-9959.

(86) Keegan, N.; Wright, N. G.; Lakey, J. H. *Angewandte Chemie-International Edition* **2005**, *44*, 4801-4804.

(87) Dieudonne, D.; Gericke, A.; Flach, C. R.; Jiang, X.; Farid, R. S.; Mendelsohn, R. *Journal of the American Chemical Society* **1998**, *120*, 792-799.

(88) Cornell, D. G. *Journal of Colloid and Interface Science* **1979**, *70*, 167-180.

(89) Vilar, M. R.; do Rego, A. M. B.; Ferraria, A. M.; Jugnet, Y.; Nogues, C.; Peled, D.; Naaman, R. *Journal of Physical Chemistry B* **2008**, *112*, 6957-6964.

(90) Lang, P.; Nogues, C. *Surface Science* **2008**, *602*, 2137-2147.

(91) Song, B.; Walczyk, W.; Schoenherr, H. *Langmuir* **2011**, *27*, 8223-8232.

(92) Gupta, P.; Ulman, A.; Fanfan, S.; Korniakov, A.; Loos, K. *Journal of the American Chemical Society* **2005**, *127*, 4-5.

(93) Wang, J.; Paz, J. L. L.; Jiang, M. *Langmuir* **1999**, *15*, 1884-1886.

(94) Greenfield, N. J. *Nature Protocols* **2006**, *1*, 2876-2890.

(95) Chang, Y.; Shu, S. H.; Shih, Y. J.; Chu, C. W.; Ruaan, R. C.; Chen, W. Y. *Langmuir* **2010**, *26*, 3522-3530.

(96) L.-Viger, M.; Brouard, D.; Boudreau, D. *The Journal of Physical Chemistry C* **2011**, *115*, 2974-2981.

(97) Li, J. F.; Huang, Y. F.; Ding, Y.; Yang, Z. L.; Li, S. B.; Zhou, X. S.; Fan, F. R.; Zhang, W.; Zhou, Z. Y.; Wu, D. Y.; Ren, B.; Wang, Z. L.; Tian, Z. Q. *Nature* **2010**, *464*, 392-395.

(98) Liz-Marzan, L. M.; Giersig, M.; Mulvaney, P. *Langmuir* **1996**, *12*, 4329-4335.

(99) Vanblaaderen, A.; Vrij, A. *Langmuir* **1992**, *8*, 2921-2931.

(100) Vanblaaderen, A.; Vrij, A. *Journal of Colloid and Interface Science* **1993**, *156*, 1-18.

(101) Vandenberg, E. T.; Bertilsson, L.; Liedberg, B.; Uvdal, K.; Erlandsson, R.; Elwing, H.; Lundstrom, I. *Journal of Colloid and Interface Science* **1991**, *147*, 103-118.

(102) Liu, G.-B.; Zhao, H.-Y.; Thiemann, T. *Advanced Synthesis & Catalysis* **2007**, *349*, 807-811.

(103) Bolduc, O. R.; Clouthier, C. M.; Pelletier, J. N.; Masson, J.-F. *Analytical Chemistry* **2009**, *81*, 6779-6788.

(104) Bolduc, O. R.; Masson, J.-F. *Langmuir* **2008**, *24*, 12085-12091.

(105) Bolduc, O. R.; Live, L. S.; Masson, J.-F. *Talanta* **2009**, *77*, 1680-1687.

(106) Campbell, C. T.; Kim, G. *Biomaterials* **2007**, *28*, 2380-2392.

(107) Green, R. J.; Frazier, R. A.; Shakesheff, K. M.; Davies, M. C.; Roberts, C. J.; Tendler, S. J. B. *Biomaterials* **2000**, *21*, 1823-1835.

(108) Mullett, W. M.; Lai, E. P. C.; Yeung, J. M. *Methods* **2000**, *22*, 77-91.

(109) Yuk, J. S.; Ha, K. S. *Experimental and Molecular Medicine* **2005**, *37*, 1-10.

(110) Brockman, J. M.; Nelson, B. P.; Corn, R. M. *Annual Review of Physical Chemistry* **2000**, *51*, 41-63.

(111) Phillips, K. S.; Cheng, Q. *Anal. Bioanal. Chem.* **2007**, *387*, 1831-1840.

(112) Lavine, B. K.; Westover, D. J.; Oxenford, L.; Midankar, N.; Kaval, N. *Microchemical Journal* **2007**, *86*, 147-155.

(113) Neuert, G.; Kufer, S.; Benoit, M.; Gaub, H. E. *Review of Scientific Instruments* **2005**, *76*.

(114) Hemmi, A.; Imato, T.; Aoki, Y.; Sato, M.; Soh, N.; Asano, Y.; Akasaka, C.; Okutani, S.; Ohkubo, S.; Kaneki, N.; Shimada, K.; Eguchi, T.; Oinuma, T. *Sensors and Actuators B-Chemical* **2005**, *108*, 893-898.

(115) Naimushin, A. N.; Soelberg, S. D.; Bartholomew, D. U.; Elkind, J. L.; Furlong, C. E. *Sensors and Actuators B-Chemical* **2003**, *96*, 253-260.

(116) Akimoto, T.; Wada, S.; Karube, I. *Analytica Chimica Acta* **2008**, *610*, 119-124.

(117) Gentleman, D. J.; Booksh, K. S. *Talanta* **2006**, *68*, 504-515.

(118) Battaglia, T. M.; Masson, J. F.; Sierks, M. R.; Beaudoin, S. P.; Rogers, J.; Foster, K. N.; Holloway, G. A.; Booksh, K. S. *Analytical Chemistry* **2005**, *77*, 7016-7023.

(119) Masson, J. F.; Battaglia, T. M.; Khairallah, P.; Beaudoin, S.; Booksh, K. S. *Analytical Chemistry* **2007**, *79*, 612-619.

(120) Masson, J. F.; Obando, L.; Beaudoin, S.; Booksh, K. *Talanta* **2004**, *62*, 865-870.

(121) Slavik, R.; Homola, J.; Brynda, E. *Biosensors & Bioelectronics* **2002**, *17*, 591-595.

(122) Masson, J. F.; Kim, Y. C.; Obando, L. A.; Peng, W.; Booksh, K. S. *Applied Spectroscopy* **2006**, *60*, 1241-1246.

(123) Kim, Y. C.; Masson, J. F.; Booksh, K. S. *Talanta* **2005**, *67*, 908-917.

(124) Kim, Y. C.; Banerji, S.; Masson, J. F.; Peng, W.; Booksh, K. S. *Analyst* **2005**, *130*, 838-843.

(125) Stemmler, I.; Brecht, A.; Gauglitz, G. *Sensors and Actuators B-Chemical* **1999**, *54*, 98-105.

(126) Zhao, X. J.; Wang, Z.; Mu, Y.; Zhang, H. Q.; Jin, Q. H. *Laboratory Robotics and Automation* **2000**, *12*, 104-107.

(127) Evans, S. D.; Allinson, H.; Boden, N.; Flynn, T. M.; Henderson, J. R. *Journal of Physical Chemistry B* **1997**, *101*, 2143-2148.

(128) Jordan, C. E.; Corn, R. M. *Analytical Chemistry* **1997**, *69*, 1449-1456.

(129) Berger, C. E. H.; Beumer, T. A. M.; Kooyman, R. P. H.; Greve, J. *Analytical Chemistry* **1998**, *70*, 703-706.

(130) Beusink, J. B.; Lokate, A. M. C.; Besselink, G. A. J.; Pruijn, G. J. M.; Schasfoort, R. B. M. *Biosensors & Bioelectronics* **2008**, *23*, 839-844.

(131) Singh, B. K.; Hillier, A. C. *Analytical Chemistry* **2006**, *78*, 2009-2018.

(132) Klenkar, G.; Valiokas, R.; Lundstrom, I.; Tinazli, A.; Tampe, R.; Piehler, J.; Liedberg, B. *Analytical Chemistry* **2006**, *78*, 3643-3650.

(133) Chinowsky, T. M.; Jung, L. S.; Yee, S. S. *Sensors and Actuators B-Chemical* **1999**, *54*, 89-97.

(134) Gentleman, D. J.; Obando, L. A.; Masson, J. F.; Holloway, J. R.; Booksh, K. S. *Analytica Chimica Acta* **2004**, *515*, 291-302.

(135) Johansen, K.; Stalberg, R.; Lundstrom, I.; Liedberg, B. *Measurement Science & Technology* **2000**, *11*, 1630-1638.

(136) Tao, N. J.; Boussaad, S.; Huang, W. L.; Arechabaleta, R. A.; D'Agnese, J. *Review of Scientific Instruments* **1999**, *70*, 4656-4660.

(137) Masson, J. F.; Battaglia, T. M.; Cramer, J.; Beaudoin, S.; Sierks, M.; Booksh, K. S. *Analytical and Bioanalytical Chemistry* **2006**, *386*, 1951-1959.

(138) Livermore, D. M. *Clinical Microbiology Reviews* **1995**, *8*, 557-&.

(139) Yolken, R. H.; Hughes, W. T.; Stoppa, P. J. *The Journal of Pediatrics* **1980**, *97*, 715-720.

(140) Shankaran, D. R.; Gobi, K. V. A.; Miura, N. *Sensors and Actuators B-Chemical* **2007**, *121*, 158-177.

(141) Green, R. J.; Davies, J.; Davies, M. C.; Roberts, C. J.; Tendler, S. J. B. *Biomaterials* **1997**, *18*, 405-413.

(142) Green, R. J.; Davies, M. C.; Roberts, C. J.; Tendler, S. J. B. *Biomaterials* **1999**, *20*, 385-391.

(143) Cooper, M. A. *Nature Reviews Drug Discovery* **2002**, *1*, 515-528.

(144) Schlenoff, J. B.; Li, M.; Ly, H. *Journal of the American Chemical Society* **1995**, *117*, 12528-12536.

(145) Tour, J. M.; Jones, L.; Pearson, D. L.; Lamba, J. J. S.; Burgin, T. P.; Whitesides, G. M.; Allara, D. L.; Parikh, A. N.; Atre, S. V. *Journal of the American Chemical Society* **1995**, *117*, 9529-9534.

(146) Masson, J. F.; Barnhart, M.; Battaglia, T. M.; Morris, G. E.; Nieman, R. A.; Young, P. J.; Lorson, C. L.; Booksh, K. S. *Analyst* **2004**, *129*, 855-859.

(147) Masson, J. F.; Battaglia, T. M.; Davidson, M. J.; Kim, Y. C.; Prakash, A. M. C.; Beaudoin, S.; Booksh, K. S. *Talanta* **2005**, *67*, 918-925.

(148) Masson, J. F.; Battaglia, T. M.; Kim, Y. C.; Prakash, A.; Beaudoin, S.; Booksh, K. S. *Talanta* **2004**, *64*, 716-725.

(149) Lofas, S.; Johnsson, B. *Journal of the Chemical Society-Chemical Communications* **1990**, 1526-1528.

(150) Peluso, P.; Wilson, D. S.; Do, D.; Tran, H.; Venkatasubbaiah, M.; Quincy, D.; Heidecker, B.; Poindexter, K.; Tolani, N.; Phelan, M.; Witte, K.; Jung, L. S.; Wagner, P.; Nock, S. *Analytical Biochemistry* **2003**, *312*, 113-124.

(151) McPherson, T.; Kidane, A.; Szleifer, I.; Park, K. *Langmuir* **1998**, *14*, 176-186.

(152) Zolk, M.; Eisert, F.; Pipper, J.; Herrwerth, S.; Eck, W.; Buck, M.; Grunze, M. *Langmuir* **2000**, *16*, 5849-5852.

(153) Munson, M. S.; Hasenbank, M. S.; Fu, E.; Yager, P. *Lab on a Chip* **2004**, *4*, 438-445.

(154) Mrksich, M.; Sigal, G. B.; Whitesides, G. M. *Langmuir* **1995**, *11*, 4383-4385.

(155) Mrksich, M.; Whitesides, G. M. *Annual Review of Biophysics and Biomolecular Structure* **1996**, *25*, 55-78.

(156) Ostuni, E.; Chapman, R. G.; Liang, M. N.; Meluleni, G.; Pier, G.; Ingber, D. E.; Whitesides, G. M. *Langmuir* **2001**, *17*, 6336-6343.

(157) Statz, A. R.; Meagher, R. J.; Barron, A. E.; Messersmith, P. B. *J. Am. Chem. Soc.* **2005**, *127*, 7972-7973.

(158) Levy, R. *Chembiochem* **2006**, *7*, 1141-1145.

(159) Levy, R.; Thanh, N. T. K.; Doty, R. C.; Hussain, I.; Nichols, R. J.; Schiffrin, D. J.; Brust, M.; Fernig, D. G. *Journal of the American Chemical Society* **2004**, *126*, 10076-10084.

(160) Hsieh, K. H.; Demaine, M. M. *Synthesis-Stuttgart* **1991**, 59-62.

(161) Steglich, W. *Angewandte Chemie (International ed. in Englich)* **1978**, *17*, 522-524.

(162) Doucet, N.; Savard, P. Y.; Pelletier, J. N.; Gagne, S. M. *Journal of Biological Chemistry* **2007**, *282*, 21448-21459.

(163) Doucet, N.; Pelletier, J. N. *Proteins-Structure Function and Bioinformatics* **2007**, *69*, 340-348.

(164) Catimel, B.; Nerrie, M.; Lee, F. T.; Scott, A. M.; Ritter, G.; Welt, S.; Old, L. J.; Burgess, A. W.; Nice, E. C. *Journal of Chromatography A* **1997**, *776*, 15-30.

(165) Howell, S.; Kenmore, M.; Kirkland, M.; Badley, R. A. *Journal of Molecular Recognition* **1998**, *11*, 200-203.

(166) Su, X. L.; Li, Y. B. *Biosensors & Bioelectronics* **2004**, *19*, 563-574.

(167) Adanyi, N.; Varadi, M.; Kim, N.; Szendro, I. *Current Applied Physics* **2006**, *6*, 279-286.

(168) Khatkhatay, M. I.; Desai, M. P.; Sankolli, G. M.; Pardhe, D. K.; Joshi, U. M. *Journal of Clinical Laboratory Analysis* **1993**, *7*, 95-99.

(169) Wojtyk, J. T. C.; Morin, K. A.; Boukherroub, R.; Wayner, D. D. M. *Langmuir* **2002**, *18*, 6081-6087.

(170) Nordin, H.; Jungnelius, M.; Karlsson, R.; Karlsson, O. P. *Analytical Biochemistry* **2005**, *340*, 359-368.

(171) Livingstone, C. D.; Barton, G. J. *Computer Applications in the Biosciences* **1993**, *9*, 745-756.

(172) Xu, L. C.; Siedlecki, C. A. *Biomaterials* **2007**, *28*, 3273-3283.

(173) Huang, L.; Reekmans, G.; Saerens, D.; Friedt, J. M.; Frederix, F.; Francis, L.; Muyldermans, S.; Campitelli, A.; Van Hoof, C. *Biosensors & Bioelectronics* **2005**, *21*, 483-490.

(174) Smith, E. A.; Corn, R. M. *Applied Spectroscopy* **2003**, *57*, 320A-332A.

(175) Luppa, P. B.; Sokoll, L. J.; Chan, D. W. *Clin. Chim. Acta* **2001**, *314*, 1-26.

(176) Phillips, K.; Cheng, Q. *Anal. Bioanal. Chem.* **2007**, *387*, 1831-1840.

(177) Rich, R. L.; Myszka, D. G. *Curr. Opin. Biotechnol.* **2000**, *11*, 54-61.

(178) Porfirieva, A.; Evtugyn, G.; Hianik, T. *Electroanalysis* **2007**, *19*, 1915-1920.

(179) Sankaranarayanan, S. K. R. S.; Cular, S.; Bhethanabotla, V. R.; Joseph, B. *Physical Review E (Statistical, Nonlinear, and Soft Matter Physics)* **2008**, *77*, 066308-066319.

(180) Furuya, M.; Haramura, M.; Tanaka, A. *Biorg. Med. Chem.* **2006**, *14*, 537-543.

(181) Morimoto, N.; Iwasaki, Y.; Nakabayashi, N.; Ishihara, K. *Biomaterials* **2002**, *23*, 4881-4887.

(182) Wink, T.; vanZuilen, S. J.; Bult, A.; vanBennekom, W. P. *Analyst* **1997**, *122*, R43-R50.

(183) Satomi, T.; Nagasaki, Y.; Kobayashi, H.; Tateishi, T.; Kataoka, K.; Otsuka, H. *J. Nanosci. Nanotechnol.* **2007**, *7*, 2394-2399.

(184) Sato, Y.; Yoshioka, K.; Tanaka, M.; Murakami, T.; Ishida, M. N.; Niwa, O. *Chem. Commun.* **2008**, 4909-4911.

(185) Statz, A. R.; Barron, A. E.; Messersmith, P. B. *Soft Matter* **2008**, *4*, 131-139.

(186) Kozak, D.; Surawski, P.; Thoren, K. M.; Lu, C. Y.; Marcon, L.; Trau, M. *Biomacromolecules* **2009**, *10*, 360-365.

(187) Bolduc, O. R.; Masson, J. F. *Langmuir* **2008**, *24*, 12085-12091.

(188) Cho, Y.; Ivanisevic, A. *J. Phys. Chem. B* **2005**, *109*, 6225-6232.

(189) Duchesne, L.; Wells, G.; Ferning, D. G.; Harris, S. A.; Levy, R. *ChemBioChem* **2008**, *9*, 2127-2134.

(190) Kimura, S.; Miura, Y.; Morita, T.; Kobayashi, S.; Imanishi, Y. *Journal of Polymer Science Part a-Polymer Chemistry* **2000**, *38*, 4826-4831.

(191) Takeda, K.; Morita, T.; Kimura, S. *J. Phys. Chem. B* **2008**, *112*, 12840-12850.

(192) Venanzi, M.; Pace, G.; Palleschi, A.; Stella, L.; Castrucci, P.; Scarselli, M.; De Crescenzi, M.; Formaggio, F.; Toniolo, C.; Marletta, G. *Surf. Sci.* **2006**, *600*, 409-416.

(193) Tseng, M. C.; Chang, Y. P.; Chu, Y. H. *Anal. Biochem.* **2007**, *371*, 1-9.

(194) Fabris, L.; Antonello, S.; Armelao, L.; Donkers, R. L.; Polo, F.; Toniolo, C.; Maran, F. *Journal of the American Chemical Society* **2006**, *128*, 326-336.

(195) Pomerantz, W. C.; Cadwell, K. D.; Hsu, Y. J.; Gellman, S. H.; Abbott, N. L. *Chem. Mater.* **2007**, *19*, 4436-4441.

(196) Pyun, J. C.; Kim, S. D.; Chung, J. W. *Anal. Biochem.* **2005**, *347*, 227-233.

(197) Bui, C. T.; Ercole, F.; Pham, Y.; Campbell, R.; Rasoul, F. A.; Maeji, N. J.; Ede, N. J. *J. Pept. Sci.* **2000**, *6*, 534-538.

(198) Parsons, J. G.; Sheehan, C. S.; Wu, Z. M.; James, I. W.; Bray, A. M. In *Combinatorial Chemistry, Pt B*, 2003; Vol. 369, pp 39-74.

(199) De Gheldre, Y.; Avesani, V.; Berhin, C.; Delmee, M.; Glupczynski, Y. *J. Antimicrob. Chemother.* **2003**, *52*, 591-597.

(200) Nüesch-Inderbinen, M. T.; Hächler, H.; Kayser, F. H. *European Journal of Clinical Microbiology & Infectious Diseases* **1996**, *15*, 398-402.

(201) Hujer, A. M.; Page, M. G. P.; Helfand, M. S.; Yeiser, B.; Bonomo, R. A. *J. Clin. Microbiol.* **2002**, *40*, 1947-1957.

(202) Kaiser, E.; Colescott, R. L.; Bossinger, C. D.; Cook, P. I. *Anal. Biochem.* **1970**, *34*, 595-598.

(203) Kaiser, T.; Nicholson, G. J.; Kohlbau, H. J.; Voelter, W. *Tetrahedron Lett.* **1996**, *37*, 1187-1190.

(204) De Wals, P. Y.; Doucet, N.; Pelletier, J. N. *Protein Sci.* **2009**, *18*, 147-160.

(205) Bradford, M. M. *Anal. Biochem.* **1976**, *72*, 248-254.

(206) Bebrone, C.; Moali, C.; Mahy, F.; Rival, S.; Docquier, J. D.; Rossolini, G. M.; Fastrez, J.; Pratt, R. F.; Frere, J.-M.; Galleni, M. *Antimicrob. Agents Chemother.* **2001**, *45*, 1868-1871.

(207) Jones, R. N.; Wilson, H. W.; Novick, W. J.; Barry, A. L.; Thornsberry, C. *J. Clin. Microbiol.* **1982**, *15*, 954-958.

(208) Jung, L. S.; Campbell, C. T.; Chinowsky, T. M.; Mar, M. N.; Yee, S. S. *Langmuir* **1998**, *14*, 5636-5648.

(209) Sakurai, T.; Oka, S.; Kubo, A.; Nishiyama, K.; Taniguchi, I. *Journal of Peptide Science* **2006**, *12*, 396-402.

(210) Gooding, J. J.; Erokhin, P.; Losic, D.; Yang, W. R.; Policarpio, V.; Liu, J. Q.; Ho, F. M.; Situmorang, M.; Hibbert, D. B.; Shapter, J. G. *Anal. Sci.* **2001**, *17*, 3-9.

(211) Masson, J. F.; Kranz, C.; Booksh, K. S.; Mizaikoff, B. *Biosensors & Bioelectronics* **2007**, *23*, 355-361.

(212) Frazier, R. A.; Matthijs, G.; Davies, M. C.; Roberts, C. J.; Schacht, E.; Tendler, S. J. B. *Biomaterials* **2000**, *21*, 957-966.

(213) Silin, V.; Weetall, H.; Vanderah, D. J. *J. Colloid Interface Sci.* **1997**, *185*, 94-103.

(214) Trmcic-Cvitas, J.; Hasan, E.; Ramstedt, M.; Li, X.; Cooper, M. A.; Abell, C.; Huck, W. T. S.; Gautrot, J. E. *Biomacromolecules* **2009**, *10*, 2885-2894.

(215) Uchida, K.; Hoshino, Y.; Tamura, A.; Yoshimoto, K.; Kojima, S.; Yamashita, K.; Yamanaka, I.; Otsuka, H.; Kataoka, K.; Nagasaki, Y. *Biointerphases* **2007**, *2*, 126-130.

(216) Uchida, K.; Otsuka, H.; Kaneko, M.; Kataoka, K.; Nagasaki, Y. *Analytical Chemistry* **2005**, *77*, 1075-1080.

(217) Zareie, H. M.; Boyer, C.; Bulmus, V.; Nateghi, E.; Davis, T. P. *Acs Nano* **2008**, *2*, 757-765.

(218) Teramura, Y.; Iwata, H. *Anal. Biochem.* **2007**, *365*, 201-207.

(219) Lee, C. Y.; Gamble, L. J.; Grainger, D. W.; Castner, D. G. *Biointerphases* **2006**, *1*, 82-92.

(220) Lee, C. Y.; Nguyen, P. C. T.; Grainger, D. W.; Gamble, L. J.; Castner, D. G. *Anal. Chem.* **2007**, *79*, 4390-4400.

(221) Feller, L. M.; Cerritelli, S.; Textor, M.; Hubbell, J. A.; Tosatti, S. G. P. *Macromolecules* **2005**, *38*, 10503-10510.

(222) Tosatti, S.; Paul, S. M. D.; Askendal, A.; VandeVondele, S.; Hubbell, J. A.; Tengvall, P.; Textor, M. *Biomaterials* **2003**, *24*, 4949-4958.

(223) Jeong, J. H.; Kim, B. Y.; Cho, S. H.; Kim, J. D. *Journal of Nonlinear Optical Physics & Materials* **2004**, *13*, 525-534.

(224) Jeong, J. H.; Kim, B. Y.; Lee, S. J.; Kim, J. D. *Chem. Phys. Lett.* **2006**, *421*, 373-377.

(225) Kyo, M.; Usui-Aoki, K.; Koga, H. *Anal. Chem.* **2005**, *77*, 7115-7121.

(226) Chen, S. F.; Cao, Z. Q.; Jiang, S. Y. *Biomaterials* **2009**, *30*, 5892-5896.

(227) Vaisocherova, H.; Yang, W.; Zhang, Z.; Cao, Z. Q.; Cheng, G.; Piliarik, M.; Homola, J.; Jiang, S. Y. *Anal. Chem.* **2008**, *80*, 7894-7901.

(228) Vaisocherova, H.; Zhang, Z.; Yang, W.; Cao, Z. Q.; Cheng, G.; Taylor, A. D.; Piliarik, M.; Homola, J.; Jiang, S. Y. *Biosens. Bioelectron.* **2009**, *24*, 1924-1930.

(229) Galis, Z. S.; Sukhova, G. K.; Lark, M. W.; Libby, P. *J. Clin. Invest.* **1994**, *94*, 2493-2503.

(230) Samnegard, A. S., A.; Lundman, P.; Boquist, S.; Odeberg, J.; Hulthe, J.; McPheat, W.; Tornvall, P.; Bergstrand, L.; Ericsson, C. G.; Hamsten, A.; Eriksson, P. *J. Intern. Med.* **2005**, *258*, 411-419.

(231) Kaplan, R. C.; Smith, N. L.; Zucker, S.; Heckbert, S. R.; Rice, K.; Psaty, B. M. *Atherosclerosis* **2008**, *201*, 130-137.

(232) Kurzawski, M.; Modrzejewski, A.; Pawlik, A.; Drozdzik, M. *Clin. Exp. Dermatol.* **2009**, *34*, 613-617.

(233) Han, Z. N.; Boyle, D. L.; Manning, A. M.; Firestein, G. S. *Autoimmunity* **1998**, *28*, 197-208.

(234) Murawaki, Y.; Ikuta, Y.; Okamoto, K.; Koda, M.; Kawasaki, H. *J. Hepatol.* **1999**, *31*, 474-481.

(235) Gohji, K.; Fujimoto, N.; Komiyama, T.; Fujii, A.; Ohkawa, J.; Kamidono, S.; Nakajima, M. *Cancer* **1996**, *78*, 2379-2387.

(236) Lein, M.; Nowak, L.; Jung, K.; Koenig, F.; Schnorr, D.; Loening, S. A. *Urologe. A* **1998**, *37*, 377-381.

(237) Preece, G.; Murphy, G.; Ager, A. *J. Biol. Chem.* **1996**, *271*, 11634-11640.

(238) Simian, M.; Hirai, Y.; Navre, M.; Werb, Z.; Lochter, A.; Bissell, M. J. *Development* **2001**, *128*, 3117-3131.

(239) Sternlicht, M. D.; Bissell, M. J.; Werb, Z. *Oncogene* **2000**, *19*, 1102-1113.

(240) Sternlicht, M. D.; Lochter, A.; Sympson, C. J.; Huey, B.; Rougler, J. P.; Gray, J. W.; Pinkel, D.; Bissell, M. J.; Werb, Z. *Cell* **1999**, *98*, 137-146.

(241) McCawley, L. J.; Wright, J.; LaFleur, B. J.; Crawford, H. C.; Matrisian, L. M. *Am. J. Pathol.* **2008**, *173*, 1528-1539.

(242) Si-Tayeb, K.; Monvoisin, A.; Mazzocco, C.; Lepreux, S.; Decossas, M.; Cubel, G.; Taras, D.; Blanc, J.-F.; Robinson, D. R.; Rosenbaum, J. *Am. J. Pathol.* **2006**, *169*, 1390-1401.

(243) Stevens, A. P.; Spangler, B.; Wallner, S.; Kreutz, M.; Dettmer, K.; Oefner, P. J.; Bosserhoff, A. K. *J. Cell. Biochem.* **2009**, *106*, 210-219.

(244) Roice, M.; Suma, G.; Kumar, K. S.; Pillai, V. N. R. *J. Protein Chem.* **2001**, *20*, 25-32.

(245) Bolduc, O. R.; Live, L. S.; Masson, J. F. *Talanta* **2009**, *77*, 1680-1687.

(246) Johnsson, B.; Löfås, S.; Lindquist, G. *Anal. Biochem.* **1991**, *198*, 268-277.

(247) Johnsson, B.; Löfås, S.; Lindquist, G.; Edström, Å.; Hillgren, R.-M. M.; Hansson, A. *J. Mol. Recognit.* **1995**, *8*, 125-131.

(248) Löfås, S.; Johnsson, B.; Tegendal, K.; Rönnberg, I. *Colloids Surf. B. Biointerfaces* **1993**, *1*, 83-89.

(249) Simone, Z.; Roger, S.; Esther, Y. *Eur. J. Org. Chem.* **2003**, *2003*, 2454-2461.

(250) Chang, Y.; Chen, S. F.; Zhang, Z.; Jiang, S. Y. *Langmuir* **2006**, *22*, 2222-2226.

(251) Yang, W.; Xue, H.; Li, W.; Zhang, J. L.; Jiang, S. Y. *Langmuir* **2009**, *25*, 11911-11916.

(252) Yang, W.; Zhang, L.; Wang, S. L.; White, A. D.; Jiang, S. Y. *Biomaterials* **2009**, *30*, 5617-5621.

(253) Kurita, R.; Hirata, Y.; Yabuki, S.; Yokota, Y.; Kato, D.; Sato, Y.; Mizutani, F.; Niwa, O. *Sensors and Actuators B-Chemical* **2008**, *130*, 320-325.

(254) Duevel, R. V.; Corn, R. M. *Analytical Chemistry* **1992**, *64*, 337-342.

(255) Doneux, T.; Bouffier, L.; Mello, L. V.; Rigden, D. J.; Kejnovska, I.; Fernig, D. G.; Higgins, S. J.; Nichols, R. J. *Journal of Physical Chemistry C* **2009**, *113*, 6792-6799.

(256) Bolduc, O. R.; Clouthier, C. M.; Pelletier, J. N.; Masson, J. F. *Anal. Chem.* **2009**, *81*, 6779-6788.

(257) Dong, Y.; Wilkop, T.; Xu, D. K.; Wang, Z. Z.; Cheng, Q. *Anal. Bioanal. Chem.* **2008**, *390*, 1575-1583.

(258) Ni, J.; Lipert, R. J.; Dawson, G. B.; Porter, M. D. *Anal. Chem.* **1999**, *71*, 4903-4908.

(259) Lyon, L. A.; Musick, M. D.; Natan, M. J. *Anal. Chem.* **1998**, *70*, 5177-5183.

(260) Fan, A. P.; Lau, C. W.; Lu, J. Z. *Anal. Chem.* **2005**, *77*, 3238-3242.

(261) Dequaire, M.; Degrand, C.; Limoges, B. *Anal. Chem.* **2000**, *72*, 5521-5528.

(262) Ling, J.; Li, Y. F.; Huang, C. Z. *Anal. Chem.* **2009**, *81*, 1707-1714.

(263) Bolduc, O. R.; Lambert-Lanteigne, P.; Colin, D. Y.; Zhao, S. S.; Proulx, C.; Boeglin, D.; Lubell, W. D.; Pelletier, J. N.; Fethiere, J.; Ong, H.; Masson, J.-F. *Analyst* **2011**, *136*, 3142-3148.

(264) Chudy, M.; Grabowska, I.; Ciosek, P.; Filipowicz-Szymanska, A.; Stadnik, D.; Wyzkiewicz, I.; Jedrych, E.; Juchniewicz, M.; Skolimowski, M.; Ziolkowska, K.; Kwapiszewski, R. *Anal. Bioanal. Chem.* **2009**, *395*, 647-668.

(265) Vilarino, N.; Louzao, M. C.; Vieytes, M. R.; Botana, L. M. *Anal. Bioanal. Chem.* **2010**, *397*, 1673-1681.

(266) Warsinke, A. *Anal. Bioanal. Chem.* **2009**, *393*, 1393-1405.

(267) Willer, U.; Schade, W. *Anal. Bioanal. Chem.* **2009**, *395*, 275-282.

(268) Rusmini, F.; Zhong, Z.; Feijen, J. *Biomacromolecules* **2007**, *8*, 1775-1789.

(269) Chang, Y.; Chu, W. L.; Chen, W. Y.; Zheng, J.; Liu, L. Y.; Ruaan, R. C.; Higuchi, A. *Journal of Biomedical Materials Research Part A* **2009**, *93A*, 400-408.

(270) Vaisocherova, H.; Zhang, Z.; Yang, W.; Cao, Z. Q.; Cheng, G.; Taylor, A. D.; Piliarik, M.; Homola, J.; Jiang, S. Y. *Biosens. Bioelectron.* **2009**, *24*, 1924-1930.

(271) Bolduc, O. R.; Pelletier, J. N.; Masson, J. F. *Analytical Chemistry* **2010**, *82*, 3699-3706.

(272) Chelmowski, R.; Koster, S. D.; Kerstan, A.; Prekelt, A.; Grunwald, C.; Winkler, T.; Metzler-Nolte, N.; Terfort, A.; Woll, C. *Journal of the American Chemical Society* **2008**, *130*, 14952-+.

(273) Daw, N. C.; Billups, C. A.; Rodriguez-Galindo, C.; McCarville, M. B.; Rao, B. N.; Cain, A. M.; Jenkins, J. J.; Neel, M. D.; Meyer, W. H. *Cancer* **2006**, *106*, 403-412.

(274) Lynch, G.; Magill, G. B.; Sordillo, P.; Golbey, R. B. *Cancer* **1982**, *50*, 1724-1727.

(275) Blankespoor, R.; Limoges, B.; Schöllhorn, B.; Syssa-Magalé, J.-L.; Yazidi, D. *Langmuir* **2005**, *21*, 3362-3375.

(276) Keller, T. A.; Duschl, C.; Kröger, D.; Sévin-Landais, A.-F.; Vogel, H.; Cervigni, S. E.; Dumy, P. *Supramolecular Science* **1995**, *2*, 155-160.

(277) Kröger, D.; Liley, M.; Schiweck, W.; Skerra, A.; Vogel, H. *Biosensors and Bioelectronics* **1999**, *14*, 155-161.

(278) Tinazli, A.; Tang, J.; Valiokas, R.; Picuric, S.; Lata, S.; Piehler, J.; Liedberg, B.; Tampé, R. *Chemistry - A European Journal* **2005**, *11*, 5249-5259.

(279) Xu, F.; Zhen, G.; Yu, F.; Kuennemann, E.; Textor, M.; Knoll, W. *Journal of the American Chemical Society* **2005**, *127*, 13084-13085.

(280) Volpato, J. P.; Fossati, E.; Pelletier, J. N. *Journal of Molecular Biology* **2007**, *373*, 599-611.

(281) Bennett, B. D.; Bennett, G. L.; Vitangcol, R. V.; Jewett, J. R.; Burnier, J.; Henzel, W.; Lowe, D. G. *Journal of Biological Chemistry* **1991**, *266*, 23060-23067.

(282) Gorgani, N. N.; Parish, C. R.; Easterbrook Smith, S. B.; Altin, J. G. *Biochemistry* **1997**, *36*, 6653-6662.

(283) Igawa, T.; Tsunoda, H.; Tachibana, T.; Maeda, A.; Mimoto, F.; Moriyama, C.; Nanami, M.; Sekimori, Y.; Nabuchi, Y.; Aso, Y.; Hattori, K. *Protein Engineering Design and Selection*, *23*, 385-392.

(284) Jin, C.; Bencurova, M.; Borth, N.; Ferko, B.; Jensen-Jarolim, E.; Altmann, F.; Hantusch, B. *Glycobiology* **2006**, *16*, 349-357.

(285) Baulsir, C. F.; Simler, R. J. *Advanced Drug Delivery Reviews* **1996**, *21*, 191-203.

(286) Martin, M. A.; Olives, A. I.; del Castillo, B.; Menendez, J. C. *Current Pharmaceutical Analysis* **2008**, *4*, 106-117.

(287) Meadows, D. *Advanced Drug Delivery Reviews* **1996**, *21*, 179-189.

(288) Thillaivinayagalingam, P.; Gommeaux, J.; McLoughlin, M.; Collins, D.; Newcombe, A. R. *J. Chromatogr. B* **2010**, *878*, 149-153.

(289) Yu, D. H.; Blankert, B.; Vire, J. C.; Kauffmann, J. M. *Analytical Letters* **2005**, *38*, 1687-1701.

(290) Bodart, V.; Febbraio, M.; Demers, A.; McNicoll, N.; Pohankova, P.; Perreault, A.; Sejlitz, T.; Escher, E.; Silverstein, R. L.; Lamontagne, D.; Ong, H. *Circ. Res.* **2002**, *90*, 844-849.

(291) Demers, A.; McNicoll, N.; Febbraio, M.; Servant, M.; Marleau, S.; Silverstein, R.; Ong, H. *Biochem. J.* **2004**, *382*, 417-424.

(292) Harb, D.; Bujold, K.; Febbraio, M.; Sirois, M. G.; Ong, H.; Marleau, S. *Cardiovascular Research* **2009**, *83*, 42-51.

(293) Marleau, S.; Harb, D.; Bujold, K.; Avallone, R.; Iken, K.; Wang, Y. F.; Demers, A.; Sirois, M. G.; Febbraio, M.; Silverstein, R. L.; Tremblay, A.; Ong, H. *FASEB J.* **2005**, *19*, 1869-+.

(294) Carnazzi, E.; Aumelas, A.; Mouillac, B.; Breton, C.; Guillou, L.; Barberis, C.; Seyer, R. *J. Med. Chem.* **2001**, *44*, 3022-3030.

(295) Bolduc, O. R.; Pelletier, J. N.; Masson, J.-F. *Analytical Chemistry* **2010**, *82*, 3699-3706.

(296) Chelmowski, R.; Koester, S. D.; Kerstan, A.; Prekelt, A.; Grunwald, C.; Winkler, T.; Metzler-Nolte, N.; Terfort, A.; Woell, C. *Journal of the American Chemical Society* **2008**, *130*, 14952-+.

(297) Zhang, Z.; Chen, S.; Jiang, S. *Biomacromolecules* **2006**, *7*, 3311-3315.

(298) Bi, H.; Meng, S.; Li, Y.; Guo, K.; Chen, Y.; Kong, J.; Yang, P.; Zhong, W.; Liu, B. *Lab on a Chip* **2006**, *6*, 769-775.

(299) Terrill, R. H.; Balss, K. M.; Zhang, Y. M.; Bohn, P. W. *Journal of the American Chemical Society* **2000**, *122*, 988-989.

(300) Zhang, Y. M.; Terrill, R. H.; Bohn, P. W. *Analytical Chemistry* **1999**, *71*, 119-125.

(301) Qu, D.; Morin, M. *J. Electroanal. Chem.* **2002**, *524*, 77-80.

(302) Li, Z. G.; Niu, T. X.; Zhang, Z. J.; Bi, S. P. *Electrochim. Acta* **2010**, *55*, 6907-6916.

(303) Rivera-Gandía, J.; Cabrera, C. R. *J. Electroanal. Chem.* **2007**, *605*, 145-150.

(304) Vanderah, D. J.; Vierling, R. J.; Walker, M. L. *Langmuir* **2009**, *25*, 5026-5030.

(305) Lioubimov, V.; Kolomenskii, A.; Mershin, A.; Nanopoulos, D. V.; Schuessler, H. A. *Appl. Optics* **2004**, *43*, 3426-3432.

(306) Branca, M.; Correia-Ledo, D.; Bolduc, O. R.; Ratel, M.; Schmitzer, A. R.; Masson, J.-F. *Physical Chemistry Chemical Physics* **2011**, *13*, 12015-12023.

(307) Rapaport, H.; Kjaer, K.; Jensen, T. R.; Leiserowitz, L.; Tirrell, D. A. *Journal of the American Chemical Society* **2000**, *122*, 12523-12529.

(308) Fenter, P.; Schreiber, F.; Berman, L.; Scoles, G.; Eisenberger, P.; Bedzyk, M. J. *Surface Science* **1998**, *412-13*, 213-235.

(309) Rabe, M.; Verdes, D.; Zimmermann, J.; Seeger, S. *Journal of Physical Chemistry B* **2008**, *112*, 13971-13980.

(310) Fischer, M.; Leech, A. P.; Hubbard, R. E. *Analytical Chemistry* **2011**, *83*, 1800-1807.

(311) Rich, R. L.; Errey, J.; Marshall, F.; Myszka, D. G. *Anal. Biochem.* **2011**, *409*, 267-272.

Annexes

Annexe A : Plans de détails de l'instrumentation SPR auto-référencé

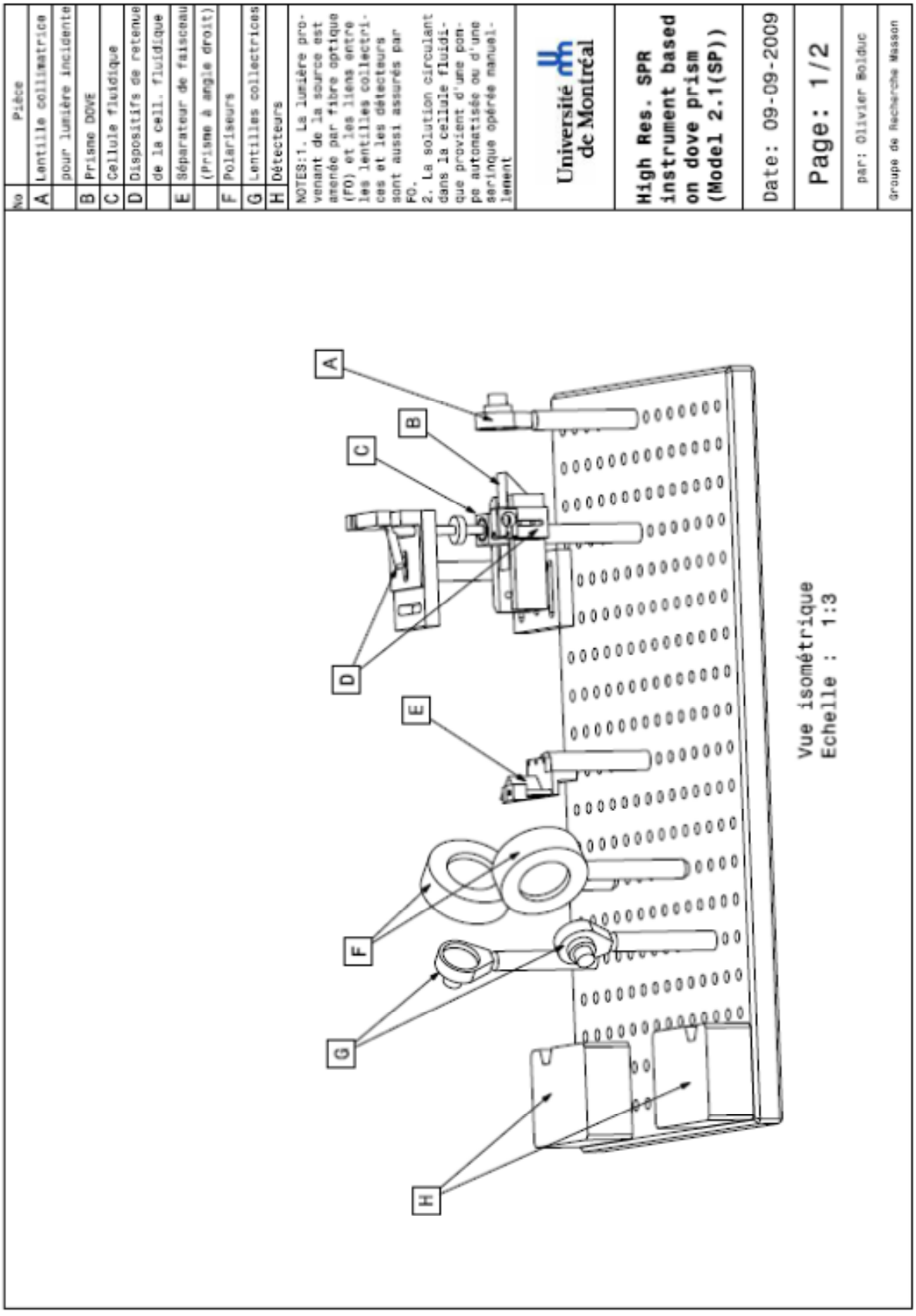

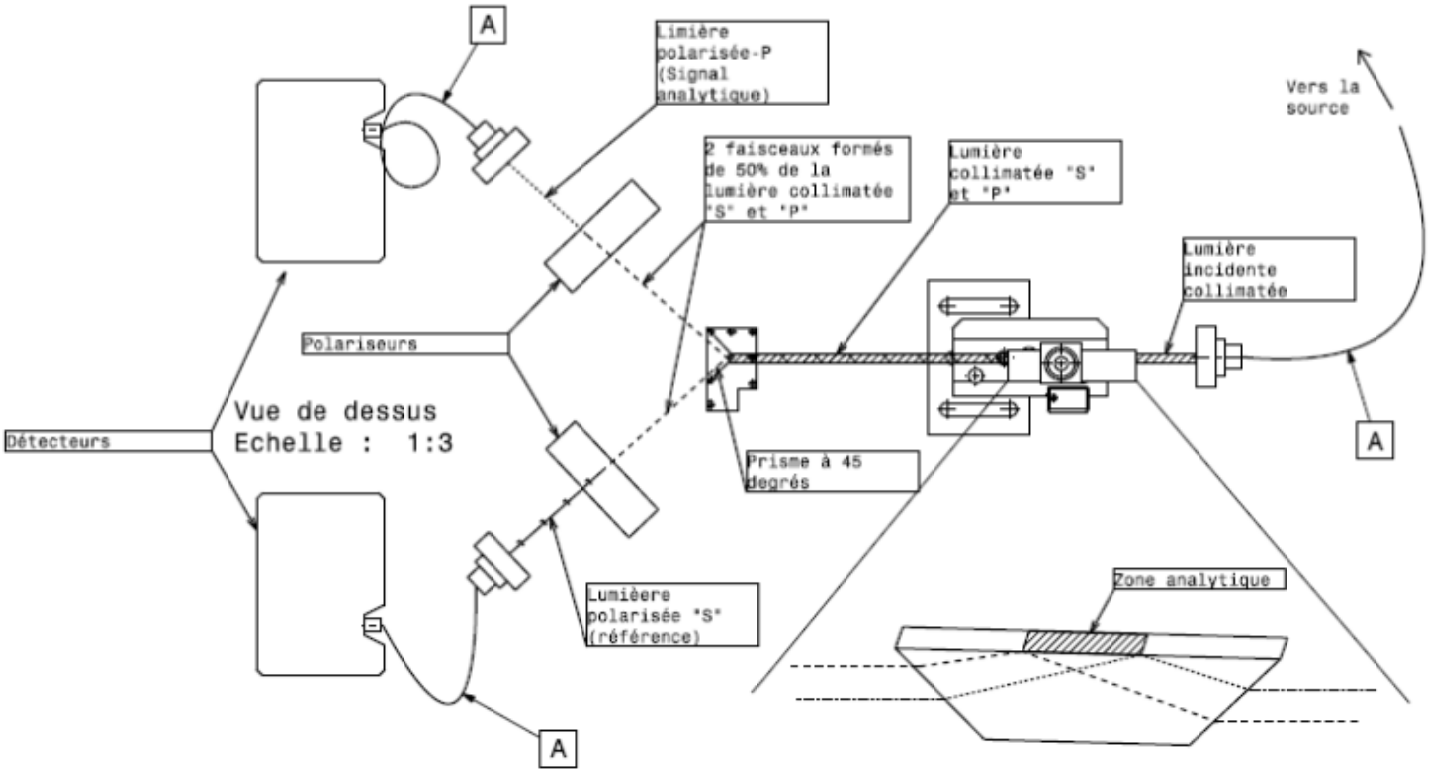

No	Pièce
A	Fibres optiques

NOTES:1. Certaines pièces sont volontairement absentes afin de montrer plus clairement les composantes optiques de l' appareil.

Université de Montréal

High Res. SPR instrument based on dove prism (Model 2.1(SP)) with light path

Date: 09-09-2009

Page: 2/2

par: Olivier Bolduc

Groupe de Recherche Masson

Annexe B : Informations supplémentaires Chapitre 6

Detailed Procedure for Preparation of 3-MPA-Peptide-OH

Hydroxymethyl polystyrene resin (100-200 mesh), protected amino acids and coupling agent were bought form Novabiochem (distributed by EMD biochemicals, Ville Mont-Royal, QC). The amino acids used in the synthesis of the peptides were purchased in the form of Fmoc-Leu-OH, Fmoc-His(Trt)-OH, Fmoc-Asp(OtBu)-OH, Fmoc-Ser(tBu)-OH to avoid multiple couplings and side reactions during the solid phase synthesis. All reactions and rinsing took place in an empty solid phase extraction (SPE) tubes equipped with 20 μm polyethylene (PE) frits. Two immersions in dichloromethane (DCM) for 30 minutes allowed the preparation of the resin for a primary coupling with the C-terminal amino acid. This was accomplished by preparing a solution of 6 equiv of amino acid with 3 equiv of diisopropylcarbodiimide (Sigma-Aldrich, Milwaukee, WI) in N,N-dimethylformamide (DMF). A catalytic amount of 4-(dimethylamino)pyridine (DMAP, Fluka, Milwaukee, WI) was rapidly added to the previous solution immediately before the reaction mixture was transferred to the SPE tube. The tubes were placed on an orbital shaker overnight at room temperature. The reaction mixture was rinsed with DMF three times followed by three rinses with methanol and three immersions in DCM, each step for three minutes in order to condition the newly coupled resin for the next reaction. This rinsing sequence was repeated after every coupling/deprotecting step. Deprotection of the N-terminal extremity from the Fmoc protective group was accomplished over two periods of 30 minutes in a 20:80 piperidine (Sigma-Aldrich, Milwaukee, WI):DMF solution. This step was previously

executed on a small amount of resin using a Kaiser test to confirm the completion of the previous coupling before proceeding with a larger scale deprotection. Subsequent coupling of amino acids were accomplished by immersing the resin for two hours in a solution of 3 equiv amino acid, 3 equiv of 2-(1H-benzotriazole-1-yl)-1,1,3,3-tetramethyluronium (HBTU, Novabiochem) and 9 equiv of N-ethyldiisopropylamine (DIEA), in DMF. The final capping of the peptides with *N*-3-mercaptopropionic acid (3-MPA, Sigma-Aldrich) was accomplished overnight using 1 equiv of 3-MPA and HBTU mixed with 3 equiv DIEA in DMF. This final coupling was verified with a 0.035% N-bromosuccinimide in chloroform (Fisher Scientific) solution, directly sprayed on a small amount of the resin. Once dry, another solution made of 3 mL of 0.1 M sodium hydroxide (Fluka, Milwaukee, WI) containing 0.33% of fluorescein mixed with 100 mL of ethanol was sprayed on the resin. A yellow color reveals the presence of a thiol group on the resin. The efficacy of this approach was confirmed for pure 3-MPA and mercaptohexadecanoic acid (16-MHA, Sigma-Aldrich, Milwaukee, WI) eluted on a TLC slide. The peptidomimetic products were cleaved with 95% trifluoroacetic acid (TFA, EMD biochemicals), 2.5% triethylsilane (TES, Alfa Aesar, Ward Hill, MA) and 2.5% water. TFA was evaporated on a rotary evaporator and the remaining TFA was evaporated using a light flow of nitrogen. Every step was confirmed for the synthesis of one peptide using liquid chromatography- positive mode electrospray ionization – mass spectrometry (LC-ESI-MS) while only the final product was analyzed for the other peptides. The overall yield varied between 15% and 70% depending on the sequence of the peptide.

Preparation and characterization of peptidic monolayers

22mm × 22mm BK7 microscope slides were coated with a 3-nm-thick Ti adhesion layer followed by a 50-nm-thick gold layer (ESPI metals) using a Cressington 308R sputter coater. A reference SPR signal in phosphate buffered saline (PBS, CellGro, Mediatech inc.) was acquired using a previously described setup based on a dove prism placed in a Kretchmann configuration. This setup uses white light in a wavelength interrogation mode and is equipped with a polarizer changing from the reference s-polarized light to p-polarized light where SPR is occurring. This provided the SPR wavelength (λ_{SPR}) through a minimum finding algorithm applied in MatLab. Each slide was immersed for 16h (overnight) in a 1 mM peptide solution in DMF to form a well-ordered monolayer. The slides were rinsed twice with absolute ethanol to wash the excess of solution. A custom-built contact angle instrument allowed the monitoring of advancing contact angles with 300 μL of PBS on each slide. Following this step, the slides were placed on the SPR instrument equipped with a custom-built 100 μL fluidic cell to monitor the shift of λ_{SPR} in PBS due to the formation of the peptidic SAM. The quantification of nonspecific interaction due to bovine serum proteins was acquired immediately afterward. This was achieved by monitoring in real-time a 5 min reference in PBS, followed by a 20 min period in bulk bovine serum and ended by a 5 min period in PBS. One slide per peptide was analyzed using a Tensor 27 (Bruker optics) equipped with a Ge attenuated total reflection (GATR).

Annexe C : Informations supplémentaires Chapitre 7

Experimental details

Synthesis and characterization of peptide-based self-assembled monolayers

The peptides were synthesized according to a previously described protocol [271]. LC-MS was used to verify the products at each step of the synthesis. The conformation of the peptides in solution was measured with circular dichroism on a Chirascan™ spectrometer (Applied Photophysics ltd) using a 1 mg/mL peptide solution in PBS. Microscope slides were coated with a 0.5 nm thick chromium adhesion layer and then with a 50 nm thick gold layer using a sputter coater (Cressington Model 308R). These SPR sensors were reacted for at least 16 h with a 5 mM peptide solution in DMF. The SAM formed on the SPR sensors was extensively rinsed with DMF and ethanol and dried. The mid-IR spectrum of the peptide monolayers immobilized on the SPR sensors was measured in attenuated total reflectance (ATR). Mid-IR spectra were recorded using a Bruker Tensor 27 equipped with a Ge-ATR module.

The synthesis of the modified peptide layer binding His-tagged biomolecules was performed directly on the SPR sensors (Figure 7-2), based on the optimal peptide 3-MPA-LHDLHD-OH. The following solutions are aqueous and the SPR sensors were rinsed in ultrapure water following each step. The peptide monolayer immobilized on the SPR sensor was reacted with a solution composed of 100 mM EDC and 20 mM NHS for 2 minutes, followed by a 1 hour reaction with 40 mM Nα,Nα-bis(carboxymethyl)-L-lysine hydrate. The final step was a 10-minute exposition to 100 mM $CuSO_4$, during which Cu^{2+} binds to the modified peptide layer. The SPR sensors were rinsed in ultrapure water and dried using a moderate flow of nitrogen. The product of each reaction was monitored using FTIR. In

this configuration, the peptide monolayer chelates copper and copper chelates His-tagged biomolecules. Thus, the surfaces were analyzed using x-ray photoelectron spectroscopy (XPS) to ensure the presence of Cu^{2+} on the SPR sensors modified with the modified peptide layer binding His-tagged biomolecules. A VG ESCALAB 3 MKII equipped with a Mg Kα source running at 300W scanning from 50 to 100 Å deep provided the XPS spectral information.

Characterization of modified peptide layer binding His-tagged proteins

The peptides were produced in large amount (hundreds of mg) and stored in an opaque and sealed container at room temperature without any further care. They were used over a period of 30 days without any change in the analytical signal. Peptides exhibit a good absorption signature in the mid-IR domain. Thus, the reactions performed on the SPR substrates were followed using FTIR as a convenient way to rapidly obtain information about the composition of the modified peptide layer at the surface of a gold-coated sensor. Every spectral acquisition was preceded by the acquisition of a blank measurement with a bare gold-coated slide. The amide I band is of primary importance in the analysis of a peptide-based self-assembled monolayer to determine the secondary structure of the peptide on the SPR sensor. The amine I band for 3-MPA-LHDLHD-OH is located at 1645 cm^{-1} typical for a α-helix. The C=O stretch of the carboxylic acid functional groups of the aspartic acid were observed at 1720 cm^{-1} and disappeared once coupled with Nα,Nα-bis(carboxymethyl)-L-lysine hydrate using EDC/NHS chemistry. This reaction was confirmed with FTIR, with the appearance of two bands at 1670 and 1740 cm^{-1} also observed on the spectra of pure Nα,Nα-bis(carboxymethyl)-L-lysine hydrate. The XPS spectrum of the modified peptide layer chelated with copper exhibited the Cu_{2p} band at

934.07 eV confirming the presence of copper at the surface of the sensors. The relative peak areas observed for sulphur, nitrogen, carbon and oxygen correspond to the values expected for this SAM. The XPS response corresponding to Au and Cu indicate a strong presence of these two metals as expected. Other metals such as Co or Ni can be used for His-tagged protein binding, the most common being Ni. Thus, Ni was also tried with the current modified peptide layer, which in this case did not appear on the XPS spectrum after exposure of the modified peptide layer to Ni. For this reason and because of its lower environmental impact, copper-functionalized surfaces were used thereafter.

Annexe D: Informations supplémentaires Chapitre 8

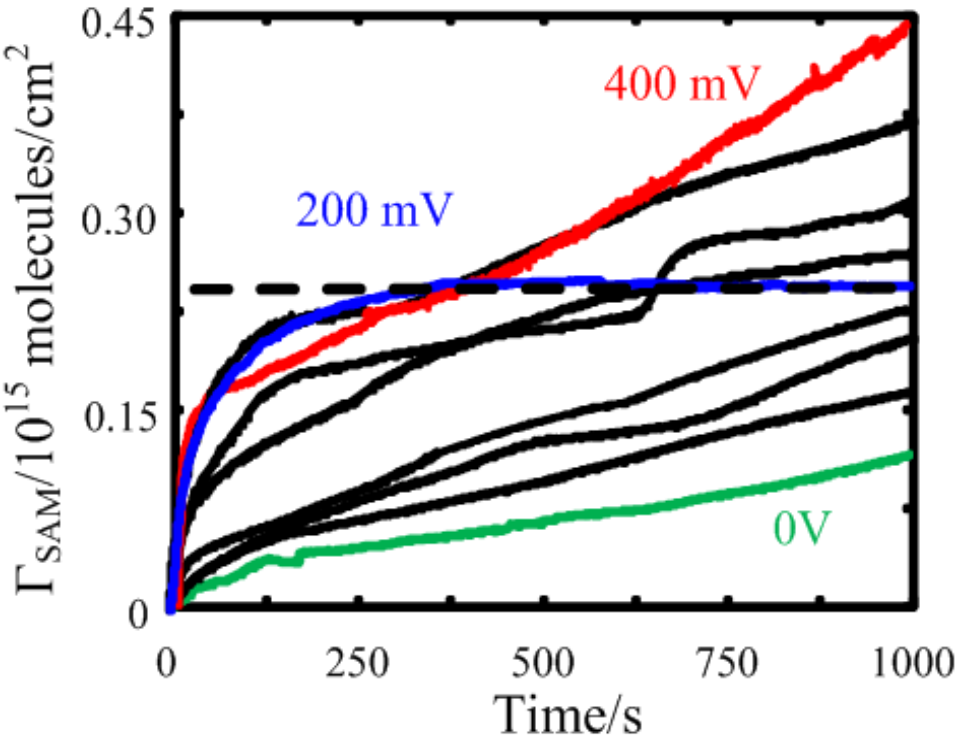

Figure D-1 Overlay of the SPR sensorgrams for the formation of a 3-MPA-H_3D_2-OH layer for ΔE vs Ag/AgCl from 0 to 400mV; each line, from the bottom to the top at 900s, represents a potential difference of 50 mV. The dashed line represents the density for a monolayer self-assembled overnight in ethanol at open circuit potential.

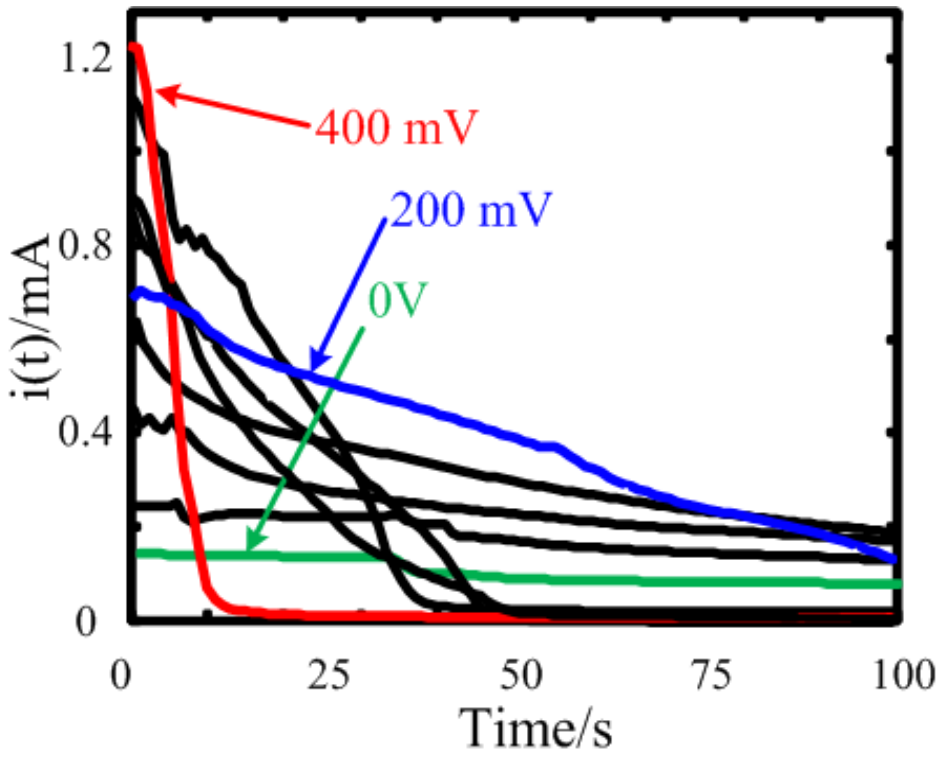

Figure D-2. Overlay of the amperometric measurements for the formation of a 3-MPA-H_3D_2-OH layer for ΔE vs Ag/AgCl from 0 to 400 mV; each line from the bottom to the top at t = 0s, represents a difference of 50 mV.